UNIVERSITÀ DEGLI STUDI DI TRIESTE

e

UNIVERSITÀ CA'FOSCARI DI VENEZIA

XXXIV CICLO DEL DOTTORATO DI RICERCA IN

CHIMICA

DESIGN, SYNTHESIS AND OPTIMIZATION OF POTENTIAL DEUBIQUITINASES INHIBITORS WITH PROMISING ANTINEOPLASTIC ACTIVITY

Settore scientifico-disciplinare: **CHIM/06**

DOTTORANDO
MATTIA VIDALI

COORDINATORE
PROF. ENZO ALESSIO

SUPERVISORE DI TESI
PROF. FULVIA FELLUGA

ANNO ACCADEMICO 2020/2021

Questo lavoro rappresenta la coronazione di una mia grande ambizione che ho a lungo perseguito e per la quale mi sono duramente impegnato. Dedico questa tesi a tutti coloro che saranno felici assieme a me per questo traguardo.

Abstract

Deubiquitinases (DUBs) are a heterogeneous family of enzymes involved in plenty of different cellular functions related to the Ubiquitin Proteasome System, in particular with the degradation of unrequired, damaged, and misfolded proteins. For this reason, they play an essential role in the regulation of the eukaryotic proteome and thus are essential for cellular homeostasis and survival. The human genome encodes approximately 100 different DUBs, most of which are cysteine-dependent isopeptidases with highly conserved catalytic domains. Since various DUB members are commonly overexpressed in numerous tumor lines, the development of DUBs inhibitors has become the focus of recent trends in drug discovery aimed at improving current cancer therapies. In this scenario, our research group previously demonstrated that a partially selective inhibitor (**2c**), containing a reactive 1,5-diaryl-3-oxo-1,4-pentadiene group as a Michael acceptor, inhibits multiple cellular nucleophilic targets, including several DUBs, and triggers a proapoptotic response in different types of tumours with micromolar IC_{50}. We also demonstrated that its cytotoxicity is directly related to the electrophilicity of both β-carbon atoms of the cross-conjugated dienone, as a further evidence of an irreversible inhibition mechanism that occurs via alkylation of the catalytic cysteine. However, if on the one hand the wide number of biological targets of **2c** contributes to boost its overall *in vivo* activity, on the other this indiscriminate reactivity could be disadvantageous due to the rise of possible adverse side effects. A typical strategy to address this common issue is the conjugation of non-specific covalent inhibitors with molecular fragments aimed at improving their selectivity simultaneously toward the enzyme's catalytic site and cancer cells.

Based on these results, in the first part of the project the compound **2c** was selected for further lead optimization. These modifications resulted in the functionalization of the inhibitor scaffold with different amino acids such as lysine, arginine, serine, alanine, aspartic and glutamic acid. Some of these derivatives were subsequently used as building blocks for the synthesis of longer peptides containing the functionalized inhibitor, mainly based on Arg-Gly-Asp, Lys-Gly-Asp and

GnRH-1 sequences. Each product was obtained via conventional peptide chemistry procedures by means of repeated steps of coupling, purification, and deprotection from the parent inhibitor. The resulting structures, generally known as Peptide-Drug Conjugates (PDCs), are emerging as powerful tools for targeted drug delivery, particularly useful for the treatment of tumours that overexpress the related peptide receptors.

The second part of this thesis was focused on the early stages of drug discovery aimed at identifying novel inhibitors of DUBs with potential antitumoral activity. These structures are based on different electrophilic Michael acceptors specific for the alkylation of cysteine-dependent proteases, such as α,β-unsaturated esters, alkynes, and vinyl sulfones. Further conjugation of the acceptor to small peptides resembling the terminal sequence of the substrate (ubiquitin) is expected to increase the binding affinity of the inhibitor for the binding site of the target enzyme, thus resulting in a higher selectivity. For this reason, all the candidates were obtained as ubiquitin-mimetic pseudopeptides, with the terminal carboxylic group of the sequence replaced by the covalent modifier.

In summary, this work presents an efficient, versatile, and reproducible protocol for the synthesis of 22 novel potential DUBs inhibitors with promising antineoplastic activity. All the compounds were isolated as products of multistep reactions in modest to very good yields. These reactions also led to the isolation and characterization of 30 intermediate products that could be useful for future developments. The high purity profile of each sample was evidenced by NMR spectroscopy and ESI mass spectroscopy, which both allowed a complete product characterization. Preliminary MTT assays identified the vinyl sulfone **51b** as a promising hit compound with potential antitumor activity against Kuramochi cell line. For this reason, it will be the subject of further optimization processes in the near future.

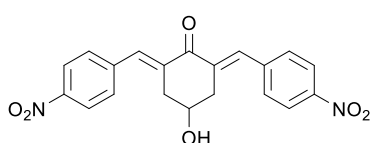
2c   **51b**
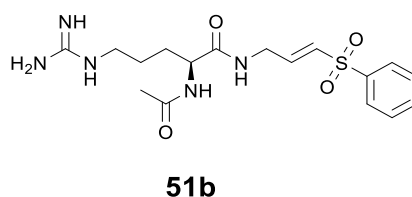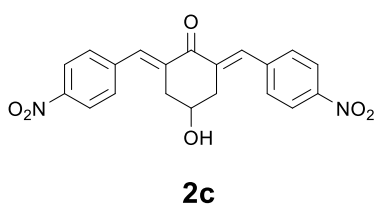
Il termine deubiquitinasi (DUBs) indica una famiglia eterogenea di enzimi coinvolti in molteplici processi cellulari connessi all'Ubiquitin Proteasome System, in particolar modo legati alla degradazione di proteine danneggiate, mal ripiegate o destinate ad avere vita breve nell'organismo. Per tale motivo, le deubiquitinasi ricoprono un ruolo essenziale nella regolazione del proteoma delle cellule eucariotiche, risultando pertanto essenziali all'omeostasi e alla sopravvivenza cellulare. L'organismo umano codifica approssimativamente un centinaio di diverse deubiquitinasi, la maggior parte delle quali sono proteasi cisteiniche aventi un dominio catalitico ben conservato tra i vari membri. Dal momento che alcuni membri sono sovraespressi in numerosi tipi di cellule tumorali, una branca molto fertile di ricerca riguarda proprio lo sviluppo di nuovi inibitori specifici per le deubiquitinasi quali potenziali farmaci antitumorali. In questo scenario, il nostro gruppo di ricerca ha precedentemente descritto come un inibitore parzialmente selettivo (**2c**), contenente il gruppo 1,5-diaril-3-osso-1,4-pentadienilico quale accettore di Michael, induca l'inibizione di svariati bersagli molecolari nucleofili, in particolar modo di molteplici deubiquitinasi. Questo composto si è mostrato anche in grado di indurre una risposta proapoptotica in diverse linee di cellule tumorali nel range micromolare. È stato inoltre dimostrato che la citotossicità del **2c** è direttamente correlata all'elettrofilicità dei due atomi di carbonio β del sistema coniugato del dienone. Questa evidenza ha ulteriormente confermato come l'inibizione delle deubiquitinasi da parte del **2c** avvenga tramite alchilazione del gruppo tiolico della cisteina catalitica. Se, da un lato, questo ampio spettro di attività biologiche conferisce a tale inibitore una spiccata efficacia *in vivo*, d'altra parte, però, questa promiscua reattività potrebbe essere la causa di possibili effetti avversi. Un tipico approccio per superare questo problema, comune alla maggior parte degli inibitori covalenti, consiste nella coniugazione di questi ultimi con frammenti molecolari finalizzati a migliorarne la selettività, sia verso il sito attivo dell'enzima bersaglio sia verso le cellule tumorali.

Sulla base di queste considerazioni, la prima parte del progetto è stata focalizzata sulla ottimizzazione della struttura **2c**: si sono in questo modo ottenuti vari derivati dell'inibitore, il cui scaffold è stato funzionalizzato con amminoacidi quali lisina, arginina, alanina, acido aspartico e acido glutammico. Alcuni di questi prodotti sono stati successivamente impiegati come reattivi di partenza per la sintesi di catene peptidiche contenenti l'inibitore funzionalizzato, basate in particolar modo su
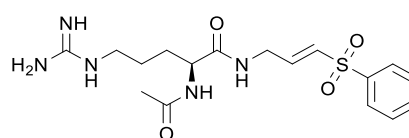
sequenze di Arg-Gly-Asp, Lys-Gly-Asp e GnRH-1. Questa serie di composti è stata ottenuta a partire dal **2c** per mezzo di sequenziali passaggi di sintesi peptidica, purificazione e deprotezione. Tali derivati peptidici, conosciuti generalmente con il termine "farmaco peptide-coniugato" (Peptide Drug Conjugates, PCDs), costituiscono un'emergente classe di fionde molecolari per il rilascio mirato di farmaci all'interno dell'organismo, potenzialmente efficaci per il trattamento di tumori che sovraesprimono tali recettori peptidici.

La seconda parte della tesi è stata invece focalizzata sullo sviluppo di nuovi inibitori covalenti delle deubiquitinasi con promettente attività antitumorale, basati su differenti accettori di Michael specifici per proteasi tioliche, quali esteri α,β-insaturi, alchini e vinil solfoni. La coniugazione di tali accettori con sequenze peptidiche che mimano la sequenza terminale del substrato dell'enzima (ubiquitina) dovrebbe risultare in una maggiore selettività dell'inibitore verso il sito di legame dell'enzima bersaglio. Per questo motivo, tutti i candidati sono stati ottenuti come pseudopeptidi ispirati alla struttura dell'ubiquitina, il cui residuo carbossi-terminale è stato sostituito dall'inibitore stesso.

In conclusione, questo lavoro presenta un protocollo efficiente, riproducibile e versatile per la sintesi di 22 potenziali nuovi inibitori delle deubiquitinasi con promettente citotossicità verso le cellule tumorali. La sintesi di tali composti è avvenuta in più passaggi, con rese che oscillano da medie a molto buone. Queste reazioni hanno portato inoltre all'isolamento di 30 intermedi di reazione, che potrebbero rivelarsi molto utili in vista di futuri sviluppi. Analisi NMR e di spettroscopia di massa hanno confermato l'elevato profilo di purezza di tutti i composti sintetizzati, consentendone inoltre una completa caratterizzazione. Una preliminare valutazione dell'attività antitumorale, effettuata tramite saggi MTT su cellule Kuramochi, ha portato all'identificazione del vinilsolfone **51b** come promettente composto attivo con potenziale attività antitumorale. Per questo motivo, tale composto sarà oggetto di futuri processi di ottimizzazione.

2c   **51b**

Contents

Index

Figures

Tables

Schemes

Abbreviations

3D	Three-Dimensional
ABPs	Activity-Based Probes
Ac	Acetyl group
ACN	Acetonitrile
ADME	Absorption, Distribution, Metabolism, Excretion
AMC	7-Amino-4-Methylcoumarin
Ala	Alanine
AMPK	Adenosine Mono Phosphate-Activated Protein Kinase
anh	Anhydrous
aq	Aqueous
Ar	Aromatic substituent
Arg	Arginine
Asp	Aspartic Acid
ATeNA	Applicazioni Tecnologiche di Nuovi Anti-Neoplastici
Bn	Benzyl
Boc	*tert*-Butoxycarbonyl
Boc$_2$O	di-*tert*-Butyldicarbonate
br	Broad Signal
BTZ	Bortezomib
CDKs	Cyclin-Dependent Kinases
COX-2	Cyclooxygenase-2
CP	Core Particle
Cys	Cysteine
d	Density
d	Doublet
dd	Doublet of Doublets
dt	Doublet of Triplets
DCM	Dichloromethane
DBF	Dibenzofulvene
DMF	N,N-Dimethylformamide
DMSO	Dimethylsulfoxide
DSC	N,N′-Disuccinimidyl carbonate
DUBs	Deubiquitinating Enzymes (Deubiquitinases)
E1	Ubiquitin-Activating Enzymes

E2	Ubiquitin-Conjugating Enzymes
E3	Ubiquitin-Ligating Enzymes (Ubiquitin Ligases)
EDC	1-Ethyl-3-(3-Dimethylaminopropyl)Carbodiimide
eq	Equivalents
ESI	Electrospray Ionization
Et	Ethyl
EtOH	Ethanol
Fmoc	Fluorenylmethyloxycarbonyl
FP	Fluorescence Polarization
Gdn	Guanidine
gCOSY	Gradient Homonuclear Correlation Spectroscopy
Glu	Glutamic Acid
Gly	Glycine
GnRH	Gonadotropinreleasing Hormone
h	Hours
HOBt	1-Hydroxybenzotriazole
His	Histidine
IC_{50}	50% Inhibitory Concentration
JAMMs	JAMM/MPN Domain-Associated Metallopeptidases
Lys	Lysine
m	Multiplet
MALDI-TOF	Matrix-Assisted Laser Desorption/Ionization Time-Of-Flight
Me	Methyl
MeOH	Methanol
Met	Methionine
min	Minutes
MJDs	Machado-Joseph Disease Protein Domain Proteases
MMPs	Matrix Metalloproteinases
MS	Mass Spectrometry
NBD	7-Nitrobenz-2-Oxa-1,3-Diazole
NF-κB	Nuclear Factor 'κ-Light-Chain-Enhancer' of Activated B-Cells
NMR	Nuclear Magnetic Resonance Spectroscopy
n.m.t.	Not More Than
Su	N-Succinimidyl
OTUs	Ovarian-Tumor Proteases
Pbf	2,2,4,6,7-Pentamethyl-Dihydrobenzofuran-5-Sulfonyl
PDCs	Peptide-Drug Conjugates
pGlu	Pyroglutamic Acid
Ph	Phenyl
PLA_2	Phospholipase PLA_2

PLPro	Papain-Like Protease
PolyUb	Polyubiquitin
Pro	Proline
pTSA	p-Toluenesulfonic Acid
Py	pyridine
q	Quartet
quint	Quintet
RGD	Arg-Gly-Asp
RP	Regulatory Particle
r.t.	Room Temperature
s	Singlet
SARS-CoV-2	Severe Acute Respiratory Syndrome Coronavirus 2
sat	Saturated Solution
Ser	Serine
t	Triplet
*t*Bu	*tert*-Butyl
*t*BuOK	Potassium *tert*-butoxide
td	Triplet of Doublets
TEA	Triethylamine
TFA	Trifluoroacetic Acid
THF	Tetrahydrofuran
TLC	Thin Layer Chromatography
TMSOTf	Trimethylsilyl Trifluoromethanesulfonate
TMS	Tetramethylsilane
Trp	Tryptophan
Tyr	Tyrosine
Ub	Ubiquitin
UCHs	Ubiquitin Carboxy-Terminal Hydrolases
UPS	Ubiquitin Proteasome System
USPs	Ubiquitin Specific Proteases

1. INTRODUCTION

2. AIM

3. RESULTS AND DISCUSSION

4. CONCLUSIONS

5. EXPERIMENTAL SECTION

6. SUPPORTING MATERIAL

The Ubiquitin Proteasome System

The Role of the Ubiquitin Proteasome System in Eukaryotes

♦ *The UPS regulates protein activity and turnover in eukaryotes and is essential for cellular integrity and survival.*

The control of proteome homeostasis is crucial for several biological processes in eukaryotes, including cellular turnover, differentiation, and metabolism. Because of this, the balance between the synthesis and degradation of proteins must be strictly regulated.[1-3] In this contest, the Ubiquitin Proteasome System (UPS) is the most representative pathway for the degradation of approximately 80% of unrequired, damaged, and misfolded proteins in eukaryotes. This process was first discovered in the early 1980s,[4-6] and its full complexity continues to emerge: in fact, the wide range of biological implications of UPS have not been fully understood yet.[7-8] However, it is well established that this mechanism regulates the activity of many proteins, each with different structure and biological role. Few examples can be found in enzymes involved in the cell cycle progression and DNA repair mechanisms (e.g., P53 tumor-suppressor),[9-16] structural and transmembrane proteins,[17-18] transporters,[19-20] receptors,[21] and many more. For this reason, misfunctions of the UPS can affect cellular integrity and phenotype, leading to an uncontrolled cell proliferation and tumorigenesis.[22-25] In addition, dysregulations of the UPS are commonly related to Alzheimer's and Parkinson's diseases,[26-27] viral infections,[28-30] immunodeficiency disorders [31] and other chronic pathologies.[32-45]

♦ *Ubiquitin tags unwanted or damaged proteins and triggers their proteasomal degradation.*

One of the main features of the UPS is that it links unnecessary or deleterious proteins to a 76-residue peptide known as Ubiquitin (Ub) and triggers a cascade of enzymatic reactions that ultimately result in the substrate digestion. Most importantly, the specificity of the entire process is ensured by Ub, which acts

as a tag for proteins to be processed through the UPS.[46-47] The Ub-mediated degradation pathway for protein substrates consists of three sequential steps (Figure 1):

- Covalent conjugation with Ub (ubiquitination) and recognition by the 26S proteasome.
- Cleavage of Ub from ubiquitinated substrates assisted by deubiquitinating enzymes (also known as deubiquitinases or isopeptidases).
- Proteolysis in the 26S proteasome.
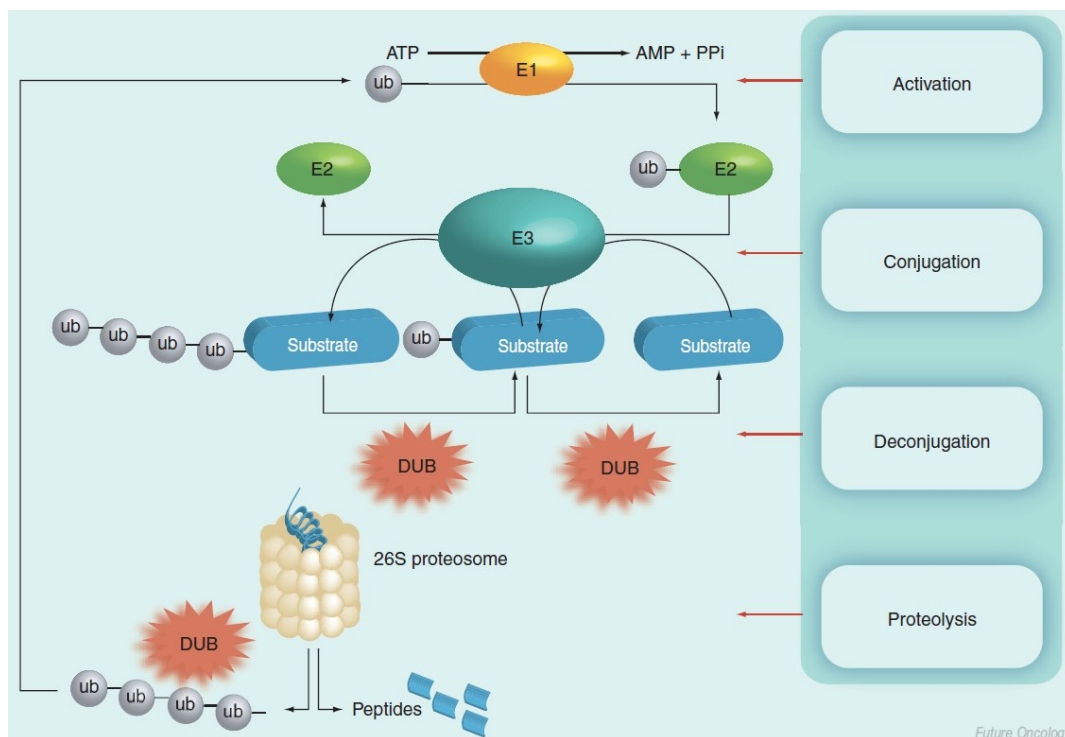
Figure 1

The UPS pathway for the degradation of proteins in eukaryotes.

Ubiquitin (Ub)

♦ *Ub has a highly conserved structure that can polymerize to generate polyUb chains.*

Due to its essential biological implications, the structure of Ub has been highly conserved throughout evolution. In fact, highly sequences homologies have been found between human and yeast Ub, with just 3 out of 76 residues of difference.[48-49] Ub has a globular three-dimensional (3D) structure characterized by the presence of a rigid and compact β-grasp fold. On the other hand, there are few flexible portions, such as the C-terminus tail consisting of Leu^{71}-Arg^{72}-Leu^{73}-Arg^{74}-Gly^{75}-Gly^{76} residues. These regions are important for the interaction with other macromolecules bearing specific ubiquitin-binding domains on their surfaces.[50-51] Other important sites include the hydrophobic pocket delimited by the Ile^{44}, Leu^{8}, Val^{70} and His^{68} residues (Figure 2a), as well as the Ile^{36} patch, which includes Leu^{71}, Leu^{73} and Ile^{36} residues (Figure 2b).[52-55]
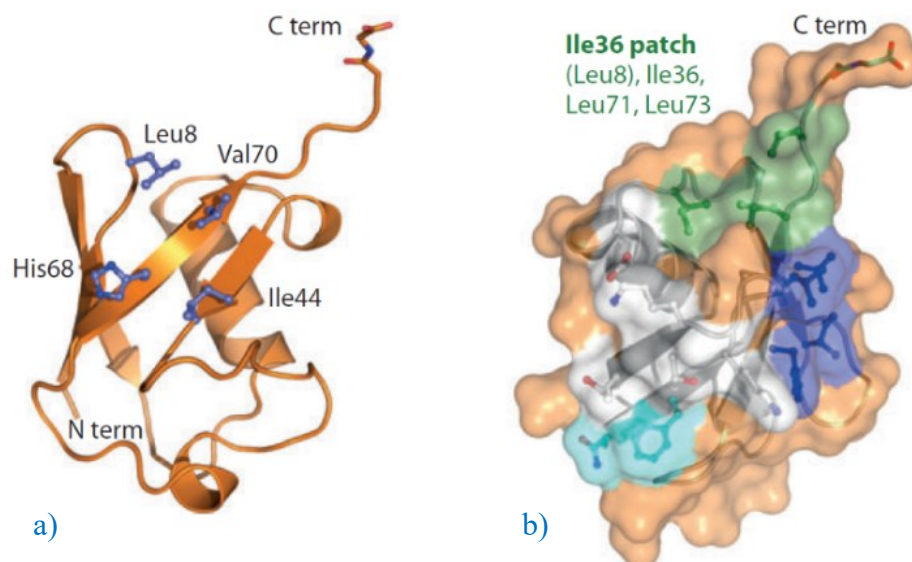
Figure 2

3D structure of the Ub monomer. There are shown:
a) the C-terminus tail and the Ile^{44}-Leu^{8}-Val^{70}-His^{68} pocket; **b)** the Ile^{36} patch.

However, the eight residues of Met[1], Lys[6], Lys[11], Lys[27], Lys[29], Lys[33], Lys[48], and Lys[63] (Figure 3a) are the most important for the transmission of the ubiquitin code. In fact, the primary amino group of each of these residues can be used as linkage site to generate an isopeptide bond with the C-terminus group of another monomer of Ub. This process can be repeated with sequential monomers of Ub, thus resulting in the formation of a poly-ubiquitin (PolyUb) chain (Figure 3b).[49]
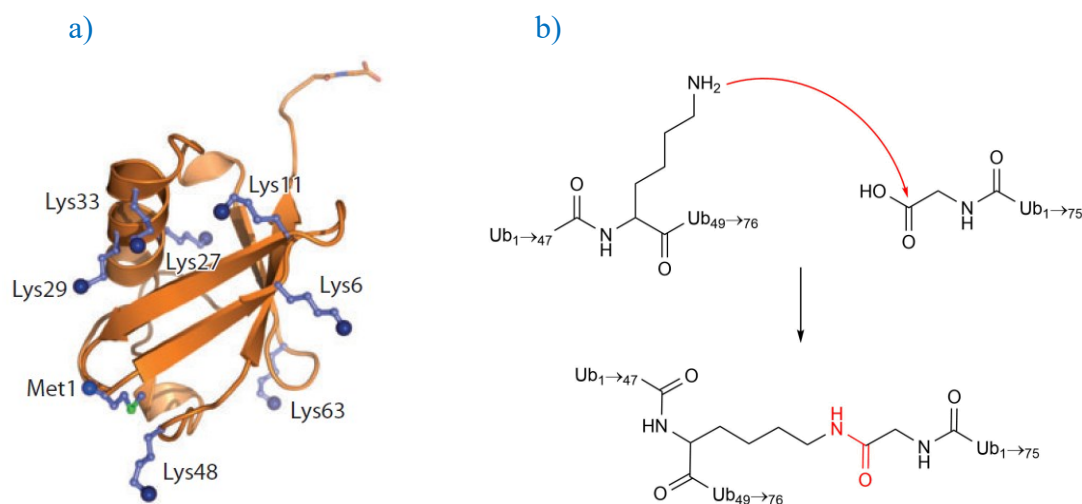
Figure 3

a) The eight free amino groups of the Ub monomer.
b) The mechanism of polyubiquitination (example of a Lys[48]-linked polyUb chain).

♦   *Protein ubiquitination is catalyzed by tree different classes of enzymes: E1, E2 and E3.*

As previously mentioned, ubiquitination is the first step of the UPS-mediated process and results in the conjugation of one or more Ub monomers to the protein substrate. This process is reversible and assisted by three different classes of enzymes: E1 (ubiquitin-activating enzymes), E2 (ubiquitin-conjugating enzymes) and E3 (ubiquitin-ligating enzymes). The human genome encodes two E1 enzymes, about fifty distinct E2 members, and more than seven hundred different E3 enzymes. Each class is then subclassified into various families and subfamilies depending on sequence similarity and substrate specificity.[56-60] In the process of ubiquitination, the Ub monomer is firstly activated via ATP-dependent thioester formation with the thiol side chain of a catalytic cysteine of an E1 enzyme. A further thioester reaction is required to transfer the Ub from the E1 enzyme to an E2 enzyme. Finally, the

activated Ub can be transferred to the substrate by a member of the E3 family (Figure 4).[49]
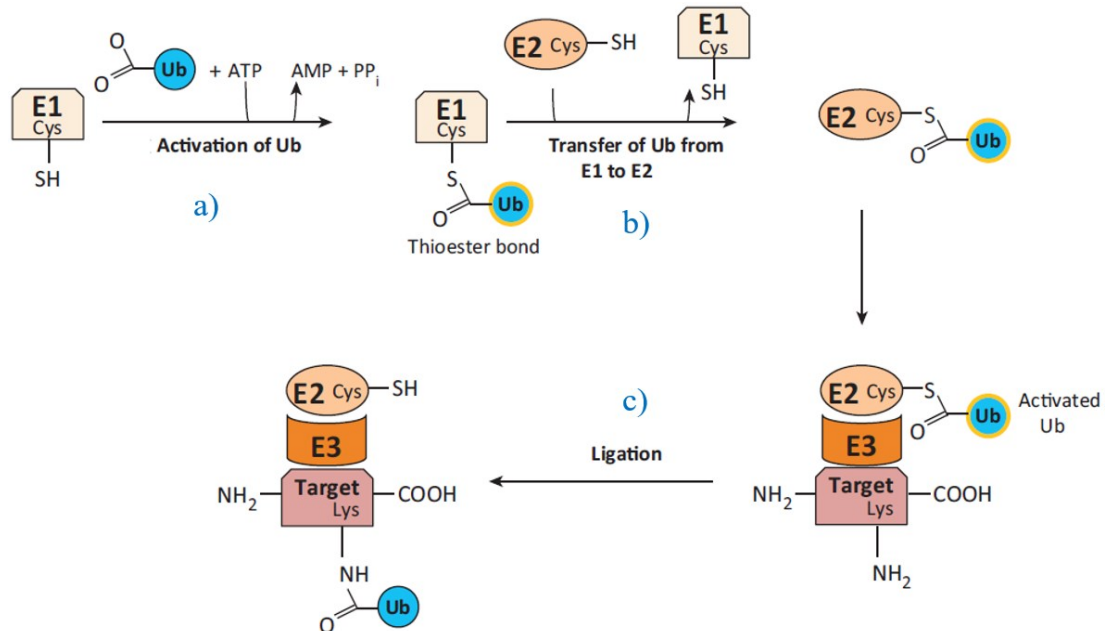
Figure 4

The three-step process of ubiquitination: **a)** *Activation*: The C-carboxy terminal residue of Ub (Gly^{76}) forms a thioester bond with a catalytic Cys of an E1 enzyme. **b)** *Conjugation*: The Ub monomer is transferred to an E2 enzyme. **c)** *Ligation*: The activated Ub joins the substrate, which can be a protein or amonomer of Ub, through the formation of an isopeptide bond that typically involves the side chain amino group of a Lys residue.

♦ *Polyubiquitination regulates many essential cellular processes.*

The Ub moiety can be added to the target protein either in its monomeric form (monoubiquitination) or as a PolyUb chain (polyubiquitination). PolyUb chains can be different in terms of length, morphologies, and connectivity (Figure 5). In general, the precise topology of a polyUb chain determines a specific outcome for the protein it is attached to. Moreover, the addition of multiple monomers of Ub to the substrate can generate a surface with multiple ubiquitinated sites.[49]
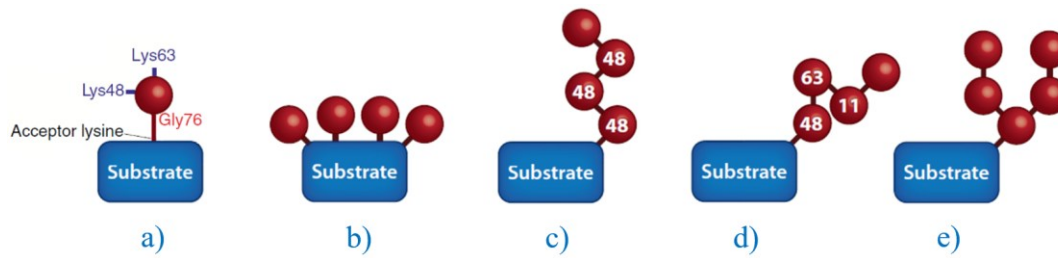
Figure 5

Different patterns of ubiquitination: **a)** Monoubiquitination.
b) Multi monoubiquitination. **c)** Homogeneous polyubiquitination.
d) Mixed polyubiquitination. **e)** Branched polyubiquitination.

Ubiquitin acts therefore as a messenger for the transmission of specific information that regulates a wide variety of cellular processes (Figure 6), including cellular reprogramming, DNA transcription, endocytosis, protein trafficking, immune response, chromatin regulation, apoptosis, oncogenesis, as well as protein degradation.[61-67, 49] For example, Lys^6- and Lys^2-linked chains play an important role in the activation of DNA repair mechanisms, and can modulate the immune response.[68-73] Lys^{33} and Lys^{27} linkages are connected to epigenetic regulation, post-Golgi transport processes and AMPK signalling,[74-77] while other chain topologies are related to signal transduction, cell cycle control, and NF-κB signalling.[78-90] Nevertheless, the Lys^{48} is the most common and characterized connectivity, and it is known to regulate proteolysis.[91-92, 49]
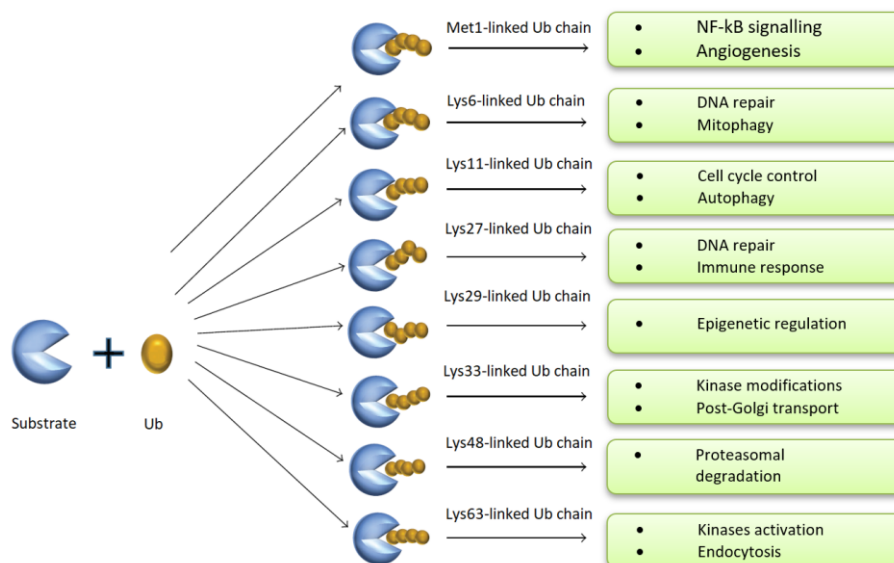
Figure 6

Cellular processes triggered by polyubiquitination.

♦ *The 26S proteasome is a multisubunit complex that degrades unfolded and deubiquitinated proteins.*

The 26S proteasome is a molecular machine designed for protein digestion in eukaryotes: it consists of a cylinder-shaped 2.5 MDa multisubunit complex known as Core Particle (CP or 20S subunit), sealed on both sides by a Regulatory Particle (RP or 19S subunit) (Figure 7). The CP consists of a cavity where a plenty of catalytic sites with chymotrypsin-like activity are exposed along the inner surface. Each RP is then splitted into a base and a lid complex: although the role of the latter is not fully clear yet, it contains several enzymes (e.g., Rpn 1, 11, 10, and 13) which all have deubiquitinating activity.[93]
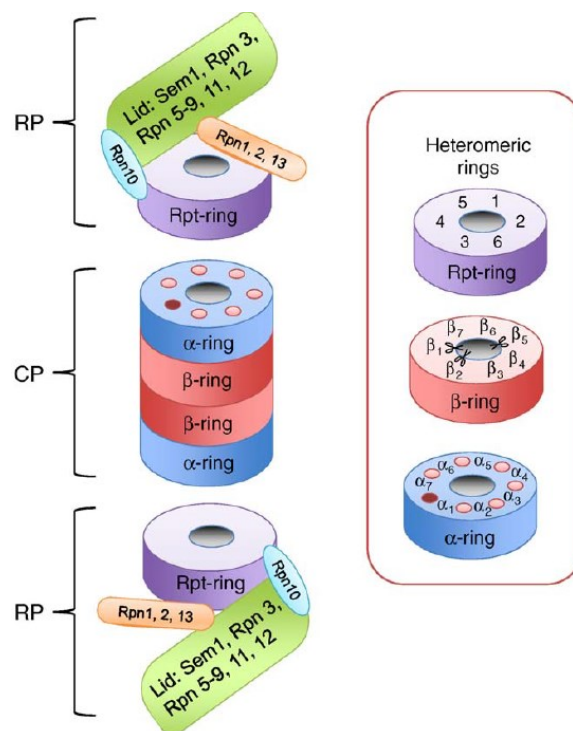
Figure 7

The structure of the 26S proteasome: each RP is made up of a lid complex (green) and a base complex (violet and orange). The CP consists instead of a narrow tunnel formed by two couples of heptameric α-rings (blue) and β-rings (red).

The narrow and elongated opening of the CP requires a steric constraint for substrates to ensure their translocation from the RP to the CP. For this reason, ubiquitinated proteins must be completely unfolded and deubiquitinated to be degraded inside the CP. It is thus obvious that DUBs play an essential regulatory function in the last step of UPS (Figure 8c).[94-96]
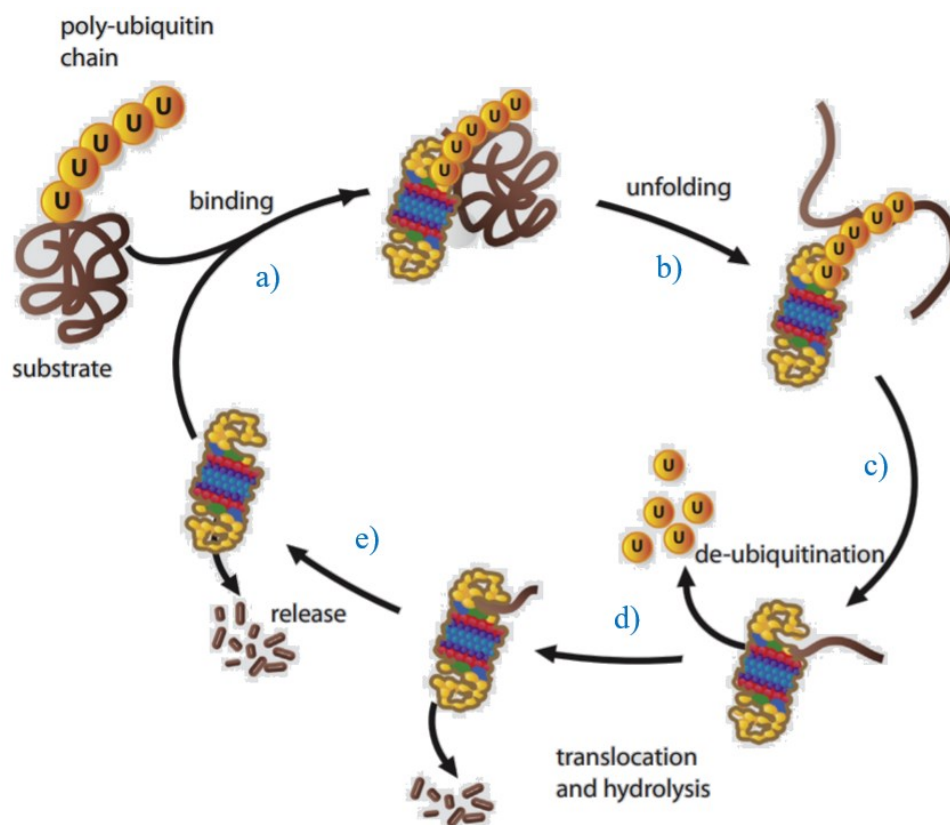
Figure 8

The UPS turnover pathway: **a)** Polyubiquitinated proteins are recognized and bound by the RP subunit of the proteasome. **b)** + **c)** The marked substrates are subsequently unfolded and deubiquitinated. **d)** Deubiquitinated substrates translocate to the CP. **(e)** The substrates can finally be hydrolyzed in shorter oligopeptides and to the corresponding amino acids.

Deubiquitinases (DUBs)

♦ *DUBs are a heterogeneous family of isopeptidases, mostly cysteine-dependent enzymes.*

The reversibility of the tagging process of ubiquitination is ensured by deubiquitinases (DUBs), a heterogeneous family of enzymes that work in an inverse fashion with respect to E3 in a process known as deubiquitination. In particular, the main role of DUBs is to bind ubiquitinated proteins or polyUb chains and to cleave the isopeptide linkage between a Lys side chain amino group and the C-terminus carboxylic group of an Ub monomer, as shown in Figure 9.[49, 97-99] For this reason, DUBs are often referred as isopeptidases.
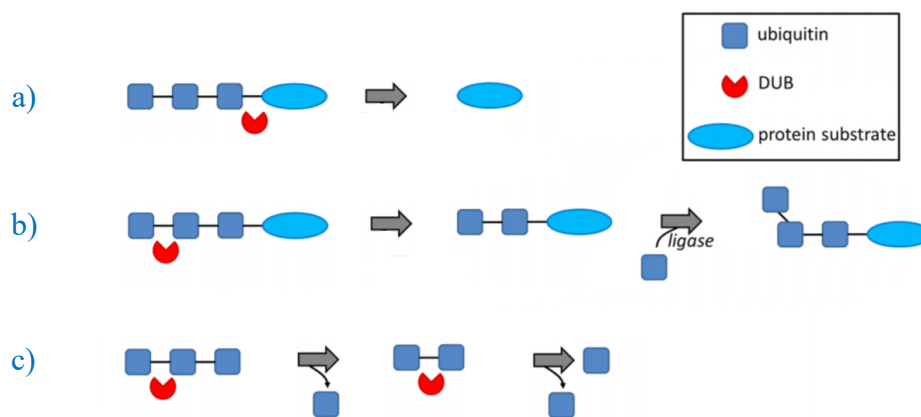
Figure 9

The catalytic role of DUBs: **a)** Cleavage of Ub monomers and PolyUb chains from substrates. **b)** Alteration of the connectivity of PolyUb chains by a combined action of E3 ligases (chain editing). **c)** Disassembling PolyUb chains and regeneration of Ub monomers.

DUBs also modulate the activity of proteins involved in DNA repair,[100] interferon signalling,[101] activation or deactivation of programmed cell death responses,[102] and can regulate other signalling pathways. Nevertheless, the role of these enzymes in determining the outcome of specific proteins continue to unfold.[103-104] Most notably, several studies reported that the dysregulation of certain DUBs leads to cancer proliferation,[105-106] infections, and neurodegenerative diseases:[107] for this reason, DUBs are considered fascinating targets for the design and development of novel chemotherapy drugs.[105-107]

As reviewed by Schauer et al. in 2020, the human genome encodes about a hundred different DUBs, classified in seven different families on the basis of the homology of the catalytic site and presence of additional non-catalytic domains (Figure 10).[108] This heterogeneity reflects the specificity of each member for different substrates and PolyUb linkages. It is reported that DUBs activity is regulated by post-translational modifications, redox reactions, allosteric regulation, protein phosphorylation, and ubiquitination itself.[109-113]
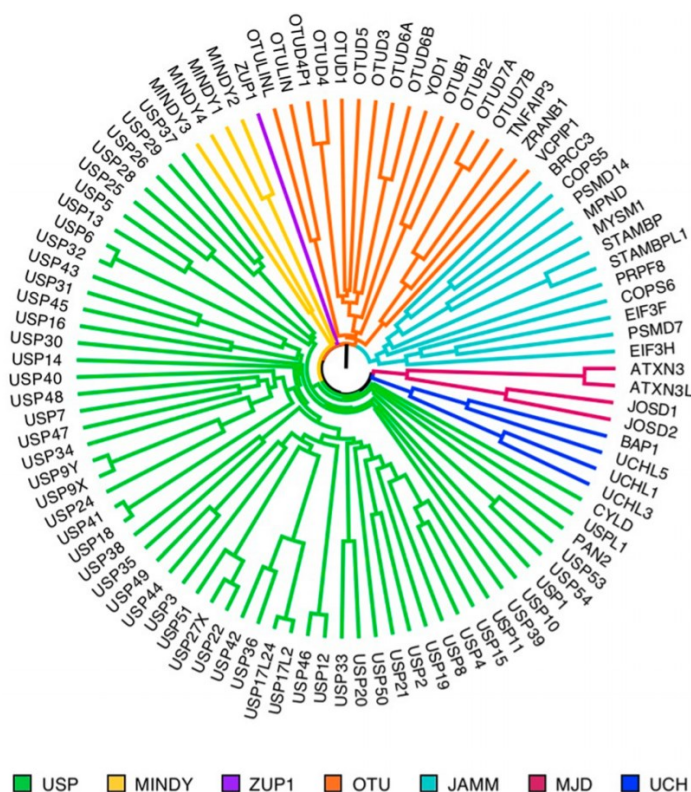
Figure 10

Classification of human DUBs based on the homology of the catalytic sites.
Each family is represented with a different colour.

As summarized in Table 1, 90% of human DUBs are cysteine-dependent enzymes whose catalytic domains are highly conserved among the distinct families. Despite significant variances in terms of size, primary sequence and 3D structure from member to member, the framework of the catalytic triad consisting of Asp-His-Cys residues is surprisingly conserved.[114] The catalytic cycle of a cysteine-dependent DUB, reported in Scheme 1, is similar to that of other papain-like

proteases, and proceeds through the nucleophilic attack of a catalytic Cys to the amidic group of the substrate. A covalent adduct (thioacyl enzyme) is then generated when the Lys residue is released from the substrate. The thioacyl enzyme subsequently reacts with water to release the Ub, regenerate the free enzyme, and start a new catalytic cycle. In contrast, in JAMM family the activation of water is assisted by the combined presence of Zn^{2+} and a residue of Glu (Scheme 2).[115-116, 97]

A number of different DUBs has been extensively reviewed in 2009 by Komander et al.;[97] however, the X-ray structure of many members remains unsolved to date. UCH and USP families are the most characterized so far, with a massive database available in the Protein Data Bank. Various crystallographic structures have been obtained using Ub-aldehyde,[55] Ub-vinyl methyl ester,[117] and Ub-propargylamide [118] complexed with different DUBs.[119]

Table 1

Classification of human DUBs based on the catalytic mechanism.

Family	Members	Mechanism
USPs (Ubiquitin Specific Proteases)	56	Cystein-dependent proteases
OTUs (Ovarian-tumor proteases)	17	
MINDYs (Motif Interacting with Ubiquitin-Containing novel DUB family proteases)	5	
UCHs (Ubiquitin carboxy-terminal hydrolases)	4	
MJDs (Machado-Joseph disease protein domain proteases)	4	
ZUP1 (Zinc Finger-Containing Ubiquitin Peptidase 1)	1	
JAMMs (JAMM/MPN domain-associated metallopeptidases)	12	Zinc metalloproteinases
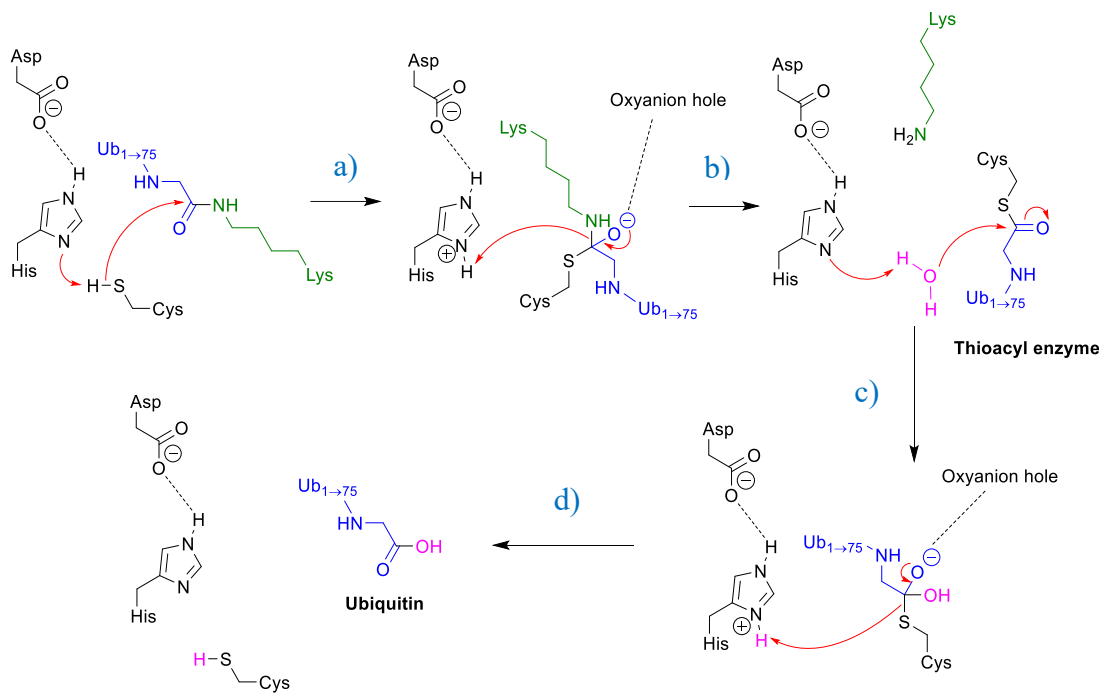
Scheme 1

Isopeptide bond hydrolysis catalyzed by a cystein-dependent DUB. *Mechanism*: **a)** The catalytic thiol of a Cys residue, usually deprotonated by the presence of the nearby Asp-His motif, generates an oxyanion intermediate via nucleophilic attack to the amidic group of the ubiquitinated substrate. **b)** The resulting tetrahedral intermediate, which is stabilized by positively charged and H-bond donating residues of the oxyanion hole, rearranges to the corresponding acyl enzyme with the release of Lys. **c)** A previously activated molecule of H_2O reacts with the acyl enzyme and generates another oxyanion intermediate. **d)** In the final step, the Ub is finally cleaved from the enzyme and a new catalytic cycle can thus begin.
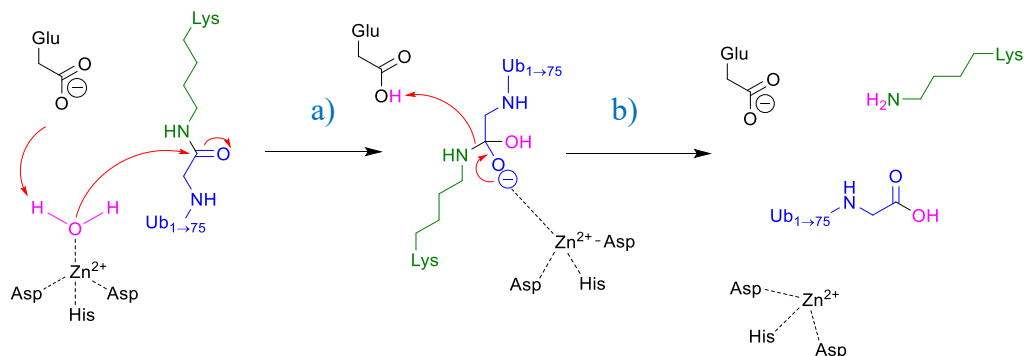
Scheme 2

Isopeptide bond hydrolysis catalyzed by a zinc-dependent DUB. *Mechanism*: **a)** The simultaneous presence of Zn^{2+} as cofactor and Glu as basic catalyst lowers the pKa of the nucleophilic H_2O molecule and leads to the formation of an oxyanion intermediate. **b)** In the second and final step, the intermediate rearranges to liberate the free DUB and the Lys amino group of the substrate.

Approximately half of human DUBs belong to USP family. Crystallographic data suggested that most of the USP members contain three highly conserved catalytic subdomains knows as palm, thumb, and finger (Figure 11). The catalytic Cys is placed between the palm and the thumb, whereas the fingers pull ubiquitinated substrates into the catalytic cleft to enable the catalysis.[104] The main characteristic of USP members is the conformational flexibility of the catalytic triad: in some cases, the spatial arrangement of the Asp-His-Cys motif is correctly aligned even in absence of the substrate, as it happens for USP14 (Figure 12a). However, other members, including USP7, have preorganized catalytic domains that need an Ub-mediated structural rearrangement to establish the catalytically active conformation (Figure 12b).[120-121, 97] Moreover, the enzymes belonging to this family usually bear additional allosteric domains that regulate the biological activity of other important macromolecules (e.g., P53 and MDM2).[122]
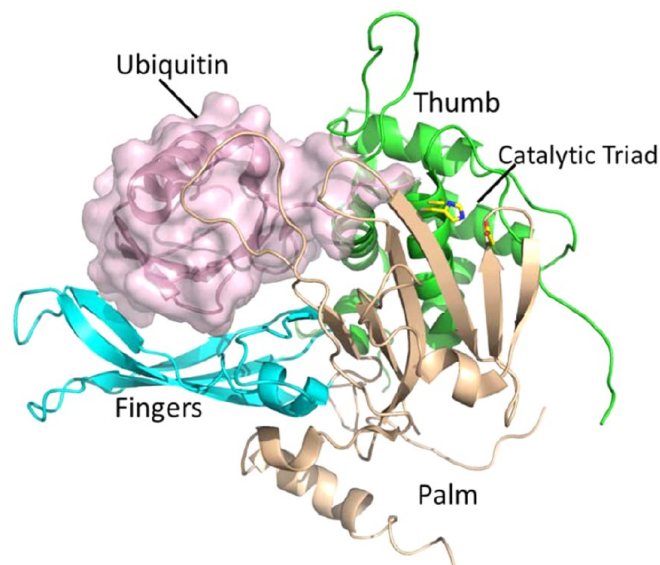
Figure 11

X-ray structure of USP 14 complexed with Ub-aldehyde (in pink).

- *UCH members have greater structural variability and different reactivity from member to member.*

The 3D structure of the four UCH enzymes is simpler compared to the USP's. However, they display greater variability in the preorganization of the catalytic site from member to member (Figure 13). This interesting feature can be exploited to design electrophilic inhibitors that can selectively affect only the most reactive members of the family.[97, 123-127]
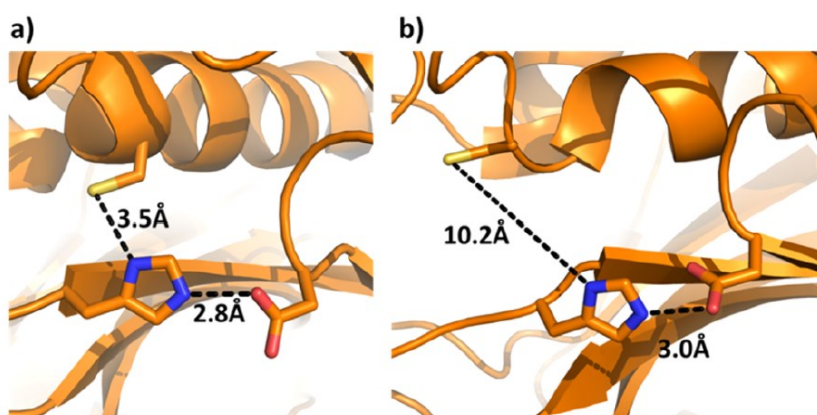
Figure 12

X-ray structures of: **a)** USP14*;* **b)** USP7*.*
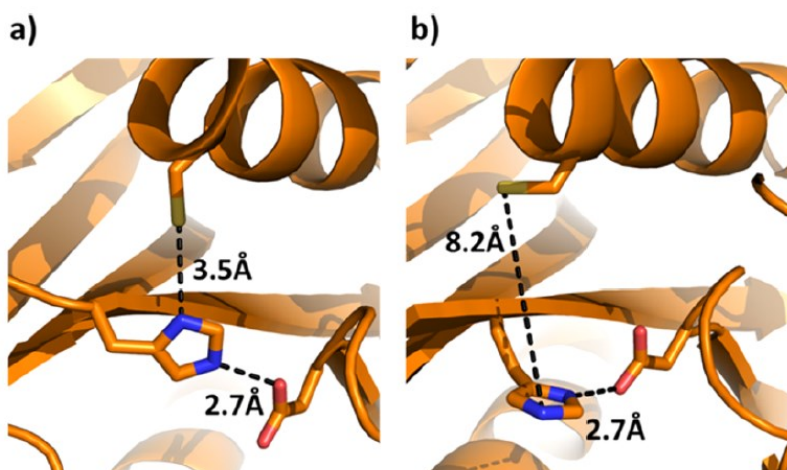
Figure 13

X-ray structures of: **a)** apo-UCHL5; **b)** UCHL1. The architecture of the active site is catalytically unproductive for UCHL5.

The development of small molecules able to modulate the activity of one or multiple DUBs represents a field of growing interest for both Pharmaceutical Industry and Academia. In fact, as will be discussed in more detail, the inhibition of different components of the UPS can trigger cell death responses in several tumor lines.[128]

Regulation of Cell Death by the UPS

♦ *Apoptosis is a regulated cell death mechanism that is necessary for cellular integrity.*

Cell death occurs through two main mechanisms: necrosis and apoptosis. The former, also known as accidental cell death, is characterized by a local acute inflammatory state that can be consequence of a thermal shock or exposure to toxic agents. Apoptosis (or programmed cell death), on the contrary, is an extremely regulated process necessary to maintain tissue homeostasis and guarantee cellular differentiation and turnover. Apoptosis can also be activated as a response to cellular stresses or irreversible damages.[129-131] A family of caspases regulates the entire apoptotic process by triggering a cascade of enzymatic reactions that lead to fragmentation of the parent cell into smaller fragments (Figure 14).[132-133] Since apoptosis is a more conserved and rationalizable mechanism than necrosis, it has been more subject to studies across the fields of biology, oncology, and medicinal chemistry.

Figure 14

Morphological changes in lymphocytic cells during apoptosis: a progressive reduction in the volume of cytoplasm, associated with DNA fragmentation, can be observed at first. Bubble-like protrusions of plasma membrane are then released as cell fragments (apoptotic bodies), which are subsequently phagocytosed.

◆ *Tumorigenesis and tumor proliferation are highly affected by UPS.*

Although apoptosis is necessary for organisms to get rid of old and damaged cells, deficiencies in its mechanisms result in an uncontrolled proliferation of abnormal cells, which can cause tumorigenesis.[134] Furthermore, the balance between proapoptotic and antiapoptotic proteins has a strong influence on tumor initiation and development. These proteins control the cell cycle progression and can contribute to activate apoptosis in cancer,[135-137] or, respectively, can be essential for cancer survival.[138] For example, the P53 tumor suppressor has been widely studied due to its overexpression in many tumours and can be activated to repair DNA damages or trigger apoptosis in the most extreme cases.[139-141] The ubiquitination and proteasomal degradation of the P53 protein is strictly regulated by MDM2 ligase; therefore, it was validated as promising anticancer drug target.[142-143]

In summary, the UPS regulates the activity of many proteins related to tumorogenesis and tumor progression: for this reason, the modulation of enzymes involved in the UPS pathway could bring benefits in the treatment of cancer.[144-147] The most significant effect of the inhibition of the UPS is the accumulation of ubiquitinated and aberrant proteins, which are deleterious for cell survival. As a consequence to the proteotoxic stress, the organism can impose cell cycle arrest or activate a safeguard apoptosis.[98] Most notably, the proteasome activity is very intense in tumor cells, and, for this reason, they are usually more susceptible to cytotoxic agents that act at the level of UPS than non-cancerous cells.[148]

UPS as Drug Target for Cancer Therapeutics

The UPS pathway can be manipulated at three different levels: inhibition of ubiquitinating enzymes, inactivation of the CP subunit of 26S proteasome, or inhibition of DUBs. It should be pointed out that, in all cases, it is essential to achieve high binding specificity with the desired target to avoid possible side effects caused by the numerous biological implications of the UPS.[149-150] A brief list of UPS inhibitors is reported in Table 2 (DUBs inhibitors will be specifically discussed in the next chapter).

- *Several E1, E2 and E3 inhibitors displayed antitumoral activity.*

PYR-41 [151-152] and **MLN4924** [153-154] inhibit the E1 enzymes and trigger apoptosis in multiple P53-mutated tumours, showing low binding affinity for other cysteine-dependent enzymes such E2 and E3. However, inhibiting the E2 and E3 enzymes seems to be a more promising approach in terms of specificity, as witnessed by the E2 inhibitor **CDC34** which arrests prostate and colon tumours proliferation.[155] The design of E3 inhibitors requires maximum selectivity, because each member of this family regulates the expression of multiple different tumor suppressors and oncogenic proteins. In this contest, the first inhibitor of the MDM2 ligase [156-157] was **Nutlin** and derivatives, which activate a P53-dependent apoptosis in ovarian and colon cancer cells.[158] The tricyclic thiophene derivative **RITA** showed similar properties to **Nutlin-3A** with comparable cytotoxicity *in vivo*.[159]

- *Drug resistance and poor selectivity are the major issues of proteasome inhibitors.*

Proteasome inhibitors became attractive drug candidates as soon as they were found to induce apoptosis preferentially in cancer cells.[160-161] This led in 2003 to the approval of Bortezomib (**BTZ**, Velcade®) as the first proteasome inhibitor used against relapses of multiple myeloma and mantle cell lymphomas.[162-163] However, heavy side effects caused by its poor selectivity have been frequently reported over the years. In addition, **BTZ** requires frequent administrations, and also many tumours developed chemoresistance.[164-165] The design and optimization of second-generation proteasome inhibitors (e.g., **Carfilzomib** [166-168]) is finalized to overcome the limitations of **BTZ** and reduce side effects.

- *DUBs are promising drug targets for the development of inhibitors with potential antitumoral activity that might also provide benefits in the treatment of SARS-CoV-2.*

Nevertheless, the existence of specific DUBs that promote or suppress apoptosis in cancer cells [102] (Figure 15) has recently shifted the emphasis toward the development of DUBs inhibitors with potential antineoplastic activity.[169] Moreover, the discovery of novel DUBs inhibitors could provide efficient therapeutic opportunities against SARS-CoV-2 viral infections and treat patients more efficiently. Despite few COVID-19 vaccines are currently available, there is an urgent need to develop alternative solutions to address the ongoing

coronavirus pandemic. In this scenario, it is well established that SARS-CoV-2 encodes a crucial papain-like protease (PLPro) that suppresses the immune response of the host and allows the uncontrolled viral replication.[170] This enzyme has deubiquitinating activity, and, therefore, it is considered an auspicious antiviral target for the development of specific inhibitors.[171-174]
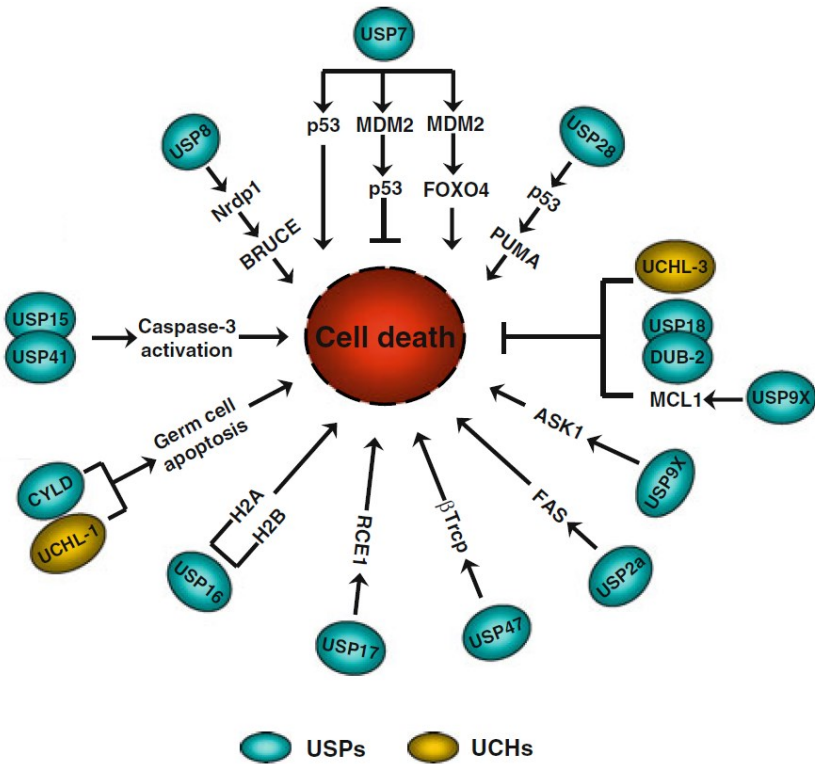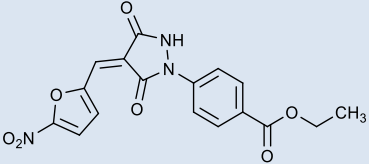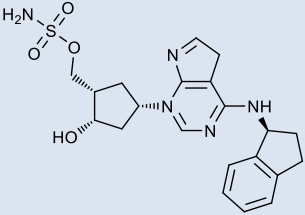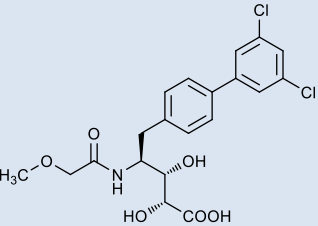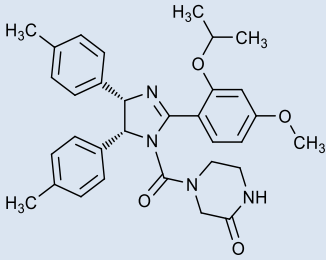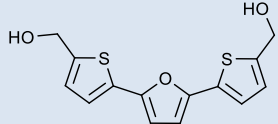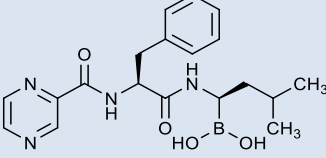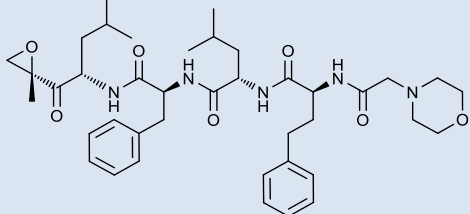
Figure 15

DUBs involved in the modulation of apoptosis: the members that activate apoptosis are represented by an arrow, while those that inhibit apoptosis by a T-shaped arrow.

Table 2

List of the above-mentioned UPS inhibitors.

Name	Target	Chemical Formula	Targeted toumors and diseases
PYR-41 [151-152]	E1		Thyroid and prostate cancers, hypertensive heart diseases.
MLN4924 [153-154]	E1		Liver, lung and pancreatic cancers, pulmonary inflammation, ischemia, mesothelioma.
CC0651 [155]	E2		Prostate and colon cancers.
Nutlin-3A [158]	E3		Pancreatic, colon, breast, ovarian, lung cancers, glioblastoma, sarcoma, leukemia.
RITA [159]	E3		Colon cancer.
Bortezomib [162-163]	CP of 26S proteasome		Multiple myeloma, mantle cell lymphoma, colonrectal, head, neck, thyroid, renal and lung cancers, neuroblastoma, leukemia.
Carfilzomib [167-168]	CP of 26S proteasome		

References

1. Ciechanover, A.; Orian, A.; Schwartz, A. L. The Ubiquitin-Mediated Proteolytic Pathway: Mode of Action and Clinical Implications. *J. Cell. Biochem. Suppl*. **2000**, 34, 40–51.

2. Schubert, U.; Anton, L. C.; Gibbs, J.; Norbury, C. C.; Yewdell, J.W.; Bennink, J. R. Rapid Degradation of a Large Fraction of Newly Synthesized Proteins by Proteasomes. *Nature* **2000**, 404, 770–774.

3. Pickart, C. M. Back to The Future with Ubiquitin. *Cell* **2004**, 116, 181–190.

4. Hershko, A. et al. Proposed Role of ATP in Protein Breakdown: Conjugation of Protein with Multiple Chains of the Polypeptide of ATP-Dependent Proteolysis. *Proc. Natl. Acad. Sci. USA* **1980**, 77, 1783-1786.

5. Ciechanover, A. et al. "Covalent Affinity" Purification of Ubiquitin-Activating Enzyme. *J. Biol. Chem.* **1982**, 257, 2537-2542.

6. Hershko, A. et al. ATP-Dependent Degradation of Ubiquitin-Protein Conjugates. *Proc. Natl. Acad. Sci. USA* **1984**, 81, 1619-1623.

7. Nandi, D.; Tahiliani, P.; Kumar, A.; Chandu, D. The Ubiquitin-Proteasome System. *J. Biosci.* **2006**, 31, 137-155.

8. Varshavsky, A. The Early History of the Ubiquitin Field. *Protein Sci.* **2006,** 15, 647–654.

9. Teixeira, L. K.; Reed, S. I. Ubiquitin Ligases and Cell Cycle Control. *Annu. Rev. Biochem*. **2013**, 82, 387-414.

10. Lukashchuk, N.; Vousden, K. H. Ubiquitination and Degradation of Mutant p53. *Mol. Cell. Biol*. **2007**, 27, 8284-8295.

11. Ulrich, H. D. Ubiquitin and SUMO in DNA Repair at a Glance. *J. Cell Sci*. **2012**, 125, 249-254.

12. Sakai, W. Functional Impacts of the Ubiquitin–Proteasome System on DNA Damage Recognition in Global Genome Nucleotide Excision Repair. *Sci. Rep.* **2020**, 10, 19704.

13. Pant, V.; Lozano, G. Limiting the Power of p53 Through the Ubiquitin Proteasome Pathway. *Genes. Dev.* **2014**, 28, 1739-1751.

14. Zhu, K. et al. The Ubiquitin-Proteasome System Regulates p53-Mediated Transcription at p21waf1 Promoter. *Oncogene* **2007**, 26, 4199-4208.

15. Dang, F.; Nie, L.; Wei, W. Ubiquitin Signaling in Cell Cycle Control and Tumorigenesis. *Cell Death Differ.* **2020** (doi: 10.1038/s41418-020-00648-0).

16. Benanti, J. A. Coordination of Cell Growth and Division by the Ubiquitin-Proteasome System. *Semin Cell Dev Biol.* **2012**, 23, 492–498.

17. Abriel, H.; Staub, O. Ubiquitylation of Ion Channels. *Physiology (Bethesda)* **2005**, 20, 398-407.

18. Foot, N.; Henshall, T.; Kumar, S. Ubiquitination and the Regulation of Membrane Proteins. *Physiol. Rev.* **2017**, 97, 253-281.

19. Lu, Q. et al. Diacylglycerol Kinase Δ Destabilizes Serotonin Transporter Protein Through the Ubiquitin-Proteasome System. *Biochim. Biophys. Acta. Mol. Cell. Biol. Lipids.* **2020**, 1865, 158608.

20. Loayza, D.; Michaelis, S. Role for the Ubiquitin-Proteasome System in the Vacuolar Degradation of Ste6p, the A-Factor Transporter in Saccharomyces Cerevisiae. *Mol. Cell. Biol.* **1998**, 18, 779-789.

21. Kondakova, I. V. Estrogen Receptors and Ubiquitin Proteasome System: Mutual Regulation. *Biomolecules* **2020**, 10, 500.

22. Devoy, A. et al. The Ubiquitin-Proteasome System and Cancer. *Essays Biochem.* **2005**, 41, 187-203.

23. Park, J. et al. Ubiquitin–Proteasome System (UPS) as a Target for Anticancer Treatment. *Arch. Pharm. Res.* **2020**, 43, 1144-1161.

24. Hanna, J. et al. Protein Degradation and the Pathologic Basis of Disease. *Am. J. Pathol*. **2019**, 189, 94, 103.

25. Jit Kong, C. Derailing the UPS of Protein Turnover in Cancer and other Human Diseases. *J. Cancer Res.* **2019**, 189, 94-103.

26. Welzel, A. T.; Walsh, D. M. Aberrant Protein Structure and Diseases of the Brain. *Ir. J. Med. Sci.* **2011**, 180, 15-22.

27. Hong, L. et al. Relationship Between Amyloid-Beta and the Ubiquitin-Proteasome System in Alzheimer's Disease. *Neurol. Res.* **2014**, 36, 276-282.

28. Kong, F. et al. The Interaction of Hepatitis B Virus with the Ubiquitin Proteasome System in Viral Replication and Associated Pathogenesis. *Virol. J.* **2019** 16, 73.

29. Gao, G.; Luo, H. The Ubiquitin-Proteasome Pathway in Viral Infections. *Can. J. Physiol. Pharmacol.* **2006**, 84, 5-14.

30. Casorla-Pérez, L. A. et al. The Ubiquitin-Proteasome System is Necessary for Efficient Replication of Human Astrovirus. *J Virol*. **2018**, 92, 1809-1817.

31. Etzioni, A.; Ciechanover, A.; Pikarsky, E. Immune Defects Caused by Mutations in the Ubiquitin System. *J Allergy Clin. Immunol.* **2017**, 139, 743-753.

32. Kitajima, et al. The Ubiquitin–Proteasome System in Regulation of the Skeletal Muscle Homeostasis and Atrophy: From Basic Science to Disorders. *J. Physiol. Sci.* **2020**, 70, 40.

33. Paul, S. Dysfunction of the Ubiquitin-Proteasome System in Multiple Disease Conditions: Therapeutic Approaches. *Bioessays*. **2008**, 30, 1172-1184.

34. Willis, M. S. et al. Sent to Destroy: The Ubiquitin Proteasome System Regulates Cell Signaling and Protein Quality Control in Cardiovascular Development and Disease. *Circ. Res.* **2010,** 106, 463–478.

35. Schwartz, A. L.; Ciechanover, A. The Ubiquitin-Proteasome Pathway and Pathogenesis of Human Diseases. *Annu. Rev. Med.* **1999**, 50, 57-74.

36. Versari, D. et al. Dysregulation of the Ubiquitin-Proteasome System in Human Carotid Atherosclerosis. Arterioscler. Thromb. Vasc. Biol. 2006, 26, 2132-2139.

37. Ciechanover, A. The Ubiquitin-Proteasome Proteolytic Pathway. *Cell* **1994**, 79, 13–21.

38. Mocciaro, A.; Rape, M. Emerging Regulatory Mechanisms in Ubiquitin-Dependent Cell Cycle Control. *J. Cell. Sci.* **2012**, 125, 255–263.

39. Liu, C.H.; Goldberg, A.L.; Qiu, X.B. New Insights into the Role of the Ubiquitin-Proteasome Pathway in the Regulation of Apoptosis. *Chang Gung Med. J.* **2007**, 30, 469–479.

40. Orlowski, R.Z. The Role of the Ubiquitin-Proteasome Pathway in Apoptosis. *Cell Death Differ.* **1999**, 6, 303–313.

41. Daulny, A.; Tansey, W.P. Damage Control: DNA Repair, Transcription, and the Ubiquitin-Proteasome System. *DNA Repair (Amst.)* **2009**, 8, 444–448.

42. Wang, J.; Maldonado, M. A. The ubiquitin-proteasome system and its role in inflammatory and autoimmune diseases. *Cell Mol Immunol.* **2006**, 3, 255-261.

43. Ciechanover A. The Ubiquitin Proteolytic System: from a Vague Idea, Through Basic Mechanisms, and onto Human Diseases and Drug Targeting. *Neurology* **2006**, 66: S7-19.

44. Ciechanover A. The Ubiquitin-Proteasome Pathway: on Protein Death and Cell Life. *EMBO J.* **1998**, 17, 7151-7160.

45. Malik B, Price SR, Mitch WE, Yue Q, Eaton DC. Regulation of Epithelial Sodium Channels by the Ubiquitin-Proteasome Proteolytic Pathway. *Am. J. Physiol. Renal Physiol.* **2006**, 290, F1285-1294.

46. Hershko, A.; Heller, H.; Elias, S.; Ciechanover, A. Components of Ubiquitin-Protein Ligase System. Resolution, a_Nity Purification, and Role in Protein Breakdown. *J. Biol. Chem.* **1983**, 258, 8206–8214.

47. Nicholson, B; Marblestone, J. G.; Butt, T. R.; Mattern, M. R., Deubiquitinating Enzymes as Novel Anticancer Targets, *Future Oncol.* **2007**, 3, 191-199.

48. Herhaus, L.; Dikic, I. Expanding the ubiquitin code through post-translational modification. *EMBO Rep.* **2015**, 16, 1071-1083.

49. Komander, D.; Rape, M. The Ubiquitin Code. *Annu. Rev. Biochem* **2012**, 81, 203-229.

50. Vijay-Kumar, S.; Bugg, C. E.; Cook W. J. 1987. Structure of Ubiquitin Refined at 1.8 Å Resolution. *J. Mol. Biol.* **1987**, 194, 531–544.

51. Lange, O. F.; Lakomek, N. A.; Fares, C; Schroder, G. F.; Walter, K.F. et al. Recognition Dynamics up to Microseconds Revealed from an RDC-Derived Ubiquitin Ensemble in Solution. *Science* 2008, 320, 1471–1475.

52. Dikic, I.; Wakatsuki, S.; Walters, K. J. Ubiquitin-Binding Domains-From Structures to Functions. *Nat. Rev. Mol. Cell Biol.* **2009**, 10, 659-671.

53. Shih, S. C.; Sloper-Mould, K. E.; Hicke, L. Monoubiquitin Carries a Novel Internalization Signal That is Appended to Activated Receptors. *EMBO J.* **2000**, 19, 187-198.

54. Sloper-Mould, K.E.; Jemc, J.C.; Pickart, C. M.; Hicke, L. Distinct Functional Surface Regions on Ubiquitin. *J. Biol. Chem.* **2001**, 276, 30483-30489.

55. Hu, M; Li, P; Li, M; Li, W; Yao, T et al. Crystal Structure of a UBP-Family Deubiquitinating Enzyme in Isolation and in Complex with Ubiquitin Aldehyde. *Cell* **2002**, 111, 1041–1054.

56. Hershko, A; Ciechanover, A. The Ubiquitin System. *Annu. Rev. Biochem*. **1998**, 67, 425–479.

57. Rieser, E.; Cordier, S. M.; Walczak, H. Linear Ubiquitination: a Newly Discovered Regulator of Cell Signalling. *Trends Biochem. Sci*. **2013**, 38, 94-102.

58. Jin, J.; Li, X.; Gygi, S.P.; Harper, J. W. Dual E1 Activation Systems for Ubiquitin di_Erentially Regulate E2 Enzyme Charging. *Nature* **2007**, 447, 1135–1138.

59. Okamoto, Y.; Ozaki, T.; Miyazaki, K.; Aoyama, M.; Miyazaki, M.; Nakagawara, A. UbcH10 is The Cancer-Related E2 Ubiquitin-Conjugating Enzyme. *Cancer Res.* **2003**, 63, 4167–4173.

60. Pickart, C. M.; Eddins, M. J. Ubiquitin: Structures, Functions, Mechanisms. *Biochim. Biophys. Acta* **2004**, 1695, 55–72.

61. Suresh, B.; Lee, J.; Kim, K-S.; Ramakrishna, S. The Importance of Ubiquitination and Deubiquitination in Cellular Reprogramming. *Stem Cells Int.* **2016**, 13, 1-14.

62. Peng, J. et al. A Proteomics Approach to Understanding Protein Ubiquitination. *Nat Biotechnol*. **2003**, 21, 921-926.

63. Amerik, A. Y.; Hochstrasser, M. Mechanism and Function of Deubiquitinating Enzymes. *Biochim Biophys Acta* **2004**, 1695, 189-207.

64. Welchman, R. L.; Gordon, C.; Mayer, R. J. Ubiquitin and Ubiquitin-Like Proteins as Multifunctional Signals. *Nat. Rev. Mol. Cell. Biol*. **2005**, 6, 599-609.

65. Kerscher, O.; Felberbaum, R; Hochstrasser, M. Modification of Proteins by Ubiquitin and Ubiquitin-Like Proteins. Annu. Rev. Cell. Dev. Biol. 2006, 22, 159-180.

66. Traub, L. M.; Lukacs, G. L. Decoding Ubiquitin Sorting Signals for Clathrin-Dependent Endocytosis by CLASPs. *J. Cell Sci.* **2007**, 120: 543-553.

67. Haglund, K.; Sigismund, S.; Polo, S.; Szymkiewicz, I.; Di Fiore P. P.; Dikic, I. Multiple Monoubiquitination of RTKs is Sufficient for their Endocytosis and Degradation. Nat Cell Biol. 2003, 5, 461-466.

68. Elia, A. E. H. et al. Quantitative Proteomic Atlas of Ubiquitination and acetylation in the DNA Damage Response. *Mol. Cell* **2015**, 59, 867-881.

69. Gatti, M. et al. RNF168 Promotes Noncanonical K27 Ubiquitination to Signal DNA Damage. *Cell Rep.* **2015**, 10, 226-238.

70. Wu, X.; Lei, C.; Xia, T.; Zhong, X.; Yang, Q.; Shu, H-B. Regulation of TRIF-Mediated Innate Immune Response by K27-Linked Polyubiquitination and Deubiquitination. *Nat. Commun.* **2019**, 10, 4115.

71. Ordureau, A. et al. Defining Roles of PARKIN and Ubiquitin Phosphorylation by PINK1 in Mitochondrial Quality Control Using a Ubiquitin Replacement Strategy. *Proc. Natl. Acad. Sci.* **2015**, 112, 6637-6642.

72. Gersch, M.; Gladkova, C.; Schubert, A. F.; Michel, M. A.; Maslen, S.; Komander, D. Mechanism and Regulation of the Lys6-Selective Deubiquitinase USP30. *Nat. Struct. Mol. Biol*. **2017**, 24, 920–930.

73. Xue, B. et al. TRIM21 Promotes Innate Immune Response to RNA Viral Infection through Lys27-Linked Polyubiquitination of MAVS. *J. Virol.* **2018**, 18.

74. Yuan, W-C. et al. K33-Linked Polyubiquitination of Coronin 7 by Cul3-KLHL20 Ubiquitin E3 Ligase Regulates Protein Trafficking. *Mol. Cell.* **2014**, 54, 586-600.

75. Jin, J.; Xie, X.; Xiao, Y.; Hu, H.; Zou, Q.; Cheng, X.; Sun, S-C. Epigenetic Regulation of the Expression of Il12 and Il23 and Autoimmune Inflammation by the Deubiquitinase Trabid. *Nat. Immunol.* **2016**, 17, 259-268.

76. Feng, X. et al. Ubiquitination of UVRAG by SMURF1 Promotes Autophagosome Maturation and Inhibit Hepatocellular Carcinoma Growth. *Autophagy* **2019**, 15, 1130–1149.

77. Al-Hakim, A. K.; Zagorska, A.; Chapman, L.; Deak, M.; Peggie, M.; Alessi, D. R. Control of AMPK-Related Kinases by USP9X and Atypical Lys(29)/Lys(33)-Linked Polyubiquitin Chains, *Biochem. J.* **2008**, 411, 249–260.

78. Ikeda, F. et al. SHARPIN Forms a Linear Ubiquitin Ligase Complex Regulating NF-κB Activity and Apoptosis. *Nature* **2011**, 471, 637–641.

79. Tokunaga, F. et al. Involvement of Linear Polyubiquitination of NEMO in NF-κB Activation. *Nat. Cell Biol.* **2009**, 11, 123–132.

80. Gerlach, B. et al. Linear Ubiquitination Prevents Inflammation and Regulates Immune Signalling. *Nature* **2011**, 471, 591–596.

81. Rivkin, E. et al. The Linear Ubiquitin-Specific Deubiquitinase Gumby Regulates Angiogenesis. *Nature* **2013**, 498, 318–324.

82. Bremm, A.; Moniz, S.; Mader, J.; Rocha, S.; Komander, D. Cezanne (OTUD7B) Regulates HIF-1α Homeostasis in a Proteasome-Independent Manner. *EMBO Rep.* **2014**, 15, 1268-1277.

83. Fritscj, J. et al. Cell fate Decisions Regulated by K63 Ubiquitination of Tumor Necrosis Factor Receptor 1, *Mol. Cell. Biol.* **2014**, 34, 3214–3228.

84. Deng, L. et al. Activation of the I κB kinase complex by TRAF6 requires a Dimeric Ubiquitin-Conjugating Enzyme Complex and a Unique Polyubiquitin Chain, *Cell.* **2000**, 103, 351–361

85. Laplantine, E. et al. NEMO Specifically Recognizes K63-Linked Poly-Ubiquitin Chains Through a New Bipartite Ubiquitin-Binding Domain, *EMBO J.* **2009**, 28, 2885–2895.

86. Duncan, S. et al. Lysine-63-Linked Ubiquitination is Required for Endolysosomal Degradation of Class I Molecules, *EMBO J.* **2006**, 25, 1635–1645.

87. Nathan, J. A.; Kim, H. T.; Ting, L.; Gygi, S. P.; Goldberg, A. L. Why Do Cellular Proteins Linked to K63-Polyubiquitin Chains not Associate with Proteasomes? *EMBO J.* **2013**, 32, 552.

88. Boname, J. M.; Thomas, M.; Stagg, H. R.; Xu, P.; Peng, J.; Lehner, P. J. Efficient Internalization of MHC I Requires Lysine-11 and Lysine-63 Mixed Linkage Polyubiquitin Chains, *Traffic*. **2010**, 11, 210–220.

89. Geetha, T.; Jiang, J.; Wooten, M. W. Lysine 63 Polyubiquitination of the Nerve Growth Factor Receptor TrkA Directs Internalization and Signaling, *Mol. Cell.* **2005**, 20, 301–312.

90. Erpapazoglou, Z.; Walker, O.; Haguenauer-Tsapis, R. Versatile Roles of K63-Linked Ubiquitin Chains in Trafficking, *Cells* **2014**, 3, 1027.

91. Ikeda, F.; Dikic, I. Atypical Ubiquitin Chains: New Molecular Signals. 'Protein Modifications: Beyond the Usual Suspects' Review Series," *EMBO Rep.* **2008**, 9, 536-542.

92. Elsasser, S. et al. Proteasome Subunit Rpn1 Binds Ubiquitin-Like Protein Domains. *Nat Cell Biol* **2002**, 4, 725-730.

93. Park, S. et al. Hexameric Assembly of the Proteasomal Atpases Is Templated Through Their C Termini. *Nature* **2009**, 459, 866–870.

94. Voges, D; Zwickl, P.; Baumeister, W. The 26S Proteasome: a Molecular Machine Designed for Controlled Proteolysis. *Annu. Rev. Biochem.* **1999**. 68, 1015-1068.

95. Bedford, L.; Paine, S.; Sheppard, P. W.; Mayer R. J.; Roelofs, J. Assembly, Structure and Function of the 26S Proteasome. *Trends Cell. Biol.* **2010**, 20, 391–401.

96. Suresh, H; Pascoe, N.; Andrews, B. The Structure and Function of Deubiquitinases: Lessons From Budding Yeast. *Open Biol.* **2020**, 10, 200279.

97. Komander, D.; Clague. M. J.; Urbé, S. Breaking the Chains: Structure and Function of the Deubiquitinases. *Nat. Rev. Mol. Cell. Biol.* **2009**, 10, 550–563.

98. Daniel E. J. The Ubiquitin-Proteasome System: Opportunities for Therapeutic Intervention in Solid Tumours. *Endocr-Relat. Cancer* **2015**, 22, T1-T17.

99. D'Arci, P.; Wang, X.; Linder, S. Deubiquitinase Inhibition as a Cancer Therapeutic Strategy. *Pharmacol. Ther.* **2014**, 147, 32-54.

100. Huang, T. T.; D'Andrea, A. D. Regulation of DNA Repair by Ubiquitylation. *Nat Rev Mol Cell Biol* **2006**, 7, 323-334.

101. Cui, J. et al. USP3 Inhibits Type I Interferon 1543 Signaling by Deubiquitinating RIG-I-Like Receptors. *Cell. Res.* **2014**, 24, 400–416.

102. Ramakrishna, S.; Suresh, B.; Baek, K-H. The Role of Deubiquitinating Enzymes in Apoptosis. *Cell. Mol. Life Sci.* **2011**, 68, 15-26.

103. Sowa, M. E.; Bennett, E. J.; Gygi, S. P.; Harper, J. W. Defining the Human Deubiquitinating Enzyme Interaction Landscape. *Cell* **2009**, 138, 389−403.

104. Ndubaku, C.; Tsui, V. Inhibiting the Deubiquitinating Enzymes (DUBs). J. Med. Chem. 2015, 58, 1581-1595.

105. Hussain, S.; Zhang, Y. Galardy, P. J. DUBs and Cancer. *Cell Cycle* **2009**, 8, 1688-1697.

106. Sacco, J. J.; Coulson, J. M.; Clague, M. J.; Urbé, S. Emerging Roles of Deubiquitinases in Cancer-Associated Pathways. *IUBMB Life* **2010**, 62, 140-157.

107. Edelmann, M. J.; Nicholson, B.; Kessler, B. M. Pharmacological Targets in the Ubiquitin System Offer New Ways of Treating Cancer, Neurodegenerative Disorders and Infectious Diseases. *Expert Rev. Mol. Med.* **2011**, 13, 1-17.

108. Schauer, N. J. et al. Advances in Discovering Deubiquitinating Enzyme (DUB) Inhibitors. *J Med Chem* **2020**, 63, 2731-2750.

109. Fraile, J. M.; Quesada, V.; Rodriguez, D.; Freije, J. M. P..; Lopez-Otin, C. Deubiquitinases in Cancer: New Functions and Therapeutic Options. *Oncogene* **2012**, 31, 2378-2388.

110. Yao, T. et al. Distinct Modes of Regulation of the Uch37 Deubiquitinating Enzyme in the Proteasome and in the Ino80 Chromatin-Remodeling Complex. *Mol. Cell* **2008**, 31, 909–917.

111. Ventii, K. H.; Wilkinson, K. D. Protein Partners of Deubiquitinating Enzymes. *Biochem. J.* **2008**, 414, 161–175.

112. Cohn, M. A.; Kee, Y.; Haas, W.; Gygi, S. P.; D'Andrea, A. D. UAF1 is a Subunit of Multiple Deubiquitinating Enzyme Complexes. *J. Biol. Chem.* **2008**, 8, 5343–5351.

113. Sarah, H. R. et al. Differential Redox Regulation Within the PTP Superfamily. *Cell Signal.* **2007**, 19, 1521-1530.

114. Kemp, M. Recent Advances in the Discovery of Deubiquitinating Enzyme Inhibitors. *Prog. Med. Chem.* **2016**, 55, 149-192.

115. Ratia, K. et al. A Noncovalent Class of Papain-like Protease/Deubiquitinase Inhibitors Blocks SARS Virus Replication. *Proc. Natl. Acad. Sci. U.S.A.* **2008**, 105, 16119−16124.

116. Ratia, K. et al. Structural Basis for the Ubiquitin-Linkage Specificity and deISGylating Activity of SARS-CoV Papain-like Protease. *PLoS Pathog.* **2014**, 10, e1004113.

117. Bordeaux, D. A., et al. Ubiquitin vinyl methyl ester binding orients the misaligned active site of the ubiquitin hydrolase UCHL1 into productive conformation. *Proc Natl Acad Sci U S A* **2010**, 107, 9117-9122.

118. Tan, X et. al. Semi-synthesis of Ubiquitin-propargylamide for identifying deubiquitinase targeting inhibitors. *Chin. Chem. Lett*. **2010**, 30, 743-746.

119. Sanman, L. E.; Bogyo, M. Activity-based profiling of proteases. *Annu Rev Biochem* **2014**, 83, 249-273.

120. Avvakumov, G. et al. Amino-Terminal Dimerization, NRDP1-Rhodanese Interaction, and Inhibited Catalytic Domain Conformation of the Ubiquitin-Specific Protease 8 (USP8). *J. Biol. Chem.* **2006**, 281, 38061−38070.

121. V.; Walker et al. Structure and Mechanisms of the Proteasome-Associated Deubiquitinating Enzyme USP14. *EMBO J.* **2005**, 24, 3747−3756.

122. Hu, M.et al. Structural Basis of Competitive Recognition of P53 and MDM2 by HAUSP/USP7: Implications for the Regulation of the P53−MDM2 Pathway. *PLoS Biol.* **2006**, 4, e27.

123. Fang, Y.; Fu, D.; Shen, X-Z. The Potential Role of Ubiquitin C-Terminal Hydrolases in Oncogenesis. *Biochim Biophys Acta* **2010**, 1806, 1-6.

124. Johnston, S. C.; Riddle, S. M.; Cohen, R. E.; Hill, C. P. Structural Basis for the Specificity of Ubiquitin C-Terminal Hydrolases. *EMBO J.* **1999**, 18, 3877−3887.

125. Larsen, C. N. C.; Krantz, B. A. B.; Wilkinson, K. D. K. Substrate Specificity of Deubiquitinating Enzymes: Ubiquitin C-Terminal Hydrolases. *Biochemistry* **1998**, 37, 3358−3368.

126. Popp, M. W.; Artavanis-Tsakonas, K.; Ploegh, H. L. Substrate Filtering by the Active Site Crossover Loop in UCHL3 Revealed by Sortagging and Gain-of-Function Mutations. *J. Biol. Chem*. **2009**, 284, 3593−3602.

127. Maiti, T. K. et al. Crystal Structure of the Catalytic Domain of UCHL5, a Proteasome-Associated Human Deubiquitinating Enzyme, Reveals an Unproductive Form of the Enzyme. *FEBS J.* **2011**, 278, 4917−4926.

128. Gupta, I. et al. Delineating Crosstalk Mechanisms of the Ubiquitin Proteasome System That Regulate Apoptosis. *Front Cell Dev Biol.* **2018**, 6:11.

129. Ouyang, L. et al. Programmed Cell Death Pathways in Cancer: a Review of Apoptosis, Autophagy. *Cell Prolif.* **2012**, 45, 487-498.

130. Ziegler, U.; Groscurth, P. Morphological Features of Cell Death. *News Physiol Sci* **2004**, 19, 124-128.

131. Cohen, J.J. Apoptosis. *Immunol Today* **1993**, 14, 126-130.

132. Riedl, S. J.; Shi, Y. Molecular Mechanism of Caspase Regulation During Apoptosis. *Nat. Rev. Mol.* **2004**, 5, 897-907.

133. Mcllwain, D.R.; Berger, T.; Mak, T.K. Caspase Functions in Cell Death and Disease. *Cold Spring Harb Perspect Biol.* **2013**, 7, a008656.

134. Lockshin, R. A.; Zakeri, Z. Cell Death in Health and Disease. *J Cell Mol Med.* **2007**, 11, 1214-1224.

135. Zhu, H. et al. Proteasome Inhibitors-Mediated TRAIL Resensitization and BIK Accumulation. *Cancer Biol Ther* **2005**, 4, 781–786.

136. Qin, J-Z. et al. Proteasome Inhibitors Trigger NOXA-Mediated Apoptosis in Melanoma and Myeloma Cells. *Cancer Res* **2005**, 65, 6282-6293.

137. Li, C. et al. Bortezomib Induces Apoptosis via BIM and BIK Up-Regulation and Synergizes with Cisplatin in the Killing of Head and Neck Squamous Cell Carcinoma Cells. *Mol Cancer Ther* **2008**, 7, 1647-1655

138. Ren, H. et al. The E3 Ubiquitin Ligases β-TrCP and FBXW7 Cooperatively Mediates GSK3-Dependent MCL-1 Degradation Induced by the Akt Inhibitor API-1, Resulting in Apoptosis. *Mol Cancer* **2013**, 12, 146.

139. Fridman, J. S.; Lowe, S. W. Control of Apoptosis by p53. *Oncogene* **2003**, 22, 9030-9040.

140. Brooks, C. L.; Gu, W. p53 Regulation by Ubiquitin. *FEBS Lett* **2011**, 585, 2803-2809.

141. Kumariya, R.; Barui, A. K.; Singh, S. p53-Cells's Inbuilt Mechanism to Inhibit Cancer Through Apoptosis. *J. Cancer Ther*. **2012**, 4, 368-370.

142. Candeias, M. M. et al. P53 mRNA Controls p53 Activity by Managing Mdm2 Functions. *Nat Cell Biol* **2008**, 10, 1098-1105.

143. Tollini, L. A.; Jin, A.; Park, J.; Zhang, Y. Regulation of P53 by MDM2 E3 Ligase Function is Dispensable in Embryogenesis and Development, but Essential in Response to DNA Damage. *Cancer Cell* **2014**, 26, 235-247.

144. Carneiro, B. A.; El-Deiry, W. S. Targeting Apoptosis in Cancer Therapy. *Nat Rev Clin Oncol* **2020**, 17, 395-417.

145. Dalla Via, L.; Nardon, C.; Fregona, D. Targeting the Ubiquitin-Proteasome Pathway with Inorganic Compounds to Fight Cancer: a Challenge for the Future. *Future Med Chem.* **2012**, 4, 525-543.

146. Wong, R. S. Y. Apoptosis in Cancer: From Pathogenesis to Treatment. *J Exp Clin Cancer Res.* **2011**, 30: 87.

147. Kerr, J. F.; Winterford, C. M.; Harmon, B. V. Apoptosis. Its Significance in Cancer and Cancer Therapy. *Cancer* **1994**, 73, 2013-2026.

148. Levin, A. et al. PSMD5 Inactivation Promotes 26S Proteasome Assembly During Colorectal Tumor Progression. *Cancer Res*, **2018**, 78, 3458-3468.

149. Zhang, W.; Sidhu, S.S. Development of Inhibitors in the Ubiquitination Cascade. *FEBS Lett* **2014**, 588, 356-367.

150. Zhang, X.; Linder, S.; Bazzaro, M. Drug Development Targeting the Ubiquitin-Proteasome System (UPS) for the Treatment of Human Cancers. *Cancers (Basel)* **2020**, 12:902.

151. Yang, Y., et al. Inhibitors of Ubiquitin-Activating Enzyme (E1), a New Class of Potential Cancer Therapeutics. *Cancer Res* **2007**, 67, 9472-9481.

152. Matsuo, S.; Sharma, A.;Wang, P.; Yang,W.L. PYR-41, a Ubiquitin-Activating Enzyme E1 Inhibitor, Attenuates Lung Injury in Sepsis. *Shock* **2018**, 49, 442–450.

153. Sarantopoulos, J. et al. Phase I Study of the Investigational NEDD8-Activating Enzyme Inhibitor Pevonedistat (TAK-924/MLN4924) in Patients with Advanced Solid Tumours. *Clin. Cancer Res.* **2016**, 22, 847–857.

154. Tong, S.; Si, Y.; Yu, H.; Zhang, L.; Xie, P.; Jiang, W. MLN4924 (Pevonedistat), a Protein Neddylation Inhibitor, Suppresses Proliferation and Migration of Human Clear Cell Renal Cell Carcinoma. *Sci. Rep.* **2017**, 7, 5599.

155. Ceccarelli, D. F. et al. An Allosteric Inhibitor of the Human Cdc34 Ubiquitin-Conjugating Enzyme. *Cell* **2011**, 145, 1075-1087.

156. Haupt, Y.; Maya, R.; Kazaz, A.; Oren, M. MDM2 Promotes the Rapid Degradation of p53. *Nature* **1997**, 387, 296–299.

157. Midgley, C.A.; Lane, D.P. p53 Protein Stability in Tumor Cells is not Determined by Mutation but is Dependent on MDM2 Binding. *Oncogene* **1997**, 15, 1179–1189.

158. Vassilev, L.T. et al. In Vivo Activation of the p53 Pathway by Small-Molecule Antagonists of MDM2. *Science* **2004**, 303, 844–848.

159. Issaeva, N. et al. Small Molecule RITA Binds to p53, Blocks p53-HDM-2 Interaction and Activates p53 Function in Tumours. *Nat. Med.* **2004**, 10, 1321-1328.

160. Adams, J. The Development of Proteasome Inhibitors as Anticancer Drugs. *Cancer Cell* **2004**, 5, 417-421.

161. Molineaux, S.M. Molecular Pathways: Targeting Proteasomal Protein Degradation in Cancer. Clin. *Cancer Res.* **2012**, 18, 15-20.

162. Kane, R.C. et al. Velcade: U.S. FDA Approval for the Treatment of Multiple Myeloma Progressing on Prior Therapy. *Oncologist.* **2003**, 8, 508-513.

163. Orlowski, R.Z et al. Phase I Trial of the Proteasome Inhibitor PS-341 in Patients with Refractory Hematologic Malignancies. *J. Clin. Oncol.* **2002**, 20, 4420-4427.

164. Nowis, D. et al. Cardiotoxicity of the Anticancer Therapeutic Agent Bortezomib. *Am. J. Pathol* **2010**, 176, 2658-2668.

165. Shin, Y.K.et al. Pathological Adaptive Responses of Schwann Cells to Endoplasmic Reticulum Stress in Bortezomib-Induced Peripheral Neuropathy. *Glia* **2010**, 58, 1961-1976.

166. Schrader, J. et al. The Inhibition Mechanism of Human 20S Proteasomes Enables Next-Generation Inhibitor Design. *Science* **2016**, 353, 594-598.

167. Arastu-Kapur, S. et al. Nonproteasomal Targets of the Proteasome Inhibitors Bortezomib and Carfilzomib: a Link to Clinical Adverse Events. *Clin. Cancer Res.* **2011**, 17, 2734-2743.

168. Vesole, D.H. et al. Phase I Study of Carfilzomib, Lenalidomide, Vorinostat, and Dexamethasone in Patients with Relapsed and/or Refractory Multiple Myeloma. *Br. J. Haematol*. **2015**, 171, 52-59.

169. Harrigan J.A., Jacq X., Martin N.M., Jackson S.P. Deubiquitylating Enzymes and Drug Discovery: Emerging Opportunities. *Nat. Rev. Drug Discov.* 2018, 17, 57–78.

170. Shin, D. et al. Papain-Like Protease Regulates SARS-Cov-2 Viral Spread and Innate Immunity. *Nature* **2020**, 587, 657-662.

171. Sivakumar, D.; Stein, M. Binding of SARS-CoV Covalent Non-Covalent Inhibitors to the SARS-CoV-2 Papain-Like Protease and Ovarian Tumor Domain Deubiquitinases. *Biomolecules* **2021**, 11, 802.

172. Xiang, R. et al. Recent Advances in Developing Small-Molecule Inhibitors Against SARS-CoV-2. *Acta Pharm Sin B* **2021** (Online ahead of print).

173. Liu, W. et al. Drug Repurposing for the SARS-CoV-2 Papain-Like Protease. *ChemMedChem* **2021** (Online ahead of print).

174. Clemente, V.; D'arcy, P.; Bazzaro, M. Deubiquitinating Enzymes in Coronaviruses and Possible Therapeutic Opportunities for COVID-19. *Int J Mol Sci* **2020**, 21, 3492.

Deubiquitinases Inhibitors as Antineoplastic Agents

Assays to Identify DUBs Inhibitors

♦ *FP assay has been extensively used in drug discovery to screen DUBs inhibitors.*

Activity-based Fluorescence Polarization (FP) assay was one of the first assay to measure the enzymatic activity of a DUB in the presence of a covalent binder, and has been extensively used for the identification of novel DUBs inhibitors.[1] FP assays are based on the change in the polarization of a sample's emitted light that can be observed after the cleavage of fluorophores from fluorescent-tagged substrates (e.g., peptides). The most used substrate is Ub-AMC (Figure 16), which bears the 7-amino-4-methylcoumarin (AMC) group coupled to the C-terminus residue of Ub.[2] If the tested candidate does not affect the isopeptidase activity, the target DUB releases the Ub from AMC and leads to depolarization of the sample's emitted light. In the opposite case, the inactivation of the DUB does not result in any change of the polarization (Figure 17).[3]
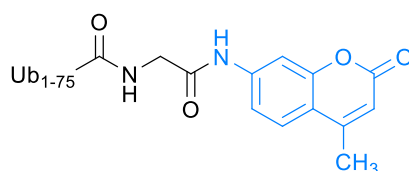
Figure 16

The structure of Ub-AMC, with highlighted the AMC fluorophore.

♦ *Ub-PLA₂, MALDI-TOF, and ABPs assays are powerful tools to study the mechanism of DUBS inhibition either in vitro or in vivo.*

Although FP assays are cheap and broadly applicable for the screening of potential DUBs inhibitors, the steric hindrance of AMC group poorly resembles the narrow C-terminus tail of Ub. A significant improvement has been implemented with Ub-PLA$_2$ assays, which use Ub conjugated to phospholipase A$_2$ (Ub-PLA$_2$) as

substrate and need lower concentrations of the tested DUBs. PLA$_2$ requires a free terminus NH$_2$ group to be catalytically active; therefore, the cleavage of Ub- PLA$_2$ amidic bond leads to the formation of a fluorescent product whose signal intensity is linearly related to the concentration of the uninhibited DUB (Figure 18).[4-6] More recently, MALDI-TOF mass spectrometry has been optimized for *in vitro* assays, and its application brings other advantages such as the use of unmodified substrates.[7]
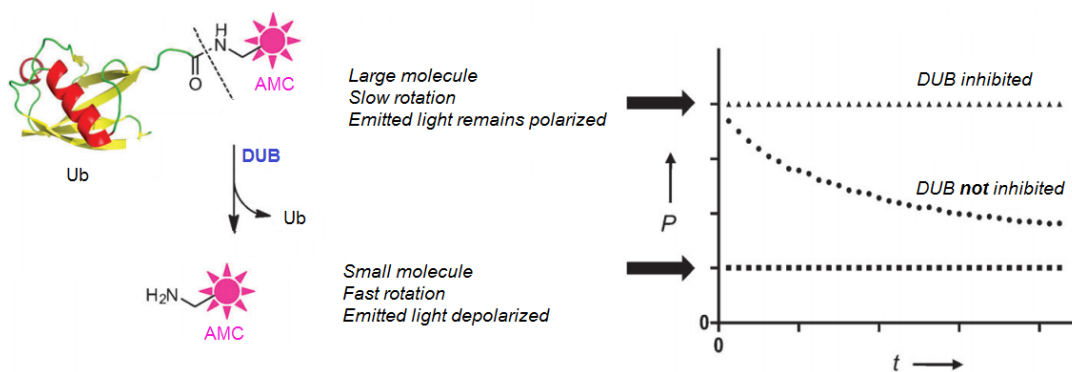
Figure 17

FP assay for the identification of DUBs inhibitors: when Ub-AMC is excited by plane-polarized light, the variation in fluorescence polarization of emitted light (y-axis) over time (x-axis) can be monitored to measure the potency of the inhibitor.
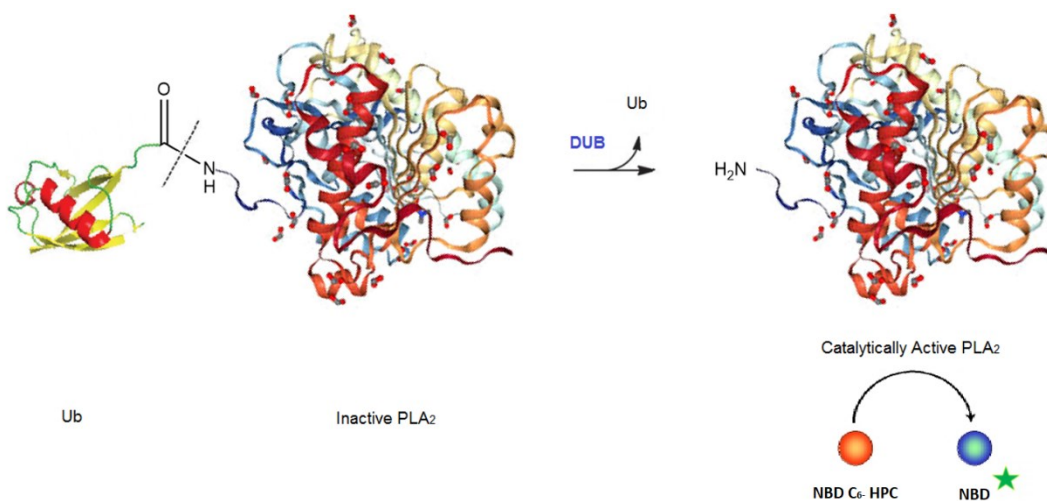
Figure 18

Ub-PLA$_2$ assay: DUB's activity releases the catalytically active PLA$_2$. Then, PLA$_2$ converts its substrate to a fluorescent product (7-nitrobenz-2-oxa-1,3-diazole, NBD), which develops a signal proportional to the concentration of the DUB in solution.

It should be noted that all the previously mentioned assays require unnatural experimental conditions, such as the addition of reducing agents to prevent cysteine oxidation, which could impact on the measured IC_{50} values.[8] Activity-Based Probes (ABPs) has overcome this limitation and led to the possibility of screening the efficacy of novel inhibitors either *in vitro* or *in vivo*. These assays are also largely used in medicinal chemistry to investigate the mechanism of interaction between a target enzyme and small-molecule probes.[9-10] The structure of an ABP consists of three main elements: the reactive group (warhead), a linker, and a tag [11] (Figure 19). The cytotoxic effects of an ABP can be quantitatively evaluated by MTT tetrazolium dye-based assay, a colorimetric assay that measures the cell viability *in vitro* at various concentration of the inhibitor.[12-14]

Tag	Spacer	Warhead
Biotin	Alkyl	Electrophile
Fluorophore	Peptide	Photocrosslinker
Radioisotope	Cleavable	Latent electrophile
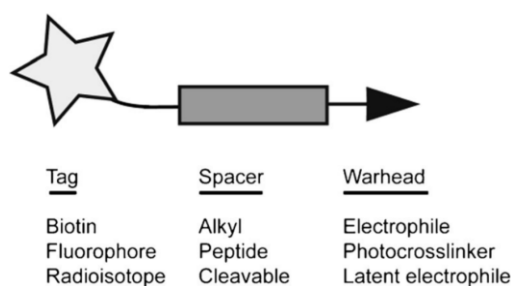
Figure 19

General structure of an ABP.

To conclude, the process of discovering new DUBs inhibitors starts from the rational drug design of small molecules made possible by the growing number of 3D structures available for several DUBs members. High-throughput screening of the active compounds then enables the selection of the most promising candidates. Finally, the structures of the hit compounds that demonstrated inhibitory activity against one or multiple DUBS can be further modified. These modifications are meant to improve the potency, selectivity, and bioavailability of selected inhibitors *in vivo* (Hit to Lead and Lead Optimization).

DUBs Inhibitors with Antineoplastic Activity

♦ *Many biologically active inhibitors of DUBs have been synthetized over the last decades.*

Following the success of **BTZ** in clinical trials, about 50 different USP and UCH inhibitors of synthetic and natural origin have been reported in the literature over the last eighteen years. As previously mentioned, some DUBs might be more susceptible to covalent warheads than others, and additional non-catalytic domains can be present as well. For this reason, the structural optimization of DUBs inhibitors might be a difficult challenge.[15-16] Similarly to **BTZ**, the administration of DUBs inhibitors leads to the weakening of proteasome activity, accumulation of ubiquitinated proteins, deprivation of the free Ub pool, and proteotoxicity.[15, 17-18]
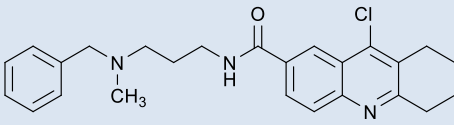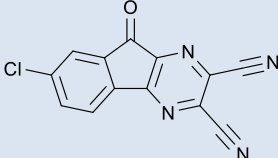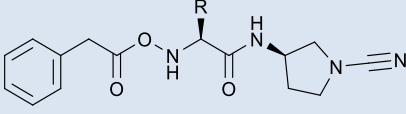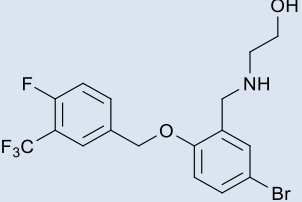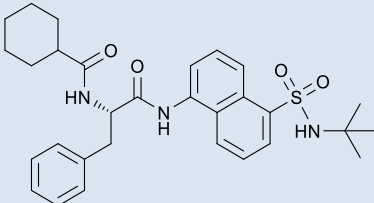
Liu and his research group discovered the first synthetic DUB inhibitor in 2003, an O-acyl isatin oxime (**LDN-57444**) capable to inactivate UCHL1.[19] This enzyme has been the subject of several studies due to its overexpression in breast, colorectal a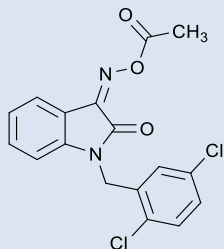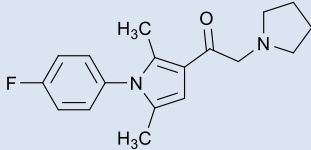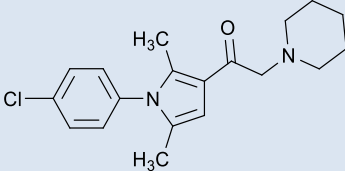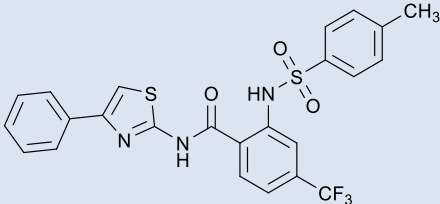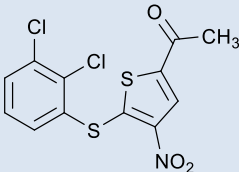nd pancreatic carcinomas.[20] Few years later, Lee and his co-workers identified the N-aryl pyrrole derivative **IU1** as a covalent inhibitor of USP14.[21] Further optimization of this compound led to its more potent version **IU1-47**, which induced tau elimination in cultured neurons.[22] However, additional studies need to be developed to test the efficacy of these inhibitors *in vivo*. USP2 is considered a fascinating drug target since its deactivation causes cell cycle arrest in several proliferative diseases.[23] In this scenario, the sulfonamide **ML364** was found to selectively inhibit USP2 and to be active against colorectal cancer and mantle cell lymphoma, with favourable ADME properties.[24] USP7 has been extensively studied due to its implications in the regulation of MDM2 levels: it was indeed reported that inactivation of USP7 causes the increase of P53 expression.[25] **P5091**,[26] **HBX-19818**,[27] and **HBX-41108** [28] are three of the most studied first-generation USP7 inhibitors: they trigger apoptosis in multiple cancer cells, overcoming **BTZ**-resistance. Despite **HBX-41108** showed the most potent inhibitory activity in the series, reasonably related to the highly electrophilic 2,3-dicyano-pyrazine ring, compound **P5091** achieved higher selectivity.[7] For this reason, **P5091** was used *in vivo* to inhibit tumours growth in mice, with no relevant toxicity observed after treatment.[29] More recently, Bashore and his team discovered that a

series of Cbz-protected cyanopyrrolidines inactivate the USP7 through a β-elimination of the catalytic cysteine, with an IC$_{50}$ range from 0.9 µM to 5.0 µM.[30] Similarly, the inhibition of USP28 was proposed as a strategy to arrest cancer development in multiple tumours, including breast and liver carcinomas.[31] USP30 is also related to tumorigenesis, and its suppression reduces the accumulation of reactive oxygen species in the body. A non-exhaustive list of DUBs inhibitors is summarized in Table 3.

Table 3

Few published DUBs inhibitors.

Name	Target	IC$_{50}$ [µM]	Formula	Year
LDN-57444 [19-20]	UCHL1	0.88		2003
IU1 [21]	USP14	4.7		2010
IU1-47 [22]		0.6		2017
ML364 [24]	USP2	1.1 ÷ 1.7		2016
P5091 [26]	USP7	4.2		2012

Name	Target	IC$_{50}$ [μM]	Formula	Year
HBX-19818 [27]		28.1		2012
HBX-41108 [28]		0.4 ÷ 0.8		2009
n.d. [30]		0.9 ÷ 5.0		2020
AZ1 [32]	USP25 and USP28	0.6 ÷ 0.7		2017
MF-094 [33]	USP30	0.12		2018

Cross-Conjugated Dienones

♦ *Several DUBs inhibitors contain an α,β-unsaturated carbonyl group that reacts as Michael acceptor with thiolic groups.*

First publications regarding natural DUBs inhibitors appeared in the literature in 2001 and reported that some prostaglandins, particularly **Δ12-PGJ₂**, induced the accumulation of polyubiquitinated proteins in the range of 100 μM.[34] UCHL1 and UCHL3 were identified as principal targets of **Δ12-**PGJ$_2$, with no direct inhibition of the 26S proteasome.[35] A similar activity was found for gambogic acid, a xanthonoid extracted from the resin of *Garcinia hanburyi* that has been widely used in traditional

Chinese medicine.[36] Both compounds contain an α,β-unsaturated ketone that reacts as Michael acceptor with the catalytic thiolic group of the DUBs and leads to the formation of a stable thioether adduct, which reasonably inactivates the enzyme (Scheme 3).[15]
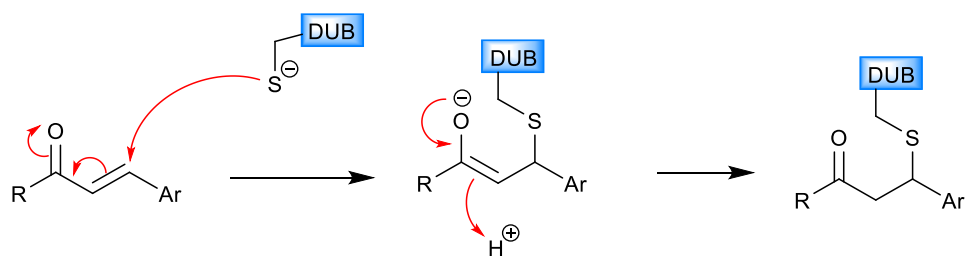
Scheme 3

Mechanism of inhibition of a cysteine-dependent DUBs by an α,β-unsaturated ketone, with the formation of the Michael addition product.

Curcumin, which also bears two α,β-unsaturated carbonyl groups, leads to UPS dysregulation and accumulation of ubiquitinated proteins at the concentration of 40 μM. The structure of curcumin and of the other mentioned compounds is illustrated in Table 4. Curcumin is present in the rhizome of various species of turmeric, mostly in *Curcuma longa*, and has been largely used for centuries in the Indian and Middle Eastern tradition for treating various diseases (Figure 20). The main biological targets of curcumin include multiple transcription factors, COX-2, kinases, and other enzymes. It was thus speculated that the wide spectrum of biological activities of this compound comes from its ability to inhibit the cysteine-dependent DUBs via Michael alkylation,[37-38] and this was subsequently corroborated by Ub-AMC assay.[39] However, curcumin has unfavourable drug-like properties due to its poor solubility, fast metabolization, and weak pharmacokinetics. For this reason, it is more suitable as a lead compound for the development of new drug candidates rather than being used in clinical trials.[40]

◆ *Synthetic cross-conjugated dienones related to curcumin are efficient DUBs inhibitors, with broad antitumoral activity and marked selectivity toward cancer cells.*

The identification of natural DUBs inhibitors opened the way to the design of synthetic analogues with similar structures. An example can be found in the curcumin analogue **AC17**, which displays anticancer activity against lung, colon, and breast cancers (IC_{50} = 4.23 μM) with improved oral bioavailability and metabolic stability.[41] Few synthetic inhibitors are currently under clinical evaluation: particularly noteworthy in this category are compounds **bAP15** and **VLX1570**. The former arrests the UPS pathway and selectively inhibits USP14 and UCHL5, leading to accumulation of misfolded proteins and exhibiting antineoplastic activity *in vivo*. However, the low solubility and poor stability in aqueous solution limited further optimization of **bAP15** toward clinic use.[42-43] A ring-expanded analogue (**VLX1570**) proved to be efficient in the treatment of colon carcinoma, displaying higher potency and selectivity compared to the parent compound. For these reasons, **VLX1570** became the first synthetic DUBs inhibitor to enter clinical trials.[43-44]
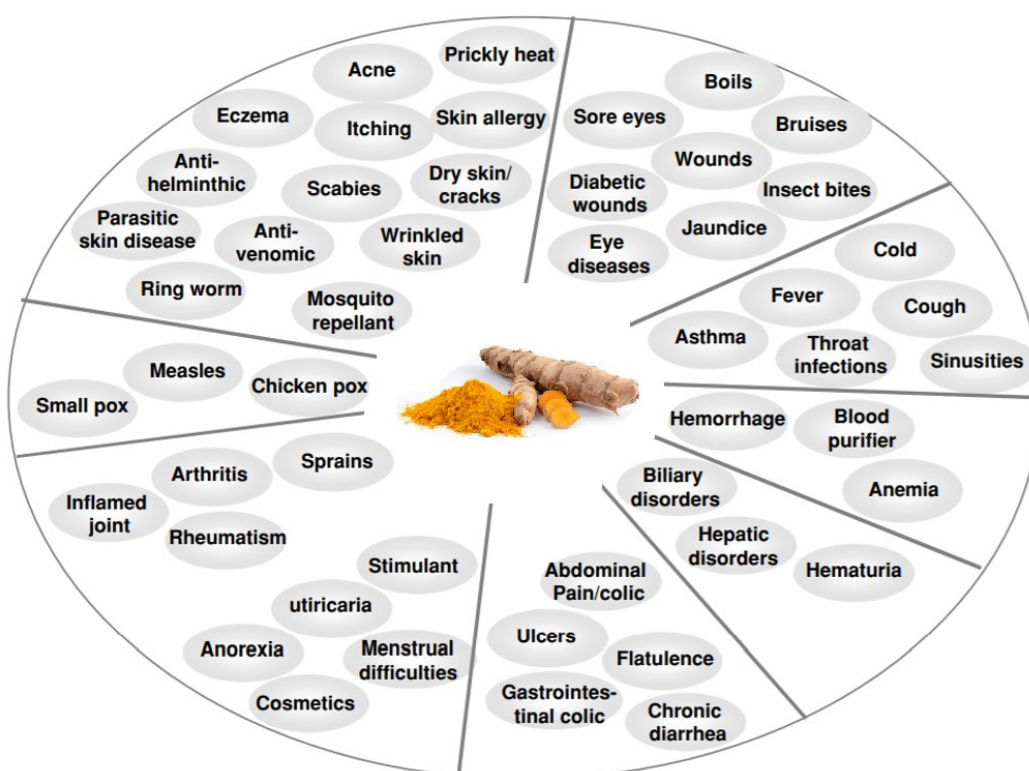
Figure 20

Traditional uses of curcumin.

Brancolini et al. (2006) reported that dienones **G5** and **F6**, both containing the unsaturated cross-conjugated 1,5-diaryl-3-oxo-1,4-pentadienilic pharmacophore (Figure 21), had deubiquitinating activity and induced cell death response in tumor cells resistant to the common chemotherapeutic agents.[45-46] Other compounds that lack the central aliphatic ring proved to be less active than the corresponding cycloketones and piperidines derivatives, probably as a consequence of the higher conformational flexibility.[47-48]
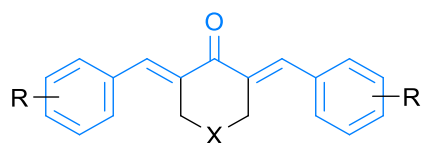
Figure 21

General structure of cyclic molecules bearing the 1,5-diaryl-3-oxo-1,4-pentadienilic core (highlighted in cyan). **X** can be a heteroatom or an electron-withdrawing group.

In summary, diaryldienones react as Michael acceptors and show marked selectivity for cysteine-dependent isopeptidases and preferential cytotoxicity toward malignant cells (Figure 22). It was also reported that this class of compounds exert other therapeutic benefits, including anti-inflammatory and antiparasitic responses.[15]
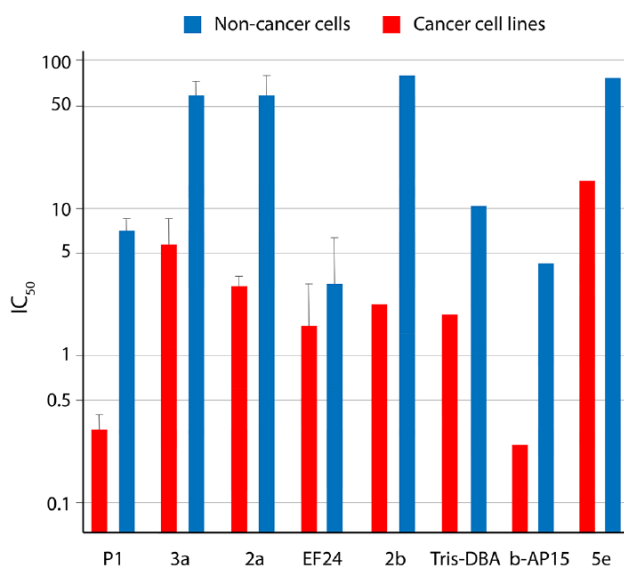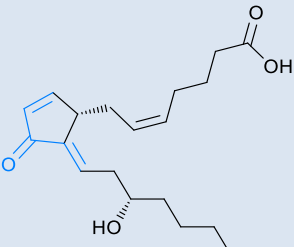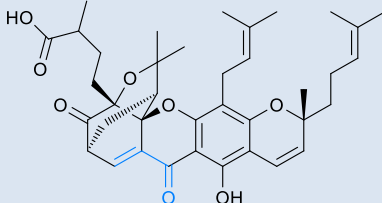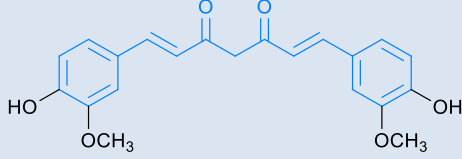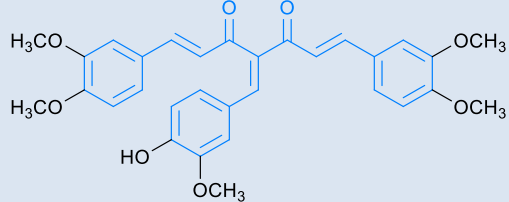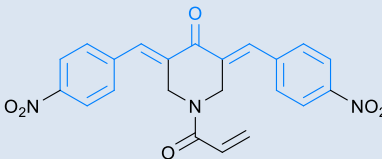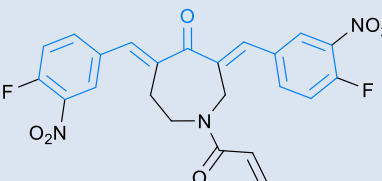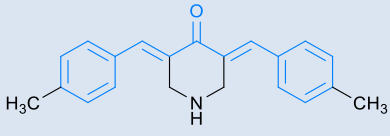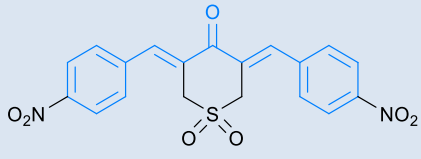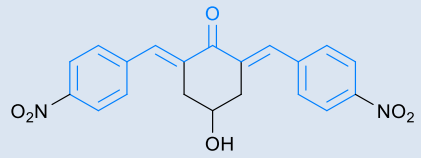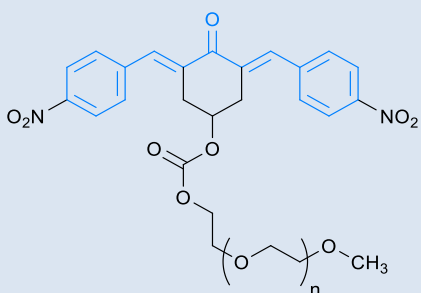
Figure 22

Selectivity of different diaryldienones toward tumor cells.

Table 4

Few DUBs inhibitors containing an α,β-unsaturated carbonyl moiety (in cyan).

Name	Targets	Chemical Formula	Year
Δ12-PGJ₂ [34-35]	UCHL1 and UCHL3		2001
Gambogic Acid [36]	n.d.		2013
Curcumin [37-40]	Multiple		n.d.
AC17 [41]	UCHL5 and USP14		2013
bAP15 [42-44]	UCHL5 and USP14		2011
VLX1570 [42-44]			2015

Name	Targets	Chemical Formula	Year
F6 [45-46]	Multiple		2006
G5 [45-46]			2006
2c [49-50]	UCHL1, UCHL5, USP2, and USP18		
2cPE [49-50]			2015

2c and Derivatives

♦ **2c** *is a partially selective and versatile DUB inhibitor with antineoplastic activity.*

As a conclusion of a study aimed to evaluate the cytotoxicity of two series of **G5**-analogues dienones against glioblastoma cells, it has emerged that the electrophilicity of both β-carbon atoms strongly impacts on the overall antitumoral activity of each dienone (Table 5). It was observed that the simultaneous presence of electronegative atoms or electron-withdrawing groups attached to both aromatic and aliphatic rings enhanced the inhibitory effect. In particular, our research group evidenced a clear linear correlation between the cytotoxicity and the Hammett σ constants for the substituted arylidene groups of dienones of the first series

(Figure 23).[49] These data were coherent with the proposed DUBs alkylation mechanism reported in Scheme 3, since the introduction of highly electron withdrawing groups (such as NO_2) on both aromatic rings results in more electrophilic, and thus reactive, dienone β-carbon atoms.

Compound **2c** represented the best compromise between a desirable antitumoral activity, reduced *in vivo* toxicity, and presence of a functionalizable secondary hydroxyl group: for this reason, it was selected for further developments. Additional studies identified other proteases besides DUBs that form stable covalent adducts with **2c** and can, therefore, contribute to magnify its biological activity. For this reason, **2c** was later identified as partially selective isopeptidase inhibitor.[50] The PEG-conjugated of **2c** (**2cPE**) was tested *in vivo* and induced significant reduction in tumor growth with an appreciable tolerability profile.
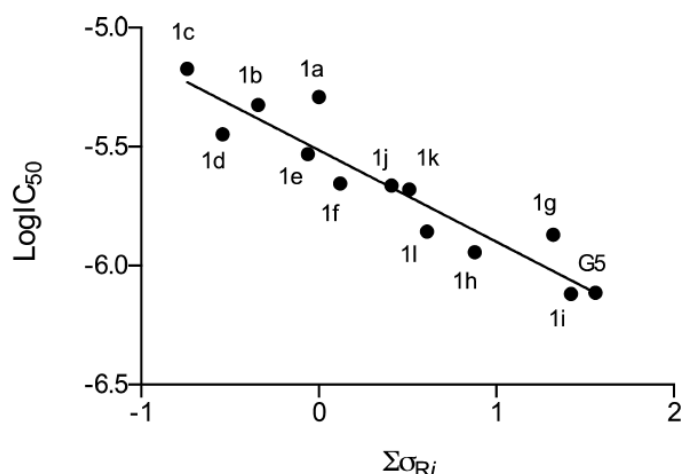
Figure 23
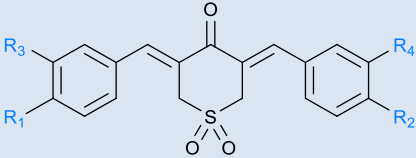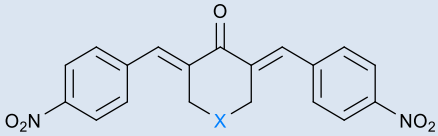
Plot of the observed log (IC_{50}) against the sum of the Hammett σ constants for the substituents on both aromatic rings of the dienones of the first series.

In conclusion, the prodrug **2cPE** and, more in general, compounds containing the 1,5-diaryl-3-oxo-1,4-pentadienilic core, proved to be efficient tumor suppressors with strong potential to be used in clinical practice in the near future

Table 5

Serie 1: cytotoxicity of Bis(arylidene)tetrahydrothiapyran-4-one 1,1-Dioxides against U87MG glioblastoma cells.
Serie 2: cytotoxicity of Nitrobenzylidene Dienones against U87MG glioblastoma cells.

Serie 1						Serie 2	
Name	R_1	R_2	R_3	R_4	IC_{50} [μM]	Name	X	IC_{50} [μM]
G5	NO_2	NO_2	H	H	0.77	G5	SO_2	0.77
1a	H	H	H	H	5.11	2a	CH_2	2.0
1b	CH_3	CH_3	H	H	4.74	2b	$CH(OCH_2–CH_2O)$	0.71
1c	OH	OH	H	H	6.73	2c	CH-OH	1.96
1d	$O–CH_3$	$O–CH_3$	H	H	3.57	2d	$CH–COOCH_2CH_3$	0.25
1e	O–Ph	O–Ph	H	H	2.94	2e	NH	2.90
1f	F	F	H	H	2.21	2f	O	14.3
1g	CN	CN	H	H	1.35	2g	S	2.01
1h	$O–CH_3$	$O–CH_3$	NO_2	NO_2	1.14	2h	SO	0.81
1i	H	H	NO_2	NO_2	0.76			
1j	NO_2	OH	H	H	2.17			
1k	NO_2	$O–CH_3$	H	H	2.09			
1l	NO_2	CH_3	H	H	1.39			

References

1. Lea, W. A.; Simeonov, A. Fluorescence Polarization Assays in Small Molecule Screening. *Expert Opin Drug Discov* **2011**, 6, 17-32.

2. Dang, L. C.; Melandri, F. D.; Stein, R. L. Kinetic and Mechanistic Studies on the Hydrolysis of Ubiquitin C-Terminal 7-Amido-4-Methylcoumarin by Deubiquitinating Enzymes. *Biochemistry* **1998**, 37, 1868-1879.

3. Geurink, P. P. A General Chemical Ligation Approach Towards Isopeptide-Linked Ubiquitin and Ubiquitin-Like Assay Reagents. *Chembiochem* **2012**, 13, 293-297.

4. Goldenberg, S. J. et al. Strategies for the Identification of Novel Inhibitors of Deubiquitinating Enzymes. *Biochem Soc Trans* **2008**, 36, 828-832.

5. Nicholson, B. et al. Characterization of Ubiquitin and Ubiquitin-Like-Protein Isopeptidase Activities. *Protein Sci* **2008**, 17, 1035-1043.

6. Cho, J.; Park, J.; Kim. E. E.; Song, E. J. Assay Systems for Profiling Deubiquitinating Activity. *Int J Mol Sci* **2020**, 21, 5638.

7. Ritorto, M. S. et al. Screening of DUB Activity and Specificity by MALDI-TOF Mass Spectrometry. *Nat Commun* **2014**, 5:4763.

8. Wrigley, J. D. et al. Enzymatic Characterisation of USP7 Deubiquitinating Activity and Inhibition. *Cell Biochem Biophys* **2011**, 60, 99-111.

9. Ovaa, H.; Kessler, B. M.; Rolen, U.; Galardy, P. J.; Ploegh, H. L.; Masucci, M. G. Activity-Based Ubiquitin-Specific Protease (USP) Profiling of Virus-Infected and Malignant Human Cells. *Proc. Natl. Acad. Sci. U. S. A.* **2004**, 101, 2253−2258.

10. Rolen, U.; Kobzeva, V.; Gasparjan, N.; Ovaa, H.; Winberg, G.; Kisseljov, F.; Masucci, M. G. Activity Profiling of Deubiquitinating Enzymes in Cervical Carcinoma Biopsies and Cell Lines. *Mol. Carcinog.* **2006**, 45, 260−269.

11. Serim, S.; Haedke, U.; Verhelst, S. H. L. Activity-Based Probes for the Study of Proteases: Recent Advances and Developments. *ChemMedChem* **2012**, 7, 1146-1159.

12. Mosmann, T. Rapid Colorimetric Assay for Cellular growth and Survival: Application to Proliferation and Cytotoxicity Assays. *J Immunol Methods* **1983**, 65, 55-63.

13. Twentyman, P. R.; Luscombe, M. A Study of Some Variables in a Tetrazolium Dye (MTT) Based Assay for Cell Growth and Chemosensitivity. *Br J Cancer* **1987**, 56, 279-285.

14. Cole, S. P. Rapid Chemosensitivity Testing of Human Lung Tumor Cells Using the MTT Assay. *Cancer Chemother Pharmacol* **1986**, 17, 259-263.

15. Schauer, N. J. et al. Advances in Discovering Deubiquitinating Enzyme (DUB) Inhibitors. *J. Med. Chem.* **2020**, 63, 2731−2750.

16. Kemp, M. Recent Advances in the Discovery of Deubiquitinating Enzyme Inhibitors. *Prog Med Chem* **2016**, 55, 149-92.

17. Ndubaku, C.; Tsui, V. Inihibiting the Deubiquitinating Enzymes (DUBs). *J Med Chem* **2015**, 58, 1581–1595.

18. Antao, A. M. et al. Advances in Deubiquitinating Enzyme Inhibition and Applications in Cancer Therapeutics. *Cancers (Basel)* **2020**, 12, 1579.

19. Liu, Y. et al. Discovery of Inhibitors That Elucidate the Role of UCH-L1 Activity in the H1299 Lung Cancer Cell Line. *Chem Biol* **2003**, 10, 837-846.

20. Hurst-Kennedy, J.; Chin, L-S; Li, L. Ubiquitin C-Terminal Hydrolase L1 in Tumorigenesis. *Biochem Res Int* **2012**, 2012:123706.

21. Lee, B. H. et al. Enhancement of Proteasome Activity by a Small-Molecule Inhibitor of USP14. *Nature* **2010**, 467, 179−184.

22. Boselli, M. et al. An Inhibitor of the Proteasomal Deubiquitinating Enzyme USP14 Induces Tau Elimination in Cultured Neurons. *J. Biol. Chem.* **2017**, 292, 19209−19225.

23. Shan, J.; Zhao, W.; Gu, W. Suppression of Cancer Cell Growth by Promoting Cyclin D1 Degradation. *Mol. Cell* **2009**, 36, 469−476

24. Davis, M. I. et al. Small Molecule Inhibition of the Ubiquitin-Specific Protease USP2 Accelerates Cyclin D1 Degradation and Leads to Cell Cycle Arrest in Colorectal Cancer and Mantle Cell Lymphoma Models. *J. Biol. Chem.* **2016**, 291, 24628−24640.

25. Li, M.; Brooks, C. L.; Kon, N.; Gu, W. A Dynamic Role of HAUSP in the P53-MDM2 Pathway. *Mol Cell* **2004**, 13, 879–886.

26. Chauhan, D. et al. A Small Molecule Inhibitor of Ubiquitin-Specific Protease-7 Induces Apoptosis in Multiple Myeloma Cells and Overcomes Bortezomib Resistance. *Cancer Cell* **2012,** 22, 345-358.

27. Reverdy, C. et al. Discovery of Specific Inhibitors of Human USP7/HAUSP Deubiquitinating Enzyme. *Chem Biol* **2012**, 19, 467-477.

28. Colland, F. et al. Small-Molecule Inhibitor of USP7/HAUSP Ubiquitin Protease Stabilizes and Activates P53 in Cells. *Mol Cancer Ther* **2009**, 8, 2286-2295.

29. Fan, Y-H et al. USP7 Inhibitor P22077 Inhibits Neuroblastoma Growth via Inducing P53-Mediated Apoptosis. *Cell Death Dis* **2013**, 4:e867.

30. Bashore, C. et al. Cyanopyrrolidine Inhibitors of Ubiquitin Specific Protease 7 Mediate Desulfhydration of the Active-Site Cysteine. *ACS Chem Biol* **2020**, 15, 1392-1400.

31. Wang, X. et al. Targeting Deubiquitinase USP28 for Cancer Therapy. *Cell Death Dis*. **2018**, 9, 186.

32. Wrigley, J. D. et al. Identification and Characterization of Dual Inhibitors of the USP25/28 Deubiquitinating Enzyme Subfamily. *ACS Chem Biol* **2017**, 12, 3113-3125.

33. Kluge, A. F. et al. Novel Highly Selective Inhibitors of Ubiquitin Specific Protease 30 (USP30) Accelerate Mitophagy. *Bioorg Med Chem Lett* **2018**, 28, 2655-2659.

34. Mullally, J. E. et al. Cyclopentenone Prostaglandins of the J Series Inhibit the Ubiquitin Isopeptidase Activity of the Proteasom Pathway. *J Biol Chem* **2001**, 276, 30366-30373.

35. Li, Z. et al. Delta12-Prostaglandin J2 Inhibits the Ubiquitin Hydrolase UCH-L1 and Elicits Ubiquitin-Protein Aggregation Without Proteasome Inhibition. *Biochem Biophys Res Commun* **2004**, 319, 1171-1180.

36. Felth, J. et al. Gambogic Acid is Cytotoxic to Cancer Cells Through Inhibition of the Ubiquitinproteasome System. *Invest New Drugs.* **2013**, 31, 587-598.

37. Rahmani, A. H.; Alsahli, M. A.; Aly, S. M.; Khan, M. A.; Aldebasi, Y. H. Role of Curcumin in Disease Prevention and Treatment. *Adv Biomed Res* **2018**, 7, 38.

38. Jana, N. R.; Dikshit, P.; Goswami, A.; Nukina, N. Inhibition of Proteasomal Function by Curcumin Induces Apoptosis through Mitochondrial Pathway. *J Biol Chem* **2003**, 279, 11680–11685.

39. Hess, W.; Mackeen, M. M.; Kramer, H. B. Natural Product Inhibitors of Ubiquitin Conjugation and Deconjugation. *Stud Nat Prod Chem.* **2016**, 49, 207–242.

40. Aggarwal, B. B. et al. Curcumin: The Indian Solid Gold. *Adv Exp Med Biol.* **2007**, 595, 1-75.

41. Zhou, B. et al. Deubiquitinase Inhibition of 19S Regulatory Particles by 4-Arylidene Curcumin Analog AC17 Causes NF-kappaB Inhibition and p53 Reactivation in Human Lung Cancer Cells. *Mol Cancer Ther.* **2013**, 12, 1381-1392.

42. D'Arcy, P. et al. Inhibition of Proteasome Deubiquitinating Activity as a New Cancer Therapy. *Nat Med* **2011**, 17, 1636–1640.

43. Wang, X. et al. Synthesis and Evaluation of Derivatives of the Proteasome Deubiquitinase Inhibitor b-AP15. *Chem Biol Drug Des* **2015**, 86, 1036–1048.

44. Wang, X. et el. The Proteasome Deubiquitinase Inhibitor VLX1570 Shows Selectivity for Ubiquitin-specific Protease-14 and Induces Apoptosis of Multiple Myeloma Cells. *Sci Rep* **2016**, 6, 26979.

45. Fontanini, A. **et al.** The Isopeptidases Inhibitor G5 Triggers a Caspase-Indipendent Necrotic Death in Cell Resistant to Apoptosis: a Comparative Study With the Proteasome Inhibitor Bortezomib. *Biol Chem* **2009**, 284, 8369-8391.

46. Aleo, E.; Henderson, C. J.; Fontanini, A.; Solazzo, B.; Brancolini, C. Identification of New Compounds that Trigger Apoptosome-Independent Caspase Activation and Apoptosis. *Cancer Res.* **2006**, 66, 9235−9244.

47. Adams, B. K. et al. Synthesis and Biological Evaluation of Novel Curcumin Analogs as Anti-Cancer and Anti-Angiogenesis Agents. *Bioorg Med Chem* **2004**, 12, 3871−3883.

48. Das, U.; Sharma, R. K.; Dimmock, J. R. 1,5-Diaryl-3-Oxo-1,4-Pentadienes: a Case for Antineoplastics with Multiple Targets. *Curr Med Chem* **2009**, 16, 2001−2020.

49. Cersosimo, U. et al. Synthesis, Characterization, and Optimization for In Vivo Delivery of a Nonselective Isopeptidase Inhibitor as New Antineoplastic Agent. *J Med Chem* **2015**, 58, 1691-704.

50. Ciotti, S. et al. The Binding Landscape of a Partially-Selective Isopeptidase Inhibitor With Potent Pro-Death Activity, Based on the Bis(Arylidene)Cyclohexanone Scaffold. *Cell Death Dis* **2018**, 9(2):184.

Targeted Drug Delivery in Cancer Therapy

The Importance of Targeted Chemotherapy

♦ *Targeted chemotherapy provides tumour-specific drug delivery and reduces common side effects of traditional treatments.*

Cancer caused approximately 50% of deaths worldwide in 2020, and this percentage is expected to rise to 70% by 2030.[1] Chemotherapy is still one of the most effective weapons to treat cancer; however, the administration of potent cytotoxic agents can lead to deleterious effects on non-cancerous cells as well. These side effects, which can manifest as pain, nausea, diarrhea, cardiotoxicity, hair loss, dry skin, or immunodepression, are the consequences of the poor tumor selectivity of most chemotherapeutic agents. Furthermore, neoplastic cells often develop chemoresistance that ultimately results in tumor recrudescence and metastasis.[2] In this scenario, there is an urgent need to tailor available chemotherapeutic agents to be converted into cancer-specific drugs (Figure 24).[3] Healthy and tumor cells display significant differences in terms of metabolism and microenvironment that can be exploited to enhance drug selectivity and reduce adverse effects.[4-6] Malignant tissues are indeed characterized by:

- Overexpression of surface receptors, including gonadotropin-releasing hormone receptors (GnRH-R),[7] membrane transporters,[8] and G protein-coupled receptors.
- Overexpression of matrix-metalloproteinases (MMPs).[9]
- Enhanced levels of reactive oxygen species.[10]
- Slightly acidic pH.[11]
- Increased glutathione levels.[12]
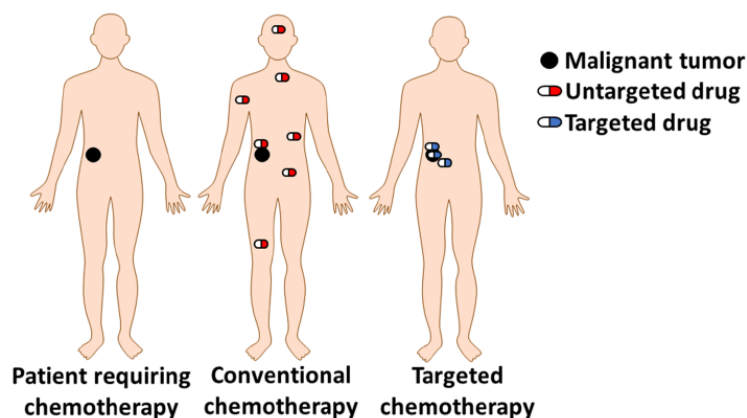
Comparison between traditional and cancer-targeted chemotherapy: the former indiscriminately kills both cancer and non-cancerous cells, while the latter delivers the drug straight to the tumor site.

♦ *The clinical development of peptides has been limited by unfavourable pharmacokinetic properties, which, however, can be improved by chemical modification of the sequences.*

The discovery of tumor-targeting peptides opened the door for the development of more effective and selective anticancer drugs for the future.[13] In fact, peptides have recently emerged as promising therapeutic agents, and their application in the treatment of various diseases is growing rapidly.[14] In general, the use of peptides in clinic is attractive due to their enhanced tissue penetration, high target specificity, reduced immunogenicity, and low toxicity. From a chemical point of view, they are easy to synthetize from cheap starting materials, simple to purify, and easily functionalizable.[5, 14] However, in practice several drawbacks hinder the clinical application of peptides and make them poor drug candidates. Few examples are the poor bioavailability and hydrosolubility, short half-life, rapid clearance, tendency to denature and to be digested by proteolytic enzymes. Chemical modifications have been implemented to overcome these limitations and increase the plasma stability of peptides *in vivo*, including cyclization, C-terminus amidation, N-terminus acetylation, and introduction of non-natural amino acids.[14-16] For example, peptide cyclization reduces the flexibility of linear sequences and can result in higher binding affinity for biological targets and improved ADME profile.

Peptide-Drug Conjugates (PCDs)

♦ *PCDs are emerging as promising agents for selective and controlled drug delivery.*

Despite their low druggability, peptides can be used as drug carriers for the design of peptide-drug conjugates (PCDs),[17-19] which combine three different elements that contribute to the overall biological activity: a tumor-homing peptide, a linker (or spacer),[20-21] and a cytotoxic agent (Table 6).

Table 6
The general structure of a PDC.

Component	Role	Effect
Peptide	Binds with high affinity to target receptors overexpressed in tumor cells and triggers receptor-mediated internalization of the PDC.	Responsible for the selectivity of the PDC.
Linker	Releases the cargo in a programmed manner upon the exposure of specific stimuli (such as decrease of pH or MMPs-dependent release).	Impacts on localization and timing of drug release.
Drug	Active principle.	Determines the potency and the therapeutical properties.

The cytotoxic agent and the peptide carrier are usually joined together by a cleavable linker, whose main function is to overcome any steric interference between these two components, thus resulting in an improved pharmacokinetic and pharmacodynamic profile of the PDC. An ideal linker should be chemically and enzymatically stable during blood circulation yet sufficiently labile to allow a controlled release of the drug at the target site via stimulus-mediated cleavage. In the case of neoplastic cells, several pH- and redox-sensitive spacers with tunable chemical properties are known (e.g., disulfide and hydrazone linkers):[22]

they efficiently reach the tumor site and release the cargo in the malignant intracellular environment, reducing potentially off-target toxicity.[20-21]

Peptides should be appropriately selected according to the investigated tumor and to the required physiochemical properties (e.g., solubility). An exhaustive list of tumor-specific peptides was reviewed by Vrettos et al.[4] and is summarized in Table 7. Moreover, the coupling with other components of the PDC must be enabled by the presence of specific functional groups within the amino acid sequence of the peptide. It should be noted, however, that the conjugation site must be carefully selected in order not to perturb or delete the binding affinity for the target receptor.[4]

Table 7

Few peptide-binding receptors overexpressed in tumor cells.

Receptors	Peptide ligand	Tumor Expression
Integrin αvβ3	RGD-related peptides	Glioblastoma, melanoma, breast, prostate, ovaian cancers
EGFR	GE11	Glioblastoma, lung, head and neck cancer
SSTR2	Octreotide	NETs, breast, ovarian, cervical cancer
GnRH-R	GnRH analogues	Ovarian, breast, endometrial, prostate, lung cancer
Bn receptors	[D-Tyr6, β-Ala11, Phe13, Nle14]-Bn(6-14) yQWAV-βAla-HF-Nle-NH$_2$	Prostate, breast, small cell lung, pancreatic cancer
VIP receptors	Vasoactive intestinal peptide	Endocrine tumours, colon, breast cancer
CCK2R	Minigastrin 11	Gastrointestinal, thyroid, lung, pancreas, liver cancer

♦ *Several PDCs are based on RGD and GnRH analogues peptides.*

Worthy of mention in this context are RGD-containing peptides and GnRH peptide analogues. The RGD (Arg-Gly-Asp) motif was first identified in the early 1980s.[23] Is known to bind over 10 different integrins, including integrin αvβ3 which is necessary for cell adhesion, migration, and positioning.[24] Due to the high expression of αvβ3 in many tumours, several RGD variants have been studied.[25] The conjugation of chemotherapeutic agents to RDG-bearing peptides results in an increased selectivity toward glioblastoma, prostate, ovarian,[26] and breast cancers among others (Figure 25).

On the other hand, ovarian, breast and lung cancers mainly overexpress the GnRH-R receptor: because of this, GnRH analogues are emerging as promising tumor-homing peptides for these types of cancers.[27] Multiple GnRH analogues have been thus developed with the incorporation of D- or unnatural amino acids at different sites within the primary sequence to increase the proteolytic stability of the peptide.[28] One of the most frequently used GnRH analogue is the decapeptide [D-Lys^6]-GnRH-I (Figure 26), which contains a free amino group on Lys^6 residue that can be used for the coupling with electrophilic cytotoxic warheads.[29]
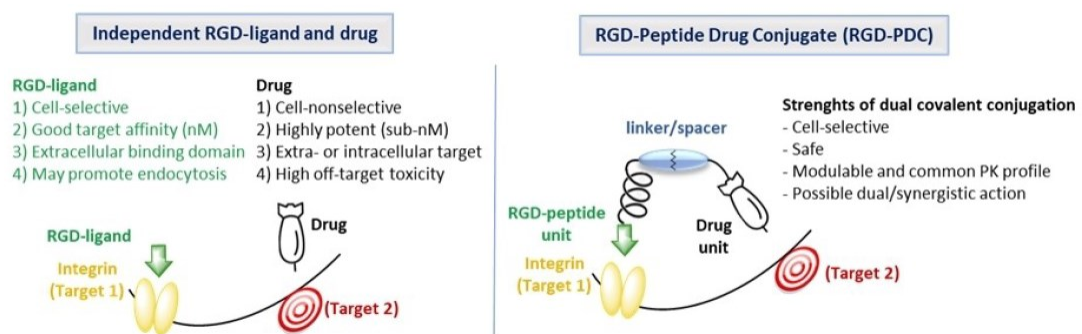
Figure 25

Conventional drug administration versus RGD-targeted administration
(left and right respectively).

In summary, recent achievements in the field of PCDs represent an important step for the development of innovative targeted therapies for future. The growing impact of these structures in the pharmaceutical industry is also witnessed by the approval of the first PDC in 2018 for the treatment of neuroendocrine tumours (^{177}Lu-dotatate).[30]
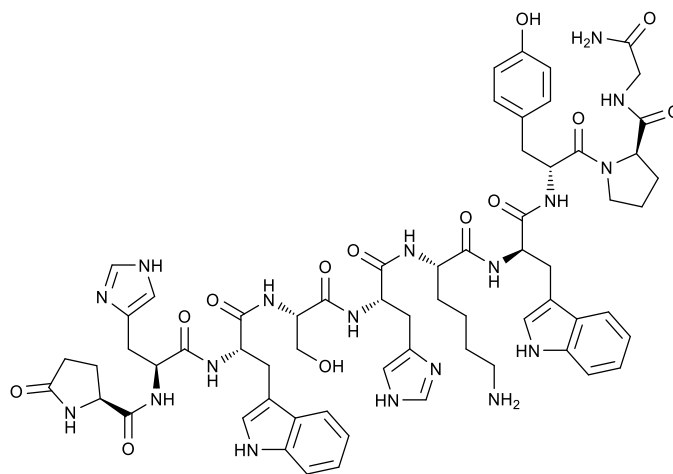
pGlu-His-Trp-Ser-His-$^{\mathbf{D}}$Lys-Trp-Tyr-Pro-Gly-NH$_2$

Figure 26

Structure of [D-Lys^6]-GnRH-I decapeptide.

References

1. Ferlay, J. et al. Cancer Statistics for the Year 2020: An Overview. *Int J Cancer* **2021** (Online ahead of print).

2. Strebhardt, K; Ullrich, A. Paul Ehrlich's Magic Bullet Concept: 100 Years of Progress. *Nat Rev Cancer* **2008**, 8, 473-80.

3. Baudino, T. A. Targeted Cancer Therapy: The Next Generation of Cancer Treatment. *Curr Drug Discov Technol* **2015**, 12, 3-20.

4. Vrettos, E. I.; Mezo, G.; Tzakos, A. G. On the Design Principles of Peptide-Drug Conjugates for Targeted Drug Delivery to the Malignant Tumor Site. *Beilstein J Org Chem* **2018**, 14, 930–954.

5. Cooper, B. M et al. Peptides as a Platform for Targeted Therapeutics for Cancer: Peptide-Drug Conjugates (PDCs). *Chem Soc Rev* **2021**, 50, 1480-1494.

6. DeBerardinis, R. J.; Chandel, N. S. Fundamentals of Cancer Metabolism. *Sci Adv* **2016**, 2, e1600200.

7. Argyros, A. et al. Peptide–Drug Conjugate GnRH–Sunitinib Targets Angiogenesis Selectively at the Site of Action to Inhibit Tumor Growth. *Cancer Res.* **2016**, 76, 1181–1192.

8. Kellici, T. F. Rational Design and Structure–Activity Relationship Studies of Quercetin–Amino Acid Hybrids Targeting the Anti-Apoptotic Protein Bcl-xL. *Org. Biomol. Chem*. **2017**, 15, 7956–7976.

9. Poreba, M. Protease-Activated Prodrugs: Strategies, Challenges, and Future Directions. *FEBS J* **2020**, 287, 1936-1969.

10. Trachootham, D.; Alexandre, J.; Huang, P. Targeting Cancer Cells by ROS-Mediated Mechanisms: a Radical Therapeutic Approach? *Nat. Rev. Drug Discovery* **2009**, 8, 579–591.

11. Kato, Y. et al. Acidic Extracellular Microenvironment and Cancer. *Cancer Cell Int*. **2013**, 13, 89.

12. Balendiran, G. K.; Dabur, R; Fraser, D. The Role of Glutathione in Cancer. *Cell Biochem Funct* **2004**, 22, 343-352.

13. Boohaker, R. J. et al. The Use of Therapeutic Peptides to Target and to Kill Cancer Cells. *Curr Med Chem* **2012**, 19, 3794-3804.

14. Haggag, Y. A. et al. Peptides as Drug Candidates: Limitations and Recent Development Perspectives. *Biomed J Sci Technol Res* **2018**, 8, 6659–6652.

15. Werle, M.; Bernkop-Schnürch, A. Strategies to Improve Plasma Half Life Time of Peptide and Protein Drugs. *Amino Acids* **2006**, 30, 351-367.

16. Hamamoto, K. et al. Antimicrobial Activity and Stability to Proteolysis of Small Linear Cationic Peptides with D-Amino Acid Substitutions. *Microbiol Immunol* **2002**, 46, 741-749.

17. Ahrens, V. M.; Bellmann-Sickert, K; Beck-Sickinger, A. G. Peptides and Peptide Conjugates: Therapeutics on the Upward Path. *Future Med Chem* **2012**, 4, 1567-1586.

18. Cooper, B. M et al. Peptides as a Platform for Targeted Therapeutics for Cancer: Peptide-Drug Conjugates (PDCs). *Chem Soc Rev* **2021**, 50, 1480-1494.

19. Worm, D. J.; Els-Heindl, S; Beck-Sickinger, A. G. Targeting of Peptide-Binding Receptors on Cancer Cells with Peptide-Drug Conjugates. *Pept. Sci.* **2020**, e24171.

20. Bargh, J. D. et al. Cleavable Linkers in Antibody-Drug Conjugates. *Chem Soc Rev* **2019**, 48, 4361-4374.

21. Chang, M. et al. Smart Linkers in Polymer-Drug Conjugates for Tumor-Targeted Delivery. *J Drug Target* **2016**, 24, 475-491.

22. Srinivasarao, M.; Low, P. S. Ligand-Targeted Drug Delivery. Chem Rev 2017, 117, 12133-12164.

23. Pierschbacher, M. D.; Ruoslahti, E. Cell Attachment Activity of Fibronectin Can be Duplicated by Small Synthetic Fragments of the Molecule. *Nature* **1984**, 309, 30–33.

24. Cox, D; Brennan, M; Moran, N. Integrins as Therapeutic Targets: Lessons and Opportunities. *Nat. Rev. Drug Discovery* **2010**, 9, 804–820.

25. Battistini, L. et al. RGD Peptide-Drug Conjugates as Effective Dual Targeting Platforms: Recent Advances. *Eur J Org Chem* **2021**, 2506–2528.

26. Seraya-Bareket, C. et al. The Identification of Nuclear αvβ3 Integrin in Ovarian Cancer: Non-Paradigmal Localization with Cancer Promoting Actions. *Oncogenesis* **2020**, 9(7):69.

27. Limonta, P. et al. GnRH Receptors in Cancer: From Cell Biology to Novel Targeted Therapeutic Strategies. *Endocr Rev* **2012**, 33, 784-811.

28. Padula, A. M. GnRH Analogues-Agonists and Antagonists. *Anim. Reprod. Sci*. **2005**, 88, 115-126.

29. Karampelas, T. et al. GnRH-Gemcitabine Conjugates for the Treatment of Androgen-Independent Prostate Cancer: Pharmacokinetic Enhancements Combined with Targeted Drug Delivery. *Bioconjugate Chem*. **2014**, 25, 813-823.

30. Demirci, E et al. ^{177}Lu-Dotatate Therapy in Patients with Neuroendocrine Tumours Including High-Grade (WHO G3) Neuroendocrine Tumours: Response to Treatment and Long-Term Survival Update. *Nucl Med Commun* **2018**, 39, 789-796.

1. Introduction

2. Aim

3. Results and Discussion

4. Conclusions

5. Experimental Section

6. Supporting Material

State of the Art and Aim of the Project

State of the Art

The discovery of new DUBs inhibitors has experienced significant progress over the last decade, as witnessed by the plenty of novel lead compounds with improved drug-like properties. Furthermore, the development of S-alkylating agents has contributed to expand the scope of covalent inhibitors in drug discovery (Scheme 3), in particular when a cysteine-dependent protease is the inhibitor's target.[1-2] The use of covalent drugs over the more common non-covalent therapeutic agents has been encouraged by their usual higher potency, prolonged effects, and reduced drug resistance.[3-5] However, the lack of specificity is a recurring limitation that hinder further developments of such type of drugs through medicinal chemistry. In this contest, it would be desirable to design more target-specific DUBs inhibitors to achieve better clinical applicability in the future.

The present Ph.D. work is part of the interdisciplinary ATeNA project [6] (Applicazioni Tecnologiche di Nuovi Anti-Neoplastici), aimed at synthetizing, characterizing, and testing the efficacy of novel DUBs inhibitors against several types of tumours, as well as optimizing the structure of already existing ones. This Project can be divided in two main parts:

The focal point of the first part is the synthesis of optimized versions of the partially selective isopeptidases inhibitor **2c**, with the aim to enhance its tumor delivery efficiency in the light of possible applications *in vivo*. These structural refinements will be performed through the insertion of specific recognition elements, such as amino acids or tumor homing peptides at the bis(arylidene)cyclohexanone scaffold (Figure 27). In particular, as previously explained, the main interest will be the conjugation of **2c** with RDG-bearing peptides and GnRH-I analogues, which should boost the selectivity of the parent inhibitor against several types of tumours, including ovarian, breast and prostate carcinomas.
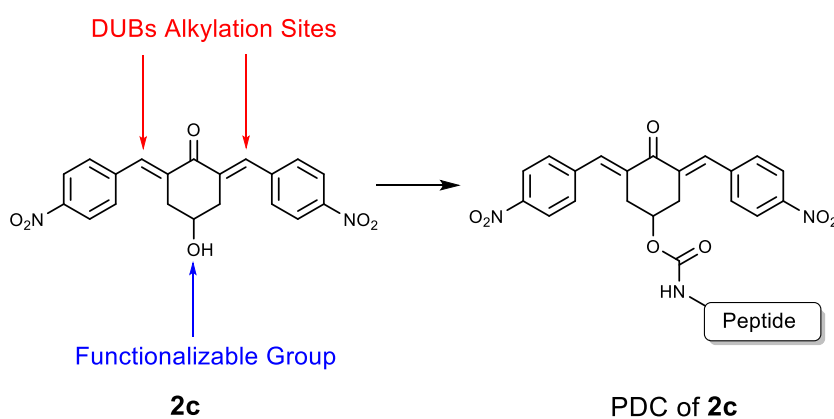
Figure 27

General structure of peptide conjugates of the inhibitor **2c**.

Part 2: Design of Novel DUBs inhibitors

The aim of the second part of the Project is the design, synthesis, and evaluation of the antitumoral activity of a small library of potential next-generation DUBs inhibitors. Such structures can be designed using electrophilic warheads specific for cysteine proteases, including Michael acceptors [7-9] such as α,β-unsaturated ketones,[10] α,β-unsaturated esters,[11] vinyl sulfones,[12-13] and propargylamides.[14-16] These moieties can be inserted into small peptide fragments resembling the C-terminal portion of Ub (Figure 28), whose function is to favour the correct positioning of the pharmacophore into the proximity of the enzyme's catalytic cleft by formation of non-covalent interactions with the active site residues.

a)
MQIFVKTLTGKTITLEVEPSDTIENVKAKIQDKEGIPPD
QQRLIFAGKQLEDGRTLSDYNIQKESTLHLVLRL**RGG**

b)
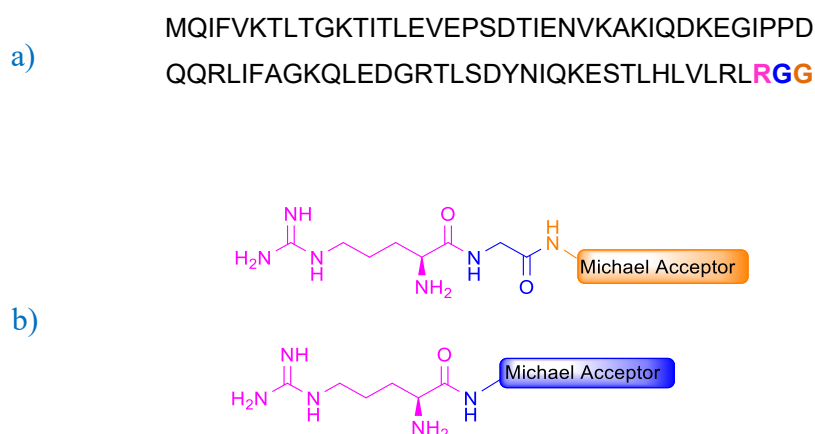
Figure 28

a) The primary sequence of the Ub monomer, with highlighted the C-terminal residues of $R^{74}G^{75}G^{76}$. **b)** General structures of pseudopeptides based on the Arg-Gly-Gly sequence in which one or both terminal residues of Gly are replaced by the Michael acceptor.

References

1. Jackson, P. A.; Widen, J. C.; Harki, D. A.; Brummond, K. M. Covalent Modifiers: A Chemical Perspective on the Reactivity of α,β-Unsaturated Carbonyls with Thiols via Hetero-Michael Addition Reactions. *J Med Chem* **2017**, *60*, 839–885.

2. Zhao, Z.; Liu, Q.; Bliven, S.; Xie, L.; Bourne, P. E. Determining Cysteines Available for Covalent Inhibition Across the Human Kinome. *J Med Chem* **2017**, *60*, 2879–2889.

3. Lagoutte, R.; Patouret, R.; Winssinger, N. Covalent Inhibitors: An Opportunity for Rational Target Selectivity. *Curr Opin Chem Biol* **2017**, *39*, 54–63.

4. Baillie, T. A. Targeted Covalent Inhibitors for Drug Design. *Angew. Chemie Int. Ed*. **2016**, *55*, 13408–13421.

5. Engel, J.; Lategahn, J.; Rauh, D. Hope and Disappointment: Covalent Inhibitors to Overcome Drug Resistance in Non-Small Cell Lung Cancer. *ACS Med Chem Lett* **2016**, *7*, 2–5.

6. https://dsv.units.it/it/node/44724

7. Haj-Yahya, N. et al. Dehydroalanine-Based Diubiquitin Activity Probes. *Org. Lett.* **2014**, 16, 540-543.

8. Li, G.; Liang, Q.; Gong, P.; Tencer, A. H.; Zhuang, Z. Activity-Based Diubiquitin Probes for Elucidating the Linkage Specificity of Deubiquitinating Enzymes. *Chem. Commun.* **2014**, 50, 216−218.

9. Hemelaar, J.; Galardy, P. J.; Borodovsky, A.; Kessler, B. M.; Ploegh, H. L.; Ovaa, H. Chemistry-Based Functional Proteomics: Mechanism-Based Activity-Profiling Tools for Ubiquitin and Ubiquitin-like Specific Proteases. *J. Proteome Res.* **2004**, 3, 268−276.

10. D'Arcy, P.; Wang, X.; Linder, S. Deubiquitinase Inhibition as a Cancer Therapeutic Strategy. *Pharmacol Ther* **2015**, 147, 32-54.

11. Johansson, H et al. Fragment-Based Covalent Ligand Screening Enables Rapid Discovery of Inhibitors for the RBR E3 Ubiquitin Ligase HOIP. *J Am Chem Soc* **2019**, 141, 2703-2712.

12. Borodovsky, A. et al. A Novel Active Site-Directed Probe Specific for Deubiquitylating Enzymes Reveals Proteasome Association of USP14. *EMBO J* **2001**, 20, 5187-5196.

13. Zhang, H. et al. Vinyl Sulfone-Based Inhibitors of Trypanosomal Cysteine Protease Rhodesain with Improved Antitrypanosomal Activities. *Bioorg Med Chem Lett* **2020**, 30, 127217.

14. Ekkebus, R. et al. On Terminal Alkynes That Can React with Active-Site Cysteine Nucleophiles in Proteases. *J Am Chem Soc* **2013**, 135, 2867-2870.

15. Arkona, C; Rademann, J. Propargyl Amides as Irreversible Inhibitors of Cysteine Proteases- A Lesson on the Biological Reactivity of Alkynes. *Angew Chem Int Ed Engl* **2013**, 52, 8210-8212.

16. Mons, E. et al. The Alkyne Moiety as a Latent Electrophile in Irreversible Covalent Small Molecule Inhibitors of Cathepsin K. *J. Am. Chem. Soc.* **2019**, 141, 3507–3514.

1. INTRODUCTION

2. AIM

3. RESULTS AND DISCUSSION

4. CONCLUSIONS

5. EXPERIMENTAL SECTION

6. SUPPORTING MATERIAL

Based on the chemical structure of the lead compound **2c**, various optimization strategies could be exploited to enhance its intracellular drug delivery both *in vitro* and *in vivo*. As previously discussed in chapter 1.3, a promising approach consists in the conjugation of the cytotoxic agent to tumor-specific peptide carriers. In this work, the synthetic process to obtain an amino acid or peptide conjugate of **2c** follows three principal routes (Scheme 4):

a) Synthesis of the inhibitor (**2c**) and functionalization of the hydroxyl group as succinimidyl ester (**2c-OSu**) to enable further modifications of the cycloaliphatic scaffold, including b) the introduction of a bifunctional linker via carbamate linkage to give **2c-Linker** .

c) Coupling of **2c-OSu** or **2c-Linker** to amino acids such as Lys, Arg, Glu, Asp, and Ser.

d) Incorporation of the so obtained amino acid conjugates into complementary peptide fragments to form the desired PDCs.

All the derivatives of **2c** can be grouped in two main sets: the compounds of the first set have the parent inhibitor directly functionalized on the ciclohexanone ring upon the formation of a carbamate junction. It should be reminded that the carbamate group is getting renewed attention in drug design, as carbamate-based drugs are generally characterized by an enhanced plasma membrane permeability and increased metabolic stability.[1-2] For compounds of the second set, instead, the funcionalization occurs through a diamino linker (**2c-Linker**), whose role is to provide a functionalizable amino group that can be exploited to introduce different amino acids to the scaffold of **2c** via C-terminus amidation. A recent literature review suggested that a minimum length of three carbon atoms is required to avoid the intramolecular cyclization of the carbamate linker and consequent release of the parent drug, which occurs with a 1,2-diaminoethane linker (Scheme 5).[1]
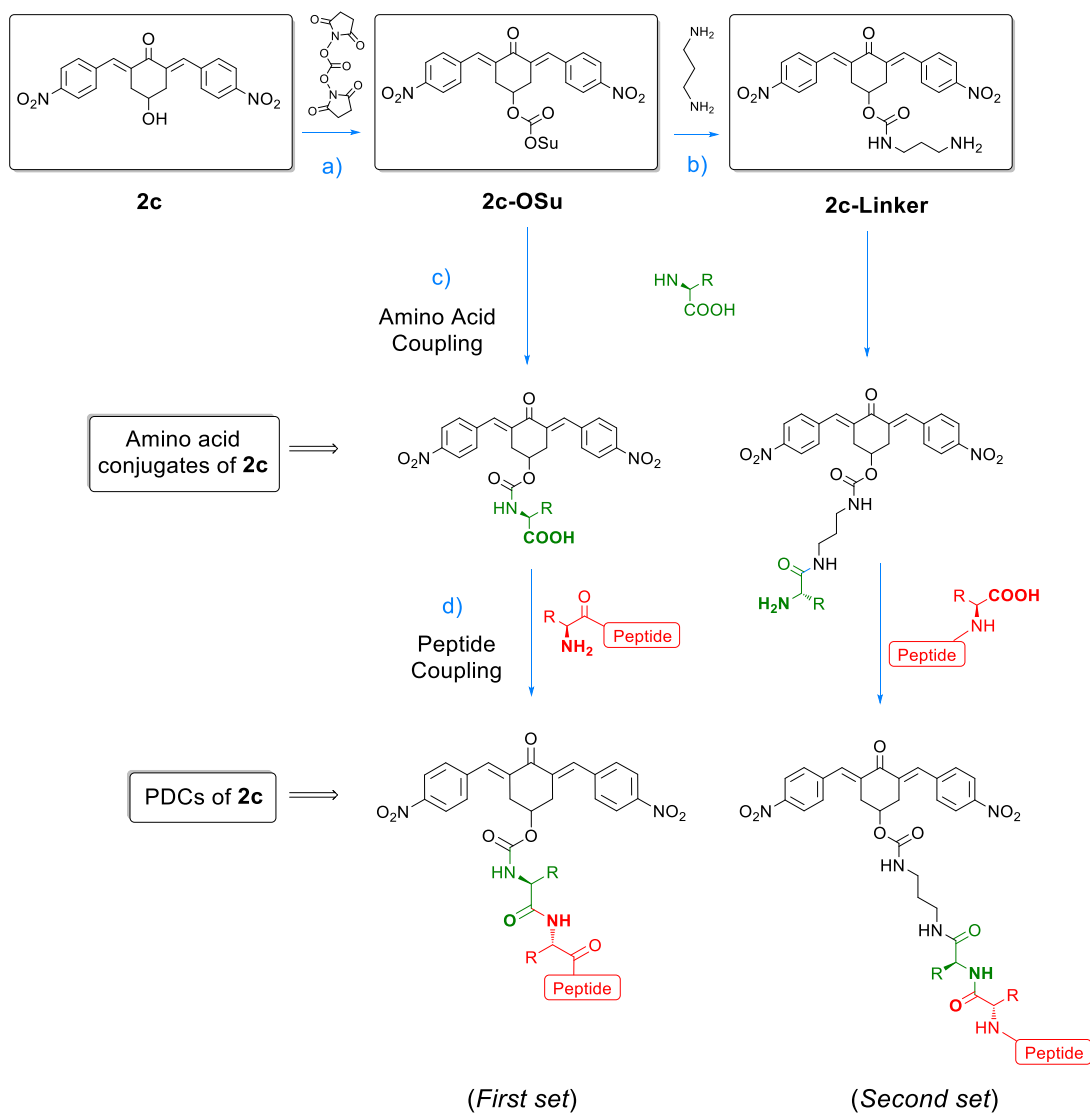
Scheme 4

General scheme for the synthesis of amino acid and peptide conjugates of **2c**.
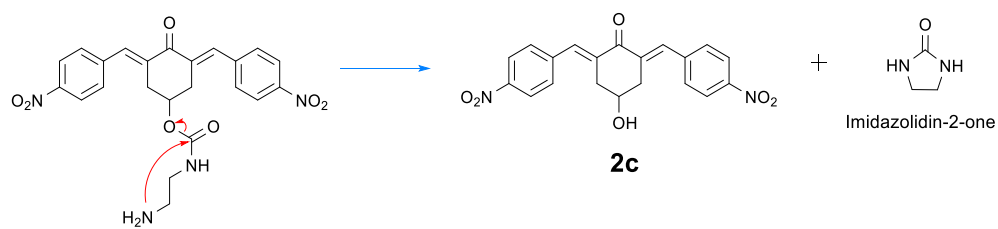
Scheme 5

Mechanism of cyclization-elimination of 1,2-diamino linkers.

Synthesis of 2c

The parent inhibitor **2c** was obtained by a slightly modified version of the classic base-catalyzed Knoevenagel condensation between 4-hydroxycyclohexanone and 4-nitrobenzaldehyde, previously carried out in our laboratory.[3] Knoevenagel condensations are nucleophilic addition-type reactions that undergo either with acid or basic catalysts and typically involve an enolyzable ketone and an aromatic aldehyde. The mechanism proceeds through the formation of an intermediate β-hydroxyketone, which is rapidly converted to the corresponding α,β-unsaturated ketone after spontaneous dehydration *in situ*. Mineral acids or strong organic acids such as pTSA promote an acid-catalyzed mechanism (Scheme 6a), whereas weak organic amines or ammonium salts are conventionally used as base catalysts (Scheme 6b). If the ketone is enolizable at both α-positions, a slight excess of the aldehyde directly leads to the more thermodynamically-favoured dienones (Scheme 6c).[4-6]
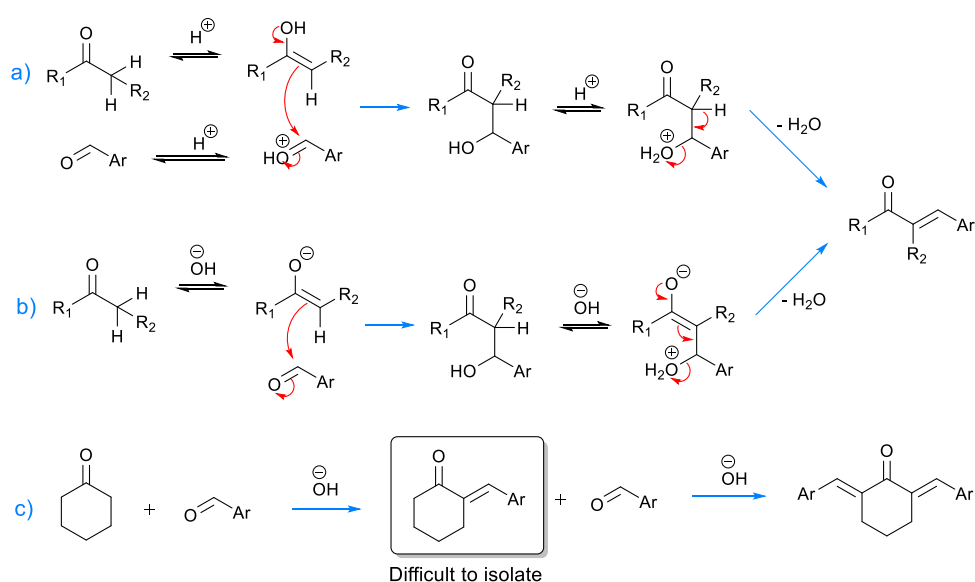
Scheme 6

a) General mechanism of an acid-catalyzed Knoevenagel condensation.
b) General mechanism of a base-catalyzed Knoevenagel condensation.
c) Formation of dienones.

The ketone precursor of **2c** was synthetized from 1,4-cyclohexanedione monoethylene acetal, first reduced to the corresponding alcohol **1** with NaBH$_4$ and then deprotected to 4-hydroxycyclohexanone **2** under strong acidic conditions. In the next step, the ketone **2** reacted with two equivalents of 4-nitrobenzaldehyde in the presence of a catalytic amount of NaOH to generate the aldol product **3** (**2c**) (Scheme 7), which precipitated from ethanol and was isolated pure in 72% yield after cristallization. Spectroscopic data of **3** were in agreement with the published data.[3]
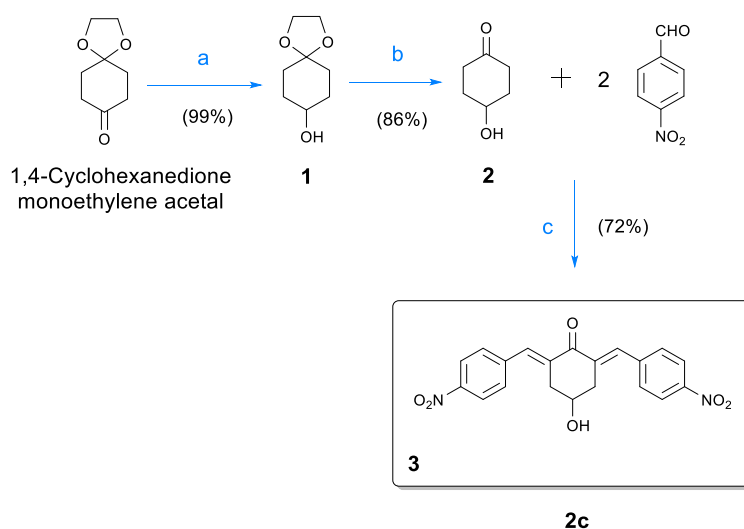
Scheme 7

Synthesis of **2c** (**3**).
Reagents and conditions: **a)** NaBH$_4$, EtOH, 0 °C → r.t., 4h. **b) (i)** pTSA$_{(aq)}$ (pH=1), reflux, 23h. **(ii)** KHCO$_3$ (pH 6÷7). **c)** EtOH, NaOH$_{(aq)}$, r.t., 18h.

The cycloaliphatic hydroxy group of **2c** was then converted to succinimidyl ester using N,N′-disuccinimidyl carbonate (DSC) as a carbonylating agent: the resulting product **4** (**2c-OSu**) was isolated with a 78% yield. The activated succinimidyl carbonate **2c-OSu** undergoes nucleophilic attack of different amines: in particular, the nucleophilic acyl substitution with the diamino linker **5** (blocked at one side as Boc) afforded the carbamate **6** (**2c-Linker**) in excellent yield after quantitative deprotection of the Boc protecting group (Scheme 8). The synthesis of **5** was accomplished according to a literature procedure that operated with a large stochiometric excess of 1,3-diaminopropane with respect to Boc$_2$O and under strictly

controlled conditions of temperature [7] to suppress the formation of the undesired bis-protected product.
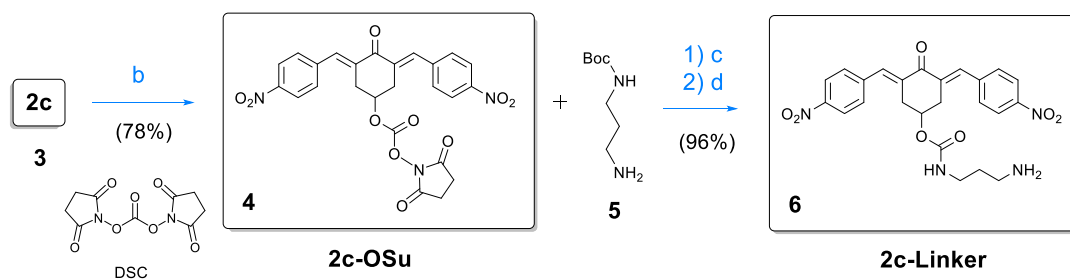
Scheme 8

Synthesis of **2c-OSu** (**4**) and **2c-Linker** (**6**).
Reagents and conditions: **a)** DCM/ACN/Py, r.t., 4h. **b)** DCM, r.t., 16h.
c) TFA/CHCl₃ 20:80, r.t., 16h.

Functionalization of **2c** with Amino Acids

Each lysine and arginine conjugate of **2c** of the first set of compounds was obtained as a product of a multi-step reaction from **2c-OSu** and the properly protected amino acid (Scheme 9). The first step proceeded via coupling of the substrate with the unprotected α- or ε-amino group of the amino acid in dichloromethane, which proceeded straightforwardly under mild basic conditions without the addition of coupling agents. Two Boc-protected conjugates of Lys (**7a** and its isomer **8a**) and the Pbf-protected Arg derivative **9a** were obtained in good to excellent yield after an aqueous workup to get rid of the water-soluble hydroxysuccinimide by-product. Final protecting groups removal provided the final products **7b**, **8b**, and **9b** respectively.
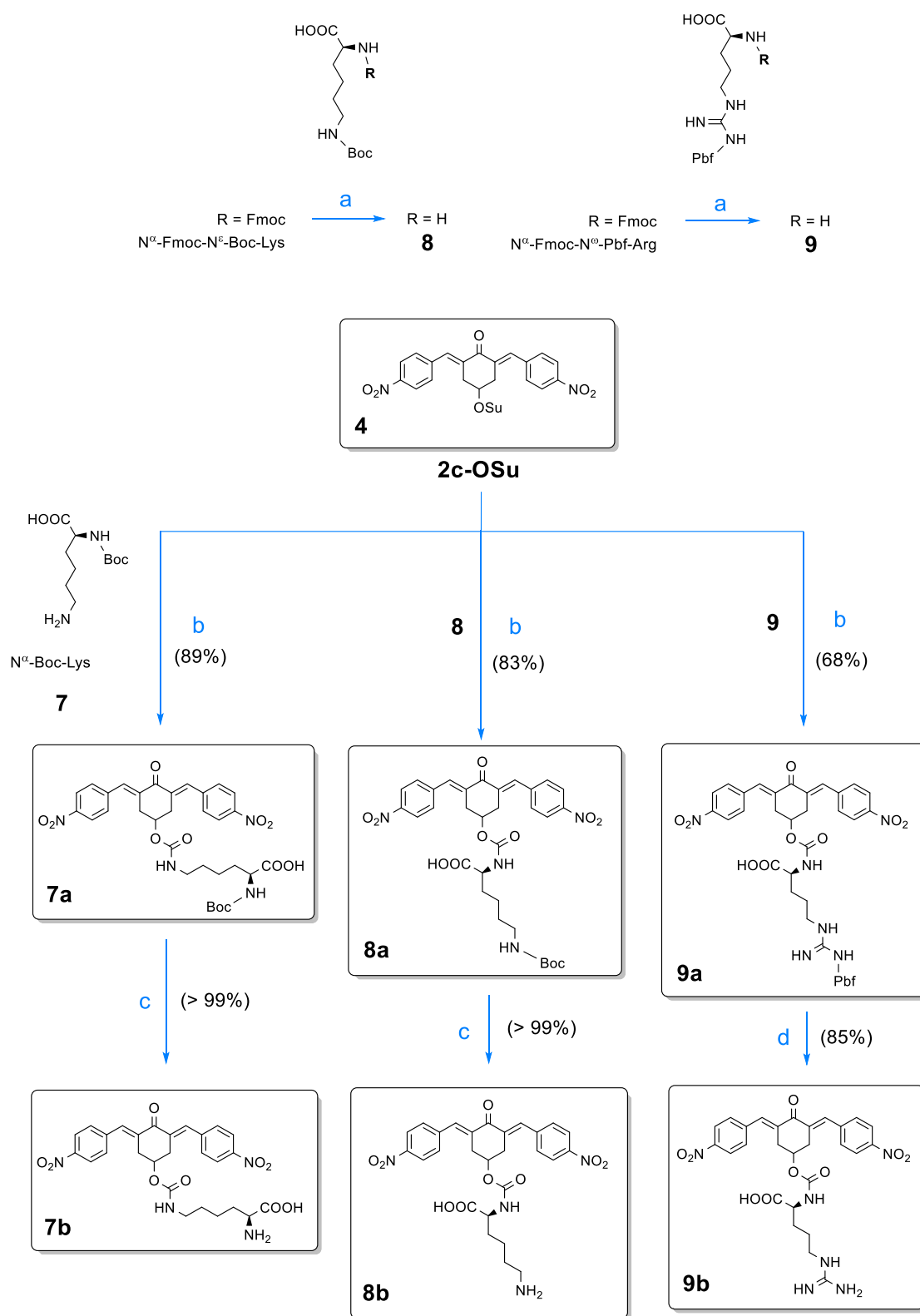
Scheme 9

Synthesis of Lys conjugates of **2c** (**7a-b** and **8a-b**) and Arg conjugates (**9a-b**). *Reagents and conditions*: **a)** NHEt₂/DCM 50:50, r.t., 20h. **b)** DCM, TEA (pH 8÷9), r.t., 18h. **c)** TFA/CHCl₃ 20:80, r.t., 6h. **d)** TFA/CHCl₃ 70:30, r.t., 16h

All the obtained products were fully characterized by NMR spectroscopy and mass spectrometry (MS): in particular, the formation of the carbamate proton resulting from the coupling was confirmed by its characteristic signal in the ^{1}H NMR spectra, which spanned between 5.5 ppm and 6.5 ppm in CDCl$_3$. The associated peak at 156 ppm in the ^{13}C NMR spectra was also diagnostic of products formation. The ESI-MS spectra of the Boc-protected derivatives typically show several intense fragmentation peaks, each related to the loss of isobutene (Δ=56 m/z) and isobutene + CO$_2$ (Δ=100 m/z) from the molecular ion, as shown in Figure 29. An additional peak at m/z = 363.1, corresponding to the alkene product of elimination of the carbamate group, can be also present (Figure 30).
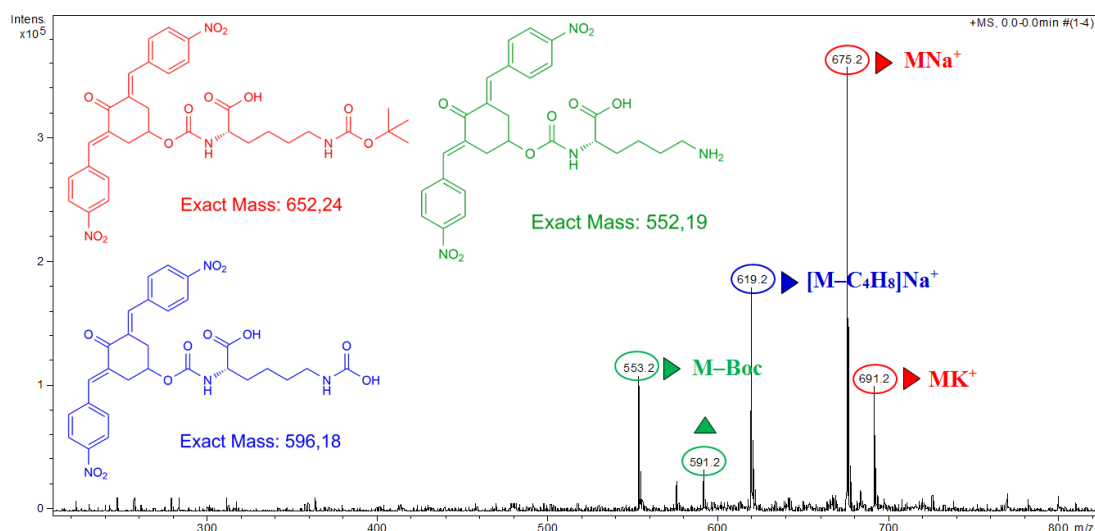
Figure 29

ESI-MS spectrum of compound **8a**. *Significant peaks of fragmentation*: molecular ion (red): m/z 691.2 (MK$^+$) and 675.2 (MNa$^+$); loss of isobutylene (blue): m/z 619.2 ([M–C$_4$H$_8$]Na$^+$); loss of isobutylene + CO$_2$ (green): m/z 591.2 ([M–Boc]K$^+$) and 553.2 ([M–Boc]H$^+$).

The Lys conjugate **7a** was synthetized in 89% yield by coupling of **2c-OSu** with the free ε-amino group of the N$^\alpha$-Boc-protected Lys **7**, while its isomer **8a** was obtained in comparable yield from N$^\varepsilon$-Boc-Lys **8**. The step of selective α-Fmoc deprotection, necessary to afford **8** from the commercial precursor, was initially carried out using the classical piperidine/DMF 20:80 methodology; however, the workup was significantly improved using 50% of diethylamine as base catalyst in dichloromethane.[8] Both intermediates **7a** and **8a** were then quantitatively converted to **8a** and **8b**, respectively, by acidolysis with TFA.[9-10] A complete list of all the protecting groups used in this thesis is summarized in Table 8 on page 77.[11-12]

The side chain group of arginine was the source of a few difficulties in coupling reactions, mostly due to the partial *in situ* lactamization of Arg (Scheme 10), which typically resulted in poor coupling yields.[12-13] For this reason, the protection of the guanidine side chain function was crucial for the synthesis of the arginine conjugate **9a**. The introduction of highly electron-withdrawing groups such as 2,2,4,6,7-Pentamethyl-dihydrobenzofuran-5-sulfonyl (Pbf) [14] or NO$_2$ [15] is known to suppress or, at least, minimize the formation of the unwanted δ-lactam. However, the ω-NO$_2$ protecting group requires harsh conditions to be removed

(most commonly, fluorolysis in anhydrous HF or catalytic hydrogenation), which makes it unsuitable for unsaturated compounds such as **2c**.
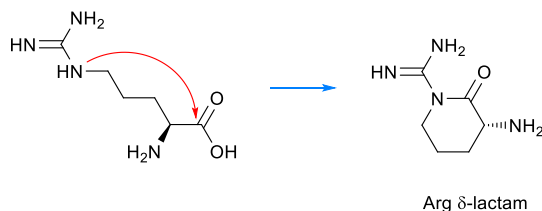
Scheme 10

Base-catalyzed cyclization of unprotected Arg.

Because of this, the derivative **9a** was synthetized by reacting a slight stoichiometric excess of Pbf-protected Arg **9** with **2c-OSu** to give the coupling product **9a,** which was subsequentely deprotected from Pbf to release the guanidinium salt of the final product **9b**. The cleavage of Pbf needed stronger acid conditions than those required for the more labile Boc protecting group (70% of TFA in chloroform overnight).[7] Moreover, unlike the one pot Boc deprotection, the workup procedure for the Pbf removal typically involves two consecutive steps of precipitation from diethyl ether and filtration, which often led to hygroscopic and sticky solids that were difficult to isolate and handle.

The second set of derivates includes glutamic and aspartic acid conjugates of **2c-Linker 6,** which were synthetized via standard EDC/HOBt amidation of the linker with the corresponding carboxylic group of the amino acid. Asp and Glu contain an additional carboxylic group that can interfere with the others and lead to the formation of undesired branched products: for this reason, all the functions that were not involved in the coupling with the inhibitor must be carefully blocked. The most used protecting groups for carboxylic acids are alkyl esters (Table 8); however, methyl esters are generally difficult to hydrolyze even under strong basic conditions,[16] whereas *tert*-butyl and benzyl esters can be easily converted to the carboxylic acids under acidic conditions. In particular, *tert*-butyl esters are labile to

TFA[19] and can be cleaved under the same conditions used for Boc deprotection. The benzyl group, on the other hand, can be removed either by acidolysis with 30% of hydrogen bromide in glacial acetic acid [17] or by catalytic hydrogenation.[18]

The glutamic acid conjugates **10b**, **11b**, and **11c** were obtained in an overall 69%, 75%, and 47% yield respectively (Scheme 11). The synthesis of **10b** started with **2c-Linker 6** and glutamic acid **10** orthogonally protected as α-Boc and γ-COOBn. The resulting intermediate of the coupling reaction **10a**, which bears the inhibitor linked to the C-terminus group of Glu, was purified by flash chromatography and then deprotected with TFA to afford the Bn-protected product **10b**. However, all the attempts to cleave the benzyl ester of **10b** never resulted in the corresponding carboxylic acid **10c**. The glutamic acid can alternatively be functionalized at the side chain position, such as in the case of compounds **11b** and **11c**, each obtained from the common precursor **11a**. The presence of two orthogonal protecting groups in **11a** can selectively lead either to **11b** or **11c** according to deprotection conditions: the former was obtained by ester cleavage with TFA, while the latter via Fmoc removal in basic conditions.

The same orthogonal protecting group strategy was applied for the synthesis of the Asp derivative **12a**, synthetized in 65% yield from **2c-Linker 6** and the bis-protected precursor **12** under the same conditions described above. This product was used as starting material for the synthesis of RGD conjugates of **2c** containing the inhibitor attached to the Asp terminal residue of the tripeptide (chapter 3.3). The fully deprotected version of **12a** (**13b**) was obtained in two steps from Asp **13**, whose conjugation with **2c-Linker 6** first led to **13a** and then to the final product **13a** after simultaneous acidolysis of Boc and COOtBu protecting groups with TFA (Scheme 12).
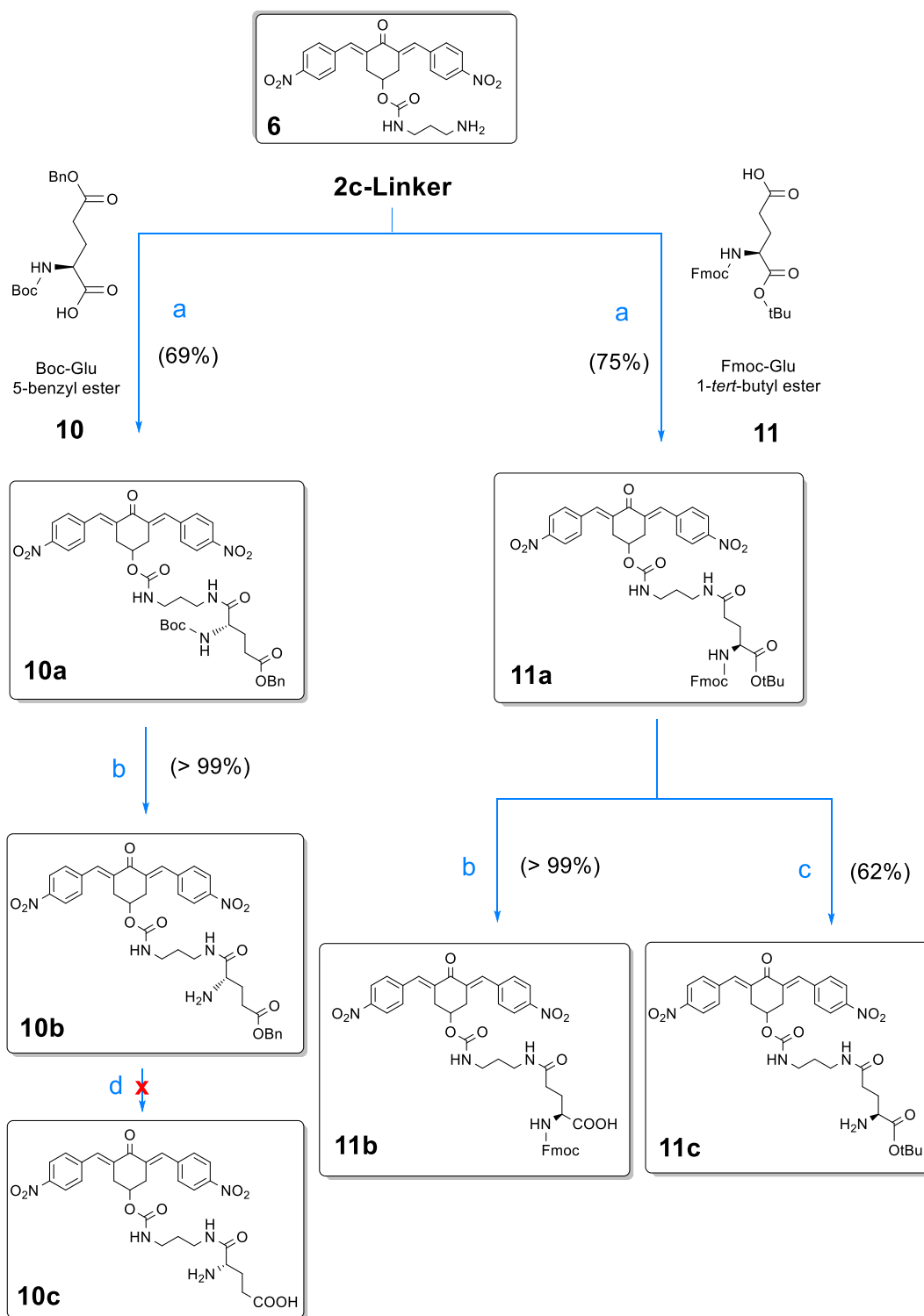
Scheme 11

Synthesis of Glu conjugates of **2c-Linker** (**10a-b** and **11a-c**).

Reagents and conditions: **a)** EDC (1.5 eq.), HOBt (1.5 eq.), DCM, TEA (pH 8÷9), r.t., 18h. **b)** TFA/CHCl₃ 20:80, r.t., 18h. **c)** NHEt₂/DCM 50:50, r.t., 20h. **d)** HBr (solution 30% in acetic acid), r.t., 16h
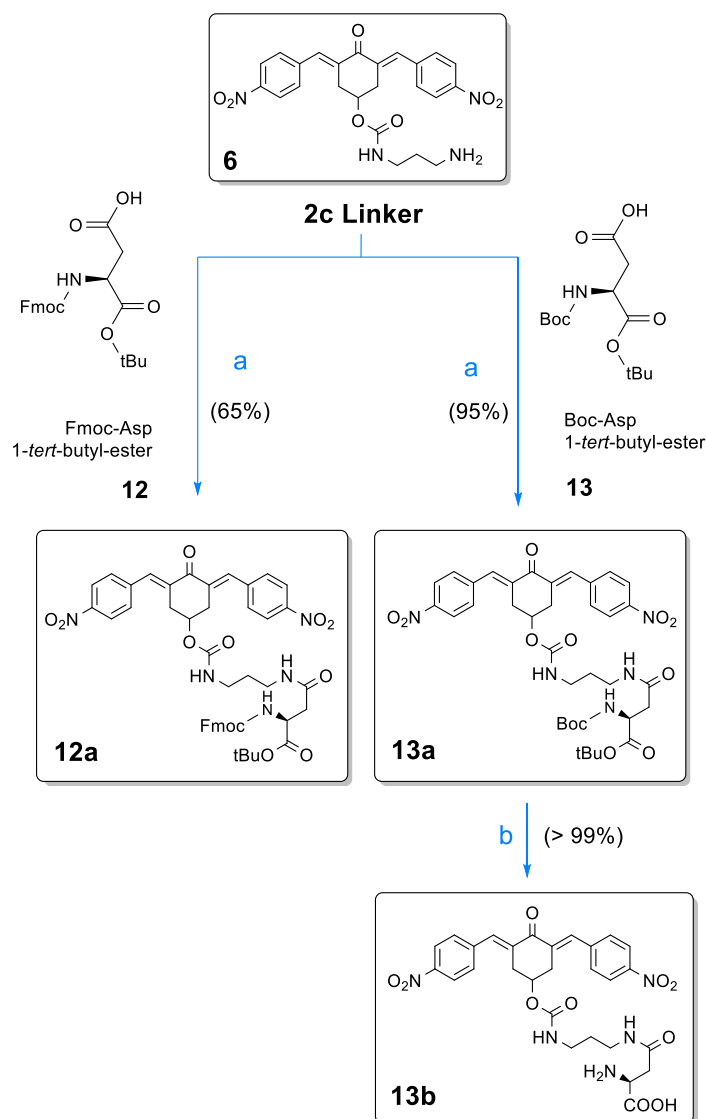
Scheme 12

Synthesis of Asp conjugates of **2c-Linker** (**12a** and **13a-b**).
Reagents and conditions: **a)** EDC (1.5 eq.), HOBt (1.5 eq.), DCM, TEA (pH 8÷9),
r.t., 18h. **b)** TFA/CHCl₃ 20:80, r.t., 18h.

The last amino acid conjugates of the second set were synthetized from **2c-Linker 6** and the Boc-protected serine β-Lactone **14**.[20] This latter precursor was isolated in 23% yield by Mitsunobu lactonization [21-22] of Boc-Ser (Scheme 13). This reaction was performed at – 78° C with diethyl azodicarboxylate (DEAD) and triphenylphosphine (PPh₃) in anhydrous THF, and the obtained product was purified by flash chromatography.[23] The yield was poor, in accordance with literature,[24] likely due to the instability of the DEAD-PPh₃ adduct formed in the first step, which tends to rapidly decompose before completing the reaction.
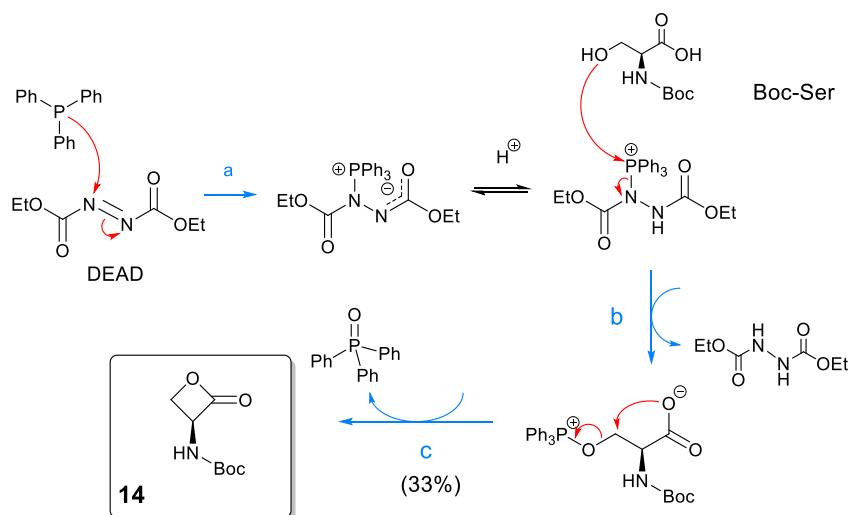
Scheme 13

Mitsunobu cyclization of Boc-Ser for the synthesis of the lactone **14**.
Reagents and conditions: THF$_{(anh)}$, -78° C→ r.t., 1h + 18h.
Mechanism: **a)** *In situ* formation of the highly electrophilic DEAD-PPh$_3$ adduct.
b) Activation of the OH group of Ser and displacement of the reduced form of
DEAD. **c)** Intramolecular S$_N$2 reaction and formation of the product **14** and
triphenylphosphine oxide.

The nucleophilic ring opening of **14** [23, 25] by the amino group of **2c-Linker 6**
occurred with poor regioselectivity, thus resulting in a mixture of serine amide **15a**
(29% yield) and β-functionalized alanine **16a** (10%) as the products of O-acyl and
O-alkyl fission respectively (Scheme 14). Most remarkably, the control of the
regioselectivity was a preeminent issue for the synthesis of **16a**, whose formation
was significantly disfavoured with respect to its isomer **15a**. The unreacted
2c-Linker precipitated from acetonitrile and was removed by filtration, then the
products **15a** and **16a** were easily separated by flash chromatography. The ^{1}H NMR
profile of **15a** is similar to that of **16a**, except for the presence of a broad signal at
6.72 ppm related to the amidic proton of the linker, which was absent in **16a**.
Few minor variations can also be detected in the ^{13}C NMR spectra.
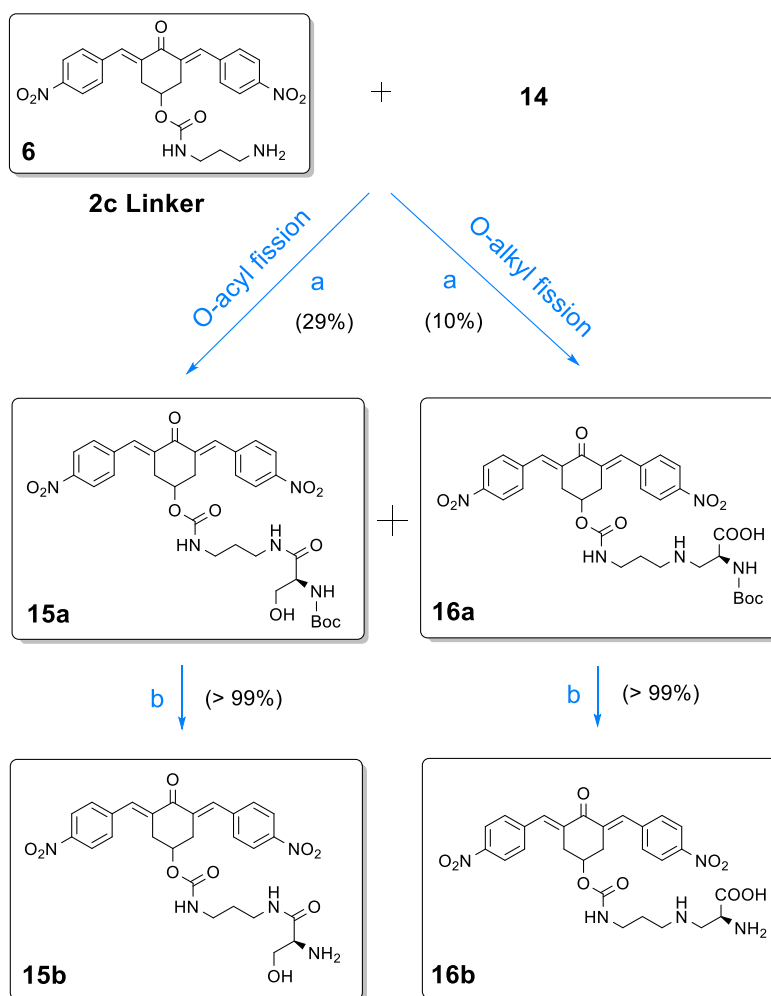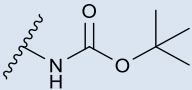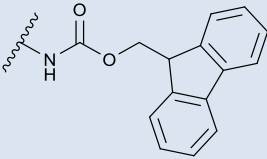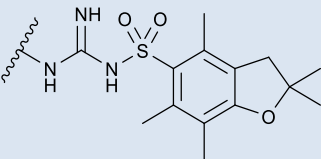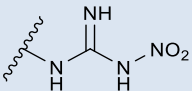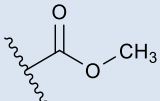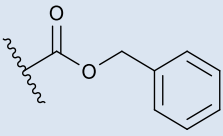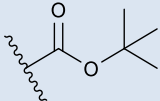
Scheme 14

Synthesis of Ser and Ala conjugates of **2c-Linker** (**15a-b** and **16a-b** respectively).
Reagents and conditions: **a)** ACN, TEA (pH 8÷9), r.t., 18h. **b)** TFA/CHCl₃ 20:80,
r.t., 18h.

As a natural development of the project, a selection of the previously collected conjugates were used as starting materials for the synthesis of the corresponding KGD and RGD conjugates of the inhibitor.

Table 8

List of the protecting groups for amines, guanidines, and carboxylic acids used in this work.

Protection	Name	Structure	Removal	Orthogonal to
NH$_2$	Boc [9-10]		→ CHCl$_3$/TFA 80:20 r.t., 1h up to 18h	Fmoc, COOMe, COOBn
	Fmoc [8]		→ NHEt2/DCM 50:50 18÷48 h. → H$_2$ (Pd/C) (Partially)	Boc, Pbf, COOtBu, COOBn, COOMe
Guanidine	Pbf [14]		→ CHCl$_3$/TFA 30:70 r.t., 1 up to 4 h	Fmoc, COOMe, COOBn
	NO$_2$ [15]		→ H$_2$ (Pd/C)*	Boc, Pbf, COOMe, COOtBu
COOH	COOMe [12, 16]		→ NaOH, H$_2$O (pH 14, Δ)	Boc, Pbf
	COOBn [18-17]		→ H$_2$ (Pd/C)* → HBr 30% in acetic acid	Depends on deprotection conditions**
	COOtBu [9-10, 19]		→ CHCl$_3$/TFA 20:80 r.t., 1 up to 4 h	Fmoc, COOMe, COOBn

* These conditions lead to the conjugate reduction of 2c.

** Orthogonal to Boc, COOMe, and COOtBu if removed by hydrogenolysis.

Orthogonal to Fmoc and NO$_2$ and partially orthogonal to COOMe and COOBn if removed by acidolysis.

As previously introduced, the conjugation of **2c** with peptide carriers bearing the Arg-Gly-Asp (RGD) motif should promote cell adhesion via integrine-binding, thus resulting in an increased selectivity against cancer cells. The cyclohexanone scaffold of **2c** was successfully functionalized with the RGD tripeptide and with the RGD-mimetic sequence KGD, in which the N-terminal Arg was replaced by a residue of Lys.[26] The synthesis of both KGD and RGD derivatives was aimed to evaluate the biological activities of the functionalized structures and compare them to that of the parent inhibitor. However, the synthesis of arginine-bearing peptides was complicated by the high robustness of the protecting groups necessary to mask the high nucleophilicity of the side chain guanidine groups and by the *in situ* cyclization of Arg, which often resulted in modest yields.[12, 13] On the other hand, the substitution of Arg with Lys usually improved the purification processes and led to peptide derivates that were easier to synthetize and purify compared to the Arg analogues. For this reason, the synthesis started with the KGD conjugates of **2c** and continued with the respective RGD analogues.

The Boc-protected Lys conjugates **7a** and **8a** were used as efficient building blocks to synthetize the KGD dimethyl ester derivatives **18a** and **19a**, each obtained via EDC/HOBt conventional peptide synthesis conditions with the complementary dipeptide fragment of Gly-Asp dimethyl ester **17** (Scheme 15). Both products were isolated in high purity by flash chromatography in 39% and 44% yields respectively. The removal of the Boc protection from **18a** and **19a** led quantitatively to the corresponding dimethyl esters **18b** and **19b**. However, multiple attempts to hydrolyze both methoxy groups of **19b** under different basic conditions always suffered from poor yields and conversions (Table 9) and did not lead to the desired product **19c**.
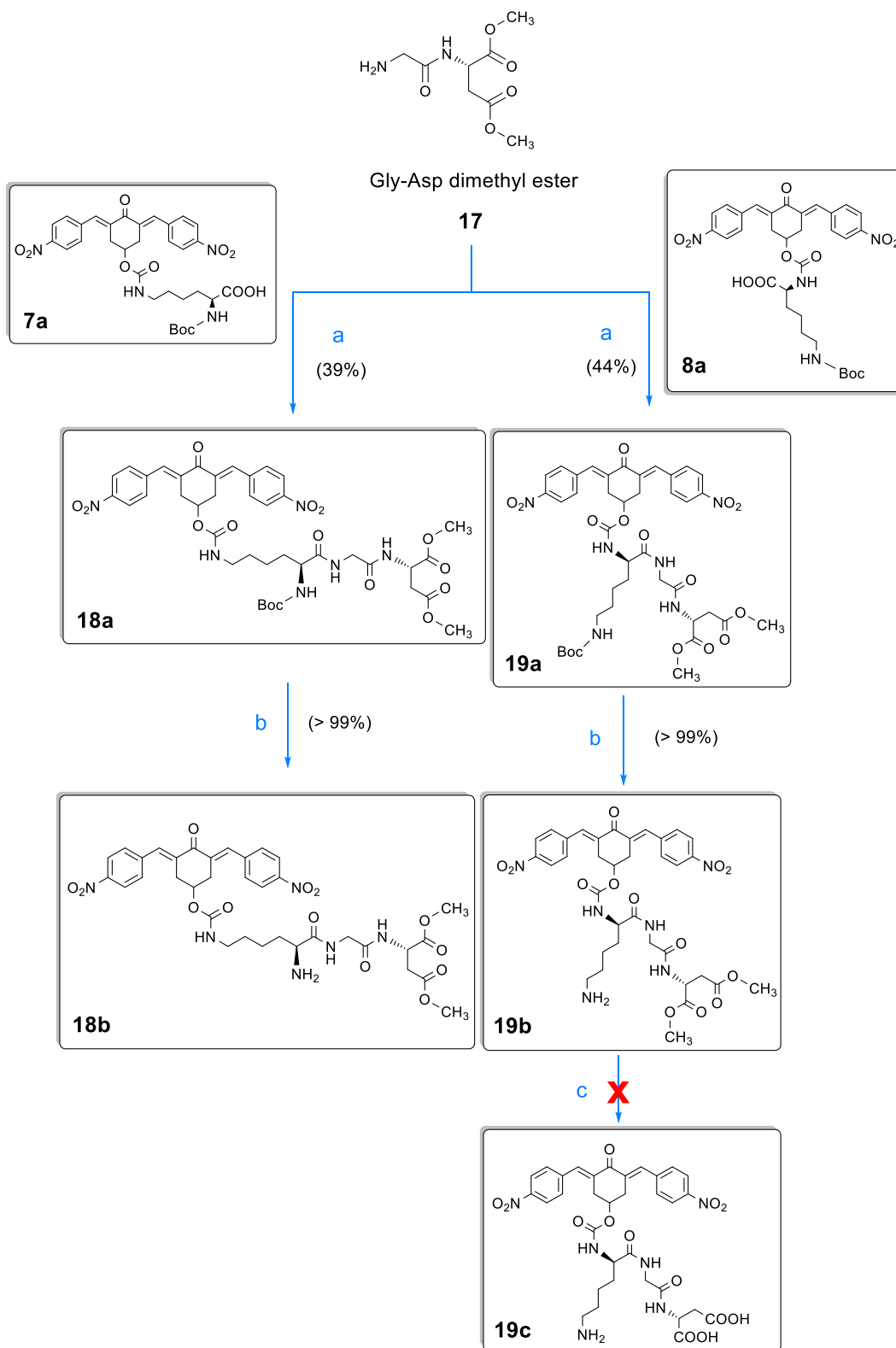
Scheme 15

Synthesis of KGD dimethyl esters conjugates of **2c** (**18a-b** and **19a-b**).
Reagents and conditions: **a)** EDC (1.5 eq.), HOBt (1.5 eq.), DCM, TEA (pH 8÷9),
r.t., 6÷18h. **b)** TFA/CHCl$_3$ 20:80, r.t., 18h. **c)** See Table 9.

Table 9

Attempts at basic hydrolysis of diester **19c**.

Base	Eq. of base per mol of diester	Solvent	Temperature	Time [h]	Result
KOH [16]	10:1	MeOH	Reflux	2	Decomposition of the mixture
	6:1	MeOH	50 °C	1	Poor conversion and mixture of partially-hydrolized products
	2:1	MeOH	25 °C	72	
	2:1	MeOH	25 °C	3	
	2:1	MeOH	25 °C	16	
NaOH	3:1	H$_2$O	Reflux	14	Full conversion, but difficult workup and product isolation

The ^{1}H NMR spectral window of this series of tripeptides can be divided in four regions of interest (Figure 31):

- The most downfield region of the spectrum, from 8.5 to 6.5 ppm, contains the 10 aromatic protons of the cross-conjugated dienone and the two peptidic N*H* protons of the backbone. In particular, the aromatic system of **2c** resonates in CDCl$_3$ as two AA'XX' multiplets system at 8.3 ppm and 7.6 ppm. The two vinylic protons, strongly deshielded due to the cross-conjugation, typically resonate as one broad singlet around 7.9 ppm.

- The 5.5 ÷ 4.5 ppm region is dominated by three well-resolved signals: the multiplet from 5.3 to 5.1 ppm contains two overlapped signals corresponding to the N*H* proton of Boc and to the C*H*-OCO proton of the cyclohexanone ring. The other signals, centered at 4.94 ppm and 4.83 ppm respectively, are referred to the urethane N*H* proton and to the C*H*^{α} proton of the Asp residue.

- The CH^α protons of Lys and Gly are slightly more shielded than that of Asp and are sometimes detected as two overlapping signals resonating from 4.2 ppm to 3.8 ppm. The CH_2^ϵ protons of Lys and the CH_2^β of Asp fall in the range $3.3 \div 2.8$ ppm, overlapped with the signal of the remaining methylene protons of the cyclohexanone scaffold as a complex multiplet. Each diastereotopic CH^β proton of Asp often appears as a narrow doublet of doublets at 2.99 ppm and 2.83 ppm respectively.

- The 9 protons of Boc and the CH_2^β, CH_2^γ, and CH_2^δ protons of the Lys side chain group span from 2.0 to 1.0 ppm.
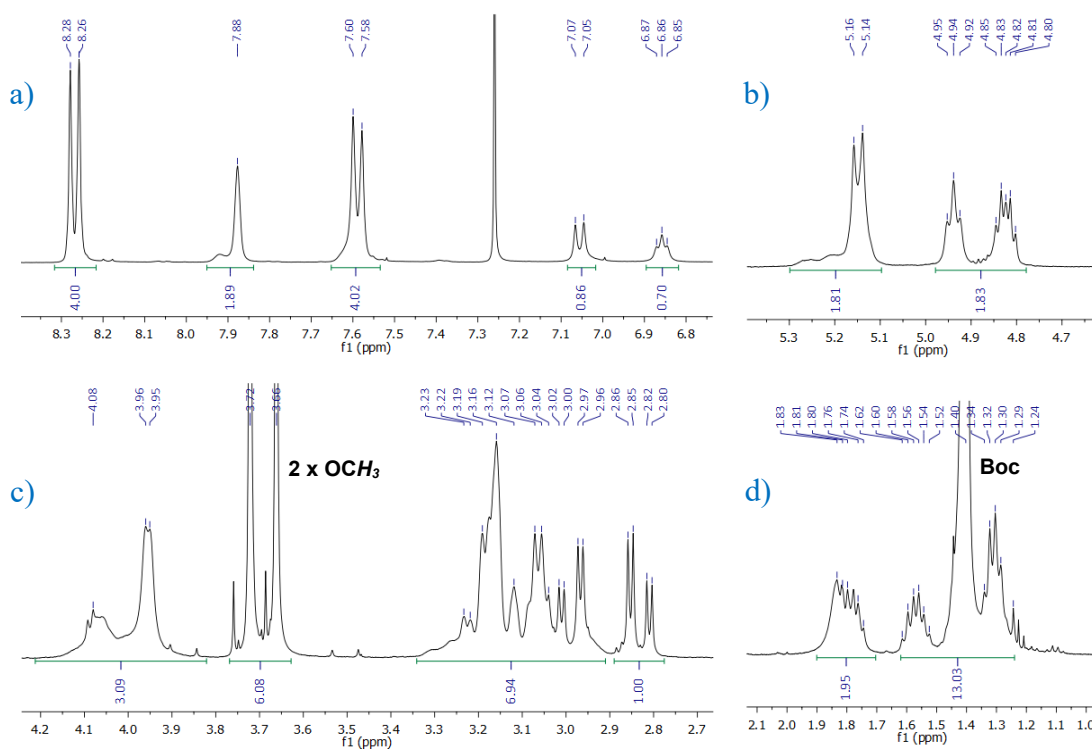
Figure 31

Partial ^{1}H NMR (CDCl$_3$, 500 MHz) spectra of **18a**: **a)** $8.5 \div 6.5$ ppm region. **b)** $5.5 \div 4.5$ ppm region. **c)** $4.2 \div 2.8$ ppm region. **d)** $2.0 \div 1.0$ ppm region. The full ^{1}H NMR spectrum of **18a** is reported on page 203 of the supporting material section (Figure 74).

A more efficient approach to remove the carboxylic protections from the Asp residue involved the use of the more labile benzyl esters: on the basis of this consideration, the tripeptide **19c** was obtained by two different synthetic routes, each starting from the dipeptide Gly-Asp dibenzyl ester **20** (Scheme 16). The first route proceeded through the formation of the KGD tripeptide **21a** via coupling of the free amino group of **20** with the commercially available N$^\alpha$-Fmoc-N$^\varepsilon$-Boc-Lys, and was followed by catalytic hydrogenation of benzyl esters and Fmoc removal to afford **21b**. The next steps consisted of the incorporation of **2c-OSu** into the peptide skeleton through the free α-amino group of the Lys residue, followed by final Boc deprotection. An alternative synthetic approach started with the conjugation of **20** to the C-terminus group of the Boc-protected Lys derivative **8a**, which led to the tripeptide **22a** with 56% of yield. At this point, the product **19a** could be either obtained by a two-steps deprotection or straightforwardly from **22a** using HBr/acetic acid. In the former case, the Boc protecting group was selectively removed with TFA, and the resulting diester **22b** was hydrolyzed to the corresponding dicarboxylic acid **19a** in the final step. In summary, the first synthetic route led to the deprotected product **19a** in five steps under milder reaction conditions, whereas the second path involved fewer reaction steps but under detrimental more aggressive acid conditions that resulted in a more difficult workup.

Gly-Asp dibenzyl ester

20

route I   *route II*

a
(51%)

N^{α}-Fmoc-N^{ε}-Boc-Lys

a
(56%)

8a

21a

(61%)

1) b
2) c

21b

4

2c-OSu

d
(56%)

21c

f
(86%)

22a

e
(> 99%)

22b

e
(> 99%)

f
(91%)

19c
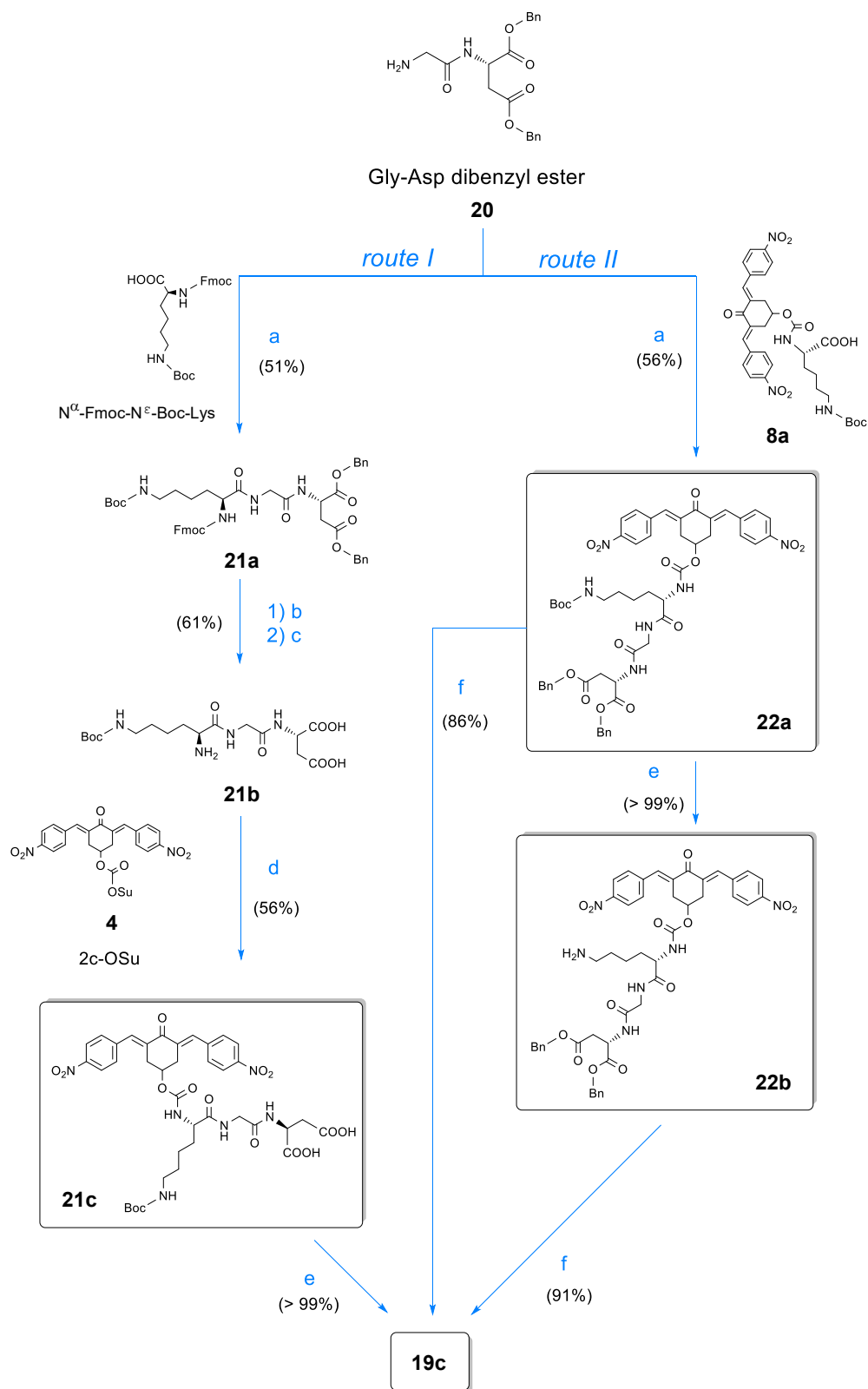
Scheme 16

Synthesis of KGD tripeptide conjugates of **2c** (**19c**, **21c**, and **22a-b**).
Reagents and conditions: **a)** EDC (1.5 eq.), HOBt (1.5 eq.), DCM, TEA (pH 8÷9),
r.t., 6÷18h. **b)** H_2 (10% Pd/C), MeOH, r.t., 22h. **c)** NHEt$_2$/DCM 50:50, r.t., 20h.
d) DMF, TEA (pH 8÷9), r.t., 20h. **e)** TFA/CHCl$_3$ 20:80, r.t., 18h. **f)** HBr (solution
30% in acetic acid), r.t., 16h.

The RGD conjugate **23a** was obtained from the coupling of the dipeptide Gly-Asp di-*tert*-butyl ester **23** with the Arg conjugate **9a** under the same conditions previously described for analogous compounds **18a**, **19a**, and **22a**. The final cleavage of both *tert*-butyl esters and Pbf protecting groups from **23a** was accomplished using a mixture of 75% of TFA in chloroform and led to the unprotected RGD tripeptide **23b** (Scheme 17) in 46% of overall yield.
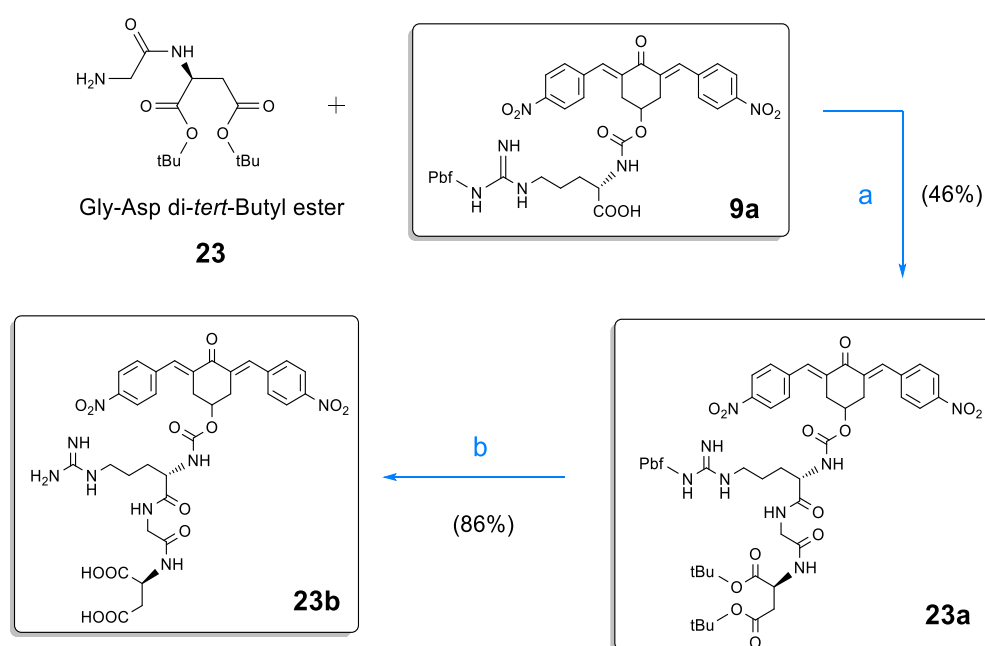
Scheme 17

Synthesis of RGD tripeptide conjugates of **2c** (**23a-b**).
Reagents and conditions: **a)** EDC (1.5 eq.), HOBt (1.5 eq.), DCM, TEA (pH 8÷9), r.t., 15h. **b)** TFA/CHCl$_3$ 75:25, r.t., 18h.

A further RGD conjugate of **2c-Linker** (**24c**) resulted to be the only derivative of the series with the pharmacophore linked to the C-terminal residue of the peptide carrier, and was synthetized to evaluate the effect of the functionalization of the terminal COOH group on the *in vitro* cytotoxicity. The product **24c** was obtained as a product of a five-step reaction from the Asp derivative **12a** and was isolated with a total yield of 19%. The synthetic procedure started with the cleavage of the α-Fmoc protecting group of **12a** and was followed by the coupling with Fmoc-Gly to afford the Fmoc-protected Gly-Asp dipeptide conjugate **24a**. A further Fmoc deprotection was needed to enable the final coupling with the bis-protected

arginine **24**, which led to the fully protected RGD conjugate **24b**. The final product **24c** was obtained after simultaneous acidolysis of all the protecting groups with TFA (Scheme 18).
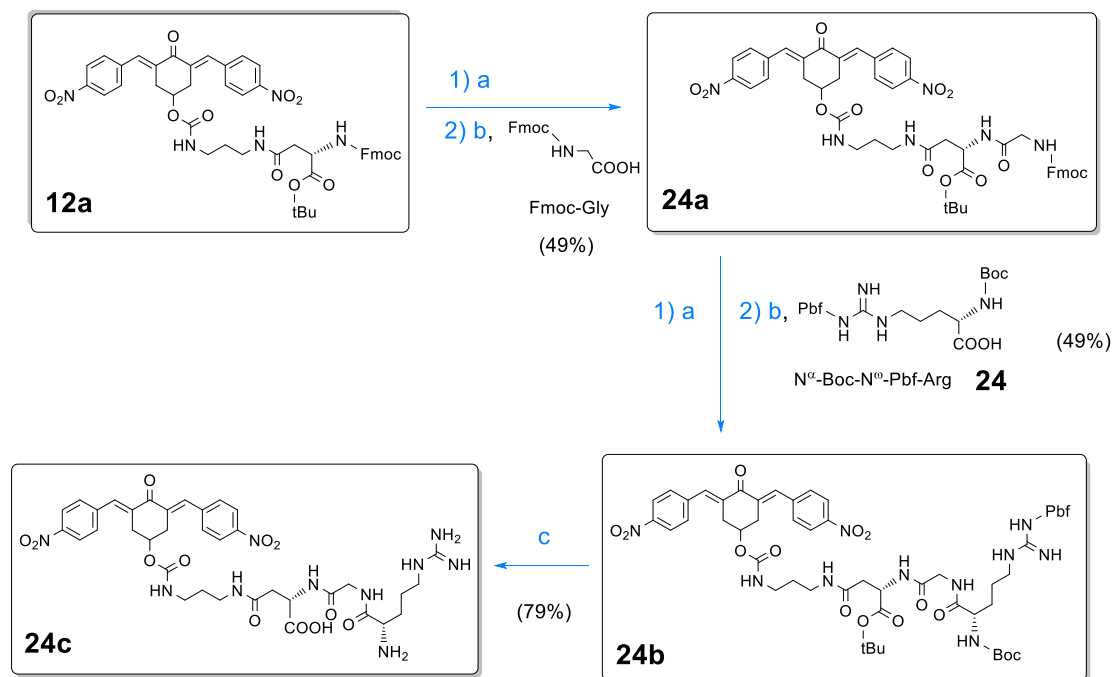
Scheme 18

Synthesis of RGD tripeptide conjugates of **2c-Linker** (**24b-c**).
Reagents and conditions: **a)** NHEt$_2$/DCM 50:50, r.t., 20h. **b)** EDC (1.5 eq.), HOBt (1.5 eq.), DCM, TEA (pH 8÷9), r.t., 15h. **c)** TFA/CHCl$_3$ 75:25, r.t., 18h.

Synthesis of the [D-Lys^6]-GnRH-I Conjugate

The reaction of **2c-OSu** with the commercially available decapeptide **25** under mild base catalysis in DMF led straightforwardly to the corresponding conjugate **25a** (Scheme 19). Since the various side chain groups of the peptide did not interfere with the coupling, no protecting groups were needed: for this reason, the product **25a** was easily purified in 77% yield after solvent evaporation and precipitation from chloroform. The formation of the product was evidenced by the prominent peak at 1713.8 m/z in the ESI-MS spectrum, corresponding to the protonated molecular ion. The complete assignment of all the proton resonances in

the ^{1}H NMR spectrum of **25a** was allowed by a combination of 1D and 2D NMR experiments. Most notably, the multiplet at 5.1 ppm, related to the cycloaliphatic C*H*-OCO proton highlighted in red, is, particularly diagnostic. In addition, the resonance of the carbamate N*H* proton (in cyan) at 7.0 ppm (detectable in the COSY NMR spectrum) also confirmed the formation of the coupling product. The peaks at 187.7 ppm and 155.6 ppm in the ^{13}C NMR spectrum, assigned to the carbonyl groups of the ketone and carbamate respectively, are also characteristic. It is also important to point out that the compound **25a** is the only hydrosoluble derivative of the entire library, and this promising feature makes it particularly suitable for further developments.
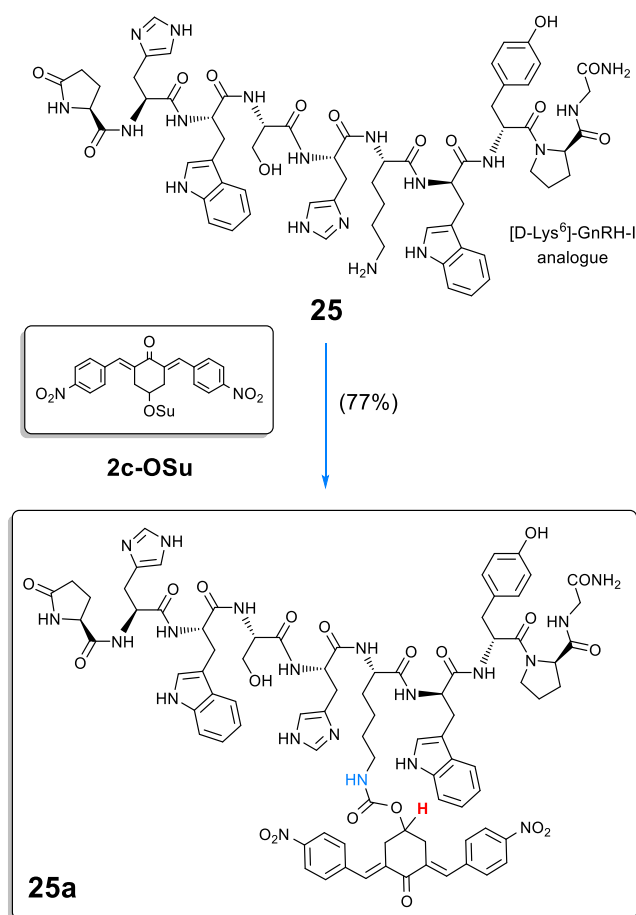
Scheme 19

Synthesis of the GnRH-I conjugate of **2c** (**25a**).
Reagents and conditions: DMF, TEA (pH 8÷9), r.t., 4h.
The most significant protons necessary for the characterization of the product **25a**
are highlighted in red and cyan.

Formation of the Michael Addiction Products

As thoroughly discussed in chapter 1.2, diaryldienones such as **2c** undergo Michael adduct formation with a broad range of cellular thiol targets,[27] displaying a remarkable selectivity for DUBs; however, the exact mechanism of DUBs inhibition exerted by **2c** has not been fully cleared yet. Because of this, a further extension of this project was the investigation of the reactivity of a simplified analogue of **2c** (**26**) toward sulphide nucleophiles that are supposed to mimic the catalytic Cys of a DUB. The compound **26** was obtained as a base-catalyzed Knoevenagel product from cyclohexanone and 4-nitrobenzaldehyde in the presence of Mg^{2+}, whose role was to generate a chelate complex of the intermediate β-hydroxyketone, thus preventing a further enolization.[28] The resulting intermediate was then dehydrated with $HCl_{(aq)}$ at pH 1 for 4 hours to finally afford the mono-enone **26**. The reaction of **26** with an equivalent amount of methyl thioglycolate at pH 8÷9 gave the Michael addition product **27 as** an approximately 1:1 mixture of sin and anti diastereoisomers (Scheme 20). The progress of the reaction was followed by NMR spectroscopy: as expected, the formation of the Michael adduct occurred rapidly within 30 minutes.
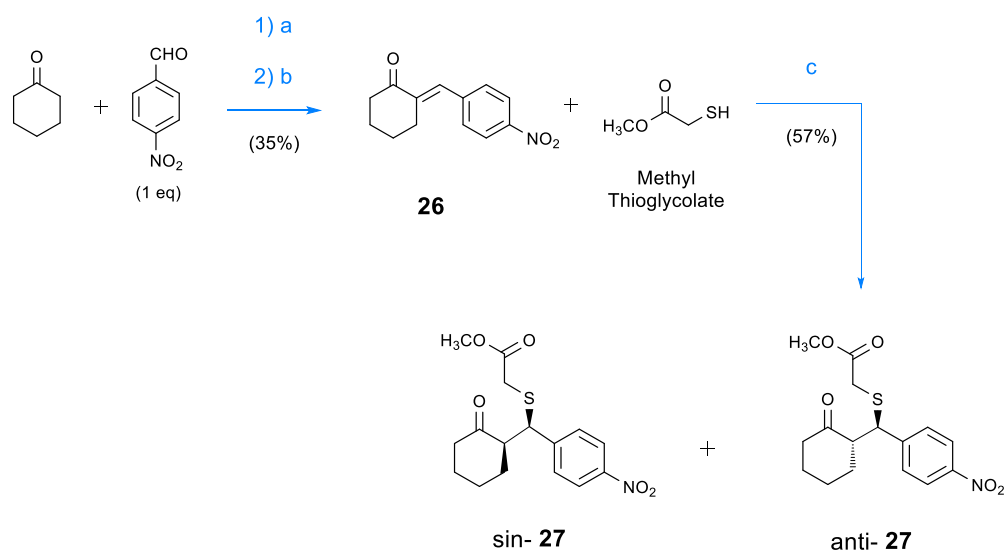
Scheme 20

a) $NaOH_{(aq)}$ 2% vol., $MgSO_4 \cdot 7H_2O$ (1 eq.) r.t., 18h. **b) (i)** $HCl_{(aq)}$ 0.1 M (pH 1), reflux, 4h. **(ii)** $KHCO_3$ (pH 6÷7). **c)** DCM, TEA (pH 8÷9), r.t., 30 min.

The ^{1}H spectrum of the quenched reaction showed the disappearance of the vinyl proton of **26** at 7.40 ppm and, most significantly, the formation of two well resolved pairs of doublets at 4.61 and 4.53 ppm for the C*H*-S proton of the two stereoisomers of the product, integrating jointly for a single proton (Figure 32). The other signals of the spectrum are also compatible with the structure of **27**, whose formation was also evidenced by the intense peak of the molecular ion found in the ESI-MS spectrum. In conclusion, the facile and rapid formation of the Michael addition product in solution further corroborates the proposed DUBs inhibition mechanism illustrated in Scheme 3.

Figure 32
a) ^{1}H NMR (CDCl$_3$, 500 MHz) of the precursor **26**.
b) ^{1}H NMR (CDCl$_3$, 500 MHz) of the mixture of products cis-**27** and trans-**27**.

References

1. Ghosh, A. K.; Brindisi, M. Organic Carbamates in Drug Design and Medicinal Chemistry. *J Med Chem* **2015**, 58, 2895-2940.

2. Matošević, A.; Bosak, A. Carbamate Group as Structural Motif in Drugs: a Review of Carbamate Derivatives Used as Therapeutic Agents. *Arh Hig Rada Toksikol* **2020**, 71, 285-299.
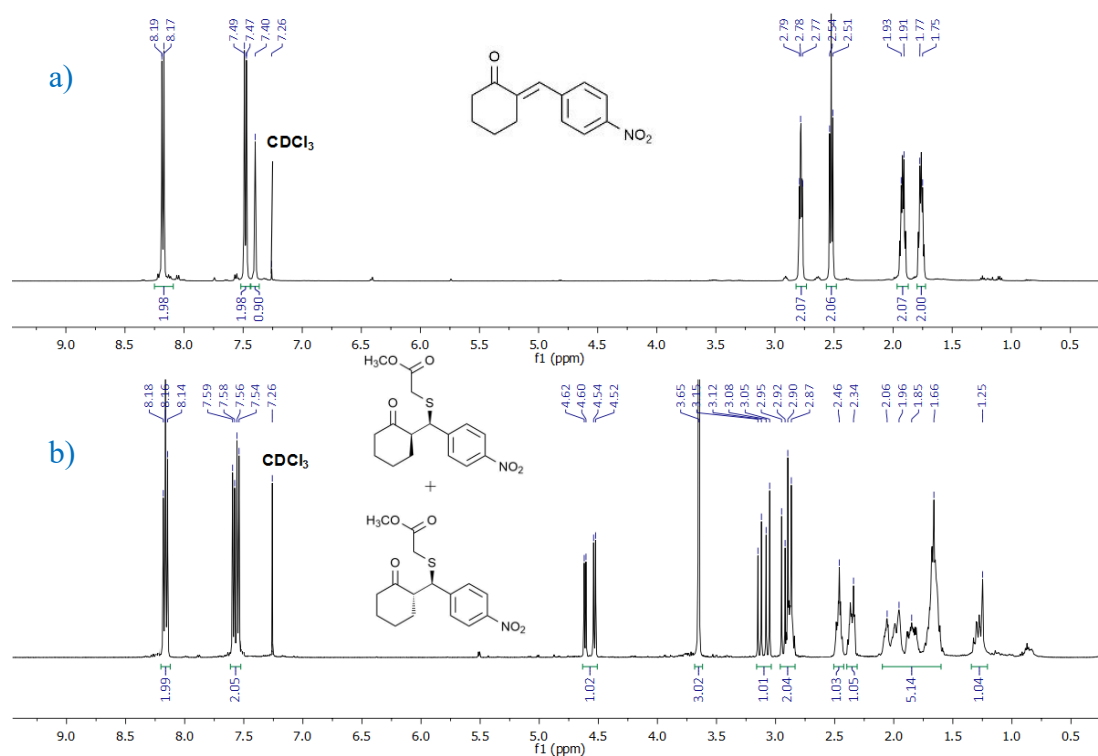
3. Cersosimo, U. et al. Synthesis, Characterization, and Optimization for In Vivo Delivery of a Nonselective Isopeptidase Inhibitor as New Antineoplastic Agent. *J Med Chem* **2015**, 58, 1691-704.

4. Jones, G. The Knoevenagel Condensation. *Org React* **1967**, 15, 204–599.

5. Tietze, L. F.; Beifuss, U. The Knoevenagel Reaction. In: *Comprehensive Organic Synthesis* **1991** (Pergamon Press).

6. Van Beurden, K.; De Koning, S.; Molendijk, D.; Van Schijndel, J. The Knoevenagel reaction: a review of the unfinished treasure map to forming carbon–carbon bonds. *Green Chem Lett Rev* **2020**, 13, 349-364.

7. Jalde, S. S. Synthesis of Novel Chlorin e6-Curcumin Conjugates as Photosensitizers for Photodynamic Therapy Against Pancreatic Carcinoma. Eur J Med Chem 2018, 147, 66-76.

8. Fields, G. B. Methods for Removing the Fmoc Group. *Methods Mol Biol* **1994**, 35, 17-27.

9. Anderson, G. W.; McGregor, A. C. t-Butyloxycarbonylamino Acids and Their Use in Peptide Synthesis. *J. Am. Chem. Soc*. **1957**, 79, 6180–6183.

10. Gibson, F. S.; Bergmeier, S. C.; Rapoport, H. Selective Removal of an N-BOC Protecting Group in the Presence of a tert-Butyl Ester and Other Acid-Sensitive Groups. *J. Org. Chem.* **1994**, 59, 3216–3218.

11. Greene, T. W.; Wuts, P. G. M. Protective Groups in Organic Synthesis, **1999** (Wiley).

12. Isidro-Llobet, A.; Alvarez, M.; Albericio, F. Amino Acid-Protecting Groups. *Chem Rev* **2009**, 109, 2455-2504.

13. Doherty-Kirby, A.; Lajoie, G. A. Side-Chain Protecting Groups. *Solid-Phase Synthesis, A Practical Guide*, Kates, S. A.; Albericio, F. eds., Marcel Dekker Inc.: New York. **2000**, 103-128.

14. Carpino, L. A. et al. The 2,2,4,6,7-Pentamethyldihydrobenzofuran-5-Sulfonyl Group (Pbf) as Arginine Side Chain Protectant. *Tetrahedron Lett*. **1993**, 34, 7829-7832.

15. Alhassan, M. et al. Revisiting NO_2 as Protecting Group of Arginine in Solid-Phase Peptide Synthesis. *Int. J. Mol. Sci*. **2020**, 21, 4464.

16. Khurana, J. M.; Chauhan, S.; Bansal, G. Facile Hydrolysis of Esters with KOH-Methanol at Ambient Temperature. *Monatsh. Chem*. **2004**, 135, 83–87.

17. Ben-Ishai, D. The Use of Hydrogen Bromide in Acetic Acid For The Removal of Carbobenzoxy Groups and Benzyl Esters of Peptide Derivatives. *J. Org. Chem*. **1954**, 19, 62–66.

18. Smith, H. L. Hydrogenolysis of Benzyl Esters with Palladiumon-Carbon Catalysts. *J Pharm Sci* **1965**, 54, 1269-1273.

19. Lundt, B. F.; Johansen, N. L.; Vølund, A.; Markussen, J. Removal of t-Butyl and t-Butoxycarbonyl Protecting Groups with Trifluoroacetic Acid. Mechanisms, Biproduct Formation and Evaluation of Scavengers. *Int J Pept Protein Res* **1978**, 12, 258-268.

20. Klinge, M; Vederas, J. C. N-Benzyloxycarbonyl-L-serine β-Lactone. In: *e-EROS: Encyclopedia Of reagents For organic Synthesis* **2001** (Wiley).

21. Mitsunobu, O. The Use of Diethyl Azodicarboxylate and Triphenylphosphine in Synthesis and Transformation of Natural Products. *Synthesis* **1981**, 1, 1-28.

22. Hughes, D. The Mitsunobu Reaction. In: *Organic Reactions* **1992** (Wiley), 42, 335-395.

23. Arnold, L. D.; Kalantar, T. H.; Vederas, J. C. Conversion of Serine to Stereochemically Pure β-Substituted α-Amino Acids via β-Lactones. *J. Am. Chem. Soc.* **1985**, 107, 7105-7109.

24. Schneider, A. et al. Stereoselective Synthesis of Boc-Protected L-Seleno- and Tellurolanthionine, L-Seleno- and Tellurocystine and Derivatives. *Tetrahedron Lett.* **2006**, 47, 1019-1021.

25. Ramer, S. E.; Moore, R.N.; Vederas, J. C. Mechanism of Formation of Serine β-Lactones by Mitsunobu Cyclization: Synthesis and Use of L-Serine Stereospecifically Labelled With Deuterium at C-3. *Can. J. Chem.* **1986**, 64, 706-713.

26. Wermuth, J.; Goodman, S. L.; Jonczyk, A.; Kessler, H. Stereoisomerism and Biological Activity of the Selective and Superactive αvβ3 Integrin Inhibitor cyclo(-RGDfV-) and Its Retro-Inverso Peptide. J. Am. Chem. Soc. **1997**, 119, 1328–1335.

27. Sauerland, M. et al. Kinetic Assessment of Michael Addition Reactions of α,β -Unsaturated Carbonyl Compounds to Amino Acid and Protein Thiols. *Free Radic. Biol. Med.* **2021**, 169, 1–11.

28. House, H. O. et al. Chemistry of Carbanions. XXIII. Use of Metal Complexes to Control the Aldol Condensation. *J. Am. Chem. Soc.* **1973**, 95, 3310-3324.

The Figure 33 shows the crystallographic structure of the UCHL5 member complexed with Ub: particularly noteworthy, the C-terminal residue of Ub (Gly[76]) is placed in the close proximity of the DUB's catalytic site loop. By this way, a 180° flip of the ubiquitinated substrate aligns the isopeptide bond with the catalytic Cys[88] residue of the enzyme and triggers the deubiquitinating process.
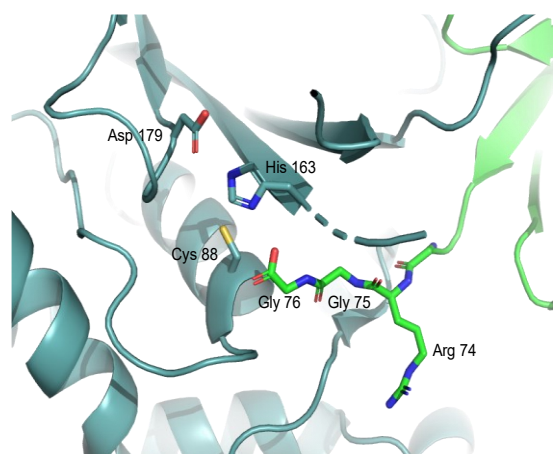
Figure 33

Structure of the non-covalent complex between UCHL5 (in blue) and Ub (in green): the residues of Asp[179], His[163] and Cys[88] of the catalytic triad are pointed out, together with the Arg[74]-Gly[75]-Gly[76] residues of the C-terminal portion of Ub.

The concept of the second part of the Project was inspired by the three-dimensional architecture of this complex and was focused on the design and synthesis of Ub-mimetic potential DUBs inhibitors. The pharmacophore portion was derived from the structure of typical cysteine protease inhibitors and was subsequently conjugated to the C-terminal sequence of the Ub monomer (consisting of the residues of Arg[74]-Gly[75]-Gly[76]) to ensure site-specific delivery.[1] The whole synthetic approach to obtain each compound of interest can be divided into the following main steps:

- Synthesis of the Michael acceptor if not readily available from commercial sources.

- Conjugation of the acceptor to the carboxylic group of Boc-Gly and subsequent coupling with Pbf-protected Arg, affording the final pseudopeptide (in which the Michael acceptor replaces the terminal residue of Gly[76]) via repeated steps of coupling/purification/deprotection (Scheme 21).
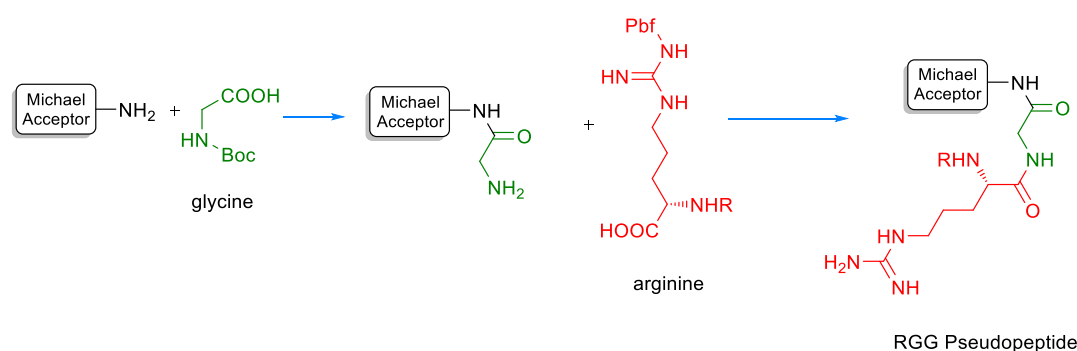
Scheme 21

General scheme for the synthesis of DUBs inhibitors based on the terminal tail of Ub.

Inhibitors Based on α,β-Unsaturated Esters

The first candidates as Michael acceptors were α,β-unsaturated esters [2-3] incorporated in an azetidenyl-based scaffold. Such four-membered rings are commonly found in several natural bioactive compounds and their application in the development of novel therapeutic agents is becoming wider.[4-7] Moreover, the intrinsic rigidity introduced by the azetidine ring typically confers to drugs an increased potency and binding affinity for cellular targets compared to more flexible analogues.[8-9]

The synthesis of compounds **31b** and **32b** started with the Boc deprotection of the commercial precursor *tert*-butyl 3-(2-ethoxy-2-oxoethylidene)azetidine-1-carboxylate, which led to the corresponding amine **28** whose structure comprises the

Michael acceptor (responsible for the alkylation of the catalytic thiol of DUBs), the azetidine core, and a secondary amino group necessary for the peptide bond formation. The next steps involved two sequential peptide couplings of **28** with Boc-Gly and N^α-Boc-N^ω-Pbf-Arg **24** to afford the Pbf-protected intermediate **31a** with 54% yield. The same procedure carried out with N^α-Acetyl-N^ω-Pbf-Arg **30** gave the acetylated analogue **32a** in 47% yield. The final TFA cleavage of the residual protecting group(s) led to the fully deprotected products **31b** (78%) and **32b** (71%), respectively. The complete reaction scheme is reported in Scheme 22.
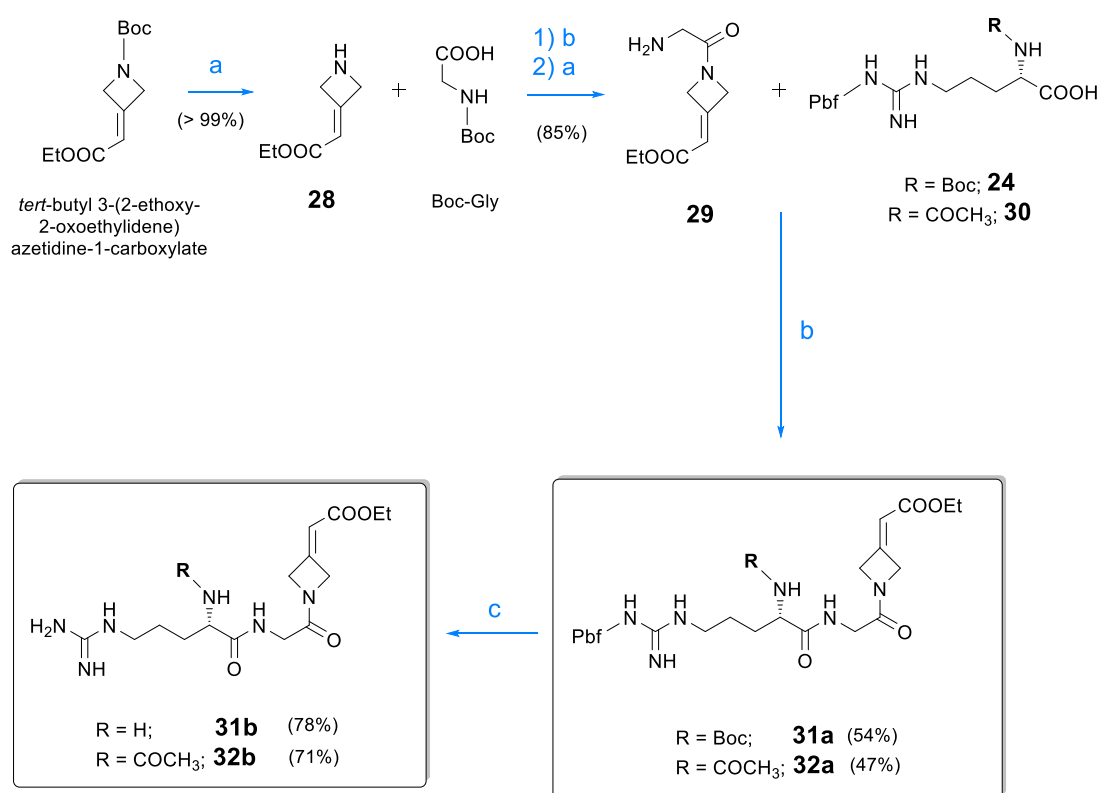
Scheme 22

Synthesis of azetidin-3-ylidenemethyl propionate derivatives **31a-b** and **32a-b**.
Reagents and conditions: **a)** TFA/CHCl$_3$ 20:80, r.t., 6h. **b)** DCM, TEA (pH 8÷9), r.t., 18h. **c)** TFA/CHCl$_3$ 70:30, r.t., 16h.

The synthesis of a N-acetylated analogue of **31b** was aimed to evaluate how the presence of an acetylated amino group within the primary sequence of the pseudopeptide impacts on the overall cytotoxic activity of the inhibitor. In addition,

as previously introduced, the N-acetylation of peptide-based drugs usually improves both *in-vivo* performance and druggability.[10]

The number of resonance signals found in the ^{1}H and ^{13}C NMR spectra of **31b** and **32b** evidenced that each compound exists as a mixture of two major conformers that interconvert by rotation around the CH–COOEt σ-bond (Scheme 23).[11] In some cases, it was possible to estimate the equilibrium ratio of the two conformers by integration of the corresponding signals in the ^{1}H NMR spectrum of the mixture. For example, the s-cis and s-trans rotamers of **31b** gave two well separated signals at 6.02 and 5.92 ppm, respectively, for the vinyl proton; therefore, the percentage of the more stable s-trans rotamer was calculated to be approximately 85%. The presence of two slow rotating conformers in solution was also revealed by the related carbon spectra. As expected, the effect was more pronounced for the nucleus close to the rotation centre, such as for those of the alkene (151 and 114 ppm), ester (60 and 13 ppm), and the remaining methylene carbons of the azetidine ring. The high purity profile of the final products was confirmed by the dominant peaks observed at m/z = 355.2 for **31b** and m/z = 397.2 for **32b** in the ESI-MS spectra, each due to the corresponding protonated compound.
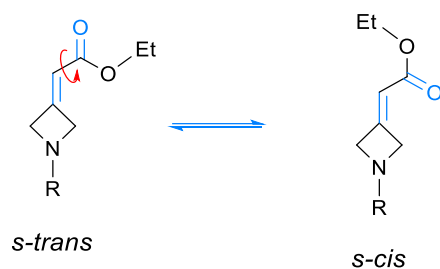
Scheme 23

The s-trans/s-cis equilibrium in compounds **28**, **29**, **31a-b**, and **32a-b**.
The two π-bonds of the alkene and carbonyl ester can be either on the same side of
the σ-bond (*s-cis* conformer) or on the opposite (*s-trans* conformer).

The α,β-unsaturated esters **37a** and **37b** were structurally based on the linear methyl (E)-4-aminobut-2-enoate scaffold,[12-17] and were obtained from 3-amino-1,2-propanediol following the protocol published by Johansson, H. et al (Scheme 24).[14]
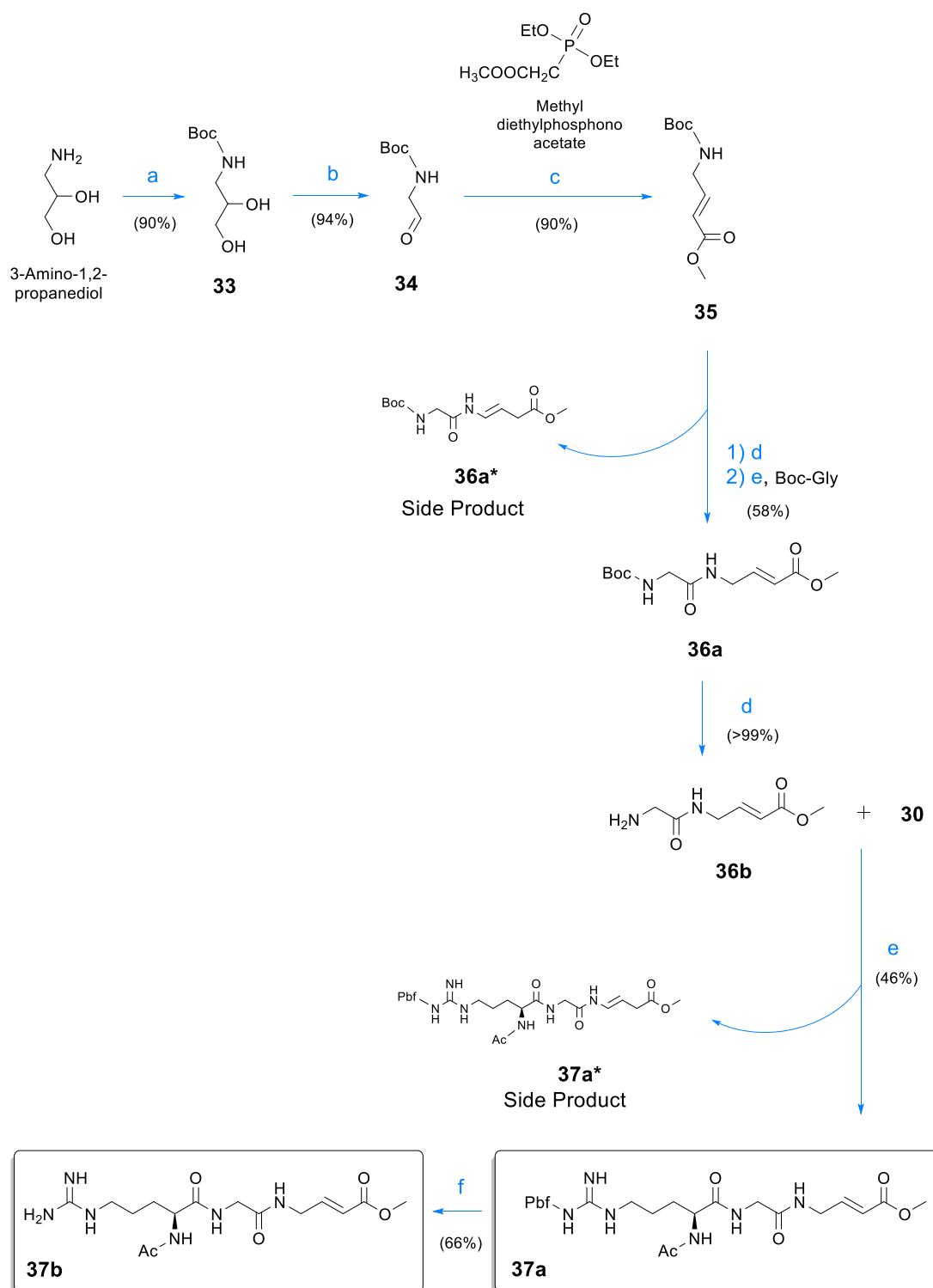
Scheme 24

Synthesis of methyl (E)-4-aminobut-2-enoate derivatives **37a-b**. *Reagents and conditions*: **a)** Boc$_2$O (1 eq.), DCM, MeOH, r.t., 18h. **b)** NaIO$_4$ (1 eq), H$_2$O, r.t., 1h. **c)** *t*-BuOK (1 eq), THF$_{(anh)}$, 0°C → r.t., 38 min + 3h. **d)** TFA/CHCl$_3$ 20:80, r.t., 18h. **e)** DCM, TEA (pH 8÷9), r.t., n.m.t. 45 min. **f)** TFA/CHCl$_3$ 75:25, r.t., 8h.

This procedure involved the oxidation-decarboxylation of the Boc-protected diol **33** with sodium periodate (NaIO$_4$), which gave the corresponding aldehyde **34** that was subsequently reacted in a Horner–Wadsworth–Emmons reaction [18] with an equivalent amount of methyl diethyl phosphonoacetate and potassium *tert*-butoxide (*t*-BuOK) to afford the conjugated alkene **35** in a total yield of 76% and in the expected E-configuration. The last stages of the synthesis consisted of the incorporation of the Michael acceptor **35** into the dipeptide sequence of N$^\alpha$-Acetyl-Arg-Gly under the conditions previously described, followed by Pbf removal to obtain the desired product **37b** (18% yield).

However, the yield in **37b** was lowered by the partial lactamization of the precursor **30** and formation of two unwanted enamines **36a*** and **37a*** during the two coupling steps. These latter side products were generated *in-situ* via double bond isomerization of the parent α,β-unsaturated esters and were removed by flash column chromatography. Since these parallel reactions are proved to be catalyzed by triethylamine (Scheme 25), yield could be improved by avoiding strong basic conditions and prolonged reaction. The ^{1}H NMR spectrum of **36a*** evidenced the presence of the enamine proton as a broad doublet at 8.8 ppm, as well as other significant differences from that of the related α,β-unsaturated ester **36a**, especially in the chemical shift and multiplicity of the vinyl protons signals (Figure 34).

36a   **36a***
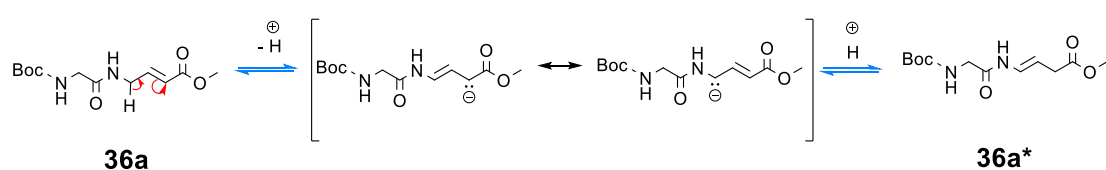
Scheme 25

Mechanism of base-catalyzed isomerization of the α,β-unsaturated ester **36a** into the corresponding enamine **36a***.
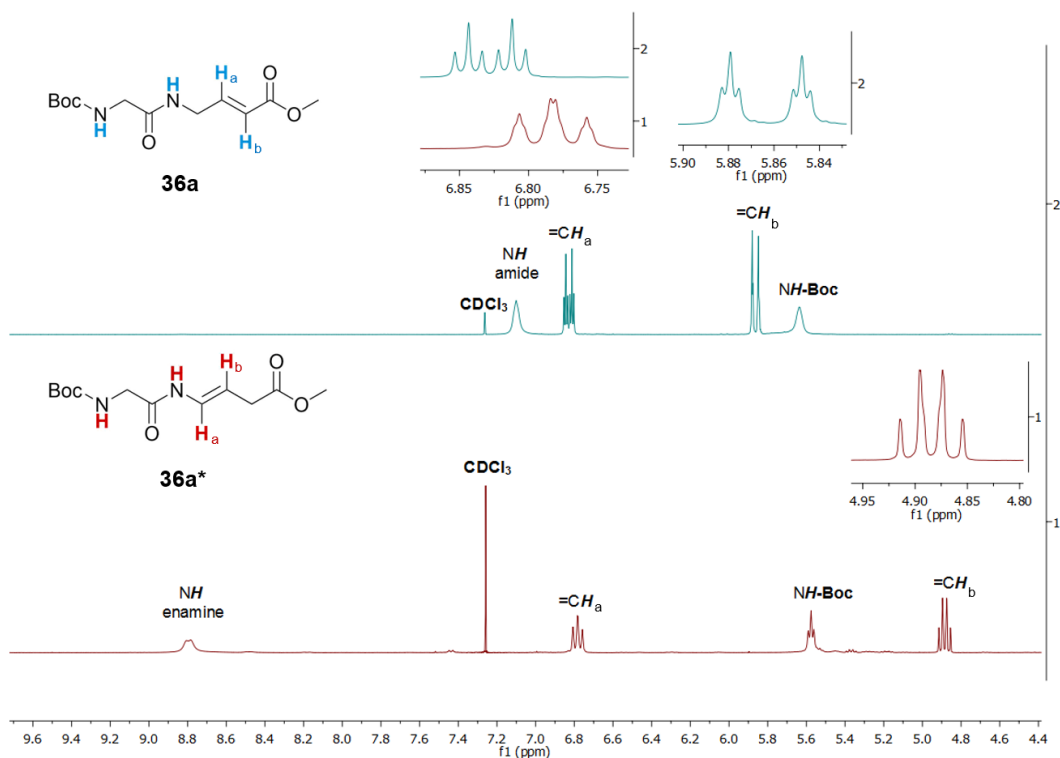
Figure 34

Overlay of the partial ¹H NMR spectra of the two isomers **36a** (cyan) and **36a*** (red)
in the region 4.5 ÷ 9.5 ppm.

The spectroscopic characterization of the final product **37b** confirmed the trans configuration of the alkene, as suggested by the values of the coupling constant of the two olefinic protons ($^3J_{trans}$ = 15.8 Hz). In particular, the vinyl proton adjacent to the carbonyl group of the ester appears as a doublet at 5.88 ppm, while the other resonates at 6.81 ppm as a doublet of triplets due to the coupling with the vicinal methylene protons. The complete characterization of the product was allowed by a combination of DEPT, COSY and HSQC experiments.

Alkynes are known to be mild electrophilic probes with a high affinity for cysteine proteases and reduced reactivity toward other cellular nucleophiles.[19-20] Molecules that bear this functional group undergo photochemically-induced thiol-yne addition with several protein thiols, resulting in the formation of alkenyl sulfide adducts [21-22] that lead to enzyme inactivation.

Based on this, we took into account two candidates containing an alkyne pharmacophore bonded to a piperazine scaffold. They were synthetized from 1-(prop-2-yn-1-yl)piperazine **38** via peptide coupling with either amino acid precursors **24** or **30**, affording products **39a** (52%) and **40a** (82%) respectively (Scheme 26). The former was purified by flash chromatography and then deprotected from Pbf to afford the product **39b** in 74% yield. The workup procedure to isolate the acetylated analogue **40a** was slightly different and involved an acidic workup with diluted HCl and extraction of the basified solution with dichloromethane. This procedure avoided tedious flash chromatography and resulted in pure **40a** with excellent yield. The final deprotection of **40a** to **40b** occurred in 69% yield.
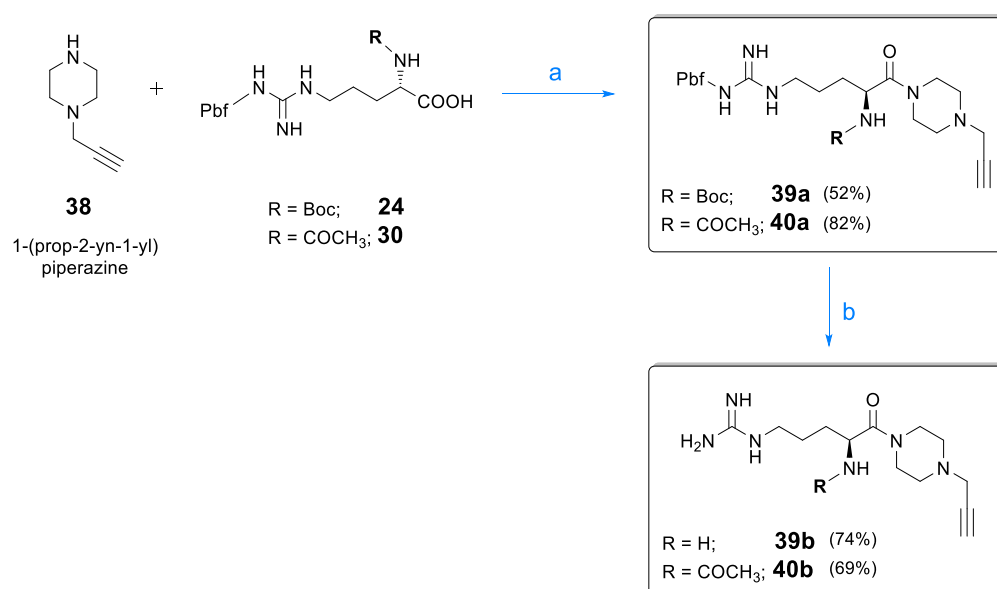
Scheme 26

Synthesis of 1-(prop-2-yn-1-yl)piperazine derivatives **39a-b** and **40a-b**. *Reagents and conditions*: **a)** DCM, TEA (pH 8÷9), r.t., 18h. **b)** TFA/CHCl$_3$ 75:25, r.t., 18h.

The second group of alkyne-bearing compounds that were synthetized have a propargylamide group [23-24] linked to the carboxylic group of the Arg-Gly dipeptide, whose terminal α-amino group can alternatively be free (**43b**), acetylated (**44b**), or Fmoc-protected (**45a**) (Scheme 27). Products **43b** and **44b** were obtained in four steps from propargylamine with a total yield of 35% and 39%, respectively, according to standard coupling procedures previously reported. The two orthogonal protecting groups in **45a** (Fmoc and Pbf) made it a suitable building block for further additions of amino acids to the N-terminal site of the sequence, resulting thus in longer pseudopeptides with a C-terminal acetylene group. All the products share the characteristic triplet signal of the acetylene proton, which spanned between 2.2. and 3.1 ppm in the ^{1}H NMR spectrum depending on the deuterated solvent. The triple bond was also identified in the carbon spectra, with the signals at 71.5 and 79.5 ppm in CDCl$_3$, or at 81.3 and 73.6 ppm in DMSO-d$_6$.
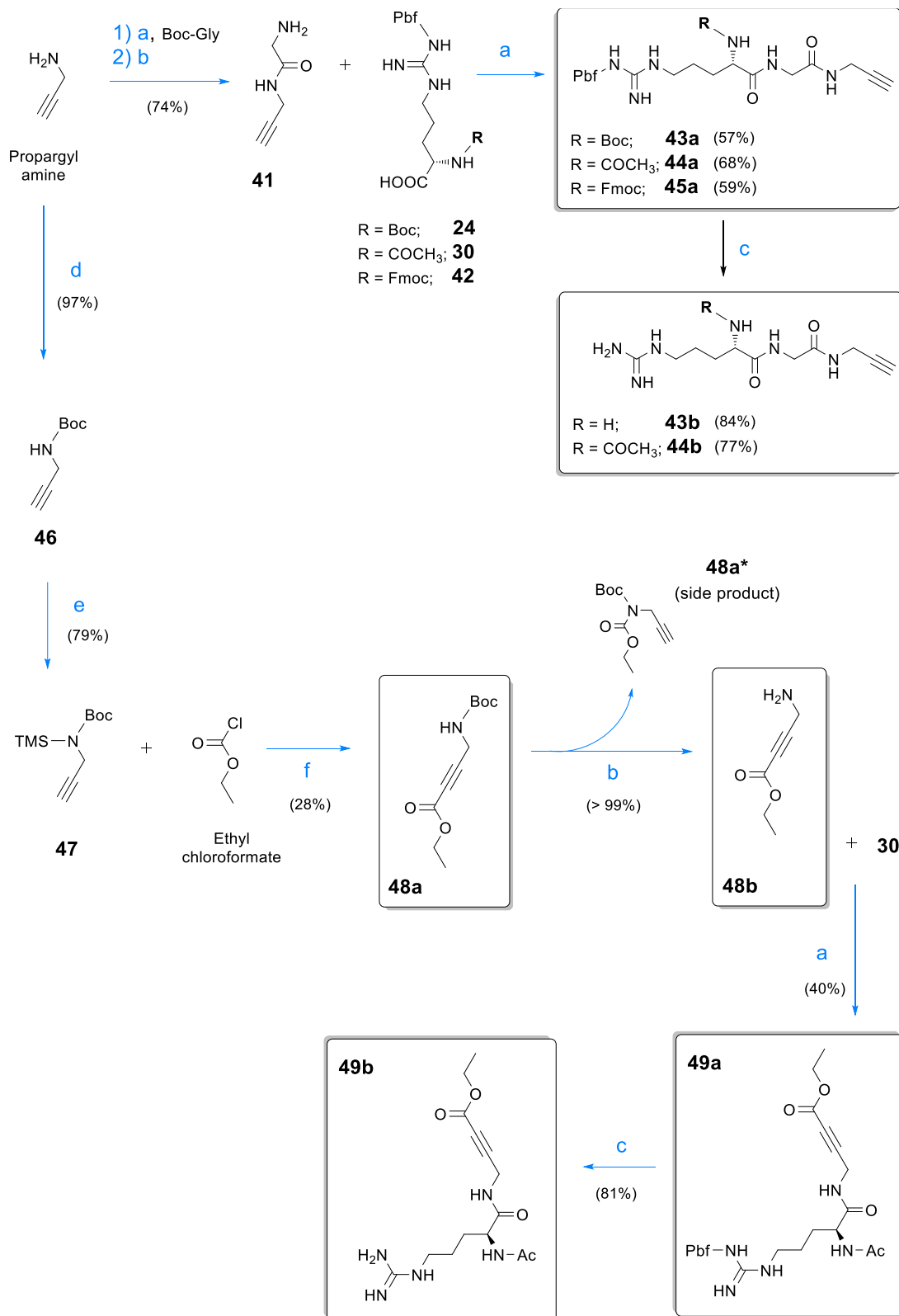
Scheme 27

Synthesis of propargylamide derivatives **43a-b**, **44a-b, 45a-b,** and **49a-b**. *Reagents and conditions*: **a)** DCM, TEA (pH 8÷9), r.t., n.m.t. 18h. **b)** TFA/CHCl₃ 20:80, r.t., 8h. **c)** TFA/CHCl₃ 75:25, r.t., 18h. **d)** Boc₂O (1 eq.), DCM, r.t., 18h. **e)** TMSOTf (1 eq.), TEA (1 eq.), DCM₍anh₎, 0°C → r.t., 40 min. **f)** LiN(SiMe₃)₂ (1 eq.), THF₍anh₎, −90°C → r.t., 40 min + 8h.

The direct conjugation of a terminal alkyne to electron withdrawing groups such as ketones, esters, or amides leads to the corresponding α,β-alkynyl carbonyl derivatives, which are versatile intermediates frequently used in medicinal chemistry. Despite such moieties can undergo nucleophilic attack either to the carbonyl or alkyne carbons, it is acknowledged that soft nucleophiles such as thiols prefer to furnish the 1,4-addition product (Scheme 28).[25-26] The synthesis of the Michael acceptor **48b** was inspired by a literature protocol [27-28] that involved the sequential deprotonation of the terminal alkyne of the Bis-N-protected propargylamine **47** with Lithium bis(trimethylsilyl)amide (LiN(SiMe$_3$)$_2$) and quenching with ethyl chloroformate (Scheme 27). The presence of Boc and trimethylsilyl protections at the amino group of **47** was required to minimize the formation of the N-acylated side product **48a***, recognizable by the triplet at 2.19 ppm of the acetylene proton. The α,β-alkynyl ester **48a** was thus isolated in 28% yield. Spectroscopic data matches those reported in literature for analog compounds.[29] The synthesis of the final product continued with the Boc-deprotection of **48a** and coupling of the resulting amino group with N^α-Acetyl-N^ω-Pbf **30**, followed by Pbf cleavage. In summary, the synthesis of **48b** occurred in six steps with a total yield of 7%.

R$_1$ = Et;
R$_2$ = CH$_2$NH$_2$;

48b
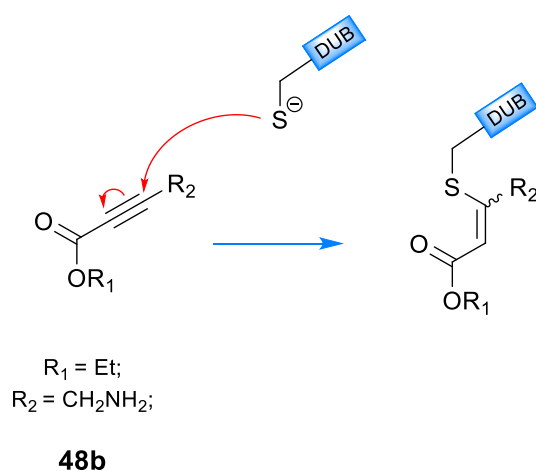
Scheme 28

1,4-conjugate additions to activated alkynes (thiol-yne addition).

Inhibitors Based on Vinyl Sulfones

The last compounds contain a phenyl vinyl sulfone pharmacophore, which is characteristically susceptible to the nucleophilic addition of catalytic thiols at the double bond (Scheme 29). Because of that, this group has received considerable attention over the last decade as an irreversible cysteine protease inhibitor.[30-33]

R = CH$_2$NH$_2$;

50b
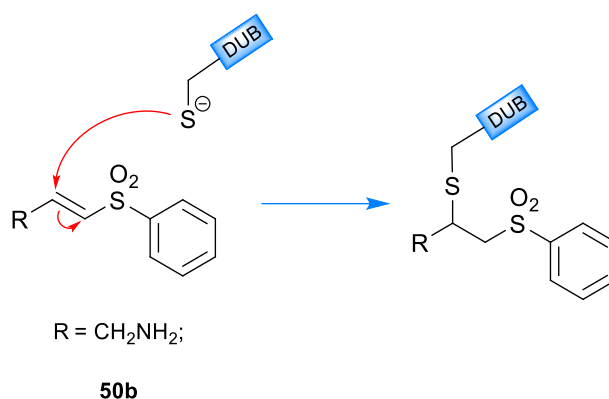
Scheme 29

1,4-conjugate additions to vinyl sulfones.

The synthesis of the pharmacophore **50b** was run following the procedure carried out by Zhang, H. et al.[31] and involved a Horner–Wadsworth–Emmons reaction of diethyl (phenylsulfonyl)methylphosphonate and the Boc-protected aldehyde **34** (Scheme 30). The reaction proceeded in three steps: first, formation of the phosphonate enolate intermediate, followed by reaction with **34** to afford the E-configured vinyl sulfone **50a**, and final Boc removal to give **50b** in 56% overall yield. The conjugation of the Michael acceptor **50b** with N$^\alpha$-Acetyl-N$^\omega$-Pbf **30** suffered from a partial *in-situ* isomerization of the product **51a** to the corresponding enamine **51a***, similarly to what reported for products **36a** and **37a**. The final compound **51b** was obtained in 67% yield from **51a** after TFA acidolysis of the Pbf protecting group. Spectroscopic data of **51b** were in accordance with the reported structure and stereochemistry.
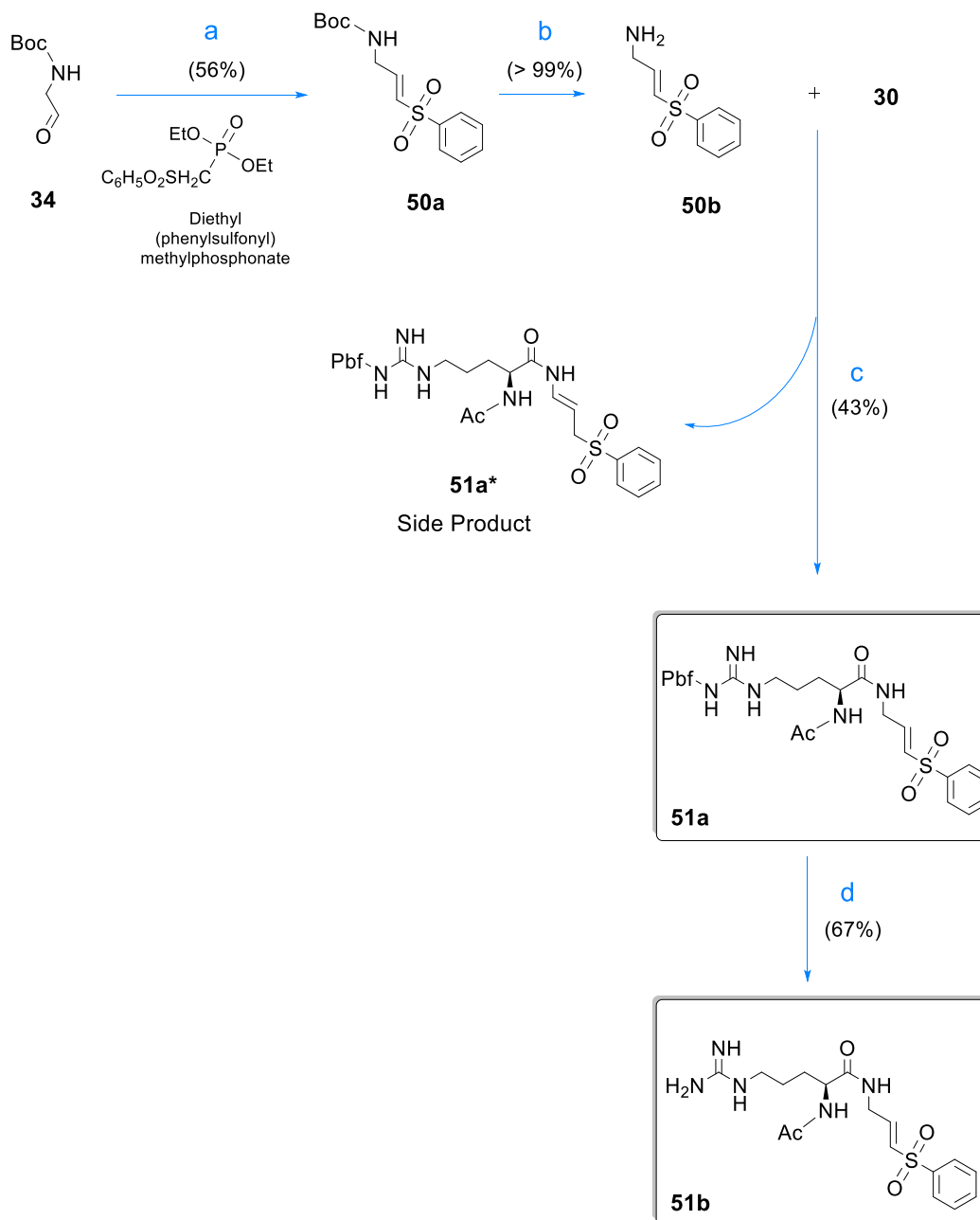
Scheme 30

Synthesis of phenyl vinyl sulfone derivatives **51a-b**. *Reagents and conditions*:
a) NaH (1.5 eq.), THF$_{(anh)}$, 0°C, 20 min + 5 min. **b)** TFA/CHCl$_3$ 20:80, r.t., 8h.
c) DCM, TEA (pH 8÷9), r.t., n.m.t. 1h. **d)** TFA/CHCl$_3$ 75:25, r.t., 18h.

In Vitro Evaluation of Antitumoral Activity

The potential antitumoral activity of each candidate was evaluated in collaboration with the group of Professor Gabriele Grassi (Università degli Studi di Trieste) using Kuramochi cell line as an *in vitro* model of human ovarian carcinoma. Among the tested compounds, only the derivatives **43b**, **44b**, and **51b** displayed a promising cytotoxic effect according to MTT test, a cell viability assay that was performed at various concentration of each inhibitor (1, 2, 4, and 10 µM) after 24 hours of exposure (Table 10 on page 106). The activity of these three samples was reported as % cell viability and compared to that of **2c** (reference) with the aim to identify novel hit compounds that displayed a similar dose-dependent cytotoxicity (Figure 35). The reduction of the carbonyl group of **2c** deletes the biological activity of the parental compound, and the resulting inactive isoform **VV1** was chosen as negative control in all experiments.

VV1
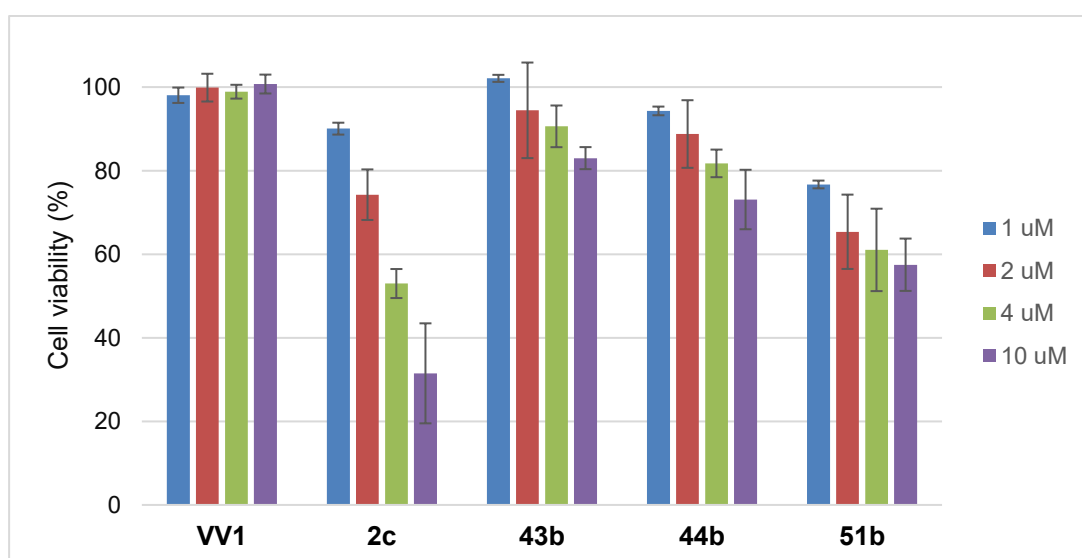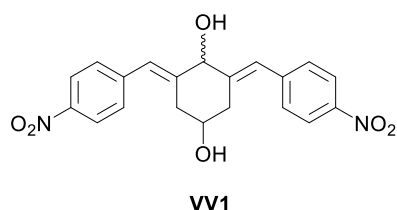
Figure 35

Citotoxicity of compounds **43b**, **44b**, and **51b** against Kuramochi cell line.

As shown in Figure 35, the compound **VV1** was inactive as expected, whereas compounds **43b**, **44b**, and **51b** induced a dose-dependent cell viability reduction. However, the overall effect was stronger for **2c**, which decreased the viability of Kuramochi cells more than the others for the entire range of concentrations tested, except for **51b** at 1 μM. On the basis of the half maximal inhibitory concentration values (IC$_{50}$), the most biologically active compound was **2c**, followed in order by the vinyl sulfone **51b** and propargylamide derivatives **44b** and **43b**. The last two compounds showed more or less the same activity, which was considerably lower to that of **51b**. The other candidates did not show appreciable cytotoxicity under the conditions of the assay. For this reason, the concentration range of **51b** was extended up to 200 μM, and it was found that this compound induced a 93% mortality at the highest concentration tested (Figure 36).
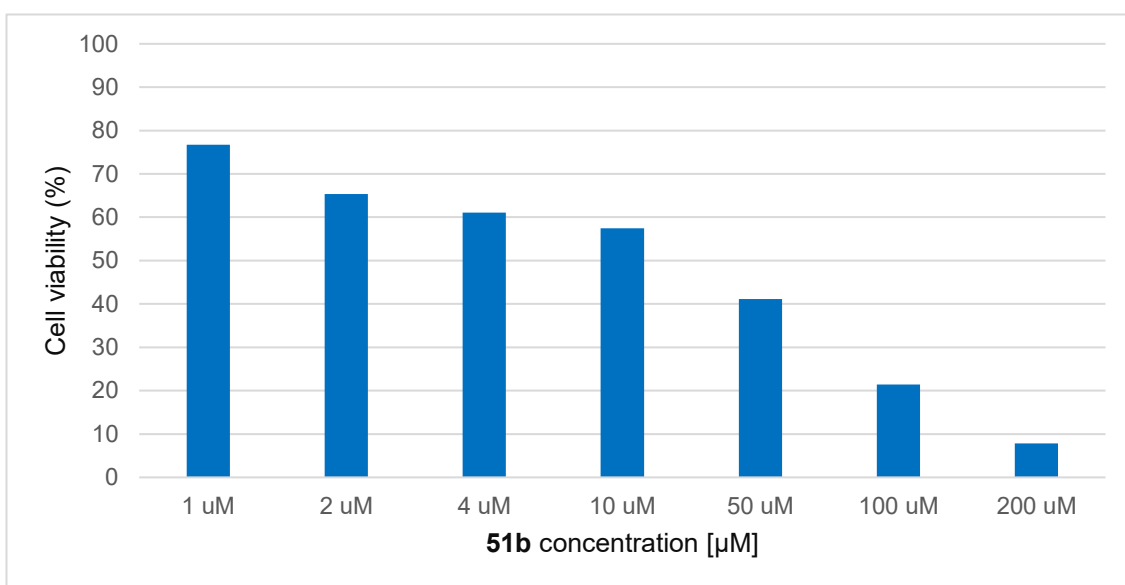
Figure 36

Cytotoxicity of **51b** against Kuramochi cell line in the concentrations range of
1 ÷ 200 μM.

Table 10

IC$_{50}$ values of tested candidates.

Compound	Structure	IC50 [μM]
2c (Reference)		4.85 ± 1.10
31b		Not Active
32b		Not Active
37b		Not Active
39b		Not Active
40b		Not Active
43b		46.71 ± 2.41
44b		40.18 ± 1.69
49b		Not Active
51b		10.95 ± 1.23

References

1. Hruby, V. J.; Olson, G. L. Prospects and Progress in Drug Design Based on Peptides and Proteins. *J Cell Biochem Suppl* **1993**, 17C, 201-237.

2. Jackson, P. A.; Widen, J. C.; Harki, D. A.; Brummond, K. M. Covalent Modifiers: A Chemical Perspective on the Reactivity of α,β-Unsaturated Carbonyls with Thiols via Hetero-Michael Addition Reactions. *J Med Chem* **2017**, 60, 839–885.

3. Amslinger, S. The Tunable Functionality of α,β-Unsaturated Carbonyl Compounds Enables Their Differential Application in Biological Systems. *ChemMedChem* **2010**, 5, 351-356.

4. Brandi, A.; Cicchi, S.; Cordero, F. M. Novel Syntheses of Azetidines and Azetidinones. *Chem Rev* **2008**, 108, 3988-4035.

5. Parmar, D. R. et al. Azetidines of Pharmacological Interest. *Arch Pharm.* **2021**; e2100062.

6. Mughal, H; Szostak, M. Recent Advances in the Synthesis and Reactivity of Azetidines: Strain-Driven Character of the Four-Membered Heterocycle. *Org Biomol Chem* **2021**, 19, 3274-3286.

7. Alcaide, B.; Almendros, P.; Aragoncillo, C. Highly Reactive 4-Membered Ring Nitrogen-Containing Heterocycles: Synthesis and Properties. *Curr Opin Drug Discov Devel* **2010**, 13, 685-697.

8. Pavone, V.; Lombardi, A.; Maggi, C. A.; Quartara, L.; Pedone, C. Conformational Rigidity Versus Flexibility in a Novel Peptidic Neurokinin A Receptor Antagonist. *J Pept Sci* **1995**, 1, 236-240.

9. Lawson, A. D. G.; MacCoss, M; Heer, J. P. Importance of Rigidity in Designing Small Molecule Drugs To Tackle Protein-Protein Interactions (PPIs) through Stabilization of Desired Conformers. *J Med Chem* **2018**, 61, 4283-4289.

10. Di, L. Strategic Approaches to Optimizing Peptide ADME Properties. *AAPS J* **2015**, 17, 134-143.

11. Hu, D. X.; Grice, P.; Ley, S. V. Rotamers or Diastereomers? An Overlooked NMR Solution. *J Org Chem* **2012**, 77, 5198-5202.

12. Liu, S.; Hanzlik, R. P. Structure-Activity Relationships for Inhibition of Papain by Peptide Michael Acceptors. *J Med Chem* **1992**, 35, 1067-1075.

13. Thompson, S. A.; Andrews, P. R.; Hanzlik, R. P. Carboxyl-Modified Amino Acids and Peptides as Protease Inhibitors. *J Med Chem* **1986**, 29, 104-111.

14. Johansson, H. et al. Fragment-Based Covalent Ligand Screening Enables Rapid Discovery of Inhibitors for the RBR E3 Ubiquitin Ligase HOIP. *J. Am. Chem. Soc.* **2019**, 141, 6, 2703–2712.

15. Kathman, S. G.; Xu, Z.; Statsyuk, A.V. A Fragment-Based Method to Discover Irreversible Covalent Inhibitors of Cysteine Proteases. *J Med Chem* **2014**, 57, 4969–4974.

16. McShan, D. et al. Identification of Non-Peptidic Cysteine Reactive Fragments as Inhibitors of Cysteine Protease Rhodesain. *Bioorg. Med Chem Lett* **2015**, 25, 4509-4512.

17. Kathman, S. G. A Small Molecule That Switches a Ubiquitin Ligase from a Processive to a Distributive Enzymatic Mechanism. *J Am Chem Soc* **2015**, 137, 12442–12445.

18. Wadsworth, W. Synthetic Applications of Phosphoryl Stabilized Anions. In: *Organic Reactions* **1977** (Wiley), 25, 73–250.

19. Talete, T. T. Acetylene Group, Friend or Foe in Medicinal Chemistry. *J. Med. Chem.* **2020**, 63, 11, 5625–5663.

20. Mons, E. et al. The Alkyne Moiety as a Latent Electrophile in Irreversible Covalent Small Molecule Inhibitors of Cathepsin K. *J Am Chem Soc* **2019**, 141, 3507-3514.

21. Lowe, A. B.; Hoyleb, C. E.; Bowman, C. N. Thiol-Yne Click Chemistry: A Powerful and Versatile Methodology for Materials Synthesis. *J Mater Chem* **2010**, 20, 4745-4750.

22. Minozzi, M. et al. An Insight into the Radical Thiol/Yne Coupling: The Emergence of Arylalkyne-Tagged Sugars for the Direct Photoinduced Glycosylation of Cysteine-Containing Peptides. *J. Org. Chem*. **2011**, 76, 450–459.

23. Ekkebus, R. et al. On Terminal Alkynes That Can React with Active-Site Cysteine Nucleophiles in Proteases. *J Am Chem Soc* **2013**, 135, 2867-2870.

24. Arkona, C.; Rademann, J. Propargyl Amides as Irreversible Inhibitors of Cysteine Proteases-A Lesson on the Biological Reactivity of Alkynes. *Angew Chem Int Ed Engl* **2013**, 52, 8210-8212.

25. Worch, J. C.; Stubbs, C. J.; Price, M.; Dove, A. P. Click Nucleophilic Conjugate Additions to Activated Alkynes: Exploring Thiol-yne, Amino-yne, and Hydroxyl-yne Reactions from (Bio)Organic to Polymer Chemistry. *Chem. Rev.* **2021**, 121, 6744–6776.

26. Fraile, A.; Parra, A.; Tortosa, M.; Organocatalytic Transformations of Alkynals, Alkynones, Propriolates, and Related Electron-Deficient Alkynes. *Tetrahedron* **2014**, 70, 9145–9173.

27. Reginato, G.; Mordini, A.; Caracciolo, M. Synthetic Elaboration of the Side Chain of (*R*)-2,2-Dimethyl-3-(*tert*-butoxycarbonyl)-4-ethynyloxazolidine: A New Regio- and Stereoselective Strategy to δ-Functionalized β-Amino Alcohols. *J. Org. Chem.* **1997**, 62, 18, 6187–6192.

28. Trost, B. M.; Lumb, J-P; Azzarelli, J. M. An Atom-Economic Synthesis of Nitrogen Heterocycles from Alkynes. *J. Am. Chem. Soc.* **2011**, 133, 740–743.

29. Paul, A. et al. Novel Triazolopeptides: Chirospecific Synthesis and Conformational Studies of Proline Derived Analogs. *Tetrahedron* **2009**, 65, 6156-6168.

30. Palmer, J. T.; Rasnick, D.; Klaus, J. L.; Bromme, D. Vinyl Sulfones as Mechanism-Based Cysteine Protease Inhibitors. *J Med Chem* **1995**, 38, 17, 3193–3196.

31. Zhang, H. et al. Vinyl Sulfone-Based Inhibitors of Trypanosomal Cysteine Protease Rhodesain with Improved Antitrypanosomal Activities. *Bioorg Med Chem Lett* **2020**, 30, 127217.

32. Schneider, T. H. et al. Vinyl Sulfone Building Blocks in Covalently Reversible Reactions with Thiols. *New J Chem* **2015**, 39, 5841–5853.

33. Breuer, C.; Lemke, C.; Schmitz, J.; Bartz, U.; Gütschow, M. Synthesis and Kinetic Evaluation of Ethyl Acrylate and Vinyl Sulfone Derived Inhibitors for Human Cysteine Cathepsins. *Bioorg Med Chem Lett* **2018**, 28, 2008-2012.

1. INTRODUCTION

2. AIM

3. RESULTS AND DISCUSSION

4. CONCLUSIONS

5. EXPERIMENTAL SECTION

6. SUPPORTING MATERIAL

Conclusions and Future Perspectives

DUBs are involved in multiple cellular processes and are commonly overexpressed in different tumours, suggesting an important role in cancer onset and development. For this reason, they have become an attractive drug target for the design of irreversible small molecules inhibitors with potential antineoplastic activity. However, the lack of selectivity represents a common issue for the development of covalent inhibitors, particularly when a DUB is the inhibitor's target. This thesis proposes an efficient and reproducible methodology for the synthesis of 22 selective inhibitors of cysteine-dependent DUBs based on different Michael acceptor pharmacophores.

The first part was focused on the structural optimization of the partially selective inhibitor **2c** via insertion of tumor-targeting peptides on the cyclohexanone scaffold, aiming at the enhancement of its selectivity and targeted drug delivery. This led to the synthesis of 12 derivatives of the bis(arylidene) cyclohexanone scaffold compound **2c**, each obtained via standard peptide coupling of the parent inhibitor with different amino acids and peptides (such as RGD and GnRH-I analogues), together with the isolation of 20 different intermediates particularly useful for future developments. The inhibitory activity of these compounds is related to the presence of the 1,5-diaryl-3-oxo-1,4-pentadienilic core, which selectively react as Michael acceptor with multiple cellular thiols, including cysteine-dependent DUBs. The cytotoxic effect of this series of peptide conjugates of **2c** is still under investigation towards different types of tumours, including ovarian carcinoma and leiomyosarcoma. In addition, their potential antiviral properties are currently being evaluated against PLpro from SARS-CoV-2.

The second part of the thesis reported the synthetic protocol for 10 Ub-mimetic pseudopeptides bearing an electrophilic probe specific for the alkylation of the catalytic Cys residue of DUBs. Each of these compounds was obtained as a product of a multi-step reaction from inexpensive and commercially available starting materials in modest to good yields. Nevertheless, the reaction conditions

should be further optimized, especially regarding the coupling steps that leads to the α,β-unsaturated ester **37b** and vinyl sulfone **51b**.

In conclusion, compounds **43b**, **44b** and **51b** reduced the cell viability of Kuramochi tumor cell line on preliminary MTT assays, suggesting a potential antitumoral activity. Based on these encouraging results, the compound **51b** has been selected as promising lead compound for further optimizations. Such optimization processes include, but are not limited to, the synthesis of vinyl sulfone analogues, introduction of withdrawing substituents on the aromatic ring to increase the reactivity, and elongation of the peptide chain attached to the acceptor (Figure 37). Despite the other compounds did not significantly reduce the Kuramochi cells viability, their cytotoxicity will be further tested *in vitro* on different ovarian tumor cell lines to evaluate their antineoplastic activity.
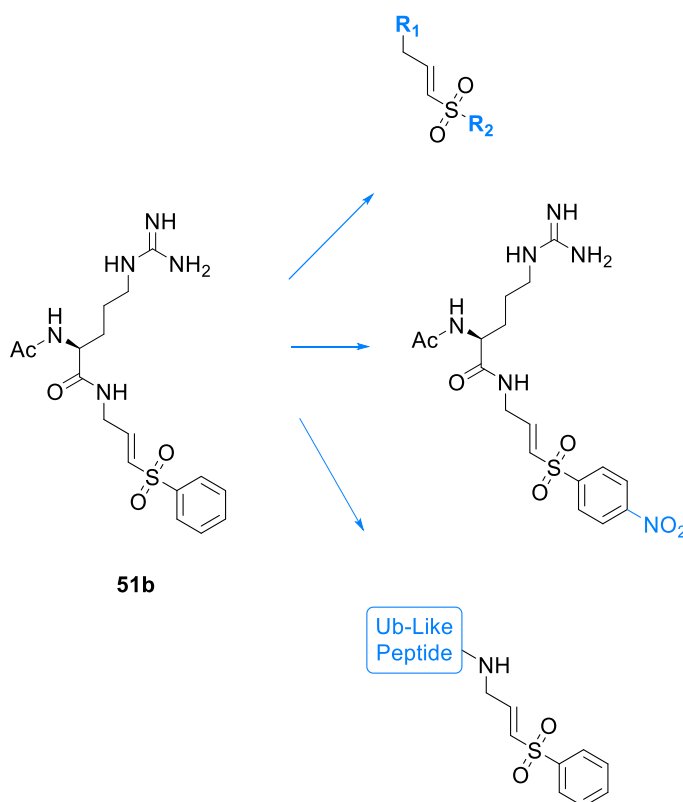

Figure 37

Future perspectives for compound **51b**.

1. INTRODUCTION

2. AIM

3. RESULTS AND DISCUSSION

4. CONCLUSIONS

5. EXPERIMENTAL SECTION

6. SUPPORTING MATERIAL

Materials and Instrumentation

Commercial reagents and solvents were used without further purification and purchased from Sigma Aldrich, Fluka, Carlo Erba, and Honeywell. All the amino acids have S-configuration, unless otherwise specified. All moisture-sensitive reactions were carried out under Ar with oven-dried glassware and anhydrous solvents. THF was dried by distillation over sodium/benzophenone ketyl under Ar. All the mixture of solvents are reported as v/v percentages. pH values were measured by litmus paper. Organic and aqueous mixtures were concentrated under reduced pressure on a Büchi evaporator.

Flash column chromatography was performed on Merck silica gel 60 (230-240 Mesh), using a mixture of solvents as mobile phase whose nature and composition is specified each time. Thin layer chromatography (TLC) and NMR were used to monitor the reactions progression and characterize the products. TLC were carried out using pre-coated fluorescent plastic sheets with 0.25mm Merck silica gel 60F-254 and were visualized with UV light (254 nm) and/or by staining with $KMNO_4$ solution.

Electrospray mass spectra (ESI-ESI-MS) were obtained on a Bruker Daltonics Esquire 4000 spectrometer. NMR spectra were recorded on Varian 500 MHz and Varian 400 MHz spectrometers using deuterated solvents whose nature is specified each time. Chemical shifts values (δ) are given in parts per million (ppm), with $CDCl_3$ ($\delta = 7.26$ for ^1H NMR and 77.2 for ^{13}C NMR), $(CD_3)_2SO$ ($\delta = 2.50$ for ^1H NMR and 39.5 for ^{13}C NMR), or CD_3OD ($\delta = 3.31$ for ^1H NMR and 49.0 for ^{13}C NMR) as references. Proton and carbon resonances have been assigned by a combination of DEPT, COSY and HSQC spectra. The multiplicity of each signal is described as s (singlet), d (doublet), t (triplet), q (quartet), m (multiplet), dd (doublet of doublets), dt (doublet of triplets), and br (broad signal). Coupling constants (J) are given in Hz.

Procedure *A*: Coupling with **2c-OSu**

2c-OSu was dissolved in dichloromethane with an equimolar amount of the amino acid, peptide, or amine. The resulting mixture was adjusted to pH ~ 8÷9 with the minimum amount of triethylamine, then stirred from 2h to 18h until complete conversion was observed (TLC), and finally washed 3X with $20\%_{(aq)}$ citric acid. The organic layer was dried over Na_2SO_4 and evaporated to afford the desired product without further purifications, unless otherwise specified. Reaction details and spectroscopic data are given below for each product.

Procedure *B*: Boc and COOtBu Protecting Groups Removal

The Boc-protected (or, alternatively, *tert*-butyl ester) compound was dissolved in a solution of 20% TFA in $CHCl_3$. The resulting mixture was stirred at r.t. from 2h to 18h till complete conversion (TLC). The solvents were removed *in vacuo* to afford the deprotected product as trifluoroacetate salt (or, respectively, carboxylic acid) without further purifications. Reaction details and spectroscopic data are given below for each product.

Procedure *C*: Fmoc Protecting Groups Removal

The Fmoc-protected compound was dissolved in a 1:1 solution of dichloromethane and diethylamine. The mixture was stirred at r.t. for at least 18h till complete conversion (TLC). Solvents were evaporated and the resulting product was precipitated from diethyl ether, filtered, and washed 4-8 times with cold diethyl ether. Reaction details and spectroscopic data are given below for each product.

Procedure *D:* Pbf Protecting Groups Removal

The Pbf-protected Arg derivative was dissolved in a 75% solution of TFA in CHCl$_3$ and left on stirring overnight (a change in the colour of the mixture is visible after 20 minutes). The solvent mixture was evaporated afterwards, and the crude precipitated from diethyl ether and filtered to afford the deprotected product as the guanidinium trifluoroacetate salt. Reaction details and spectroscopic data are given below for each product.

Procedure *E:* Amide Bond Formation and Peptide Coupling

The N-protected amino acid or peptide derivative was stirred at 0 °C for 30 min with 1.5 equivalents of EDC·HCl (MW = 191.70) and 1.5 equivalents of HOBt (MW = 135.12) in dichloromethane. After 10 minutes, 1.0 equivalent of the amino partner, previously dissolved in dichloromethane, was slowly added to the mixture together with the minimum volume of triethylamine to reach an apparent pH 8÷9. The resulting solution was stirred at r.t. from 2h to 18h till the limiting reactant was completely converted to the product (TLC). When the reaction was completed, the mixture was washed 3÷5 times with 20% of citric acid$_{(aq)}$ and 3÷5 times with sat NaHCO$_{3(aq)}$. The organic layer was dried over Na$_2$SO$_4$ and evaporated *in vacuo* to afford the crude product, which was subsequently purified by silica gel flash chromatography. Purification details and characterising data are given below for each purified product.

Procedure *F:* Catalytic Hydrogenation of Benzyl Esters

The benzyl ester was dissolved in methanol with a catalytic amount of 10% Pd/C. The resulting mixture was hydrogenated at 1 atm for 18h at r.t., then the catalyst was filtered off through a layer of celite and washed with methanol. The organic phase was evaporated to dryness *in vacuo* to afford the corresponding carboxylic acid product.

Procedure *G*: Hydrolysis of Benzyl Esters with Hydrobromic Acid

The benzyl ester was dissolved in the minimum volume of a 30% HBr in acetic acid solution and then stirred at r.t. overnight. The resulting carboxylic acid was precipitated with cold diethyl ether, then filtered, further washed with ether, and dried *in vacuo.*

Procedure *H*: Acetylation of Arginine

Pbf-protected Arg was dissolved in $CHCl_3$ with an equimolar amount of acetic anhydride (MW = 102.09). The resultant mixture was stirred at 60°C overnight, then washed 3x with 20% of citric acid$_{(aq)}$. The organic layer was dried over Na_2SO_4 and evaporated *in vacuo* to afford the acetylated product.

Compound **3** (**2c**)
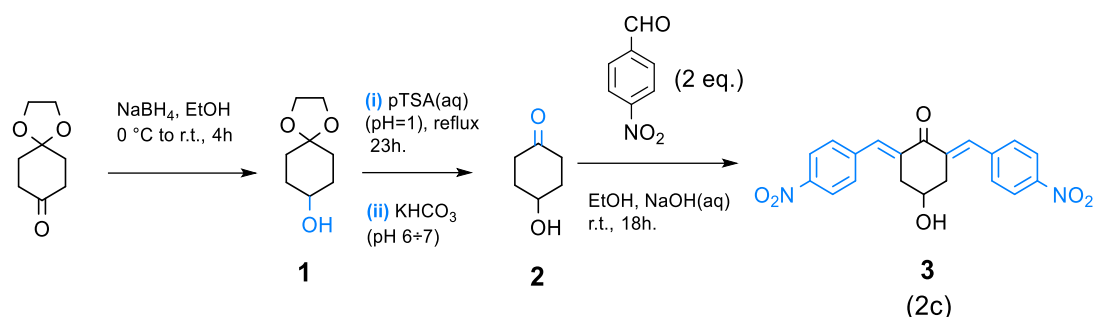
4-hydroxycyclohexanone ethylene acetal (**1**): 1,4-Cyclohexanedione monoethylene acetal (10.545 g, MW = 156.08; 67.56 mmol) was suspended in 70 mL ethanol at 0 °C with 7.212 g of NaBH$_4$ (MW = 37.84; 190.6 mmol). The reaction mixture was stirred for 4 hours at r.t. and then quenched with 200 mL of cold H$_2$O. The solution was extracted 4x with ethyl acetate, the combined organic phases were then dried over Na$_2$SO$_4$ and concentrated *in vacuo* to give compound **1**

- MW = 158.09; yield = 99% from 1,4-Cyclohexanedione monoethylene acetal; pale-yellow viscous oil.
- ^{1}H NMR (CDCl$_3$, 400 MHz) δ_H 3.97 – 3.89 (m, 4H, 2 x CH_2 acetal), 3.83 – 3.76 (m, 1H, CH-OH), 1.92 – 1.75 (m, 4H, 2 x ring CH_2), 1.71 – 1.51 (m, 4H, 2 x ring CH_2).

4-Hydroxycyclohexanone (**2**): compound **1** (10.612 g, MW = 158.09; 67.13 mmol) was dissolved in 25 mL H$_2$O. 10 g pTSA were then slowly added to pH ~1. The mixture was refluxed for 23 hours and then neutralized with sat KHCO$_{3(aq)}$. The product was extracted 15 x with ethyl acetate, the combined organic phases were dried over Na$_2$SO$_4$ and then concentrated *in vacuo* to give the crude product **2**, which was used in the next step without further purifications.

- MW = 114.07; yield = 86% from **1**; dark brown viscous oil.
- ^{1}H NMR (CDCl$_3$, 400 MHz) δ$_H$ 4.18 – 4.11 (m, 1H, C*H*-OH), 2.62 – 2.49 (m, 2H, ring C*H*$_2$), 2.33 – 2.21 (m, 2H, ring C*H*$_2$), 2.10 – 1.86 (m, 4H, 2 x ring C*H*$_2$).

4-hydroxy-2,6-bis((E)-4-nitrobenzylidene)cyclohexan-1-one **2c** (**3**): the crude ketone **2** (1.248 g, MW = 114.07; n.m.t. 10.9 mmol) and 4-nitrobenzaldehyde (2.781 g, MW = 151.12; 18.40 mmol) were suspended in 30 mL ethanol. 1.0 mL of a 2.9 M NaOH solution of was slowly added dropwise to the reaction mixture until complete solubilization. The system was left on stirring at r.t. overnight, then 20 mL of H$_2$O were added, the precipitated solid was filtered, washed with small amounts of cold ethanol, and dried at 60 °C overnight to give pure **2c** (**3**).

- MW = 380.10; yield = 72% from 4-nitrobenzaldehyde; yellow solid.
- ^{1}H NMR ((CD$_3$)$_2$SO, 400 MHz) δ$_H$ 8.27 (app d, *J* = 8.8 Hz, 4H, 2 x o-NO$_2$ Ph*H*), 7.79 (app d, *J* = 8.8 Hz, 4H, 2 x m-NO$_2$ Ph*H*), 7.72 (br s, 2H, C*H*=C), 5.00 (d, *J* = 2.6 Hz, 1H, O*H*), 4.14 – 4.03 (m, 1H, C*H*-OH), 3.13 – 2.91 (m, 4H, 2 x ring C*H*$_2$).

Compounds **4** (**2c-OSu**) and **6** (**2c-Linker**)

4
(2c-OSu)

6
(2c-Linker)
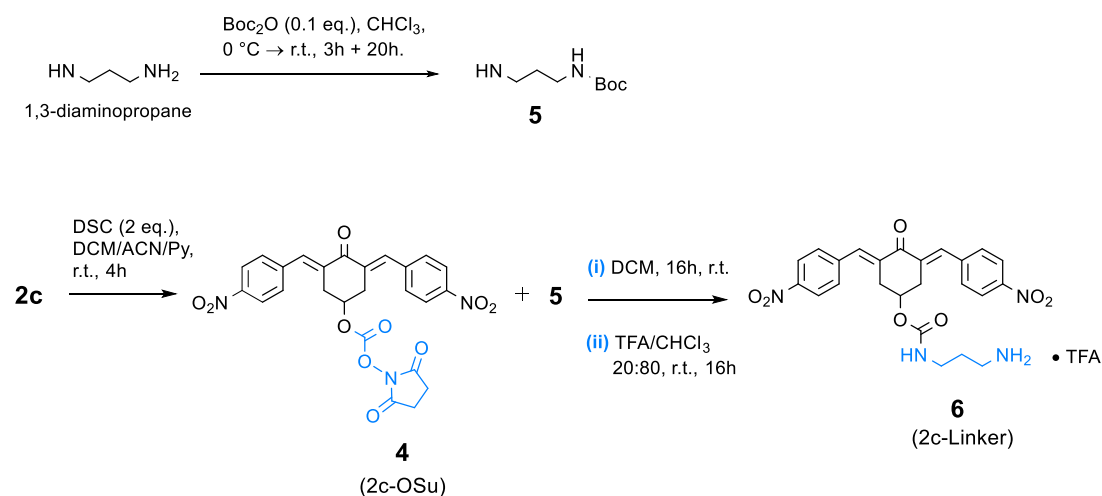
3,5-bis((E)-4-nitrobenzylidene)-4-oxocyclohexyl(2,5-dioxopyrrolidin-1-yl)carbonate **2c-OSu** (**4**): N,N′-Disuccinimidyl carbonate (2.326 g, MW = 256.17; 9.08 mmol) was added to a suspension **2c** (1.709 g, MW = 380.10; 4.50 mmol) in 40 mL of 1:1 dichloromethane/acetonitrile. Approximately 5 mL pyridine were slowly added till complete solubilization, and the resulting solution was left on stirring at r.t. After 4 hours, the mixture was concentrated to half its volume, and the product **4** was precipitated with diethyl ether, filtered, and purified by flash chromatography (eluent: CHCl₃).

- MW = 521.11; yield = 71% from **2c**; yellow solid.
- ^{1}H NMR ((CD₃)₂SO, 400 MHz) δ_H 8.27 (app d, J = 8.8 Hz, 4H, 2 x o-NO₂ Ph*H*), 7.85 (br s, 2H, C*H*=C), 7.78 (app d, J = 8.8 Hz, 4H, 2 x m-NO₂ Ph*H*), 5.36 – 5.30 (m, 1H, C*H*-OCO), 3.41 – 3.26 (m, 4H, 2 x ring C*H₂*), 2.70 (s, 4H, 2 x Osu C*H₂*).

tert-butyl (3-aminopropyl)carbamate (**5**): a solution of Boc₂O (0.956 g, MW = 218.25; 4.38 mmol) in 23 mL of CHCl₃ was slowly added at 0 °C over 3h to 65 mL of 1,3-diaminopropane (65 mL, MW = 74.12; d = 0.888 g/mL; 43.7 mmol) dissolved in 45 mL CHCl₃. The reaction mixture was stirred at r.t. for further 20h, then filtered. The organic phase was washed 6 times with small volumes of 20% citric acid$_{(aq)}$, dried over Na₂SO₄, and concentrated *in vacuo* to give compound **5**.

- MW = 174.14; yield = 83% from 1,3-diaminopropane; viscous colourless oil that tends to solidify at r.t.
- ^{1}H NMR (CDCl₃, 400 MHz) δ_H 4.92 (br s, 1H, CON*H*), 3.19 (br q, 2H), 2.74 (t, J = 6.7 Hz, 2H), 1.59 (quint, J = 6.7 Hz, 2H), 1.44 (s, 9H, Boc (C*H₃*)₃), 1.22 (br s, 2H, N*H₂*).

3,5-bis((E)-4-nitrobenzylidene)-4-oxocyclohexyl(3-aminopropyl)carbamate trifluoroacetate salt **2c-Linker** (**6**): obtained from **2c-Osu** (0.832 g, MW = 521.11; 1.65 mmol) and **5** (0.290 g, MW = 174.14; 1.67 mmol) according to *Procedure A*. The resulting product was deprotected according to *Procedure B*.

- MW = 594.16 as TFA salt; yield = 96% from **2c-Osu**; yellow solid.
- ^{1}H NMR ((CD$_3$)$_2$SO, 500 MHz) δ$_H$ 8.28 (app d, J = 8.8 Hz, 4H, 2 x o-NO$_2$ PhH), 7.82 – 7.74 (m, 6H, 2 x m-NO$_2$ PhH + CH=C), 7.64 – 7.40 (br m, 3H, NH_3^+), 7.18 (t, J = 5.8 Hz, 1H, NH), 5.06 – 4.97 (m, 1H, CH-OCO), 3.36 – 3.10 (m, 4H, 2 x ring CH_2), 2.87 (q, J = 6.6 Hz, 2H, linker CH_2), 2.67 – 2.60 (m, 2H, linker CH_2), 1.50 (quint, J = 6.4 Hz, 2H, linker CH_2).

Compounds **7a-b** (2c-Lys)
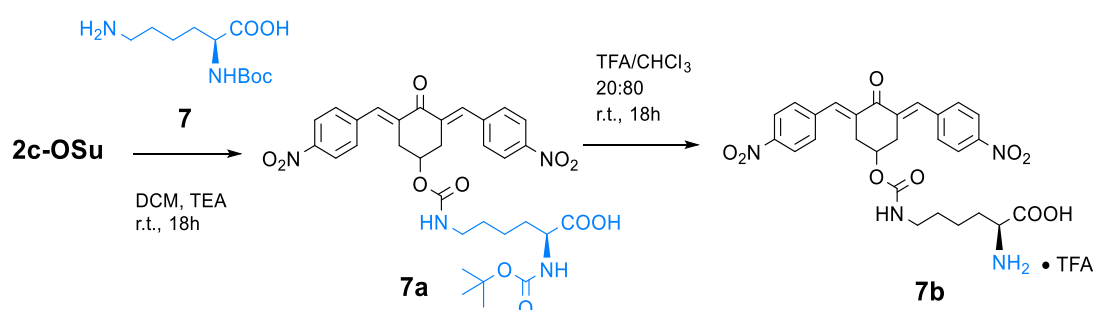
N^6-(((3,5-bis((E)-4-nitrobenzylidene)-4-oxocyclohexyl)oxy)carbonyl)-N^2-(tert-butoxycarbonyl)-L-lysine (**7a**): obtained from N^α-Boc-Lys **7** (0.458 g, MW = 246.16; 1.86 mmol) and **2c-OSu** (0.856 g, MW = 521.11; 1.64 mmol) according to *Procedure A*.

- MW = 652.66; yield = 86% from **2c-OSu**; yellow solid.
- ^{1}H NMR (CDCl$_3$, 500 MHz) δ$_H$ 8.30 – 8.26 (m, 4H, 2 x o-NO$_2$ PhH), 7.93 – 7.87 (m, 2H, 2 x CH=C), 7.62 – 7.57 (m, 4H, 2 x m-NO$_2$ PhH), 5.24 – 5.12 (m, 1H, CH-OCO), 5.07 (d, J = 7.3 Hz, 1H, NH-Boc), 4.73 (t, J = 5.9 Hz, 1H, NH urethane), 4.32 – 4.04 (m, 1H, Lys CH^α), 3.31 – 2.93 (m, 6H, 2 x ring CH_2 + Lys CH_2^ε), 1.86 – 1.57 (m, 2H, Lys CH_2^β), 1.53 – 1.24 (m, 13H, Lys CH_2^δ + CH_2^γ + Boc (CH_3)$_3$ [1.42 (s)]).
- ^{13}C{^{1}H} NMR (CDCl$_3$, 400 MHz) δ$_c$ 187.9 (C=O), 175.9 (COOH), 155.9, 155.5 (2 x CONH), 147.7, 141.7, 137.4, 134.6, 130.9, 124.0, 80.5 (Boc), 67.2

(CH-OCO), 53.2 (Lys C^α), 40.6 (Lys C^ε), 33.4 (ring CH$_2$), 32.0 (Lys C^β), 29.3 (Lys C^δ), 28.5 (Boc), 22.8 (Lys C^γ).

- ESI-MS: m/z 553.2 [M – Boc]H$^+$, 619.2 [M – C$_4$H$_8$]Na$^+$, 675.2 MNa$^+$, 691.2 MK$^+$.

N^6-(((3,5-bis((E)-4-nitrobenzylidene)-4-oxocyclohexyl)oxy)carbonyl)-L-lysine *trifluoroacetate salt* (**7b**): obtained from **7a** according to *Procedure B*.

- MW = 666.54 as TFA salt; quantitative yield from **7a**; yellow solid.
- ^{1}H NMR ((CD$_3$)$_2$SO, 400 MHz) δ_H 8.32 – 8.10 (m, 7H, 2 x o-NO$_2$ PhH + NH_3^+), 7.84 – 7.76 (m, 6H, 2 x CH=C, 2 x m-NO$_2$), 7.08 (t, J = 5.4 Hz, 1H, NH urethane), 5.11 – 4.96 (m, 1H, CH-OCO), 3.87 – 3.75 (m, 1H, Lys CH^α), 3.33 – 3.11 (m, 4H, 2 x ring CH_2), 2.89 – 2.67 (m, 2H, Lys CH_2^ε), 1.75 – 1.57 (m, 2H, Lys CH_2^β), 1.34 – 1.11 (m, 4H, Lys CH_2^γ + CH_2^δ).
- ^{13}C{^{1}H} NMR ((CD$_3$)$_2$SO, 400 MHz) δ_c 187.2 (C=O), 171.0 (COOH), 158.1, 155.2 (CONH urethane), 147.0, 141.5, 135.8, 135.4, 131.3, 123.6, 66.5 (CH-OCO), 51.8 (Lys C^α), 40.2 (Lys C^ε - overlapped to DMSO signal), 32.3 (ring CH$_2$), 29.6 (Lys C^β), 28.7 (Lys C^δ), 21.5 (Lys C^γ).
- ESI-MS: m/z 363.1 [C$_{20}$H$_{14}$N$_2$O$_5$]H$^+$, 553.2 MH$^+$.

Compounds **8a-b** (2c-Lys)

8a

8b
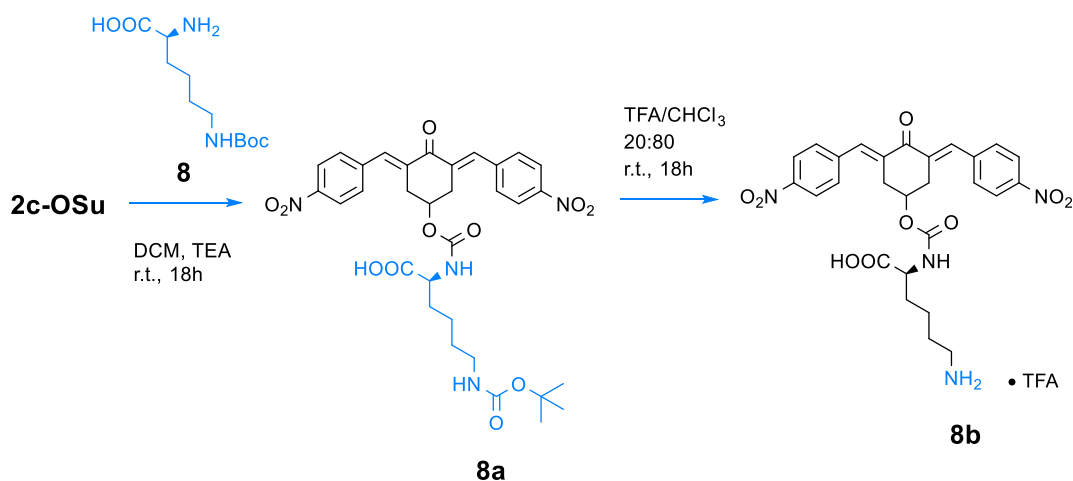
N^ε-*Boc-Lys* (**8**): obtained from commercial N^α-Fmoc-N^ε-Boc-Lys according to *Procedure C*.

N^2-*(((3,5-bis((E)-4-nitrobenzylidene)-4-oxocyclohexyl)oxy)carbonyl)-N^6-(tert-butoxycarbonyl)-L-lysine* (**8a**): obtained from N^ε-Boc-Lys **8** (0.361 g, MW = 246.16; 1.47 mmol) and **2-OSu** (0.639 g, MW = 521.11; 1.22 mmol) according to *Procedure A*.

- MW = 652.66; yield = 83% from **2-OSu**; yellow solid.
- ^{1}H NMR (CDCl$_3$, 400 MHz) δ_H 8.27, 8.24 (2 app. d, J = 8.7 Hz each, 4H, 2 x o-NO$_2$ PhH), 7.92 – 7.84 (m, 2H, 2 x CH=C), 7.59, 7.54 (2 app. d, J = 8.7 Hz each, 4H, 2 x m-NO$_2$ PhH), 5.43 (br d, 1H, NH urethane), 5.25 – 5.07 (m, 1H, CH-OCO), 4.79 – 4.55 (m, 1H, NH-Boc), 4.34 – 3.89 (m, 1H, Lys CH^α), 3.39 – 2.85 (m, 6H, 2 x ring CH_2 + Lys CH_2^ε), 1.86 – 1.54 (m, 2H, Lys CH_2^β), 1.51 – 1.20 (m, 13H, Lys CH_2^δ + CH_2^γ + Boc (CH_3)$_3$ [1.40 (s)]).
- ^{13}C{^{1}H} NMR (CDCl$_3$, 400 MHz) δ_c 187.6 (C=O), 175.6 (COOH), 156.5, 155.2 (2 x CONH urethane), 147.6, 141.7, 137.6, 134.4, 130.9, 123.9, 79.7 (Boc), 67.8 (CH-OCO), 53.7 (Lys C^α), 40.0 (Lys C^ε), 33.3 (ring CH$_2$), 31.6 (Lys C^β), 29.8 (Lys C^δ), 28.5 (Boc), 22.3 (Lys C^γ).
- ESI-MS: m/z 553.2 [M – Boc]H$^+$, 591.1 [M – Boc]K$^+$, 619.2 [M – C$_4$H$_8$]Na$^+$, 675.2 MNa$^+$, 691.2 MK$^+$.

(((3,5-bis((E)-4-nitrobenzylidene)-4-oxocyclohexyl)oxy)carbonyl)-L-lysine trifluoroacetate salt (**8b**): obtained from **8a** according to *Procedure B*.

- MW = 666.54 as TFA salt; quantitative yield from **8a**; yellow solid.
- ^{1}H NMR ((CD$_3$)$_2$SO, 400 MHz) δ_H 12.46 (br, 1H, COOH), 8.30 – 7.50 (m, 14H, 2 x o-NO$_2$ PhH + 2 x CH=C + 2 x m-NO$_2$ PhH + NH_3^+ + NH urethane), 5.05 (br, CH-OCO), 4.18 – 3.61 (m, 1H, Lys CH^α), 3.44 – 2.95 (m, 4H, partially overlapped to the signal of H$_2$O, 2 x ring CH_2), 2.69 (br, 2H, partially overlapped to the signal of DMSO, Lys CH_2^ε), 1.72 – 1.23 (m, 6H, Lys CH_2^β + CH_2^δ + CH_2^γ).

- $^{13}C\{^1H\}$ NMR ($(CD_3)_2SO$, 400 MHz) δ_c 187.2 (C=O), 173.6 (COOH), 155.3 (CONH urethane), 147.0, 141.6, 135.8, 135.4, 131.1, 123.6, 66.9 (CH-OCO), 53.5 (Lys C^α), 38.5 (Lys C^ε), 32.3 (ring CH$_2$), 29.9 (Lys C^β), 26.4 (Lys C^δ), 22.5 (Lys C^γ).

- ESI-MS: m/z 363.1 [$C_{20}H_{14}N_2O_5$]H$^+$, 553.2 MH$^+$.

Compounds **9a-b** (2c-Arg)

9a
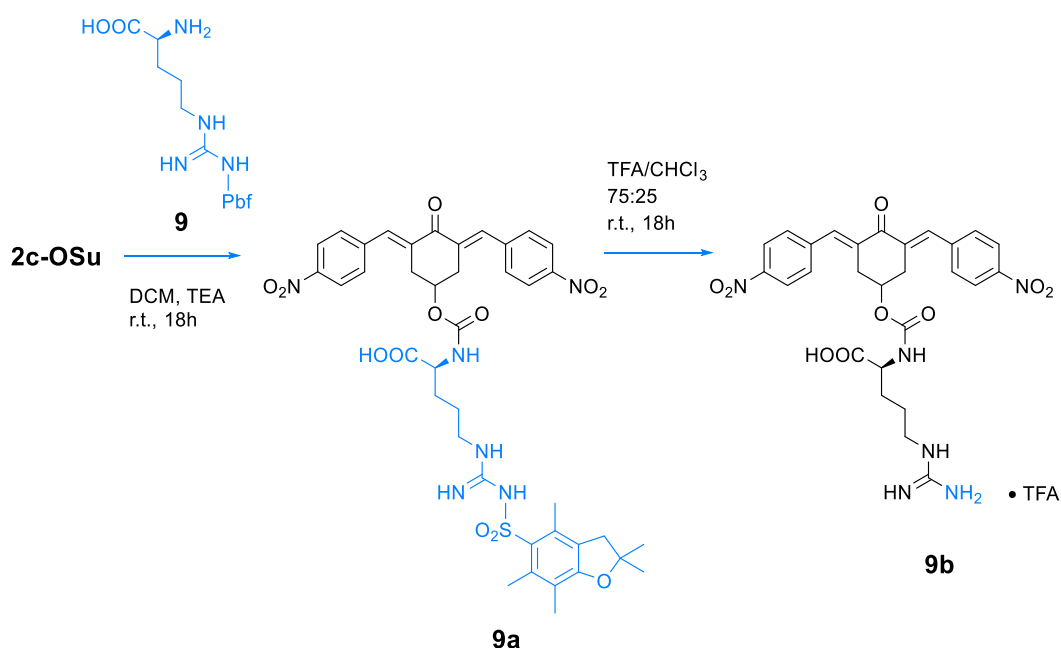
N^ω-*Pbf-Arg* (**9**): obtained from commercial N^α-Fmoc-N^ω-Pbf-Arg according to *Procedure C*.

N^2-*(((3,5-bis((E)-4-nitrobenzylidene)-4-oxocyclohexyl)oxy)carbonyl)-N^ω-((2,2,4,6,7-pentamethyl-2,3-dihydrobenzofuran-5-yl)sulfonyl)-L-arginine* (**9a**): N^ω-Pbf-Arg **9** (0.830 g, MW = 426.19; 1.95 mmol) was reacted with **2c-OSu** (0.813 g, MW = 521.11; 1.56 mmol) according to *Procedure A* to give compound **9a**.

- MW = 832.27; yield = 68% from **2c-OSu**; yellow solid.
- ^1H NMR ($(CD_3)_2SO$, 400 MHz) δ_H 8.29 – 8.20 (m, 4H, 2 x o-NO$_2$ PhH), 7.82 – 7.70 (m, 6H, 2 x CH=C + 2 x m-NO$_2$ PhH), 7.48 – 6.35 (br m, 4H, Gdn +

NH urethane), 5.07 – 4.90 (m, 1H, CH-OCO), 3.51 (br q, 1H, Arg CH^α), 3.27 – 3.07 (m, 4H, 2 x ring CH_2), 2.94 – 2.81 (m, 4H, Arg CH_2^δ + Pbf CH_2 [2.91 (s)]), 2.43, 2.38, 1.94 (3s, 3H each, 3 x CH_3 Pbf), 1.57 – 1.14 (m, 10H, Arg CH_2^β + Arg CH_2^γ + Pbf (CH_3)$_2$ [1.37 (s, 6H)]).

- ^{13}C{^{1}H} NMR ((CD$_3$)$_2$SO, 400 MHz) δ_c 187.2 (C=O), 175.9 (COOH), 157.3 (Pbf), 156.2 (C=NH), 154.5 (CONH urethane), 146.9, 141.5, 137.2 (Pbf), 135.8, 135.4, 134.3 (Pbf), 131.3 (Pbf), 131.2, 124.2 (Pbf), 123.6, 116.2 (Pbf), 86.2 (Pbf), 66.6 (CH-OCO), 55.0 (Arg C^α), 42.4 (Pbf), 40.6 (Arg C^δ), 32.7 (ring CH$_2$), 29.7 (Arg C^β), 28.3 (Pbf), 25.5 (Arg C^γ), 18.9 (Pbf), 17.6 (Pbf), 12.2 (Pbf).

- ESI-MS: m/z 833.3 MH$^+$, 855.2 MNa$^+$, 871.2 MK$^+$.

(((3,5-bis((E)-4-Nitrobenzylidene)-4-oxocyclohexyl)oxy)carbonyl)-L-arginine trifluoroacetate salt (**9b**): obtained from **9a** according to *Procedure D*.

- MW = 964.19 as TFA salt; yield = 85% from **9b**; yellow solid.

- ^{1}H NMR ((CD$_3$)$_2$SO, 400 MHz) δ_H 8.40 – 8.18 (m, 4H, 2 x o-NO$_2$ PhH), 7.92 – 7.68 (m, 6H, 2 x CH=C + 2 x m-NO$_2$ PhH), 7.52 – 6.50 (br m, 4H, NH amide + NH urethane + Gdn), 5.05 (br s, 1H, CH-OCO), 3.89 – 3.68 (m, 1H, Arg CH^α) , 3.30 – 3.05 (m, partially overlapped to the signal of H$_2$O, 4H, 2 x ring CH_2), 3.05 – 2.91 (m, 2H, Arg CH_2^δ), 1.70 – 1.28 (m, 4H, Arg CH_2^β + C$H^{\beta 2}$ + CH_2^γ).

- ^{13}C{^{1}H} NMR ((CD$_3$)$_2$SO, 400 MHz) δ_c 187.2 (C=O), 173.6 (COOH), 158.6, 156.7 (C=NH), 155.4 (CONH urethane), 147.1, 141.6, 136.0, 135.3, 131.2, 123.7, 67.1 (CH-OCO), 53.5 (Arg C^α), 40.3 (Arg C^δ), 32.4 (ring CH$_2$), 27.7 (Arg C^β), 25.3 (Arg C^γ).

- ESI-MS: m/z 581.2 MH$^+$.

Compounds **10a-b** (2c-Linker-Glu)

10a

10b
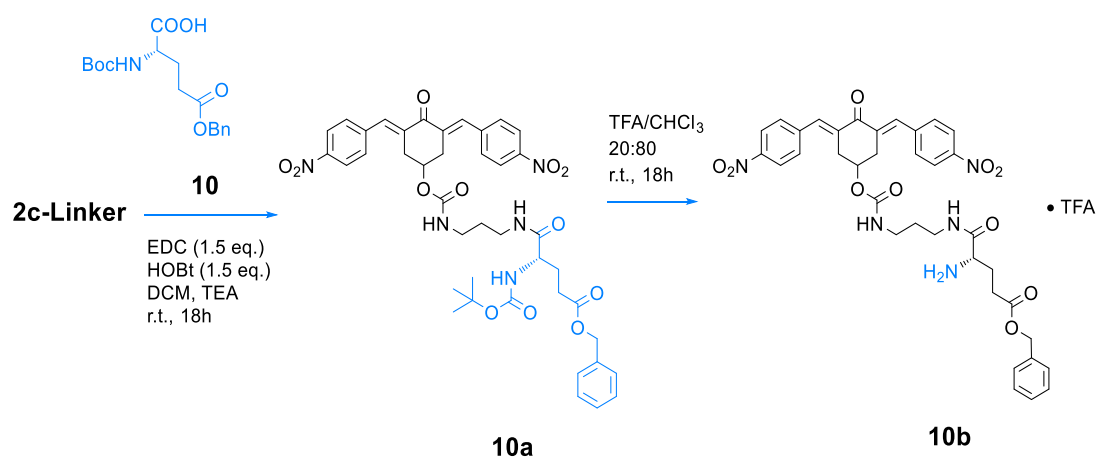
Benzyl   *(S)-5-((3-(((((3,5-bis((E)-4-nitrobenzylidene)-4-oxocyclohexyl)oxy) carbonyl)amino)propyl)amino)-4-((tert-butoxycarbonyl)amino)-5-oxopentanoate* (**10a**): obtained from **2c-Linker** (0.478 g, MW = 594.16 as TFA salt; 0.804 mmol) and Boc-Glu-5-benzyl ester **10** (0.299 g, MW = 337.37; 0.886 mmol) according to *Procedure E*. Compound **10a** was separated as a pure compound by flash chromatography (eluent: CHCl₃/MeOH 99:1).

- MW = 799.31; yield = 69% from **2c-Linker**; yellow solid.
- ^{1}H NMR (CDCl₃, 400 MHz) δ_H 8.26 (app d, J = 8.7 Hz, 4H, 2 x o-NO₂ Ph*H*), 7.90 – 7.86 (m, 2H, 2 x C*H*=C), 7.58 (app d, J = 8.7 Hz, 4H, 2 x m-NO₂ Ph*H*), 7.37 – 7.29 (m, 5H, Bn Ph*H*), 6.30 (br t, 1H, N*H* amide), 5.45 (br t, 1H, N*H* urethane), 5.30 (br d, 1H, N*H*-Boc), 5.21 – 5.06 (m, 3H, C*H*-OCO + Bn C*H₂*), 4.32 – 4.22 (m, 1H, Glu C*H*$^\alpha$), 3.24 – 2.98 (m, 8H, 2 x ring C*H₂* + 2 x C*H₂* linker), 2.28 – 2.08 (m, 3H, Glu C*H₂*$^\gamma$ + C*H*$^{\beta 1}$), 1.96 – 1.82 (m, 1H, Glu C*H*$^{\beta 2}$), 1.53 (quint, J = 6.1 Hz, 2H, C*H₂* linker), 1.40 (s, 9H, Boc (C*H₃*)₃).
- ^{13}C{^{1}H} NMR (CDCl₃, 400 MHz) δ_c 187.4 (*C*=O), 172.6, 172.0 (*C*ONH and *C*OO), 155.8, 155.3 (2 x *C*ONH urethane), 147.3, 141.6, 137.0, 135.2 (Bn), 134.5, 130.7, 128.5 (Bn), 128.4 (Bn), 128.2 (Bn) 123.7, 80.0 (Boc), 67.1 (2C, Bn + *C*H-OCO), 53.1 (Glu *C*$^\alpha$), 37.3, 35.9 (2 x *C*H₂ linker), 33.2 (ring *C*H₂), 32.3 (Glu *C*$^\gamma$), 29.7 (*C*H₂ linker), 28.5 (Glu *C*$^\beta$), 28.2 (Boc).

- ESI-MS: m/z 700.2 [M–CO$_2$–C$_4$H$_8$]H$^+$, 722.2 [M–CO$_2$–C$_4$H$_8$]Na$^+$, 766.2 [M – CO$_2$]H$^+$, 822.2 MNa$^+$.

Benzyl (S)-4-amino-5-((3-((((3,5-bis((E)-4-nitrobenzylidene)-4-oxo cyclohexyl)oxy)carbonyl)amino)propyl)amino)-5-oxopentanoate trifluoroacetate salt (**10b**): obtained from **10a** according to *Procedure B*.

- MW = 813.25 as TFA salt; quantitative yield from **10a**; yellow solid.
- ^{1}H NMR (CDCl$_3$, 400 MHz) δ_H 8.23 (app d, J = 8.7 Hz, 4H, 2 x o-NO$_2$ PhH), 7.87 (s, 2H, 2 x CH=C), 7.56 (app d, J = 8.7 Hz, 4H, 2 x m-NO$_2$ PhH), 7.34 – 7.26 (m, 5H, partially overlapped to the signal of CDCl$_3$, Bn PhH), 7.00 – 6.91 (m, 1H, NH amide), 6.70 – 5.98 (br, 3H, NH_3^+), 5.24 – 5.06 (m, 4H, NH urethane + CH-OCO + Bn CH_2), 4.23 – 4.10 (m, 1H, Glu CH^α), 3.28 – 2.92 (m, 8H, 2 x ring CH_2 + 2 x CH_2 linker), 2.55 – 2.09 (m, 4H, Glu CH_2^γ + CH_2^β), 1.58 – 1.43 (m, 2H, CH_2 linker).
- ^{13}C{^{1}H} NMR (CDCl$_3$, 400 MHz) δ_c 188.5 (C=O), 174.1, 168.8 (CONH and COO), 156.6 (CONH urethane), 147.5, 141.6, 137.8, 134.4 (Bn), 134.0, 130.9, 129.1 (Bn), 128.8 (Bn), 128.6 (Bn) 123.7, 69.0 (Bn), 68.0 (CH-OCO), 53.3 (Glu C^α), 37.8, 36.9 (2 x CH$_2$ linker), 33.0 (ring CH$_2$), 32.0 (Glu C^γ), 28.9 (CH$_2$ linker), 25.5 (Glu C^β).
- ESI-MS: m/z 700.3 MH$^+$.

Compounds 11a-c (2c-Linker-Glu)
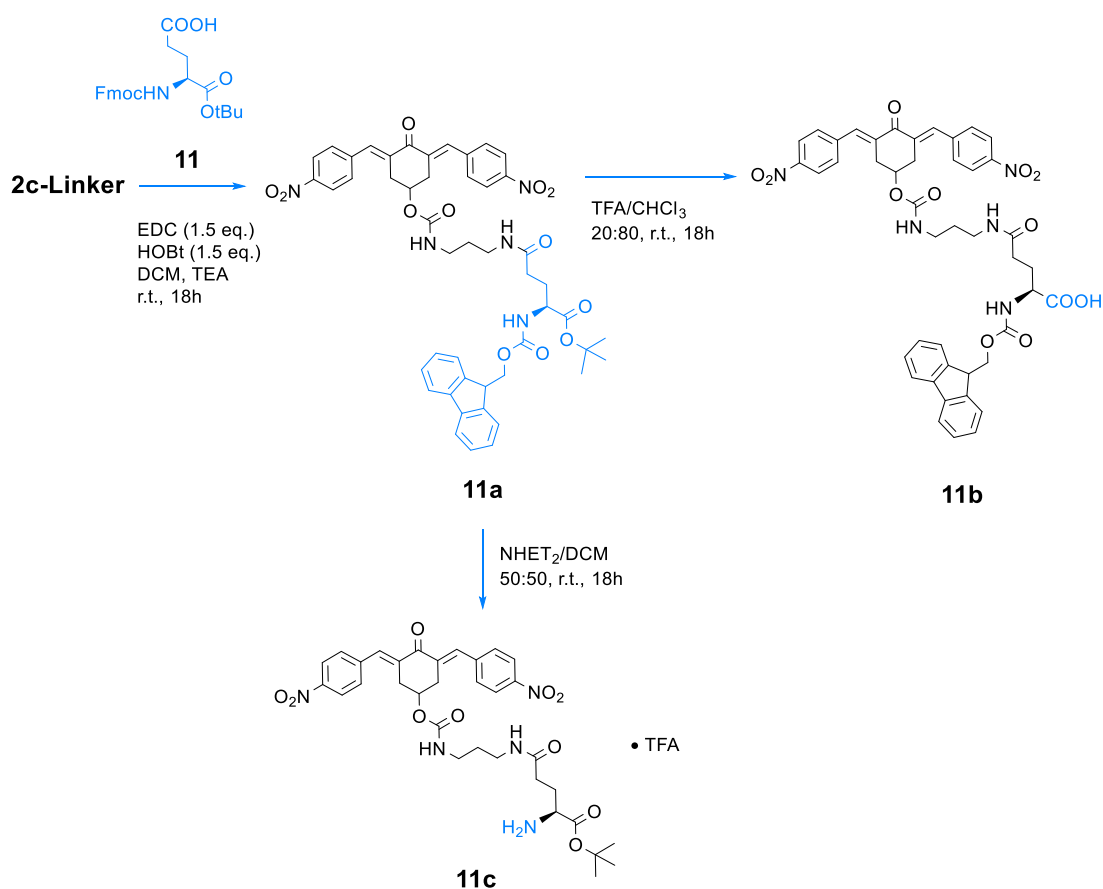
tert-butyl N²-(((9H-fluoren-9-yl)methoxy)carbonyl)-N⁵-(3-((((3,5-bis((E)-4-nitrobenzylidene)-4-oxocyclohexyl)oxy)carbonyl)amino)propyl)-L-glutaminate (**11a**): obtained from **2c-Linker** (0.360 g, MW = 594.16 as TFA salt; 0.606 mmol) and Fmoc-Glu-tert-butyl ester **11** (0.279 g, MW = 425.50; 0.656 mmol) according to *Procedure E*. The crude was separated by flash chromatography (eluent: CHCl₃/MeOH 99:1 → 96:4) to give pure **11a**.

- MW = 887.34; yield = 75% from **2c-Linker**; yellow solid.
- ¹H NMR (CDCl₃, 500 MHz) δ$_H$ 8.28 – 8-23 (m, 4H, 2 x o-NO₂ Ph*H*), 7.88 – 7.86 (m, 2H, 2 x C*H*=C), 7.75 (app d, *J* = 7.6 Hz, 2H, 2 x Fmoc Ph*H*), 7.61 – 7.53 (m, 6H, 2 x m-NO₂ Ph*H* + 4 x Fmoc Ph*H*), 7.39 (app t, *J* = 7.6 Hz, 2H, 2 x Fmoc Ph*H*), 7.33 – 7.27 (m, 2H, 2 x Fmoc Ph*H*), 6.33 (br t, 1H, N*H* amide), 5.59 (d, *J* = 7.8 Hz, 1H, N*H*-Fmoc), 5.45 (t, *J* = 5.9 Hz, 1H, N*H* urethane), 5.12 – 5.03 (m, 1H, C*H*-OCO), 4.42 – 4.33 (m, 2H, Fmoc C*H₂*),

4.23 – 4.15 (m, 2H, Fmoc CH + Glu CH^{α}), 3.30 – 3.04 (m, 8H, 2 x ring CH_2 + 2 x CH_2 linker), 2.28 – 2.13 (m, 3H, CH_2^{γ} + Glu C$H^{\beta 1}$), 1.59 – 1.51 (m, 1H, Glu C$H^{\beta 2}$), 1.59 – 1.51 (m, 2H, CH_2 linker), 1.46 (s, 9H, tBu (CH_3)$_3$).

- ^{13}C{^{1}H} NMR (CDCl$_3$, 500 MHz) δ_c 187.1 (C=O), 172.4, 170.7 (CONH and COO), 156.2, 155.3 (2 x CONH urethane), 147.1, 143.5 (Fmoc), 143.0 (Fmoc), 141.3, 140.9 (Fmoc), 136.7, 134.3, 130.5, 127.5 (Fmoc), 126.8 (Fmoc), 124.8 (Fmoc), 123.4, 119.7 (Fmoc), 82.3 (tBu), 66.8 (2C, Fmoc + CH-OCO), 53.7 (Glu C^{α}), 46.8 (Fmoc), 37.1, 35.7 (2 x CH$_2$ linker), 32.9 (ring CH$_2$), 32.2 (Glu C^{γ}), 29.5 (CH$_2$ linker), 28.7 (Glu C^{β}), 27.7 (tBu).

- ESI-MS: m/z 610.2 [M – CO$_2$ – C$_4$H$_8$ – DBF]H$^+$, 832.3 [M –C$_4$H$_8$]H$^+$, 854.3 [M –C$_4$H$_8$]Na$^+$, 910.3 MNa$^+$, 926.3 MK$^+$.
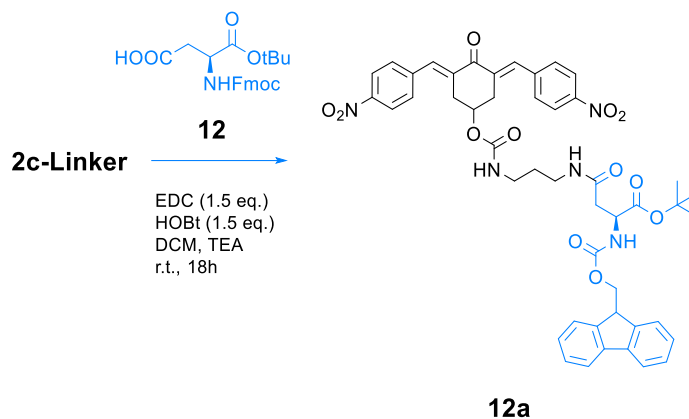
N^2-(((9H-fluoren-9-yl)methoxy)methyl)-N^5-(3-(((((3,5-bis((E)-4-nitrobenzylidene)-4-oxocyclohexyl)oxy)carbonyl)amino)propyl)-L-glutamine **(11b)**: obtained from **11a** according to *Procedure B*.

- MW = 817.30; quantitative yield from **11a**; sticky yellow solid.

- ^{1}H NMR (CDCl$_3$, 400 MHz) δ_H 10.74 (br s, 1H, COOH), 8.27 – 8-17 (m, 4H, 2 x o-NO$_2$ PhH), 7.89 – 7.84 (m, 2H, 2 x CH=C), 7.72 (app d, J = 7.6 Hz, 2H, 2 x Fmoc PhH), 7.60 – 7.46 (m, 6H, 2 x m-NO$_2$ PhH + 4 x Fmoc PhH), 7.36 (app t, J = 7.6 Hz, 2H, 2 x Fmoc PhH), 7.30 – 7.23 (m, partially overlapped to the signal of CDCl$_3$, 2H, 2 x Fmoc PhH), 7.03 (br s, 1H, NH amide), 5.96 (br s, 1H, NH-Fmoc), 5.25 (br s, 1H, NH urethane), 5.13 – 5.05 (m, 1H, CH-OCO), 4.45 – 4.24 (m, 3H, Fmoc CH_2 + Glu CH^{α}), 4.24 – 4.11 (m, 1H, Fmoc CH), 3.31 – 2.96 (m, 8H, 2 x ring CH_2 +2 x CH_2 linker), 2.46 – 2.05 (m, 4H, Glu CH_2^{γ} + CH_2^{β}), 1.63 – 1.50 (m, 2H, CH_2 linker).

- ^{13}C{^{1}H} NMR (CDCl$_3$, 400 MHz) δ_c 187.7 (C=O), 174.3, 174.0 (CONH and COOH), 156.8, 156.1 (2 x CONH urethane), 147.5, 143.7 (Fmoc), 143.5 (Fmoc), 141.5, 141.3 (Fmoc), 137.3, 134.4, 130.8, 127.9 (Fmoc), 127.2 (Fmoc), 125.2 (Fmoc), 123.8, 120.1 (Fmoc), 67.6 (CH-OCO), 67.4 (Fmoc), 53.4 (Glu C^{α}), 47.0 (Fmoc), 37.8, 36.7 (2 x CH$_2$ linker), 33.1 (ring CH$_2$), 32.3 (Glu C^{γ}), 29.8 (CH$_2$ linker), 28.5 (Glu C^{β}).

- ESI-MS: m/z 830.3 M$^-$.

tert-butyl N^5-*(3-((((3,5-bis((E)-4-nitrobenzylidene)-4-oxocyclohexyl)oxy) carbonyl)amino)propyl)-L-glutaminate* (**11c**): obtained from **11a** according to *Procedure C*.

- MW = 665.27; yield = 62% from **11a**; sticky yellow solid.

- ^{1}H NMR (CDCl$_3$, 400 MHz) δ_H 8.35 – 8-18 (m, 4H, 2 x o-NO$_2$ Ph*H*), 7.88 (s, 2H, 2 x C*H*=C), 7.65 – 7.51 (m, 4H, 2 x m-NO$_2$ Ph*H*), 6.47 – 6.37 (m, 1H, N*H* amide), 5.52 (br t, 1H, N*H* urethane), 5.22 – 5.01 (m, 1H, C*H*-OCO), 3.39 – 2.92 (m, 9H, Glu C*H*$^\alpha$ + 2 x ring C*H*$_2$ + 2 x C*H*$_2$ linker), 2.48 – 1.08 (br m, 15H, Glu C*H*$_2$$^\beta$ + C*H*$_2$$^\gamma$ + C*H*$_2$ linker + tBu (C*H*$_3$)$_3$ [1.45 (s)]).

- ^{13}C{^{1}H} NMR (CDCl$_3$, 500 MHz) δ_c 187.5 (*C*=O), 174.7, 173.4 (*C*ONH and *C*OOtBu), 155.6 (*C*ONH urethane), 147.5, 141.7, 137.2, 134.7, 130.8, 123.8, 81.4 (tBu), 67.1 (*C*H-OCO), 54.5 (Glu *C*$^\alpha$), 37.4, 35.8 (2 x *C*H$_2$ linker), 33.4 (ring *C*H$_2$), 33.0 (Glu *C*$^\gamma$), 30.4 (Glu *C*$^\beta$), 29.9 (*C*H$_2$ linker), 28.1 (tBu).
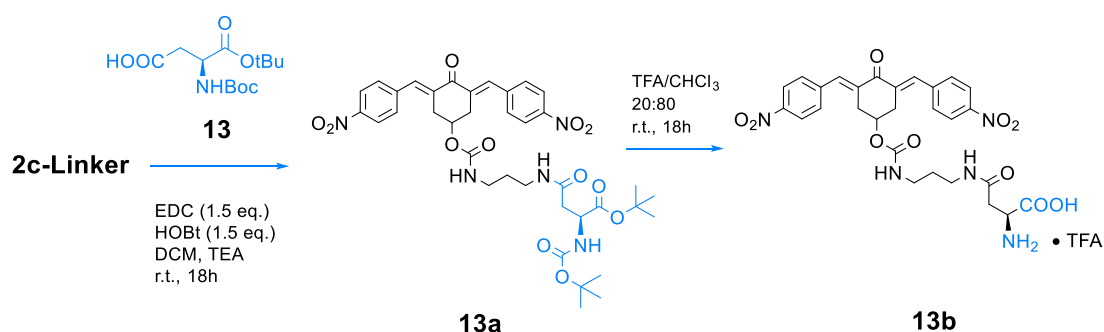
Compound **12a** (2c-Linker-Asp)

tert-butyl N2-(((9H-fluoren-9-yl)methoxy)carbonyl)-N4-(3-((((3,5-bis((E)-4-nitrobenzylidene)-4-oxocyclohexyl)oxy)carbonyl)amino)propyl)-L-asparaginate (**12a**): obtained from **2c-Linker** (0.955 g, MW = 594.16 as TFA salt; 1.61 mmol) and Fmoc-Asp $^\alpha$-*tert*-butyl ester **12** (0.831 g, MW = 411.20; 2.02 mmol) according to

Procedure E. The crude mixture was separated on flash chromatography (eluent: ethyl acetate:hexane 40:60 → 80:20) affording pure **12a**.

- MW = 873.32; yield = 65% from **2c-Linker**: yellow solid.
- ^{1}H NMR (CDCl$_3$, 500 MHz) δ_H 8.26, 8.25 (2 app d, J = 8.7 Hz each, 4H, 2 x o-NO$_2$ PhH), 7.89 – 7.86 (m, 2H, 2 x CH=C), 7.74 (app d, J = 7.6 Hz, 2H, 2 x Fmoc PhH), 7.60 – 7.54 (m, 6H, 2 x m-NO$_2$ PhH + 2 x Fmoc PhH), 7.38 (app t, J = 7.6 Hz, 2H, 2 x Fmoc PhH), 7.32 – 7.26 (m, 2H, partially overlapped to the signal of CDCl$_3$, 2 x Fmoc PhH), 6.07 – 5.86 (m, 2H, NH-Fmoc + NH amide), 5.23 (br t, 1H, NH urethane), 5.13 – 5.05 (m, 1H, CH-OCO), 4.49 – 4.26 (m, 3H, Asp CH^α + Fmoc CH_2), 4.26 – 4.16 (m, 1H, Fmoc CH), 3.29 – 3.01 (m, 8H, 2 x ring CH_2 + 2 x CH_2 linker), 2.86 – 2.65 (m, 2H, Asp C$H_2{}^\beta$), 1.56 – 1.38 (m, 11H, CH_2 linker + tBu (CH_3)$_3$ [1.45 (s)]).
- ^{13}C{^{1}H} NMR (CDCl$_3$, 500 MHz) δ_c 187.4 (C=O), 170.4, 170.1 (CONH amide and COOtBu), 156.2, 155.4 (2 x CONH urethane), 147.5, 143.8 (Fmoc), 141.6, 141.2 (Fmoc), 137.1, 134.5, 130.8, 127.8 (Fmoc), 127.1 (Fmoc), 125.1 (Fmoc), 123.8, 120.0 (Fmoc), 82.4 (tBu), 67.21 (CH-OCO), 67.15 (Fmoc CH$_2$), 51.5 (Asp C^α), 47.1 (Fmoc CH), 38.1 (Asp C^β), 37.3, 35.9 (2 x CH$_2$ linker), 33.3 (ring CH$_2$), 29.9 (CH$_2$ linker), 27.9 (tBu).
- ESI-MS: m/z 596.2 [M – COOtBu – C$_{14}$H$_{10}$]H$^+$, 818.2 [M – C$_4$H$_8$]H$^+$, 840.4 [M – C$_4$H$_8$]Na$^+$, 896.3 MNa$^+$.

Compounds **13a-b** (2c-Linker-Asp)

tert-butyl N^4-(3-((((3,5-bis((E)-4-nitrobenzylidene)-4-oxocyclohexyl)oxy) carbonyl)amino)propyl)-N^2-(tert-butoxycarbonyl)-L-asparaginate (**13a**): obtained from **2c-Linker** (0.099 g, MW = 594.16 as TFA salt; 0.17 mmol) and Boc-Asp α-*tert*-butyl ester **13** (0.050 g, MW = 289.15; 0.17 mmol) according to *Procedure E*. The product was purified by flash chromatography (eluent: CHCl$_3$/MeOH 99:1).

- MW = 751.31; yield = 95% from **2c-Linker**; yellow solid.
- ^{1}H NMR (CDCl$_3$, 500 MHz) δ_H 8.28 – 8.24 (m, 4H, 2 x o-NO$_2$ PhH), 7.88 (br, 2H, 2 x CH=C), 7.58 (app d, J = 8.6 Hz, 4H, 2 x m-NO$_2$ PhH), 6.15 (br t, 1H, NH amide), 5.61 (br d, 1H, NH-Boc), 5.39 (t, J = 6.3 Hz, 1H, NH urethane), 5.12 – 5.07 (m, 1H, CH-OCO), 4.38 – 4.30 (m, 1H, Asp CH^α), 3.28 – 3.00 (m, 8H, 2 x ring CH_2 + 2 x CH_2 linker), 2.78 – 2.60 (m, 2H, 2 x Asp CH_2^β), 1.52 (quint, J = 6.3 Hz, 2H, CH_2 linker), 1.42, 1.40 (2s, 9H each, 2 x (CH_3)$_3$).
- ^{13}C{^{1}H} NMR (CDCl$_3$, 500 MHz) δ_c 187.5 (*C*=O), 170.7, 170.5 (*C*ONH and *C*OOtBu), 155.7, 155.6 (2 x *C*ONH urethane), 147.5, 141.7, 137.1, 134.6, 130.8, 123.8, 82.2 (tBu), 79.9 (Boc), 67.2 (*C*H-OCO), 51.1 (Asp *C*$^\alpha$), 38.3 (Asp *C*$^\beta$), 37.3, 35.9 (2 x *C*H$_2$ linker), 33.3 (ring *C*H$_2$), 29.9 (*C*H$_2$ linker), 28.3 (Boc), 27.9 (tBu).

N^4-(3-((((3,5-bis((E)-4-nitrobenzylidene)-4-oxocyclohexyl)oxy)carbonyl) amino)propyl)-L-asparagine trifluoroacetate salt (**13b**): obtained from **13a** according to *Procedure B*.

- MW = 709.21 as TFA salt; quantitative yield from **13a**; yellow solid.
- ^{1}H NMR ((CD$_3$)$_2$SO, 400 MHz) δ_H 8.30 (app. d, J = 8.7 Hz, 4H, 2 x o-NO$_2$ PhH), 8.22 – 8.03 (m, 4H, NH_3^+ + NH amide), 7.84 – 7.76 (m, 6H, 2 x m-NO$_2$ PhH + 2 x CH=C), 7.07 (t, J = 5.7 Hz, 1H, NH urethane), 5.10 – 4.99 (m, 1H, CH-OCO), 4.19 – 4.08 (m, 1H, Asp Asp CH^α), 3.32 – 3.13 (m, 4H, 2 x ring CH_2), 2.94 (br q, 2H, CH_2 linker), 2.84 (q, J = 6.7 Hz, 2H, CH_2 linker), 2.72 – 2.63 (m, 2H, Asp CH_2^β), 1.39 (quint, J = 6.7 Hz, 2H, CH_2 linker).
- ^{13}C{^{1}H} NMR ((CD$_3$)$_2$SO, 400 MHz) δ_c 187.3 (*C*=O), 170.3, 168.3 (*C*ONH amide and *C*OOH), 155.3 (*C*ONH urethane), 147.1, 141.6, 135.9, 135.5, 131.1, 123.7, 66.3 (*C*H-OCO), 48.8 (Asp *C*$^\alpha$), 37.9, 36.3 (2 x *C*H$_2$ linker), 34.4 (Asp *C*$^\beta$), 32.6 (ring *C*H$_2$), 29.2 (*C*H$_2$ linker).

- ESI-MS: m/z 363.1 [$C_{20}H_{14}N_2O_5$]H$^+$, 596.2 MH$^+$.

Compounds **14**, **15a-b** (2c-Linker-Ser), and **16a-b** and (2c-Linker-Ala)
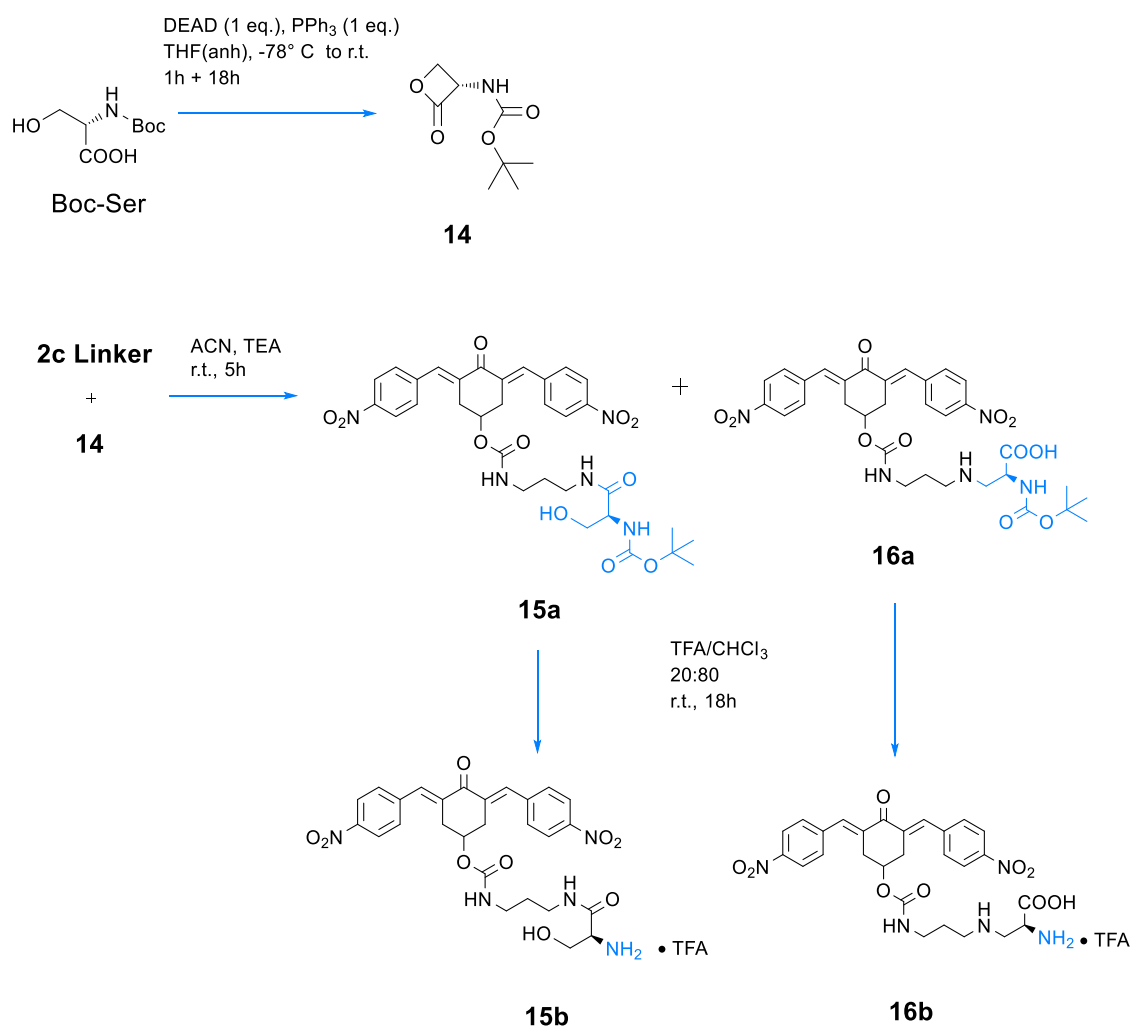
tert-butyl (S)-(2-oxooxetan-3-yl)carbamate (**14**): 6.003 g of triphenylphosphine (MW = 262,29; 22.9 mmol), previously dried *in vacuo* for 3 hours, were dissolved at -78° C in 100 mL of anhydrous THF under Ar flow. After ten minutes, a solution of 4.379 g of diethyl azodicarboxylate (MW = 174.15; 25.1 mmol) in 15 mL of anhydrous THF was added dropwise over eight minutes. After 15 minutes, a solution of 4.650 g of Boc-Ser (MW = 205.21; 22.7 mmol) in 55 mL of anhydrous THF was slowly added to the mixture, which was subsequently stirred at

–78° C for other 60 minutes and then slowly warmed to r.t. After 18 hours, the solvent was removed *in vacuo* and the crude was purified by flash chromatography (eluent: hexane/ethyl acetate 80:20 → 40:60).

- MW = 187.19; yield = 33% from Boc-Ser-OH.
- ^{1}H NMR (CDCl$_3$, 500 MHz) δ$_H$ 5.23 (m, 1H, N*H*), 5.10 (m, 1H, C*H*), 4.46–4.39 (m, 2H, C*H$_2$*), 1.45 (s, 9H, Boc (C*H$_3$*)$_3$).

    2c-Linker (0.192 g, MW = 594.16 as TFA salt; 0.323 mmol) and **14** (0.055 g, MW = 187.20; 0.294 mmol) were added to a solution of 4 mL of acetonitrile and 0.2 mL of TEA. The resulting mixture was left on stirring at r.t. for 5h and then filtered. The mother liquor was concentrated *in vacuo* to give a crude mixture of regioisomeric products **15a** and **16a**, which were separated by flash chromatography (eluent: CHCl$_3$/MeOH 98:2 for **15a** → 90:10 for **16a**).

    3,5-bis((E)-4-nitrobenzylidene)-4-oxocyclohexyl   *(3-((S)-2-((tert-butoxy carbonyl)amino)-3-hydroxypropanamido)propyl)carbamate* (**15a**):

- MW = 667.25; yield = 29% from **14**; yellow solid.
- ^{1}H NMR (CDCl$_3$, 400 MHz) δ$_H$ 8.28 (app. d, *J* = 8.7 Hz, 4H, 2 x o-NO$_2$ Ph*H*), 7.89 (s, 2H, 2 x C*H*=C), 7.59, 7.58 (2 app. d, *J* 8.7 Hz each, 4H, 2 x m-NO$_2$ Ph*H*), 6.72 (br s, 1H, N*H* amide), 5.47 (br d, 1H, N*H*-Boc), 5.19 (t, *J* = 6.3 Hz, 1H, N*H* urethane), 5.16 – 5.09 (m, 1H, C*H*-OCO), 4.12 – 4.01 (m, 2H, Ser C*H^α* + C*H^{β1}*), 3.62 (dd, *J* = 11.4, 5.0 Hz, 1H, Ser C*H^{β2}*), 3.34 – 3.05 (m, 8H, 2 x ring C*H$_2$* + 2 x C*H$_2$* linker), 1.79 (br s, 1H, O*H*), 1.57 (quint, *J* = 6.2 Hz, 2H, C*H$_2$* linker), 1.42 (s, 9H, Boc (C*H$_3$*)$_3$).
- ^{13}C{^{1}H} NMR (CDCl$_3$, 400 MHz) δ$_c$ 187.5 (*C*=O), 171.9 (*C*ONH amide), 155.7 (*C*ONH urethane), 155.5 (O-*C*ONH), 147.5, 141.5, 137.2, 134.4, 130.7, 123.8, 80.6 (Boc), 67.2 (*C*H-OCO), 62.8 (Ser *C^β*), 55.1 (Ser *C^α*), 37.2, 35.8 (2 x *C*H$_2$ linker), 33.2 (ring *C*H$_2$), 29.7 (*C*H$_2$ linker), 28.2 (Boc).
- ESI-MS: m/z 363.1 [C$_{20}$H$_{14}$N$_2$O$_5$]H$^+$, 568.2 [M – Boc]H$^+$, 590.2 [M – Boc]Na$^+$, 690.2 MNa$^+$.

(S)-3-((3-((((3,5-Bis((E)-4-nitrobenzylidene)-4-oxocyclohexyl)oxy)

carbonyl)amino)propyl)amino)-2-((tert-butoxycarbonyl)amino)propanoic acid (**16a**):

- MW = 667.25; yield = 10% from **14**; sticky yellow solid.
- ^{1}H NMR (CDCl$_3$, 400 MHz) δ_H 8.26, 8.25 (2 app. d, J = 8.7 Hz, 4H, 2 x o-NO$_2$ PhH), 7.86 (s, 2H, 2 x CH=C), 7.63 – 7.45 (m, 4H, 2 x m-NO$_2$ PhH), 5.67 (br s, 1H, NH-Boc), 5.22 – 5.04 (m, 2H, NH urethane + CH-OCO), 4.31 (br s, 1H, Ala CH^α), 3.40 – 2.87 (m, 10H, 2 x ring CH_2 + 2 x CH_2 linker + Ala CH_2^β), 2.03 – 1.83 (m, 2H, CH_2 linker), 1.42 (s, 9H, Boc (CH_3)$_3$).
- ^{13}C{^{1}H} NMR (CDCl$_3$, 400 MHz) δ_c 187.5 (C=O), 162.6 (COOH), 155.8 (2 x CONH urethane), 147.6, 141.7, 137.3, 134.6, 130.9, 123.9, 80.6 (Boc), 67.6 (CH-OCO), 50.0 (Ser C^α), 45.7 (Ser C^β), 39.3, 37.5 (2 x CH$_2$ linker), 33.3 (ring CH$_2$), 28.3 (Boc), 26.1 (CH$_2$ linker).
- ESI-MS: *m/z* 363.1 [C$_{20}$H$_{14}$N$_2$O$_5$]H$^+$, 568.2 [M – Boc]H$^+$, 590.2 [M – Boc]Na$^+$, 612.2 [M – C$_4$H$_8$]H$^+$, 668.3 MH$^+$, 690.2 MNa$^+$, 706.2 MK$^+$.

3,5-bis((E)-4-nitrobenzylidene)-4-oxocyclohexyl (3-((S)-2-amino-3-hydroxy propanamido)propyl)carbamate trifluoroacetate salt (**15b**): obtained from **15a** according to *Procedure B*.

- MW = 681.20 as TFA salt; quantitative yield from **15a**; yellow solid.
- ^{1}H NMR ((CD$_3$)$_2$SO, 400 MHz) δ_H 8.40 – 8.21 (m, 4H, 2 x o-NO$_2$ PhH + NH amide), 8.11 – 7.97 (m, 3H, NH_3^+), 7.84 – 7.75 (m, 6H, 2 x m-NO$_2$ PhH + 2 x CH=C), 7.09 (t, J = 6.4 Hz, 1H, NH urethane), 5.09 – 4.97 (m, 1H, CH-OCO), 3.77 – 3.56 (m, 3H, Ser CH^α + CH_2^β), 3.32 – 3.12 (m, 4H, 2 x ring CH_2), 3.05 – 2.79 (m, 4H, 2 x CH_2 linker), 1.52 – 1.34 (m, 2H, CH_2 linker).
- ^{13}C{^{1}H} NMR ((CD$_3$)$_2$SO, 400 MHz) δ_c 187.2 (C=O), 166.5 (CONH amide), 155.2 (CONH urethane), 147.0, 141.5, 135.8, 135.4, 131.2, 123.6, 66.6 (CH-OCO), 60.3 (Ser C^β), 54.3 (Ser C^α), 37.8, 36.4 (2 x CH$_2$ linker), 32.5 (ring CH$_2$), 29.0 (CH$_2$ linker).
- ESI-MS: m/z 363.1 [C$_{20}$H$_{14}$N$_2$O$_5$]H$^+$, 568.2 MH$^{+.}$

(S)-3-((3-(((((3,5-bis((E)-4-nitrobenzylidene)-4-oxocyclohexyl)oxy)carbonyl)
amino)propyl)amino)-2-((tert-butoxycarbonyl)amino)propanoic acid trifluoroacetate
salt (**16b**): obtained from **16a** according to *Procedure B*.

- MW = 681.20 as TFA salt; quantitative yield from **16a**; sticky yellow solid.

- ^{1}H NMR ((CD$_3$)$_2$SO, 500 MHz) δ$_H$ 8.63 – 7.40 (br m, 15H, 2 x o-NO$_2$ PhH + 2 x m-NO$_2$ PhH + 2 x CH=C + NH_2^+ + NH_3^+), 7.26– 7.01 (m, 1H, NH urethane), 5.02 (br s, 1H, CH-OCO), 3.81 (br s, 1H, Ala CH^α), 3.33 – 3.04 (m, 4H, partially overlapped to the signal of H$_2$O, 2 x ring CH_2), 2.96 – 2.21 (m, 6H, partially overlapped to the signal of DMSO, Ala CH_2^β + 2 x CH_2 linker), 2.47 – 2.21 (m, 2H, CH_2 linker) , 1.69 – 1.29 (m, 2H, CH_2 linker).

- ^{13}C{^{1}H} NMR ((CD$_3$)$_2$SO, 500 MHz) δ$_c$ 187.2 (C=O), 169.9 (COOH), 155.3 (CONH urethane), 147.1, 141.5, 135.8, 135.4, 131.3, 123.7, 66.7 (CH-OCO), 54.0 (Ser C^β), 51.6 (Ser C^α), 50.7, 38.2 (2 x CH$_2$ linker), 32.6 (ring CH$_2$), 25.2 (CH$_2$ linker).

- ESI-MS: m/z 363.2 [C$_{20}$H$_{14}$N$_2$O$_5$]H$^+$, 568.2 MH$^+$.

Compounds **18a-b** (2c-KGD dimethyl ester)
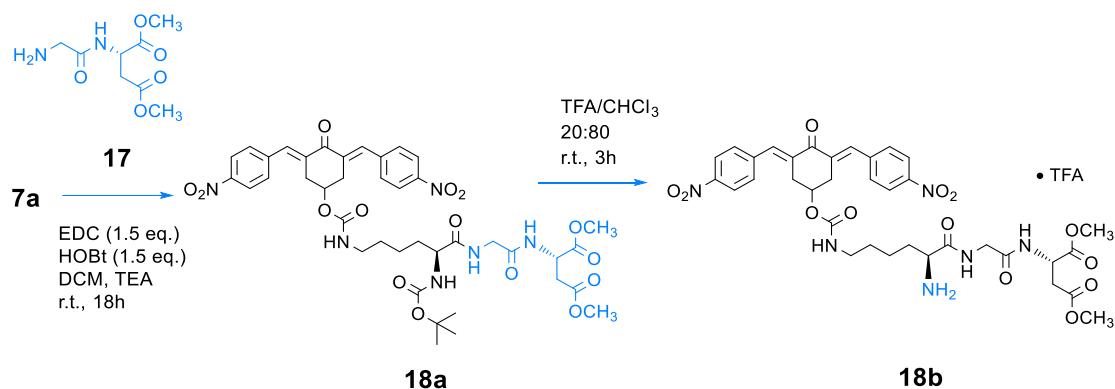
Dimethyl N^6-(((3,5-bis((E)-4-nitrobenzylidene)-4-oxocyclohexyl)oxy) carbonyl)-N^2-(tert-butoxycarbonyl)-L-lysylglycyl-L-aspartate (**18a**): obtained from the Lys conjugate **7a** (0.484 g, MW = 652.66; 0.742 mmol) and Gly-Asp dimethyl ester **17** (0.256 g, MW = 332.09 as TFA salt; 0.771 mmol) according to *Procedure E*. The crude product was purified by flash chromatography (eluent: CHCl$_3$ → CHCl$_3$/MeOH 97:3).

- MW = 852.32; yield = 39% from **7a**; yellow solid.
- ^{1}H NMR (CDCl$_3$, 400 MHz) δ_H 8.30 – 8.23 (m, 4H, 2 x o-NO$_2$ PhH), 7.95 – 7.84 (m, 2H, 2 x CH=C), 7.65 – 7.54 (m, 4H, 2 x m-NO$_2$ PhH), 7.06 (d, J = 8.1 Hz, 1H, Asp NH), 6.61 (t, J = 5.1 Hz, 1H, Gly NH), 5.30 – 5.09 (m, 2H, CH-OCO + NH-Boc), 4.94 (t, J = 5.7 Hz, 1H, NH urethane), 4.82 (dt, J = 8.1 Hz, J = 4.7 Hz, 1H, Asp CH^α), 4.15 – 3.89 (m, 3H, Lys CH^α + Gly CH_2^α), 3.72, 3.66 (2s, 3H each, 2 x O-CH_3), 3.33 – 2.91 (m, 7H, 2 x ring CH_2 + Lys CH_2^ε + Asp C$H^{\beta1}$ [2.99 (dd, J = 17.2, 4.7 Hz)], 2.83 (dd, J = 17.2, 4.7 Hz, 1H, Asp C$H^{\beta2}$), 1.93 – 1.70 (m, 2H, Lys CH_2^β), 1.69 – 1.21 (m, 13H, Lys CH_2^δ + Boc (CH_3)$_3$ [1.40 (s)] + Lys CH_2^γ).

- $^{13}C\{^1H\}$ NMR (CDCl$_3$, 400 MHz) δ_c 187.7 (C=O), 172.6, 171.4, 170.9, 168.6, 155.9, 155.4 (2 x O-CONH urethane), 147.7, 141.7, 137.3, 134.6, 130.9, 124.0, 80.4 (Boc), 67.1 (CH-OCO), 54.4 (Lys C^{α}), 53.1, 52.3 (2 x O-CH$_3$), 48.7 (Asp C^{α}), 42.9 (Gly C^{α}), 40.5 (Lys C^{ε}), 36.0 (Asp C^{β}), 33.4 (ring CH$_2$), 32.0 (Lys C^{β}), 29.3 (Lys C^{δ}), 28.4 (Boc), 22.6 (Lys C^{γ}).

- ESI-MS: m/z 775.3 [M – Boc]Na$^+$, 819.3 [M – C$_4$H$_8$]Na$^+$, 875.4 MNa$^+$, 981.3 MK$^+$.

Dimethyl N^6-(((3,5-bis((E)-4-nitrobenzylidene)-4-oxocyclohexyl)oxy) carbonyl)-L-lysylglycyl-L-aspartate trifluoroacetate salt (**18b**): obtained from **18a** according to *Procedure B*.

- MW = 866.27 as TFA salt; quantitative yield from **18a**; yellow solid.
- ^{1}H NMR (CD$_3$OD, 400 MHz) δ_H 8.41 – 8.18 (m, 4H, 2 x o-NO$_2$ PhH), 7.89 (s, 2H, 2 x CH=C), 7.80 – 7.64 (m, 4H, 2 x m-NO$_2$ PhH), 5.28 – 5.04 (m, 1H, CH-OCO), 4.78 (overlapped to the signal of H$_2$O, Asp H^{α}), 4.07 – 3.60 (m, 9H, Gly CH_2^{α} + Lys CH^{α} + 2 x O-CH_3 [3.72, 3.68 (2s)]), 3.39 – 3.17 (m, 4H, 2 x ring CH_2), 3.06 – 2.93 (m, 2H, 2 x Lys CH_2^{ε}), 2.92 – 2.78 (m, 2H, Asp CH_2^{β}), 1.93 – 1.66 (m, 2H, Lys CH_2^{β}), 1.49 – 1.27 (m, 4H, CH_2^{γ} + Lys CH_2^{δ}).
- $^{13}C\{^1H\}$ NMR (CD$_3$OD, 400 MHz) δ_c 188.9 (C=O), 172.42, 172.37, 170.7 (2C), 157.7 (CONH urethane), 148.8, 143.0, 137.7, 136.4, 132.1, 124.6, 68.7 (CH-OCO), 54.3 (Lys C^{α}), 53.1, 52.5 (2 x O-CH$_3$), 50.2 (Asp C^{α}), 43.0 (Gly C^{α}), 41.0 (Lys C^{ε}), 36.7 (Asp C^{β}), 33.9 (ring CH$_2$), 32.0 (Lys C^{β}), 30.2 (Lys C^{δ}), 22.8 (Lys C^{γ}).
- ESI-MS: m/z 363.1 [C$_{20}$H$_{14}$N$_2$O$_5$]H$^+$, 753.3 MH$^+$.

Compounds **19a-b** (2c-KGD dimethyl ester)
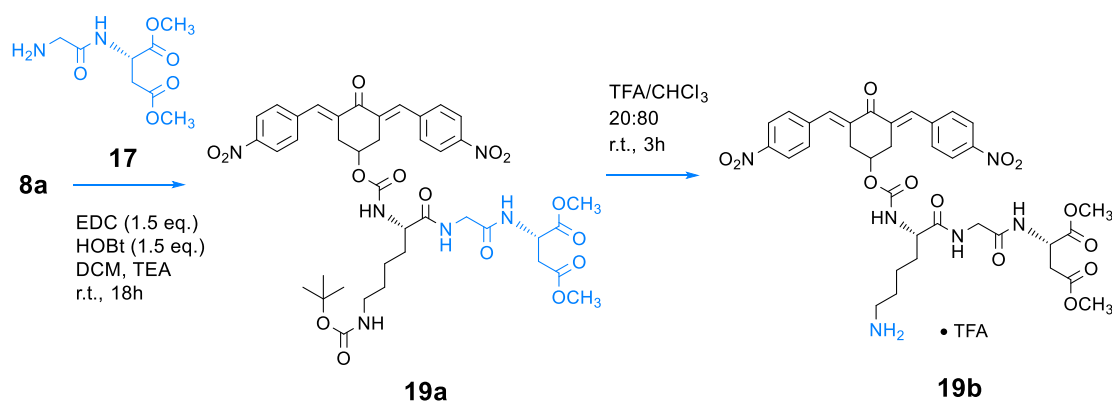
Dimethyl N^2-(((3,5-bis((E)-4-nitrobenzylidene)-4-oxocyclohexyl)oxy) carbonyl)-N^6-(tert-butoxycarbonyl)-L-lysylglycyl-L-aspartate (**19a**): obtained from the Lys derivative **8a** (0.556 g, MW = 652.66; 0.852 mmol) and Gly-Asp dimethyl ester **17** (0.307 g, MW = 332.09 as TFA salt; 0.924 mmol) according to *Procedure E*. The crude product was purified by flash chromatography (eluent: CHCl$_3$ → CHCl$_3$/MeOH 96:4).

- MW = 852.32; yield = 44% from **7a**; yellow solid.
- ^{1}H NMR (CDCl$_3$, 500 MHz) δ_H 8.28, 8.27 (2 app d, J = 8.8 Hz, 4H, 2 x o-NO$_2$ Ph*H*), 7.92 – 7.88 (m, 2H, 2 x C*H*=C), 7.62 – 7.56 (m, 4H, 2 x m-NO$_2$ Ph*H*), 6.64 (d, J = 8.2 Hz, 1H, Asp N*H*), 6.61 (br t, 1H, Gly N*H*), 5.38 (br d, 1H, N*H* urethane), 5.18 – 5.10 (m, 1H, C*H*-OCO), 4.81 (dt, J = 8.2, 4.6 Hz, 1H, Asp C*H*$^\alpha$), 4.66 (br s, 1H, N*H*-Boc), 4.05 (dt, J = 6.9, 5.9 Hz, 1H, Lys C*H*$^\alpha$), 3.97 – 3.87 (m, 2H, Gly C*H*$_2{}^\alpha$), 3.73, 3.66 (2s, 3H each, O-C*H*$_3$), 3.22 – 3.13 (m, 4H, 2 x ring C*H*$_2$), 3.10 – 2.96 (m, 3H, Lys C*H*$_2{}^\varepsilon$ + Asp C*H*$^{\beta 1}$ [3.00 (dd, J = 17.4, 4.6 Hz)]), 2.81 (dd, J = 17.4 Hz, 4.6 Hz, 1H, C*H*$^{\beta 2}$), 1.85 – 1.73 (m, 1H, Lys C*H*$^{\beta 1}$), 1.70 – 1.56 (m, partially overlapped to the signal of H$_2$O, 1H, Lys C*H*$^{\beta 2}$), 1.48 – 1.37 (m, 11H, Lys C*H*$_2{}^\delta$ + Boc (C*H*$_3$)$_3$ [1.41 (s)]), 1.34 – 1.24 (m, 2H, Lys C*H*$_2{}^\gamma$).
- ^{13}C{^{1}H} NMR (CDCl$_3$, 400 MHz) δ_c 187.5 (*C*=O), 171.9, 171.4, 170.9, 168.3, 156.4, 155.3 (2 x *C*ONH urethane), 147.7, 141.7, 137.5, 134.4, 130.9, 123.9,

79.4 (Boc), 67.9 (CH-OCO), 54.8 (Lys C^α), 53.1, 52.3 (2 x O-CH$_3$), 48.6 (Asp C^α), 42.8 (Gly C^α), 39.9 (Lys C^ε), 36.0 (Asp C^β), 33.3 (ring CH$_2$), 32.2 (Lys C^β), 29.7 (Lys C^δ), 28.6 (Boc), 22.4 (Lys C^γ).

- ESI-MS: m/z 369.2 [M – $C_{20}H_{14}N_2O_5$ – Boc – CO_2]Na$^+$, 469.3 [M – $C_{20}H_{14}N_2O_5$ – CO_2]H$^+$, 753.3 [M – Boc]H$^+$, 819.3 [M – C_4H_8]Na$^+$, 875.4 MNa$^+$, 981.3 MK$^+$.

Dimethyl (((3,5-bis((E)-4-nitrobenzylidene)-4-oxocyclohexyl)oxy)carbonyl)-L-lysylglycyl-L-aspartate trifluoroacetate salt (**19b**): obtained from **19a** according to *Procedure B*.

- MW = 866.27 as TFA salt; quantitative yield from **19a**; yellow solid.
- ^{1}H NMR (CD$_3$OD, 500 MHz) δ_H 8.30 – 8.21 (m, 4H, 2 x o-NO$_2$ PhH), 7.83 (s, 2H, 2 x CH=C), 7.74 – 7.62 (m, 4H, 2 x m-NO$_2$ PhH), 5.22 – 5.10 (m, 1H, CH-OCO), 4.79 – 4.72 (m, 1H Asp CH^α), 4.00 – 3.75 (m, 3H, Lys CH^α + Gly CH_2^α), 3.67, 3.62 (2s, 3H each, 2 x O-CH_3), 3.34 – 3.17 (m, partially overlapped to the MeOD signal, 4H, 2 x ring CH_2), 2.94 – 2.73 (m, 4H, Lys CH_2^ε + Asp CH_2^β), 1.80 – 1.55 (m, 4H, Lys CH_2^β + Lys CH_2^δ), 1.48 – 1.26 (m, 2H, Lys CH_2^γ).
- ^{13}C{^{1}H} NMR (CD$_3$OD, 400 MHz) δ_c 188.8 (C=O), 174.9, 172.33, 172.26, 172.1, 157.5 (CONH urethane), 148.8, 143.1, 137.8, 136.3, 132.1, 124.6, 69.3 (CH-OCO), 56.3 (Lys C^α), 53.1, 52.3 (2 x O-CH$_3$), 50.1 (Asp C^α), 43.2 (Gly C^α), 40.3 (Lys C^ε), 36.7 (Asp C^β), 33.9 (ring CH$_2$), 32.1 (Lys C^β), 28.0 (Lys C^δ), 23.5 (Lys C^γ).
- ESI-MS: m/z 753.3 MH$^+$.

Compounds **19c**, **21c**, and **22a-b** (2c-KGD)
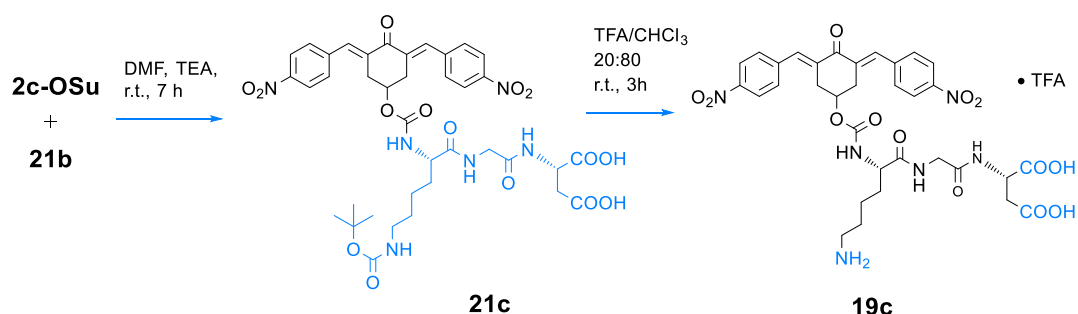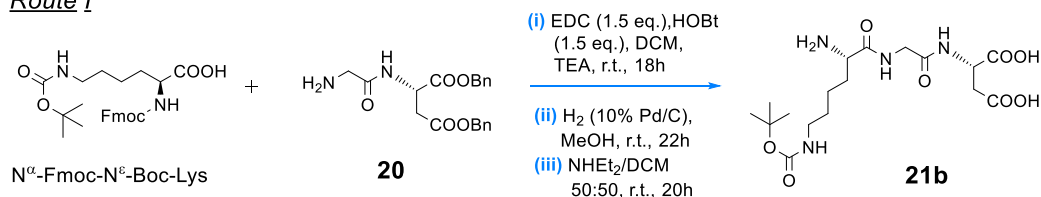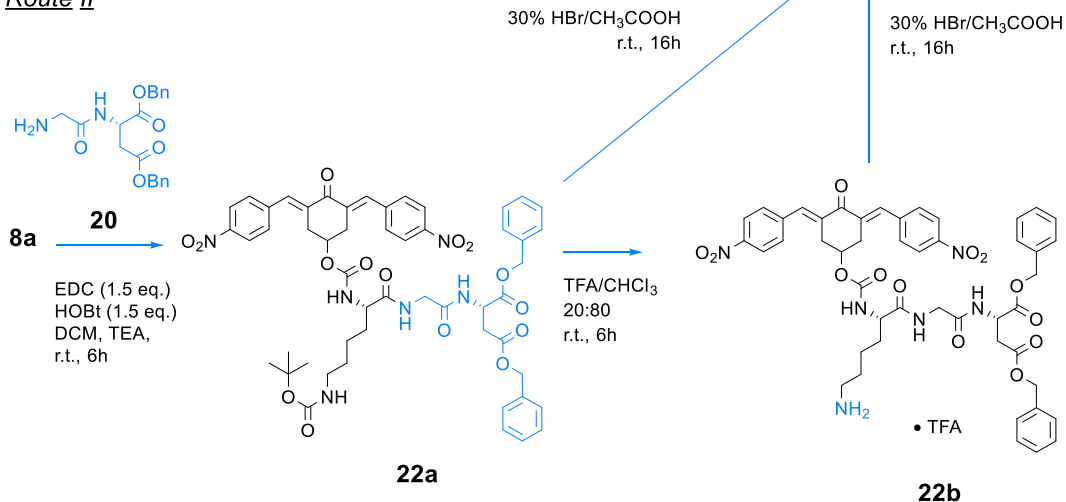
(((3,5-bis((E)-4-nitrobenzylidene)-4-oxocyclohexyl)oxy)carbonyl)-L-lysylglycyl-L-aspartic acid trifluoroacetate salt (**19c**): <u>by *route I*</u> - 0.145 g of tripeptide N^ε-Boc-Lys-Gly-Asp **21b** (MW = 418.21; 0.347 mmol) were reacted with 0.175 g of **2c-OSu** (MW = 521.11; 0.336 mmol) to afford **21c** by a slight modification of *Procedure A*, using DMF as the solvent. The crude product was purified by flash chromatography (eluent: CHCl₃/MeOH 95:5 → 90:10) and then converted to the final product **19c** according to *Procedure B*. <u>By *route II*</u> – Prepared

from the Lys derivative **8a** (0.324 g, MW = 652.66; 0.496 mmol) and Gly-Asp dibenzyl ester **20** (0.255 g, MW = 484.15 as TFA salt; 0.527 mmol) following *Procedure E*. The product was purified by flash chromatography (eluent: CHCl$_3$ → CHCl$_3$/MeOH 98:2) and then deprotected via *Procedure G*. The product was also obtained in two-steps: the first was carried out according to *Procedure B* leading to the intermediate **22b**, which was subsequently converted to **19c** according to *Procedure G*.

- MW = 838.23 as TFA salt; yield = 56% from **2c-OSu** (*route I*); 48% from **8a** (*route II*); yellow solid.

- ^{1}H NMR (CD$_3$OD, 400 MHz) δ_H 8.33 – 8.28 (m, 4H, 2 x o-NO$_2$ PhH), 7.91 – 7.86 (m, 2H, 2 x CH=C), 7.78 – 7.66 (m, 4H, 2 x m-NO$_2$ PhH), 5.20 – 5.13 (m, 1H, CH-OCO), 4.76 – 4.70 (m, 1H Asp CH^α), 3.96 – 3.89 (m, 3H, Lys CH^α + Gly CH_2^α), 3.37 – 3.16 (m, partially overlapped to the signal of MeOD, 4H, 2 x ring CH_2), 2.93 – 2.74 (m, 4H, Lys CH_2^ε + Asp CH_2^β), 1.76 – 1.54 (m, 4H, Lys CH_2^β + Lys CH_2^δ), 1.46 – 1.28 (m, 2H, Lys Lys CH_2^γ).

- ^{13}C{^{1}H} NMR (CD$_3$OD, 400 MHz) δ_c 187.9 (C=O), 174.9, 173.8 (2C), 171.1, 157.5 (CONH urethane), 148.9, 143.1, 137.9, 136.3, 132.1, 124.6, 69.3 (CH-OCO), 56.3 (Lys C^α), 50.1 (Asp C^α), 43.2 (Gly C^α), 40.3 (Lys C^ε), 36.8 (Asp C^β), 33.9 (ring CH$_2$), 32.1 (Lys C^β), 28.0 (Lys C^δ), 23.4 (Lys C^γ).

- ESI-MS: m/z 725.3 MH$^+$, 747.2 MNa$^+$, 763.2 MK$^+$.

N^5-(tert-butoxycarbonyl)glutaminylglycylaspartic acid (**21b**): prepared from Gly-Asp dibenzyl ester **20** and N$^\alpha$-Fmoc-N$^\varepsilon$-Boc-Lys according to *Procedure E*, then deprotected in two steps following *procedures F* and *C* respectively.

- ^{1}H NMR ((CD$_3$)$_2$SO, 400 MHz) δ_H 8.70 – 8.45 (m, 2H, Asp NH + Gly NH), 7.40 – 7.22 (2 x Bn PhH), 6.73 (br t, 1H, NH-Boc), 5.06, 5.08 (2s, 2H each, 2 x Bn CH_2), 4.76 (br q, 1H, Asp CH^α), 3.85 – 3.50 (m, 3H, Lys CH^α + Gly CH_2^α), 3.05 – 2.42 (m, 4H, Asp CH_2^β + Lys CH_2^ε), 1.75 – 1.50 (m, 2H, Lys CH_2^β), 1.42 – 1.14 (m, 13H, Lys CH_2^δ + Lys CH_2^γ + (CH_3)$_3$ Boc).

N²-(((3,5-bis((E)-4-nitrobenzylidene)-4-oxocyclohexyl)oxy)carbonyl)-N⁶-(tert-butoxycarbonyl)-L-lysylglycyl-L-aspartic acid (**21c**):

- MW = 824.29; yield = 56% from **2c-OSu**; yellow solid.

- ^{1}H NMR (CD$_3$OD, 500 MHz) δ_H 8.27 – 8.18 (m, 4H, 2 x o-NO$_2$ PhH), 7.84 – 7.77 (m, 2H, 2 x CH=C), 7.69 – 7.57 (m, 4H, 2 x m-NO$_2$ PhH), 5.16 – 5.09 (m, 1H, CH-OCO), 4.72 – 4.64 (m, 1H Asp CH^α), 3.92 – 3.70 (m, 3H, Lys CH^α + Gly CH_2^α), 3.32 – 3.10 (m, partially overlapped to the signal of MeOD, 4H, 2 x ring CH_2), 2.95 – 2.85 (m, 2H, Lys CH_2^ε), 2.79 – 2.70 (m, 2H, Asp CH_2^β), 1.75 – 1.13 (m, 15H, Lys CH_2^β + Lys CH_2^δ + Lys CH_2^γ + Boc (CH_3)$_3$ [1.36 (s, 9H)]).

- ^{13}C{^{1}H} NMR (CD$_3$OD, 500 MHz) δ_c 188.9 (C=O), 175.2, 173.9 (2C), 171.1, 158.5, 157.6 (2 x CONH urethane), 148.8, 143.1, 137.8, 136.3, 132.2, 124.7, 79.9 (Boc), 69.2 (CH-OCO), 56.6 (Lys C^α), 50.1 (Asp C^α), 43.3 (Gly C^α), 40.9 (Lys C^ε), 36.9 (Asp C^β), 33.8 (ring CH$_2$), 32.3 (Lys C^β), 30.4 (Lys C^δ), 28.8 (Boc), 24.0 (Lys C^γ).

- ESI-MS: m/z 319.2 [M – C$_{20}$H$_{14}$N$_2$O$_5$ – Boc – CO$_2$]H$^+$, 363.2 [C$_{20}$H$_{14}$N$_2$O$_5$]H$^+$, 341.1 [M – C$_{20}$H$_{14}$N$_2$O$_5$ – Boc – CO$_2$]Na$^+$, 419.2 [M – C$_{20}$H$_{14}$N$_2$O$_5$ – CO$_2$]Na$^+$, 725.2 [M– Boc]H$^+$, 747.2 [M– Boc]Na$^+$, 763.1 [M– Boc]K$^+$, 847.2 MNa$^+$, 863.2 MK$^+$.

Dibenzyl N²-(((3,5-bis((E)-4-nitrobenzylidene)-4-oxocyclohexyl)oxy)carbonyl)-N⁶-(tert-butoxycarbonyl)-L-lysylglycyl-L-aspartate (**22a**):

- MW = 1004.38; yield = 56% from **8a**; yellow solid.

- ^{1}H NMR (CDCl$_3$, 400 MHz) δ_H 8.31 – 8.21 (m, 4H, 2 x o-NO$_2$ PhH), 7.92 – 7.87 (m, 2H, 2 x CH=C), 7.62 – 7.53 (m, 4H, 2 x m-NO$_2$ PhH), 7.37 – 7.22 (m, partially overlapped to the signal of CDCl$_3$, 10H, 2 x Bn PhH), 6.85 (d, J = 7.9 Hz, 1H, Asp NH), 6.58 – 6.52 (br t, 1H, Gly NH), 5.38 (d, J = 7.7 Hz, 1H, NH urethane), 5.17 – 5.08 (m, 3H, CH-OCO + Bn CH_2 [5.10 (s, 2H)]), 5.02 (s, 2H, Bn CH_2), 4.86 (dt, J = 7.9, 4.6 Hz, 1H, Asp CH^α), 4.71 – 4.57 (m, 1H, NH-Boc), 4.07 – 3.98 (m, 1H, Lys CH^α), 3.94 – 3.83 (m, 2H, Gly CH_2^α), 3.22 – 3.11 (m, 4H, 2 x ring CH_2), 3.09 – 2.97 (m, 3H, Lys CH_2^ε + Asp

C$H^{\beta 1}$), 2.85 (dd, J = 17.2, 4.6 Hz, 1H, Asp C$H^{\beta 2}$), 1.83 – 1.51 (m, partially overlapped to the signal of H$_2$O, 2H, Lys CH_2^{β}), 1.49 – 1.34 (m, 11H, Lys CH_2^{δ} + (CH_3)$_3$ Boc [1.41 (s, 9H)]), 1.34 – 1.21 (m, 2H, Lys CH_2^{γ}).

- ^{13}C{^{1}H} NMR (CDCl$_3$, 400 MHz) δ_c 187.5 (*C*=O), 171.9, 170.6, 170.2, 168.4, 156.4, 155.3 (2 x *C*ONH urethane), 147.6, 141.6, 137.4, 134.4, 135.3 (Bn), 131.1 (Bn), 130.9, 128.7 (2C, 2 x Bn), 128.4 (4C, 2 x Bn), 123.9, 79.4 (Boc), 67.9 (*C*H-OCO), 67.8 (Bn), 67.0 (Bn), 54.8 (Lys *C*$^{\alpha}$), 48.8 (Asp *C*$^{\alpha}$), 42.8 (Gly *C*$^{\alpha}$), 40.0 (Lys *C*$^{\epsilon}$), 36.3 (Asp *C*$^{\beta}$), 33.3 (ring *C*H$_2$), 32.2 (Lys *C*$^{\beta}$), 29.7 (Lys *C*$^{\delta}$), 28.6 (Boc), 22.4 (Lys *C*$^{\gamma}$).

- ESI-MS: m/z 499.3 [M – C$_{20}$H$_{14}$N$_2$O$_5$ – Boc – CO$_2$]H$^+$, 521.3 [M – C$_{20}$H$_{14}$N$_2$O$_5$ –Boc–CO$_2$]Na$^+$, 599.4 [M–C$_{20}$H$_{14}$N$_2$O$_5$–CO$_2$]H$^+$, 621 [M – C$_{20}$H$_{14}$N$_2$O$_5$ – CO$_2$]Na$^+$, 637.3 [M – C$_{20}$H$_{14}$N$_2$O$_5$ – CO$_2$]K$^+$, 905.3 [M – Boc]H$^+$, 971.3 [M – C$_4$H$_8$]Na$^+$, 1027.4 MNa$^+$, 1043.3 MK$^+$.

Dibenzyl (((3,5-bis((E)-4-nitrobenzylidene)-4-oxocyclohexyl)oxy)carbonyl)-L-lysylglycyl-L-aspartate trifluoroacetate salt (**22b**):

- MW = 1018.33 as TFA salt; quantitative yield from **22a**; yellow solid.

- ^{1}H NMR ((CD$_3$)$_2$SO, 400 MHz) δ_H 8.40 – 8.33 (m, 1H, Asp N*H*), 8.33 – 8.23 (m, 4H, 2 x o-NO$_2$ Ph*H*), 8.04 (br t, 1H, Gly N*H*), 7.86 – 7.72 (m, 6H, 2 x C*H*=C + 2 x m-NO$_2$ Ph*H*), 7.58 (br s, 3H, N*H$_3^+$*), 7.39 – 7.25 (m, 11H, 2 x Bn Ph*H* + Lys N*H*), 5.10 – 4.98 (m, 5H, C*H*-OCO + 2 x Bn C*H$_2$* [5.06 (s, 2H), 5.05 (s,2H)]), 4.78 – 4.67 (m, 1H Asp C*H$^{\alpha}$*), 3.95 – 3.57 (m, 3H, Lys C*H$^{\alpha}$* + Gly C*H$_2^{\alpha}$*), 3.30 – 3.07 (m, 4H, 2 x ring C*H$_2$*), 2.95 – 2.59 (m, 4H, Asp C*H$_2^{\beta}$* + Lys C*H$_2^{\epsilon}$*), 1.60 – 1.35 (m, 4H, Lys C*H$_2^{\beta}$* + Lys C*H$_2^{\delta}$*), 1.29 – 1.10 (m, 2H, Lys C*H$_2^{\gamma}$*).

- ^{13}C{^{1}H} NMR ((CD$_3$)$_2$SO, 400 MHz) δ_c 187.5 (*C*=O), 171.9, 170.6, 170.2, 168.4, , 155.3 (*C*ONH urethane), 147.6, 141.6, 137.4, 134.4, 135.3 (Bn), 131.1 (Bn), 130.9, 128.7 (br, Bn), 128.4 (br, Bn), 123.9, 67.9 (*C*H-OCO), 67.8 (Bn), 67.0 (Bn), 54.8 (Lys *C*$^{\alpha}$), 48.8 (Asp *C*$^{\alpha}$), 42.8 (Gly *C*$^{\alpha}$), 40.0 (Lys *C*$^{\epsilon}$), 36.3 (Asp *C*$^{\beta}$), 33.3 (ring *C*H$_2$), 32.2 (Lys *C*$^{\beta}$), 29.7 (Lys *C*$^{\delta}$), 22.4 (Lys *C*$^{\gamma}$).

- ESI-MS m/z 905.4 MH$^+$.

Compounds **23a-b** (2c-RGD)
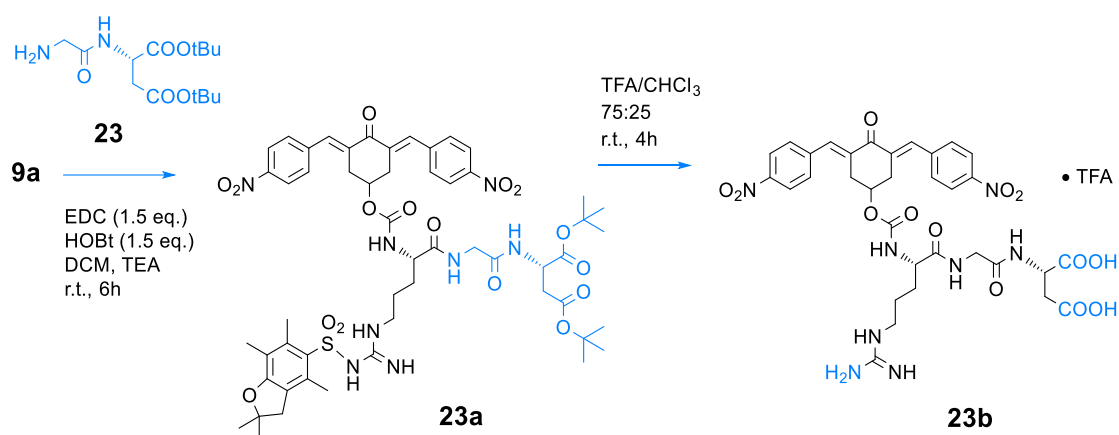
di-tert-butyl N^2-*(((3,5-bis((E)-4-nitrobenzylidene)-4-oxocyclohexyl)oxy) carbonyl)-N^ω-((2,2,4,6,7-pentamethyl-2,3-dihydrobenzofuran-5-yl)sulfonyl)-L-arginylglycyl-L-aspartate* (**23a**): obtained from the Arg conjugate **9a** (0.660 g, MW = 832.90; 0.792 mmol) and Gly-Asp di-*tert*-butyl ester **23** (0.260 g, MW = 302.20; 0.860 mmol) according to *Procedure E*. The crude product was purified by flash chromatography (eluent: CHCl$_3$/MeOH 99:1 → CHCl$_3$/MeOH 90:10).

- MW = 1116.45; yield = 46% from **9a**; yellow solid.
- ^{1}H NMR (CDCl$_3$, 400 MHz) δ$_H$ 8.27 – 8.13 (m, 4H, 2 x o-NO$_2$ PhH), 7.89 – 7.83 (m, 2H, 2 x CH=C), 7.65 – 7.50 (m, 5H, 2 x m-NO2 PhH + Gly NH), 7.06 – 6.95 (m, 1H, Asp NH), 6.38 – 5.70 (br m, 4H, Gdn + NH urethane), 5.25 – 5.09 (m, 1H, CH-OCO), 4.64 – 4.56 (m, 1H, Asp CH^α), 4.39 – 4.23 (m, 1H, Arg CH^α), 4.13 – 3.99 (m, 1H, Gly C$H^{\alpha 1}$), 3.87 – 3.71 (m, 1H, Gly C$H^{\alpha 2}$), 3.36 – 2.98 (m, 6H, Arg CH_2^δ + 2 x ring CH_2), 2.92 (s, 2H, CH_2 Pbf), 2.87 – 2.76 (m, 1H, Asp C$H^{\beta 1}$), 2.67 – 2.57 (m, 1H, Asp C$H^{\beta 2}$), 2.52, 2.46, 2.05 (3s, 3H each, 3 x CH_3 Pbf), 1.92 – 1.76 (m, 1H, Arg C$H^{\beta 1}$), 1.68 – 1.54 (m, 1H, Arg C$H^{\beta 2}$), 1.52 – 1.32 (m, 26H, Arg CH_2^γ + Pbf (CH_3)$_2$ [1.44 (s, 6H)] and 2 x (CH_3)$_3$ [1.39 (s, 18H)]).
- ^{13}C{^{1}H} NMR (CDCl$_3$, 400 MHz) δ$_c$ 187.5 (C=O), 172.6, 170.1, 169.7, 169.2, 158.7 (Pbf), 156.5 (C=NH), 155.3 (O-CONH), 147.4, 141.5, 138.2 (Pbf), 137.1,

134.5, 132.6 (Pbf), 132.2 (Pbf), 130.9, 124.7 (Pbf), 123.7, 117.5 (Pbf), 86.4 (Pbf), 82.6, 81.7 (2 x tBu), 67.6 (CH-OCO), 54.0 (Arg C^α), 49.3 (Asp C^α), 43.1 (Pbf), 42.6 (Gly C^α), 39.9 (Arg C^δ), 37.3 (Asp C^β), 33.1 (ring CH$_2$), 29.7 (Arg C^β), 28.6 (Pbf), 28.0 (tBu), 27.8 (tBu), 25.1 (Arg C^γ), 19.3 (Pbf), 17.9 (Pbf), 12.4 (Pbf).

- ESI-MS: m/z 1005.3 [M − 2 x C$_4$H$_8$]H$^+$, 1027.3 [M − 2 x C$_4$H$_8$]Na$^+$, 1061.4 [M − C$_4$H$_8$]H$^+$, 1083.3 [M − C$_4$H$_8$]Na$^+$, 1117.4 MH$^+$, 1139.4 MNa$^+$, 1155.3 MK$^+$.

(((3,5-bis((E)-4-nitrobenzylidene)-4-oxocyclohexyl)oxy)carbonyl)-L-arginyl glycyl-L-aspartic acid trifluoroacetate salt (**23b**): obtained from **23a** according to *Procedure B*.

- MW = 866.24 as TFA salt; yield = 86% from **23a**; sticky yellow solid.
- ^{1}H NMR ((CD$_3$)$_2$SO, 400 MHz) δ_H 8.34 − 8.23 (m, 4H, 2 x o-NO$_2$ PhH), 8.19 − 8.09 (m, 1H, Asp NH), 8.06 − 7.96 (m, 1H, Gly NH), 7.85 − 7.73 (m, 6H, 2 x CH=C + 2 x m-NO$_2$ PhH), 7.46 − 6.45 (m, 6H, NH urethane + protonated Gdn), 5-09 − 4.98 (m, 1H, CH-OCO), 4.50 (dt, J = 6.7, 1H, 6.4 Hz, Asp CH^α), 3.83 (br q, 1H, Arg CH^α), 3.78 − 3.57 (m, 2H, Gly C$H_2{}^\alpha$), 3.31 − 3.12 (m, 4H, 2 x ring CH_2), 2.98 (br q, 2H, Arg C$H_2{}^\delta$), 2.73 − 2.50 (m, partially overlapped to the signal of DMSO, 2H, Asp C$H_2{}^\beta$), 1.63 − 1.48 (m, 1H, Arg C$H^{\beta 1}$), 1.48 − 1.27 (m, 3H, Arg C$H^{\beta 2}$ + Arg C$H_2{}^\gamma$).
- ^{13}C{^{1}H} NMR ((CD$_3$)$_2$SO, 400 MHz) δ_c 187.2 (C=O), 172.3, 171.8, 171.7, 168.6, 156.7, 155.3, 147.1, 141.6, 136.0, 135.4, 131.3, 123.7, 67.1 (CH-OCO), 54.3 (Arg C^α), 48.6 (Asp C^α), 41.6 (Gly C^α), 40.5 (Arg C^δ), 36.1 (Asp C^β), 32.5 (ring CH$_2$), 28.8 (Arg C^β), 25.0 (Arg C^γ).
- ESI-MS: m/z 753.2 MH$^+$.
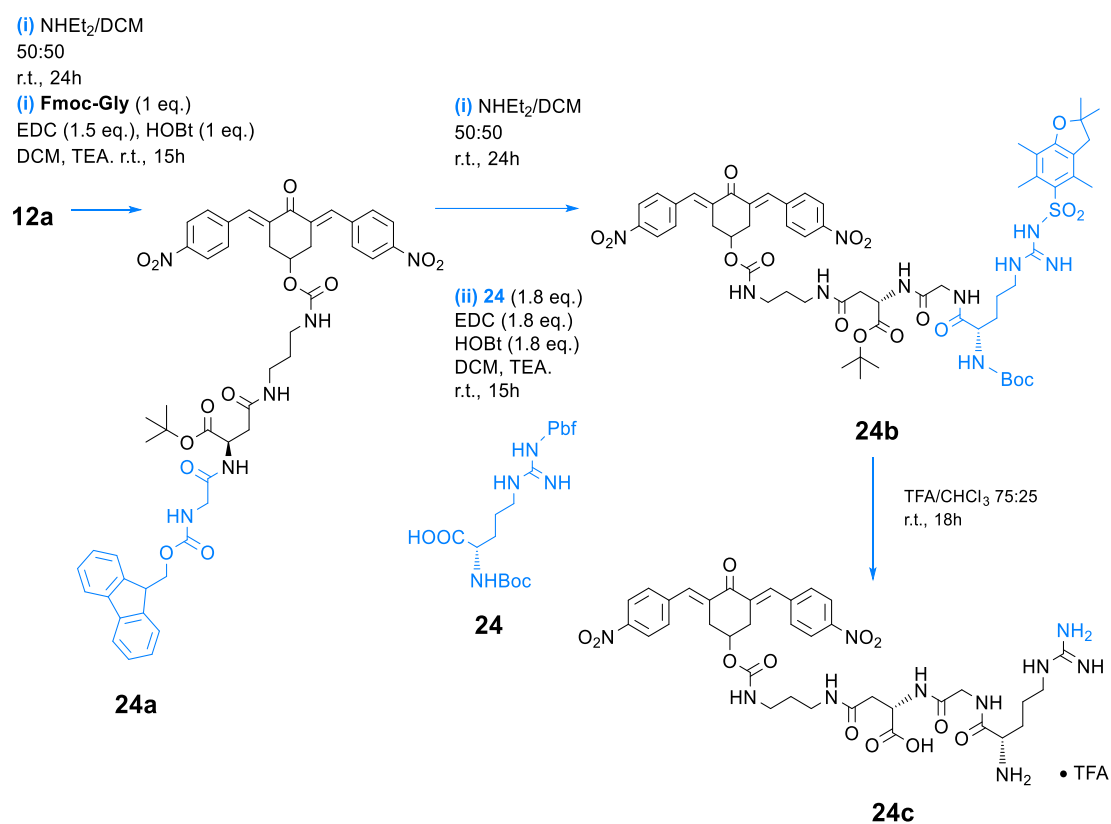
tert-butyl N^2-((((9H-fluoren-9-yl)methoxy)carbonyl)glycyl)-N^4-(3-((((3,5-bis ((E)-4-nitrobenzylidene)-4-oxocyclohexyl)oxy)carbonyl)amino)propyl)-L-asparaginate (**24a**): 0.718 g of Asp derivative **12a** (MW = 873.32; 0.822 mmol) were treated overnight with diethylamine and dichloromethane according to *Procedure C*. The filtered solid was reacted with 0.276 g of Fmoc-Gly (MW = 297.31; 0.928 mmol) according to *Procedure E*. The product **24a** was purified by flash chromatography (eluent: CHCl₃ → CHCl₃/MeOH 98:2).

- MW = 930.34; yield = 49% from **12a**; yellow solid.
- ¹H NMR (CDCl₃, 400 MHz) δ$_H$ 8.28 – 8.14 (m, 4H, 2 x o-NO₂ Ph*H*), 7.86 (br s, 2H, 2 x C*H*=C), 7.73 (app d, *J* = 7.3 Hz, 2H, 2 x Fmoc Ph*H*), 7.61 – 7.48 (m, 6H, 2 x m-NO₂ Ph*H* + 2 x Fmoc Ph*H*), 7.37 (app t, *J* = 7.3 Hz, 2H, 2 x Fmoc Ph*H*), 7.28 (app t, *J* = 7.3 Hz, 2H, 2 x Fmoc Ph*H*), 7.16 (d, *J* = 7.9 Hz, Asp N*H*), 6.09 (br t, 1H, N*H* amide), 5.67 (br t, 1H, N*H*-Fmoc), 5.28 (br t, 1H, N*H* urethane), 5.14 – 5.03 (m, 1H, C*H*-OCO), 4.63 (dt, *J* = 7.5, 4.6 Hz, 1H,

Asp CH^α), 4.40 – 4.30 (m, 2H, Fmoc CH_2), 4.20 (t, J = 7.1 Hz, 1H, Fmoc CH), 3.96 – 3.81 (m, 2H, Gly CH_2^α), 3.30 – 2.90 (m, 8H, 2 x ring CH_2 + 2 x CH_2 linker), 2.82 – 2.61 (m, 2H, Asp CH_2^β), 1.55 — 1.35 (m, 11H, CH_2 linker + tBu (CH_3)$_3$ [1.42 (s)]).

- ^{13}C NMR (CDCl$_3$, 400 MHz) 187.4 (C=O), 170.1, 169.6, 169.0, 156.7, 155.7 (2 x CONH urethane), 147.5, 143.7 (Fmoc), 141.5, 141.2 (Fmoc), 137.1, 134.5, 130.7, 127.8 (Fmoc), 127.1(Fmoc), 125.1 (Fmoc), 123.7, 120.0 (Fmoc), 82.6 (tBu), 67.2 (Fmoc CH$_2$), 49.9 (Asp C$^\alpha$), 47.0 (Fmoc CH), 44.3 (Gly C$^\alpha$), 37.9 (Asp C$^\beta$), 37.5, 35.9 (2 x CH$_2$ linker), 33.2 (ring CH$_2$), 29.7 (CH$_2$ linker), 27.9 (tBu).

- ESI-MS: m/z 653.2[M—C$_4$H$_8$–CO$_2$–DBF]H$^+$, 875.2 [M—C$_4$H$_8$]H$^+$, 897.3 [M—C$_4$H$_8$]Na$^+$, 913.2 [M—C$_4$H$_8$]K$^+$, 953.3 MNa$^+$, 969.2 MK$^+$.

tert-butyl N^4-(3-(((((3,5-bis((E)-4-nitrobenzylidene)-4-oxocyclohexyl)oxy) carbonyl)amino)propyl)-N^2-(N^2-(tert-butoxycarbonyl)-N$^\omega$-((2,2,4,6,7-pentamethyl-2,3-dihydrobenzofuran-5-yl)sulfonyl)-L-arginylglycyl)-L-asparaginate (**24b**): 0.375 g of **24a** (MW = 930.34; 0.404 mmol) were deprotected overnight with diethylamine and dichloromethane according to *Procedure C*. The obtained product was subsequentely reacted with 0.385 g of N$^\alpha$-Boc-N$^\omega$-Pbf-Arg **24** (MW = 526.65; 0.731 mmol) following *Procedure E*. The final product was purified by flash chromatography (eluent: CHCl$_3$/MeOH 99:1 → CHCl$_3$/MeOH 97:3).

- MW = 930.34; yield = 49% from **24a**; yellow solid.

- ^{1}H NMR (CDCl$_3$, 400 MHz) δ$_H$ 8.24, 8.24 (2 app. d, J = 8.8 Hz each, 4H, 2 x o-NO$_2$ PhH), 7.92 – 7.25 (m, 8H, 2 x CH=C + 2 x m-NO$_2$ PhH + Gly NH + Asp NH), 6.92 – 6.28 (m, 4H, NH amide linker + Gdn), 5.64 – 5.49 (m, 2H, NH-Boc + NH urethane), 5.24 – 5.07 (m, 1H, CH-OCO), 4.56 (br q, 1H, Asp CH^α), 4.27 – 3.97 (m, 2H, Arg CH^α + Gly C$H^{\alpha 1}$), 3.84 – 3.64 (m, 1H, Gly C$H^{\alpha 2}$), 3.42 – 2.98 (m, 10H, Arg CH_2^δ + 2 x CH_2 linker + 2 x ring CH_2), 2.93 (s, 2H, CH_2 Pbf), 2.79 – 2.68 (m, 2H, Asp CH_2^β), 2.54, 2.47, 2.06 (3s, 3H each, 3 x CH_3 Pbf), 1.88 – 1.76 (m, 1H, Arg C$H^{\beta 1}$), 1.71 – 1.25 (m, 29H, Arg C$H^{\beta 2}$ + CH_2^γ + CH_2 linker + Pbf (CH_3)$_2$ + 2 x (CH_3)$_3$ tBu).

- $^{13}C\{^1H\}$ NMR (CDCl$_3$, 400 MHz) δ_c 187.6 (C=O), 173.4, 170.4, 170.0, 169.4, 158.8 (Pbf), 156.5 (Arg C=NH), 155.8 (2C, 2 x O-CONH), 147.4, 141.7, 138.2 (Pbf), 137.1, 134.7, 132.8 (Pbf), 132.2 (Pbf), 130.9, 124.7 (Pbf), 123.8, 117.5 (Pbf), 86.5 (Pbf), 82.6 (tBu), 80.0 (Boc), 67.3 (CH-OCO), 54.0 (Arg C^α), 50.1 (Asp C^α), 43.2 (Pbf), 42.9 (Gly C^α), 40.2 (CH$_2$ linker), 38.0 (Asp C^β), 37.8 (Arg C^δ), 36.4 (CH$_2$ linker), 33.3 (ring CH$_2$), 30.0 (Arg C^β), 29.5 (CH$_2$ linker), 28.6 (Pbf), 28.4 (Boc), 27.9 (tBu), 25.3 (Arg C^γ), 19.3, 18.0, 12.5 (3 x Pbf).

- ESI-MS: m/z 1061.4 [M – 2 x C$_4$H$_8$ – CO$_2$]H$^+$, 1105.4 [M – 2 x C$_4$H$_8$]H$^+$, 1161.4 [M –C$_4$H$_8$]H$^+$, 1217.5 MH$^+$, 1239.4 MNa$^+$, 1255.4 MK$^+$.

N^2-L-arginylglycyl-N4-(3-((((3,5-bis((E)-4-nitrobenzylidene)-4-oxocyclohexyl)oxy)carbonyl)amino)propyl)-L-asparagine trifluoroacetate salt (**24c**): obtained from **24b** according to *Procedure D*.

- MW = 930.34 as TFA salt; yield = 79% from **24b**; sticky yellow solid.

- ^1H NMR ((CD$_3$)$_2$SO, 500 MHz) δ_H 9.12 – 8.85 (m, 1H, Gly NH), 8.40 – 6.91 (br m, 21H, 2 x o-NO$_2$ PhH + 2 x m-NO$_2$ PhH + 2 x CH=C + 11 x NH), 5.12 – 4.64 (m, 1H, CH-OCO), 4.33 – 4.01 (m, 1H, Asp CH^α), 3.93 – 2.68 (overlapped to the signal of H$_2$O, Gly C$H_2{}^\alpha$ + Arg C$H_2{}^\delta$ + 2 x ring CH_2 + 2 x CH_2 linker), 2.55 – 2.33 (m, partially overlapped to the signal of DMSO, 2H, Asp C$H_2{}^\beta$), 1.92 – 1.15 (m, 6H, Arg C$H_2{}^\beta$ + Arg C$H_2{}^\gamma$ + CH_2 linker).

- $^{13}C\{^1H\}$ NMR ((CD$_3$)$_2$SO, 500 MHz) δ_c 187.2 (C=O), 173.6, 169.5, 169.4, 168.0, 157.0, 155.2, 147.0, 141.5, 135.8, 135.4, 131.2, 123.6, 66.6 (CH-OCO), 51.8 (Arg C^α), 50.2 (Asp C^α), 42.2 (Gly C^α), 40.2 (overlapped to the signal of DMSO, Arg C^δ), 37.8 (2C, Asp C^β + CH$_2$ linker), 36.1 (CH$_2$ linker), 32.6 (ring CH$_2$), 29.1 (CH$_2$ linker), 28.3 (Arg C^β), 23.3 (Arg C^γ).

- ESI-MS: m/z 809.3 MH$^+$.

25

+

2c-OSu

DMF, TEA
r.t., 4h

25a
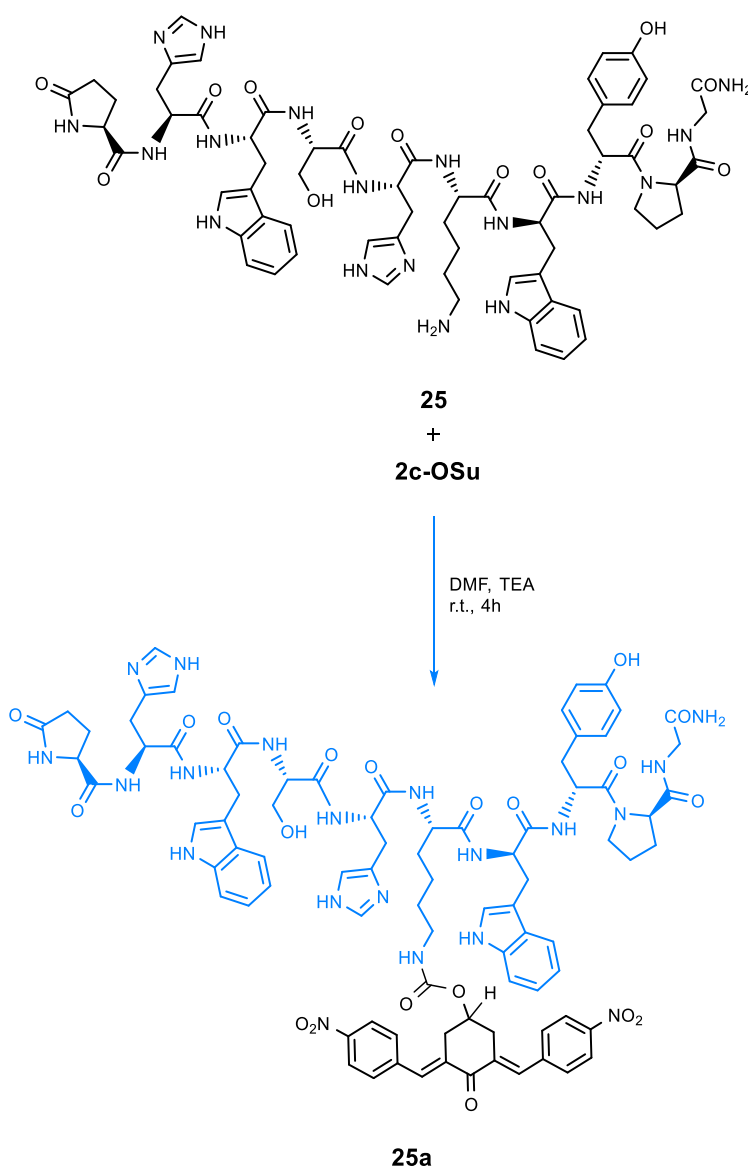
3,5-bis((E)-4-nitrobenzylidene)-4-oxocyclohexyl ((3S,6S,9S,12S,15S)-3,12-bis((1H-imidazol-4-yl)methyl)-6-((1H-indol-3-yl)methyl)-15-(((R)-1-(((R)-1-((R)-2-((2-amino-2-oxoethyl)carbamoyl)pyrrolidin-1-yl)-3-(4-hydroxyphenyl)-1-oxopropan-2-yl)amino)-3-(1H-indol-3-yl)-1-oxopropan-2-yl)carbamoyl)-9-(hydroxymethyl)-1,4,7,10,13-pentaoxo-1-((S)-5-oxopyrrolidin-2-yl)-2,5,8,11,14-pentaazanonadecan-19-yl)carbamate (**25a**): 0.045 g of decapeptide pGlu-His-Trp-Ser-His-Lys-Trp-Tyr-Pro-Gly-NH₂ **25** (MW = 1306.60; 0.033 mmol) and 0.017 g of **2c-OSu** (MW = 521.11; 0.336 mmol; 0.033 mmol) were dissolved in a solution of 0.1 mL of TEA in 2.0 mL of DMF (apparent pH = 9). The resulting mixture was stirred for 4h

and then evaporated under vacuum. The product was precipitated from chloroform, filtered, washed with cold chloroform, and dried at 60°C overnight.

- MW = 1712.68; yield = 79% from **25**; yellow solid.
- ^{1}H NMR ((CD$_3$)$_2$SO), 500 MHz) δ_H 10.86 – 10.75 (m, 1H, Trp NH), 10.75 – 10.62 (m, 1H, Trp NH), 8.75 (s, 2H, NH_2 amide), 8.37 – 7.97 (m, 11H, 2 x o-NO$_2$ PhH + 2 x Trp NH + 2 x His NH + Tyr NH + Gly NH + Ser NH), 7.95 – 7.50 (m, 10H, 2 x m-NO$_2$ PhH + 2 x C=CH + Lys NH + pGlu NH + 2 x Trp ArH), 7.35 – 6.85 (m, 15H, 8 x Trp PhH + 4 x His PhH + 2 x Tyr PhH + NH urethane), 6.70 – 6.59 (m, 2H, 2 x Tyr PhH), 5.12 – 4.97 (m, 1H, CH-OCO), 4.69 – 4.45 (m, 5H, 2 x Trp CH^α + 2 x His CH^α + Tyr CH^α), 4.36 – 4.11 (m, 3H, Ser CH^α + Pro CH^α + Lys CH^α), 4.27 – 4.21 (m, 1H,), 4.21 – 4.11 (m, 1H), 4.00 – 3.93 (m, 1H, pGlu CH^α), 3.81 – 2.56 (m, 22H, 2 x Hys C$H_2{}^\beta$ + 2 x Trp C$H_2{}^\beta$ + Tyr C$H_2{}^\beta$ + Pro C$H_2{}^\delta$ + Ser C$H_2{}^\beta$ + Gly C$H_2{}^\alpha$ + Lys C$H_2{}^\varepsilon$ + 2 x ring CH_2 (2c)), 2.19 – 1.54 (m, 8H, Pro C$H_2{}^\beta$ + Pro C$H_2{}^\gamma$ + pGlu C$H_2{}^\beta$ + pGlu C$H_2{}^\gamma$), 1.24 – 0.97 (m, 4H, Lys C$H_2{}^\beta$ + Lys C$H_2{}^\delta$), 0.84 – 0.57 (m, 2H, Lys C$H_2{}^\gamma$).
- ^{13}C{^{1}H} NMR ((CD$_3$)$_2$SO), 500 MHz) δ_c 187.66 (C=O), 177.91, 172.95, 172.08, 172.01, 171.55, 171.50, 171.23, 170.83, 170.60, 170.23, 169.99, 156.27, 155.64 (CONH urethane), 147.47, 141.95, 136.48, 136.41, 136.23, 135.85, 134.33, 134.18, 131.70, 130.68, 130.56, 130.09, 128.00, 127.73, 127.57, 124.28, 124.18, 124.07, 123.45, 121.28, 121.15, 118.96, 118.85, 118.60, 118.51, 117.34, 115.45, 111.69, 111.60, 110.22, 110.10, 79.63, 66.91, 62.04, 60.46, 55.85, 55.42, 53.75, 53.52, 53.15, 52.85, 52.31, 51.94, 47.36, 42.46, 40.41, 36.47, 33.06, 32.20, 29.54, 29.41, 29.27, 28.27, 28.08, 27.76, 27.70, 25.68, 25.45, 24.92, 22.38.
- ESI-MS: m/z 1713.7 MH$^+$.

Synthesis and Characterization of α,β-Unsaturated Esters Derivatives

Compound **29**
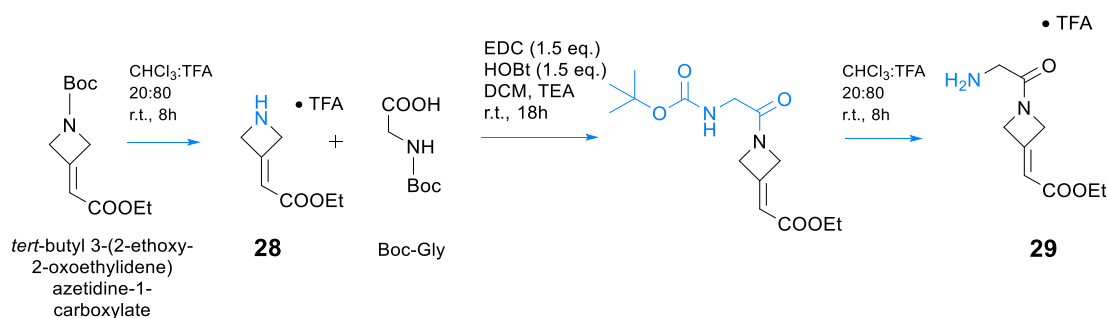
Ethyl 2-(azetidin-3-ylidene)acetate trifluoroacetate salt (**28**): obtained from *tert*-butyl 3-(2-ethoxy-2-oxoethylidene)azetidine-1-carboxylate according to *Procedure B*.

- MW = 255.10 as TFA salt; quantitative yield; viscous colourless liquid.
- ^{1}H NMR (CD$_3$OD, 400 MHz) (8:2 mixture of conformers s-cis and s-trans by analysis of C=C*H* signals at 6.20 and 5.91 ppm) δ$_H$ 6.20, 5.91 (2 quint, J = 1.8, 2.5 Hz respectively, 1H in total, C=C*H* of each rotamer), 5.08 – 5.02, 4.95 – 4.94, 4.90 – 4.86 (3m, 4H in total, 4 x C*H* ring), 4.17 (q, J = 7.1 Hz, 2H, O-C*H*$_2$), 1.26 (t, J = 7.1 Hz, 3H, C*H*$_3$).

Ethyl 2-(1-glycylazetidin-3-ylidene)acetate trifluoroacetate salt (**29**): compound **28** (0.423 g, MW = 255.10 as TFA salt; 1.66 mmol) was reacted with Boc-Gly (0.315 g, MW = 175.18; 1.80 mmol) according to *Procedure E*. The deprotection was carried out according to *Procedure B* on the crude intermediate affording the final product **29**, which was used in the next step without further purification.

- MW = 312.12 as TFA salt; yield = 85% from **28**; white solid.
- ^{1}H NMR (CD$_3$OD, 500 MHz) (8:2 mixture of conformers s-cis and s-trans by analysis of O-CH_2 signals at 4.18 and 3.60 ppm) δ_H 5.95 – 5.89 (m, 1H, C=CH), 5.34 – 5.30, 5.18 – 5.09, 5.05 – 5.00, 4.97 – 4.90, 4.90 – 4.83, 4.79 – 4.74 (6m, 4H in total, 4 x CH ring), 4.18, 3.60 (2q, J = 7.1 Hz each, 2H, O-CH_2 of each rotamer), 3.81 – 3.75 (m, 2H, Gly CH_2^α), 1.28, 1.17 (2t, J = 7.1 Hz each, 3H, CH_3 of each rotamer).
- ^{13}C NMR (CD$_3$OD, 500 MHz) (rotamer mixture) δ_C 163.4, 163.2, 150.4, 114.0 (C=CH), 60.2 (O-CH$_2$), 59.2, 58.2, 57.1, 38.1 (Gly C^α), 13.1 (CH$_3$).

Compounds **31a-b**
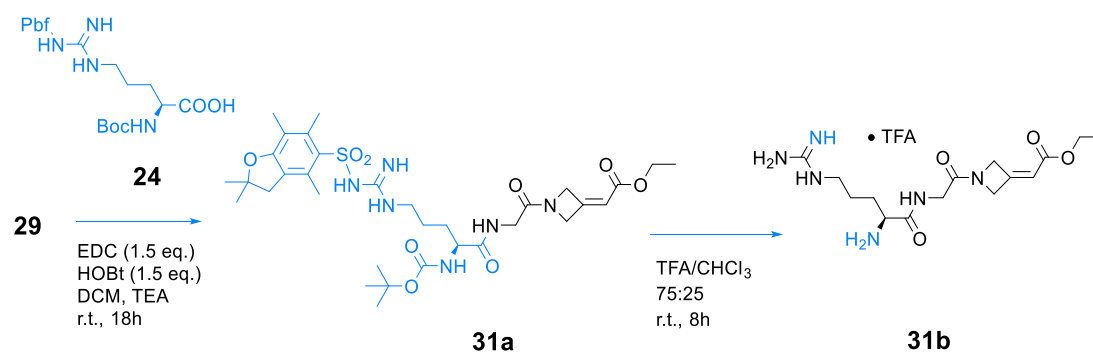
Ethyl 2-(1-(N^2-(tert-butoxycarbonyl)-N$^\omega$-((2,2,4,6,7-pentamethyl-2,3-dihydro benzofuran-5-yl)sulfonyl)-L-arginylglycyl)azetidin-3-ylidene)acetate (**31a**): obtained from 0.395 g of **29** (MW = 312.12 as TFA; 1.27 mmol) and 0.977 g of N$^\alpha$-Boc-N$^\omega$-Pbf-Arg **24** (MW = 526.65; 1.86 mmol) according to *Procedure E*. The product **31a** was purified by flash chromatography (eluent: CHCl$_3$ → CHCl$_3$/MeOH 97:3).

- MW = 706.34; yield = 54% from **29**; white to pale yellow solid.
- ^{1}H NMR (CDCl$_3$, 400 MHz) (1:1 mixture of conformers s-cis and s-trans by analysis of Arg CH_2^δ signals at 3.35 and 3.12 ppm) δ_H 7.86 – 7.70 (m, 1H, Gly NH), 6.87 – 6.07 (br m, 3H, Gdn), 5.80 (br s, 1H, C=CH), 5.71 – 5.58

(m, 1H, N*H*-Boc), 5.14 – 5.05, 4.94 – 4.80, 4.69 – 4.59 (4m, 4H in total 4 x C*H* ring), 4.35 – 4.23 (m, 1H, C*H*$^{\alpha}$ Arg), 4.16 (q, *J* = 7.1 Hz, 2H, O-C*H*$_2$), 4.06 – 3.74 (2 m, 2H in total, Gly C*H*$_2{}^{\alpha}$ of each rotamer), 3.46 – 3.01 (2m, 2H in total, C*H*$_2{}^{\delta}$ Arg of each rotamer), 2.94 (s, 2H, C*H*$_2$ Pbf), 2.56, 2.49, 2.07 (3s, 3H each, 3 x C*H*$_3$ Pbf), 1.93 – 1.79 (m, 1H, C*H*$^{\beta 1}$ Arg), 1.69 – 1.50 (m, 3H, C*H*$^{\beta 2}$ Arg + C*H*$_2{}^{\gamma}$ Arg), 1.44 (s, 6H, (C*H*$_3$)$_2$ Pbf), 1.38 (s, 9H, (C*H*$_3$)$_3$ Boc), 1.26, 1.26 (2t, *J* = 7.1 Hz each, 3H in total, C*H*$_3$ of each rotamer).

- ^{13}C{^{1}H} NMR (CDCl$_3$, 400 MHz) (rotamer mixture) δ$_c$ 173.3, 168.9, 164.9, 164.9, 158.9 (Pbf), 156.7, 156.5 (*C*=NH and *C*ONH Boc), 150.1, 149.9 (2 x *C*=CH), 138.5 (Pbf), 132.5 (Pbf), 124.7 (Pbf), 117.6 (Pbf), 114.6, 114.6 (2 x C=*C*H), 86.4 (Pbf), 79.6 (Boc), 60.8, 60.6 (O-*C*H$_2$), 59.5, 58.6, 57.2, 53.4 (*C*$^{\alpha}$ Arg), 43.2 (Pbf), 39.7, 39.6 (Gly *C*$^{\alpha}$ + Arg *C*$^{\delta}$), 30.1 (Arg *C*$^{\beta}$), 28.6 (Pbf), 28.3 (Boc), 25.2 (Arg *C*$^{\gamma}$), 19.3 (Pbf), 18.0 (Pbf), 14.2 (*C*H$_3$), 12.5 (Pbf).

- ESI-MS: m/z 607.4 [M–Boc]H$^+$, 629.4 [M–Boc]Na$^+$, 651.4 [M–C$_4$H$_8$]H$^+$, 707.4 MH$^+$, 729.4 MNa$^+$.

Ethyl 2-(1-(L-arginylglycyl)azetidin-3-ylidene)acetate trifluoroacetate salt (**31b**): obtained from **31a** according to *Procedure D*.

- MW = 468.22 as TFA salt; yield = 78% from **31a**; pale yellow sticky solid.

- ^{1}H NMR (CD$_3$OD, 400 MHz) (85:15 mixture of conformers s-cis and s-trans by analysis of C=C*H* signals at 6.02 and 5.92 ppm) δ$_H$ 6.02, 5.92 (2 br s, 1H in total, C=C*H* of each rotamer), 5.24 – 5.13, 5.06 – 4.96, 4.92 – 4.82 (overlapped to the signal of H$_2$O), 4.77 – 4.66 (4m, 4H in total 4 x C*H* ring), 4.32 – 3.84 (br m, 5H, Gly C*H*$_2{}^{\alpha}$+ O-C*H*$_2$ + C*H*$^{\alpha}$ Arg), 3.35 – 3.15 (m, partially overlapped to the signal of CD$_3$OD, 2H, C*H*$_2{}^{\delta}$ Arg), 2.12 – 1.66 (m, 4H, C*H*$_2{}^{\beta}$ Arg + C*H*$_2{}^{\gamma}$ Arg), 1.35 – 1.19 (m, 3H, C*H*$_3$)

- ^{13}C NMR (CD$_3$OD, 400 MHz) (rotamer mixture) δ$_C$ 169.5, 168.8, 165.3, 157.3 (*C*=NH), 151.2(*C*=CH), 113.7(C=*C*H), 63.8 (O-*C*H$_2$), 60.5, 60.2 (O-*C*H$_2$), 59.0, 57.0, 52.5, 40.3 (Arg *C*$^{\delta}$), 39.3 (Gly *C*$^{\alpha}$), 28.1 (Arg *C*$^{\beta}$), 23.5 (Arg *C*$^{\gamma}$), 14.0, 13.2 (2 x *C*H$_3$).

- ESI-MS: m/z 327.2 [M–C$_2$H$_5$]H$^+$, 355.2 MH$^+$.

Compounds 32a-b
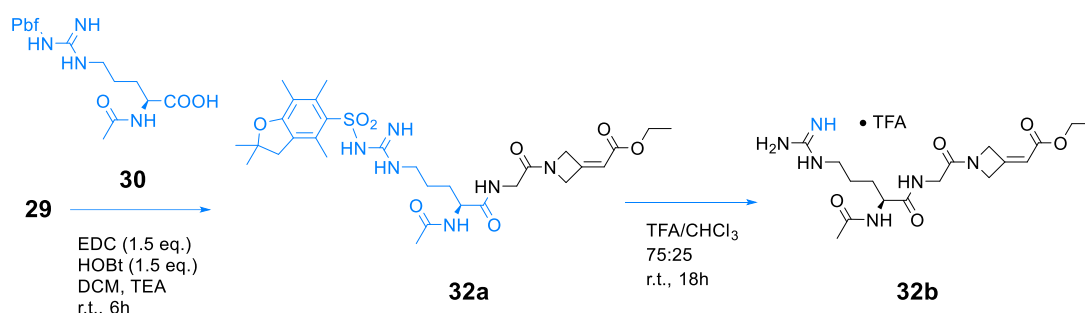
Ethyl 2-(1-(N²-acetyl-Nω-((2,2,4,6,7-pentamethyl-2,3-dihydrobenzofuran-5-yl)sulfonyl)-L-arginylglycyl)azetidin-3-ylidene)acetate (**32a**): obtained from 0.181 g of **29** (MW = 312.12 as TFA; 0.580 mmol) and 0.350 g of N^α-Acetyl-N^ω-Pbf-Arg **30** (MW = 468.20; 0.748 mmol) according to *Procedure E*. The product was purified by flash chromatography (eluent: CHCl₃/MeOH 99:1 → 95:5).

- MW = 648.29; yield = 47% from **29**; white to pale yellow solid.
- ¹H NMR (CDCl₃, 500 MHz) (1:1 mixture of conformers s-cis and s-trans by analysis of Arg CH_2^δ signals at 3.27 and 3.16 ppm) δ_H 7.92 – 7.83 (m, 1H, Gly N*H*), 7.19 – 7.07 (m, 1H, Ac N*H*), 6.80 – 6.21 (br m, 3H, Gdn), 5.83 – 5.79 (m, 1H, C=C*H*), 5.71 – 5.58, 5.11 – 5.04, 4.92 – 4.83, 4.67 – 4.62 (4m, 4H in total 4 x C*H* ring), 4.61 – 4.54 (m, 1H, CH^α Arg), 4.16 (q, *J* = 7.1 Hz, 2H, O-C*H₂*), 3.99 – 3.79 (2 m, 2H in total, Gly CH_2^α), 3.36 – 3.11 (2m, 2H in total, CH_2^δ Arg of each rotamer), 2.93 (s, 2H, C*H₂* Pbf), 2.55, 2.48, 2.06 (3s, 3H each, 3 x C*H₃* Pbf), 1.98 (s, 3H, Ac C*H₃*)1.93 – 1.83 (m, 1H, C$H^{\beta1}$ Arg), 1.74 – 1.50 (m, 3H, C$H^{\beta2}$ Arg + CH_2^γ Arg), 1.44 (s, 6H, (C*H₃*)₂ Pbf), 1.26, 1.26 (2t, *J* = 7.1 Hz each, 3H in total, C*H₃*).
- ¹³C{¹H} NMR (CDCl₃, 500 MHz) (rotamer mixture) δ_c 172.9, 170.9, 168.7, 164.9, 164.9, 158.8 (Pbf), 156.6, (*C*=NH), 150.0 (*C*=CH), 150.0 (*C*=CH), 138.3 (Pbf), 132.7 (Pbf), 132.3 (Pbf), 124.7 (Pbf), 117.6 (Pbf), 114.6, 86.4 (Pbf), 60.8, 60.5 (O-*C*H₂), 59.5, 58.6, 57.2, 52.6 (*C*$^\alpha$ Arg), 43.2 (Pbf), 40.1 (Arg *C*$^\delta$), 39.8 39.7 (2 x Gly *C*$^\alpha$), 29.7 (Arg *C*$^\beta$), 28.6 (Pbf), 25.2 (Arg *C*$^\gamma$), 23.0 (Ac *C*H₃), 19.3 (Pbf), 18.0 (Pbf), 14.2 (*C*H₃), 12.5 (Pbf).

- ESI-MS: m/z 671.3 MNa$^+$.

Ethyl 2-(1-(acetyl-L-arginylglycinyl)azetidin-3-ylidene)acetate trifluoroacetate salt (**32b**): obtained from **31a** according to *Procedure D*.

- MW = 510.23 as TFA salt; yield = 71% from **32a**; colourless/pale yellow sticky solid.

- ^{1}H NMR ((CD$_3$)$_2$SO, 400 MHz) (85:15 mixture of conformers s-cis and s-trans by analysis of Gly NH signals at 8.23 and 8.09 ppm and Arg NH signals at 8.18 and 8.08 ppm) δ_H 8.23, 8.09 (2t, J = 5.0 Hz each, 1H in total, Gly NH of each rotamer), 8.18, 8.00 (2d, J = 8.1 Hz each, 1H in total, Arg NH of each rotamer), 7.70 – 6.56 (br m, 5H, protonated Gdn), 5.99 – 5.85 (m, 1H, C=CH), 5.11 – 4.98, 4.95 – 4.86, 4.86 – 4.77, 4.75 – 4.65, 4.62 – 4.51 (5m, 4H in total, 4 x CH ring), 4.36 – 4.22 (m, 1H, Arg CH^α), 4.11 (q, J = 7.1 Hz, 2H, O-CH_2), 3.83 — 3.67 (m, 2H, Gly C$H_2{}^\alpha$), 3.14 – 3.01 (m, 2H in total, C$H_2{}^\delta$ Arg), 1.85 (s, 3H, Ac CH_3), 1.75 – 1.85 (m, 1H, C$H^{\beta 1}$ Arg), 1.58 – 1.39 (m, 3H, C$H^{\beta 2}$ Arg + C$H_2{}^\gamma$ Arg), 1.20 (t, J = 7.1 Hz, 3H, CH_3).

- ^{13}C{^{1}H} NMR (CD$_3$OD, 400 MHz) (rotamer mixture) δ_c 174.7, 173.7, 173.1, 172.1, 170.8, 169.3, 169.1, 165.3, 157.2 (C=NH), 151.2 (C=CH), 114.7, 113.7 (2 x C=CH), 60.7, 60.2 (O-CH$_2$), 58.9, 56.9, 53.7, 52.8, 42.4 (Gly C^α), 40.6 (Arg C^δ), 39.4 (Gly C^α), 28.7 (Arg C^β), 24.7 (Arg C^γ), 21.1 (Ac CH$_3$), 13.2 (CH$_3$).

- ESI-MS: m/z 397.2 MH$^+$.
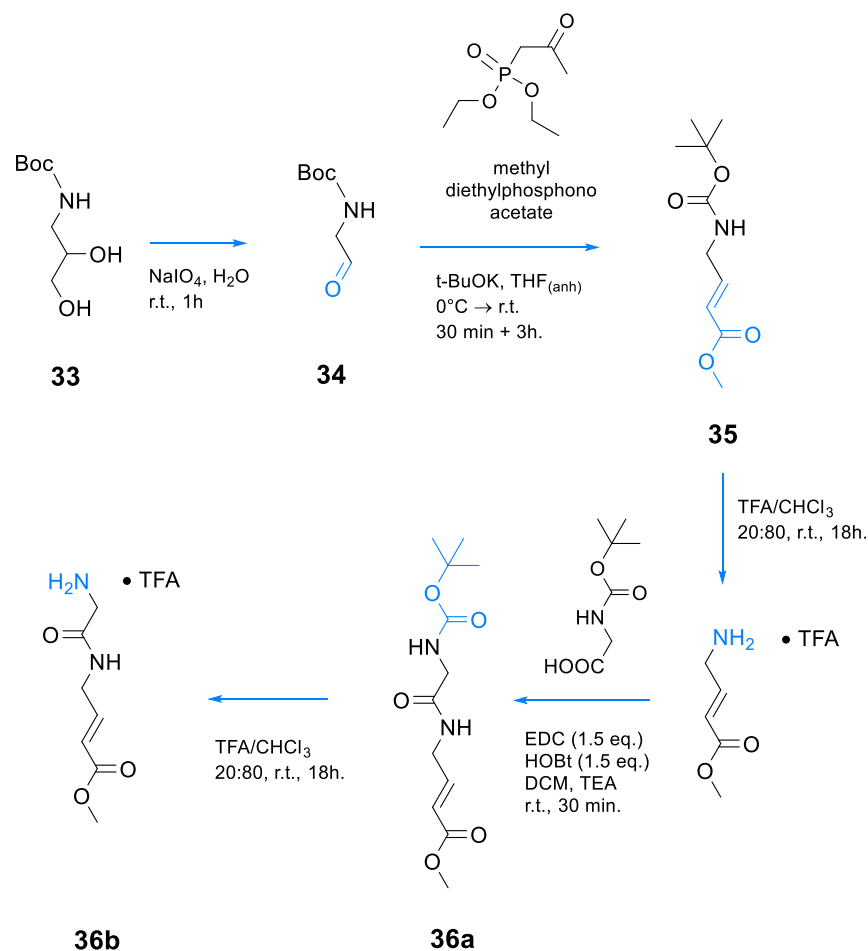
tert-butyl (2,3-dihydroxypropyl)carbamate (**33**): 3-Amino-1,2-propanediol (7.942 g, MW = 91.11; 87.17 mmol) and Boc$_2$O (19.534 g, MW = 218.25; 89.50 mmol) were dissolved in 70 mL of dichloromethane and 10 mL of methanol. The resulting mixture was stirred overnight, then evaporated under vacuum to afford a crude product **33** which was used without further purification in the next step.

- MW = 191.12; yield = 90%; viscous colourless liquid that tends to solidify at r.t.
- ^{1}H NMR (CDCl$_3$, 400 MHz) δ$_H$ 5.30 - 4.74 (br, 1H, N*H*-Boc), 3.74 (quint, *J* = 5.2 Hz, 1H), 3.57 (m, 2H), 3.31 – 2.77 (m, 2H), 1.44 (s, 9H, Boc (C*H$_3$*)$_3$).

tert-butyl (2-oxoethyl)carbamate (**34**): a misture of compound **33** (1.974 g, MW = 191.12; 10.31 mmol) and NaIO$_4$ (2.655 g, MW = 213.84; 12.4 mmol) in 17 mL of water was stirred at r.t. in a flask wrapped in aluminum foil to avoid light exposure. After 1h, the solid formed was filtered and washed with small volumes of

cold water (beware: the solid is partially hydrosoluble). The mother liquor was extracted 6 x with ethyl acetate, the combined organic phases were dried over Na_2SO_4 and evaporated to afford the crude product **34**.

- MW = 159.09; yield = 94% from **33**; viscous pale-yellow liquid that tends to solidify at r.t.
- ^{1}H NMR (CDCl$_3$, 400 MHz) δ_H 9.65 (s, 1H, C*H*O), 5.18 (br, 1H), 4.07 (m, 2H), 1.45 (s, 9H).

Methyl (E)-4-((tert-butoxycarbonyl)amino)but-2-enoate (**35**): 1.091 g of *t*-BuOK (MW = 112.21; 9.72 mmol) were dissolved at 0°C in 35 mL of anhydrous THF under Ar. Methyl diethylphosphonoacetate (2.0 mL, MW = 210.16, *d* = 1.145 g/mL; 10.9 mmol) was subsequently added dropwise. After 30 minutes stirring at 0°C, a solution of compound **34** (1.546 g, MW 159.09; 9.72 mmol) in 10 mL of anhydrous THF was added to the mixture over 8 minutes. The obtained solution was slowly warmed to r.t. and stirred for 3 hours, then evaporated to dryness, diluted with water, and extracted 3 x with ethyl acetate. The combined organic phases were dried over Na_2SO_4 and evaporated to afford the final product **35** as a crude that was purified by flash chromatography (eluent: hexane/ethyl acetate 70:30).

- MW = 215.12; yield = 90% from **34**; white solid
- ^{1}H NMR (CDCl$_3$, 500 MHz) δ_H 6.91 (dt, *J* = 15.7, 4.9 Hz, 1H, =C*H*-CH$_2$), 5.94 (dt, *J* = 15.7, 4.9 Hz, 1H, =C*H*-COO), 4.70 (br s, 1H, N*H*), 3.92 (m, 2H, C*H$_2$*), 3.74 (s, 3H, O-C*H$_3$*), 1.45 (s, 9H, Boc).

Methyl (E)-4-(2-aminoacetamido)but-2-enoate trifluoroacetate salt (**36b**): compound **35** was Boc-deprotected according to *Procedure B* until complete conversion (TLC), and the resulting crude was directly reacted with 1.0 eq. of Boc-Gly following *Procedure E*. The crude mixture was purified by flash chromatography (eluent: hexane/ethyl acetate 70:30 → 30:70) and the isolated product **36a** was subsequently deprotected following *Procedure B* to afford the final product **36b**.

- MW = 286.10 as TFA salt; yield = 58% from **35**; white to pale yellow solid.
- ^{1}H NMR ((CD$_3$)$_2$SO, 500 MHz) δ$_H$ 8.64 (t, J = 5.8 Hz, 1H, NH), 8.12 – 7.91 (br, 3H, NH_3^+), 6.85 (dt, J = 15.8, 4.6 Hz, 1H, =CH-CH$_2$), 5.95 (dt, J = 15.8, 4.6 Hz, 1H, =CH-COO), 4.70 (br s, 1H, NH), 3.97 – 3.93 (m, 2H, Gly CH_2^α), 3.67 – 3.56 (m, 5H, CH_2 + O-CH_3).

Compounds **37a-b**
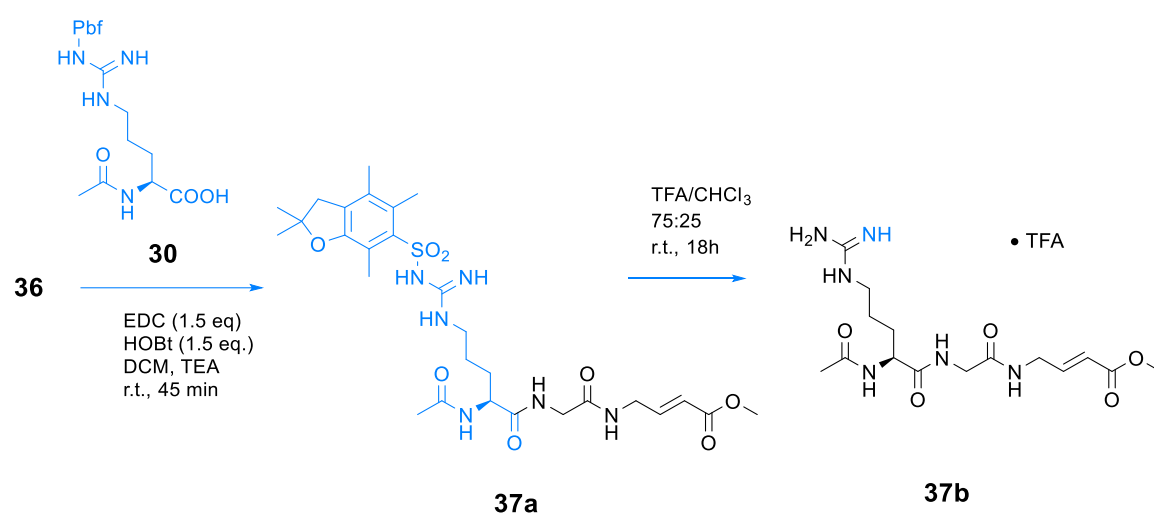
Methyl (S,E)-4-(2-(2-acetamido-5-(3-((2,2,4,5,7-pentamethyl-2,3-dihydrobenzofuran-6-yl)sulfonyl)guanidino)pentanamido)acetamido)but-2-enoate (**37a**): obtained from **36** (0.344 g, MW = 286.10 as TFA salt; 1.20 mmol) and N$^\alpha$-Acetyl-N$^\omega$-Pbf-Arg **30** (0.834 g, MW = 468.20; 1.78 mmol) according to *Procedure E*, then purified by flash chromatography (eluent: CHCl$_3$/MeOH 99:1 → 93:7).

- MW = 622.28; yield = 46% from **36**; white to pale yellow solid.
- ^{1}H NMR (CDCl$_3$, 500 MHz) δ$_H$ 8.08 (br t, 1H, NH Gly), 7.71 (br t, 1H, NH), 7.57 (br, 1H, NH Ac), 6.83 (dt, J = 15.8, 4.7 Hz, 1H, =CH-CH$_2$), 6.56 – 6.23 (m, 3H, NH Gdn), 5.88 (d, J = 15.8 Hz, 1H, =CH-COO), 4.32 (br q, 1H, CH^α Arg), 4.05 – 3.83 (m, 4H, CH_2^α Gly + CH_2-NH), 3.66 (s, 3H, O-CH_3), 3.37 – 3.07 (m, 2H, CH_2^δ Arg), 2.93 (s, 2H, CH_2 Pbf), 2.54, 2.47, 2.07 (3s, 3H

each, 3 x CH_3 Pbf), 1.96 (s, 3H, CH_3 Ac), 1.89 – 1.50 (m, 4H, CH_2^β Arg + CH_2^γ Arg), 1.45 (s, 6H, (CH_3)$_2$ Pbf).

- ^{13}C{^{1}H} NMR (CDCl$_3$, 500 MHz) δ_c 173.5, 172.1, 169.9, 166.7, 158.9 (Pbf), 156.6 (C=NH), 144.5 (CH$_2$-CH=), 138.2 (Pbf), 132.4 (Pbf), 132.1 (Pbf), 124.8 (Pbf), 120.9(=CH-COO), 117.6 (Pbf), 86.5 (Pbf), 54.0 (C^α Arg), 51.6 (O-CH$_3$), 43.2 (2C, Pbf + C^α Gly), 40.0 (2C, C^δ Arg + CH$_2$-CH=), 28.6 (2C, Pbf + C^β Arg), 25.6 (C^γ Arg), 22.7 (CH$_3$ Ac), 19.3 (Pbf), 18.0 (Pbf), 12.5 (Pbf).

- MS: m/z 623.3 MH$^+$, 645.3 MNa$^+$.

Methyl (S,E)-4-(2-(2-acetamido-5-guanidinopentanamido)acetamido)but-2-enoate trifluoroacetate salt (**37b**): obtained from **37a** according to *Procedure D*.

- MW = 484.22 as TFA salt; yield = 66% from **37a**; brownish glue.
- ^{1}H NMR ((CD$_3$)$_2$SO, 400 MHz) δ_H 8.31 (t, J = 5.5 Hz, 1H, NH), 8.17 (d, J = 7.0 Hz, 1H, NH Ac), 8.05 (t, J = 5.5 Hz, 1H, CONH Gly), 7.60 – 6.67 (br m, 6H, protonated Gdn + CH$_2$-CH= [6.81 (dt, J = 15.8, 4.4 Hz, 1H)]), 5.88 (d, J = 15.8 Hz, 1H, =CH-COO), 4.15 (br q, 1H, CH^α Arg), 3.95 – 3.78 (m, 2H, CH_2-CH=), 3.78 – 3.65 (m, 2H, CH_2 Gly), 3.63 (s, 3H, O-CH_3), 3.13 – 3.01 (m, 2H, CH_2^δ Arg), 1.84 (s, 3H, CH_3 Ac), 1.73 – 1.60 (m, 3H, C$H^{\beta1}$ Arg), 1.56 – 1.37 (m, 3H, C$H^{\beta2}$ Arg + CH_2^γ Arg).
- MS: m/z 371.2 MH$^+$.

Compounds **39a-b**
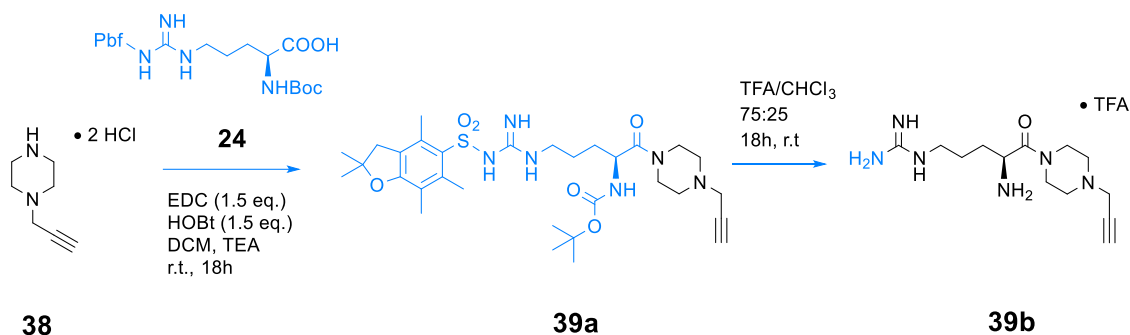
tert-butyl (S)-(1-oxo-5-(3-((2,2,4,6,7-pentamethyl-2,3-dihydrobenzofuran-5-yl)sulfonyl)guanidino)-1-(4-(prop-2-yn-1-yl)piperazin-1-yl)pentan-2-yl)carbamate (**39a**): prepared from N^α-Boc-N^ω-Pbf-Arg **24** (0.415 g, MW = 526.65; 0.788 mmol) and **38** (0.100 g, MW = 187.11 as HCl salt; 0.534 mmol) according to *Procedure E*. The product was purified by flash chromatography (eluent: $CHCl_3 \rightarrow CHCl_3/MeOH$ 98:2).

- MW = 632.34; yield = 52% from **38**; white to pale yellow solid.
- ^1H NMR (CDCl$_3$, 500 MHz) δ_H 6.30 (br, 3H, Gdn), 5.67 (d, J = 7.9 Hz, 1H, N*H*-Boc), 4.56 – 4.46 (m, 1H, Arg C*H*$^\alpha$), 3.70 – 3.40 (m, 4H, 4 x ring C*H*), 3.34 – 3.08 (m, 4H, Arg C*H*$_2^\delta$ + C*H*$_2$-C≡C), 2.93 (s, 2H, C*H*$_2$ Pbf), 2.57 – 2.45 (m, 10H, 4 x ring C*H* + 2 x C*H*$_3$ Pbf), 2.27 (t, J = 2.3 Hz, 1H, alkyne C*H*), 2.06 (s, 3H, C*H*$_3$ Pbf), 1.67 – 1.49 (m, 4H, Arg C*H*$_2^\beta$ + Arg C*H*$_2^\gamma$), 1.43 (s, 6H, (C*H*$_3$)$_2$ Pbf), 1.38 (s, 9H, (C*H*$_3$)$_3$ Boc).
- $^{13}C\{^1H\}$ NMR (CDCl$_3$, 500 MHz) δ_c 170.2, 158.6 (Pbf), 156.3, 155.9 (*C*=NH + *C*ONH), 138.2 (Pbf), 133.0 (Pbf), 132.2 (Pbf), 124.6 (Pbf), 117.4 (Pbf), 86.3 (Pbf), 79.9 (Boc), 77.8 (alkyne), 74.0 (alkyne), 51.7 (Ring *C*H$_2$), 51.2 (Ring *C*H$_2$), 49.4 (Arg *C*$^\alpha$), 46.6 (*C*H$_2$-C≡C), 45.3 (Ring *C*H$_2$), 43.2 (Pbf), 41.9

(Ring CH_2), 40.8 (Arg C^δ), 30.9 (Arg C^β), 28.6 (Pbf), 28.3 (Boc), 24.9 (Arg C^γ), 19.3 (Pbf), 17.9 (Pbf), 12.5 (Pbf).

- MS: m/z 553.4 [M–Boc]H$^+$, 577.3 [M–C$_4$H$_8$]H$^+$, 633.4 MH$^+$.

(S)-1-(4-amino-5-oxo-5-(4-(prop-2-yn-1-yl)piperazin-1-yl)pentyl)guanidine trifluoroacetate salt (**39b**): obtained from **39a** according to *Procedure D*.

- MW = 394.22 as TFA salt; yield = 74% from **39a**; sticky white to pale yellow solid.

- ^{1}H NMR ((CD$_3$)$_2$SO, 500 MHz) δ_H 8.12 (br, 3H, NH_3^+), 7.70 – 6.73 (br m, 4H, protonated Gdn), 4.40 (br, 1H, Arg CH^α), 3.83 – 3.24 (m, 7H, 4 x ring CH + CH_2-C≡C + alkyne CH), 3.20 – 3.02 (m, 2H, Arg CH_2^δ), 2.75 – 2.42 (m, 4H, partially overlapped to the signal of DMSO, 4 x ring CH), 1.72 – 1.35 (m, 4H, Arg CH_2^β + Arg CH_2^γ).

- ^{13}C{^{1}H} NMR ((CD$_3$)$_2$SO, 500 MHz) δ_c 167.5, 157.3 (C=NH), 78.2 (alkyne), 77.5 (alkyne), 51.3, 50.9 (2 x Ring CH_2), 49.6 (Arg C^α), 45.9 (CH$_2$-C≡C), 44.3 (Ring CH_2), 41.1 (Ring CH_2), 40.6 (overlapped to the signal of DMSO, Arg C^δ), 27.9 (Arg C^β), 24.1 (Arg C^γ).

- MS: m/z 281.2 MH$^+$.

Compounds **40a-b**

(S)-N-(1-oxo-5-(3-((2,2,4,6,7-pentamethyl-2,3-dihydrobenzofuran-5-yl)sulfonyl)guanidino)-1-(4-(prop-2-yn-1-yl)piperazin-1-yl)pentan-2-yl)acetamide (**40a**): prepared from 0.511 g of N^α-Acetyl-N^ω-Pbf-Arg **30** (MW = 468.20; 0.788 mmol) and 0.100 g of **38** (MW = 187.11 as HCl salt; 0.534 mmol) according to *Procedure E*. Work up was run by extracting the reaction mixture with 6 volumes of HCl 0.5 M after completion (TLC). The aqueous phase was then quickly basified with NaOH$_{(aq)}$ to pH 10÷12 and extracted with dichloromethane. The combined organic phases were dried over Na$_2$SO$_4$ and evaporated to dryness to afford the purified product **40a**.

- MW = 574.29; yield = 82% from **38**; white to pale yellow solid.
- ^{1}H NMR (CDCl$_3$, 400 MHz) δ$_H$ 6.98 (d, J = 7.9 Hz, 1H, NH Ac), 6.61 – 6.21 (m, 3H, Gdn), 4.88 – 4.79 (m, 1H, Arg CH^α), 3.72 – 3.42 (m, 4H, 4 x ring CH), 3.36 – 3.07 (m, 4H, Arg CH_2^δ + CH_2-C≡C), 2.94 (s, 2H, CH_2 Pbf), 2.59 – 2.45 (m, 10H, 4 x ring CH + 2 x CH_3 Pbf), 2.27 (t, J = 2.3 Hz, 1H, alkyne CH), 2.07 (s, 3H, CH_3 Pbf), 1.97 (s, 3H, CH_3 Ac), 1.77 – 1.48 (m, 4H, Arg CH_2^β + Arg CH_2^γ), 1.44 (s, 6H, (CH_3)$_2$ Pbf).
- ^{13}C{^{1}H} NMR (CDCl$_3$, 400 MHz) δ$_c$ 170.5, 170.0, 158.7 (Pbf), 156.3 (C=NH), 138.2 (Pbf), 133.0 (Pbf), 132.2 (Pbf), 124.6 (Pbf), 117.5 (Pbf), 86.4 (Pbf), 77.7 (alkyne), 74.1 (alkyne), 51.7 (Ring CH$_2$), 51.2 (Ring CH$_2$), 48.3 (Arg C^α), 46.6 (CH$_2$-C≡C), 45.3 (Ring CH$_2$), 43.2 (Pbf), 41.9 (Ring CH$_2$), 40.8 (Arg C^δ), 30.5 (Arg C^β), 28.6 (Pbf), 24.9 (Arg C^γ), 23.1 (Ac), 19.3 (Pbf), 17.9 (Pbf), 12.5 (Pbf).
- MS: m/z 575.4 MH$^+$, 597.4 MNa$^+$, 613.3 MK$^+$.

(S)-N-(5-guanidino-1-oxo-1-(4-(prop-2-yn-1-yl)piperazin-1-yl)pentan-2-yl) acetamide trifluoroacetate salt (**40b**): obtained from **40a** according to *Procedure D*.

- MW = 436.23 as TFA salt; yield = 69% from **40a**; sticky white to pale yellow solid.
- ^{1}H NMR ((CD$_3$)$_2$SO, 500 MHz) (8:2 mixture of conformers s-cis and s-trans by analysis of Arg CH^α signals at 4.67 and 4.13 ppm) δ$_H$ 8.22 – 8.05 (NH Ac), 7.79 – 6.67 (br m, 4H, protonated Gdn), 4.74 – 4.63, 4.21 – 4.05 (2m, 1H in total, Arg CH^α of each rotamer), 3.63 – 2.27 (3m, 13H in total, 8 x ring CH +

CH_2-C≡C + alkyne CH + Arg CH_2^δ), 1.83 (s, 3H, CH_3 Ac), 1.75 – 1.36 (m, 4H, Arg CH_2^β + Arg CH_2^γ).

- $^{13}C\{^1H\}$ NMR ((CD$_3$)$_2$SO, 500 MHz) (rotamer mixture) δ_c 174.0, 169.9, 157.2, 79.3, 78.9 (2 x alkyne), 76.8, 76.5 (2 x alkyne), 52.0 (Arg C^α), 51.3, 48.2 (2C, Arg C^α + Arg C^δ), 46.2, 45.1, 43.3, 41.7, 40.7, 29.2, 28.6 (2 x Arg C^β), 25.6, 25.2 (2 x Arg C^γ), 22.8 (Ac).

- MS: m/z 323.2 MH$^+$.

Compound 41
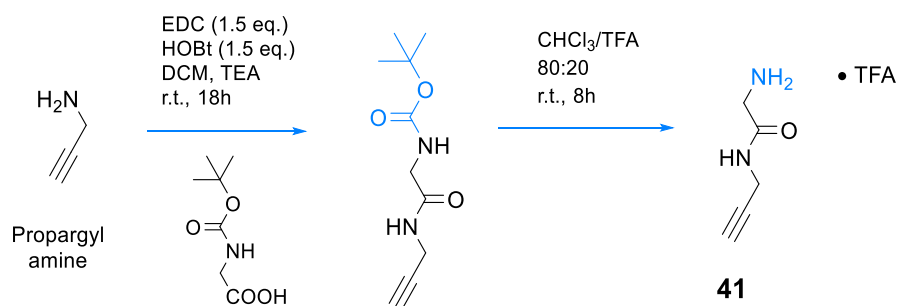
2-amino-N-(prop-2-yn-1-yl)acetamide trifluoroacetate salt (**41**): obtained by reacting 6.0 mL of propargylamine (MW = 55.08; *d* = 0.86 g/mL; 94 mmol) with 17.638 g Boc-Gly (MW = 175.18; 100.68 mmol) in 80 mL of dichloromethane according to *Procedure E*. After deprotection of the crude intermediate by Procedure *B*, compound **41** was isolated and used without further purification.

- MW = 226.08 as TFA salt; yield 74% from propargylamine; yellow glue.
- ^1H NMR (CD$_3$OD, 400 MHz) δ_H 4.03 (d, *J* = 2.6 Hz, 2H, N-CH_2), 3.67 (s, 2H, Gly CH_2^α), 2.63 (t, *J* = 2.6 Hz, 2H, alkyne CH).

Compounds 43a-b
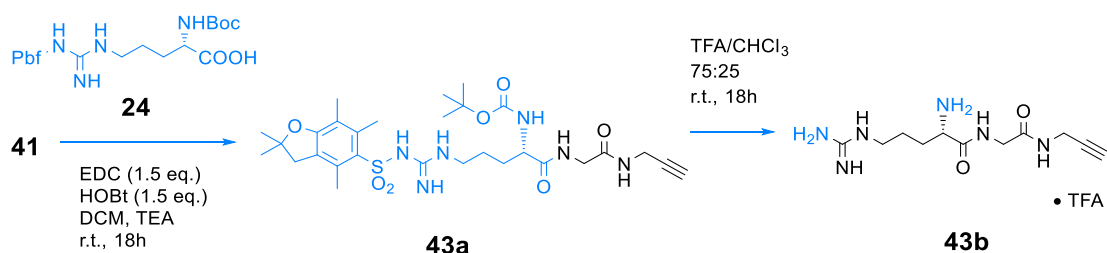
tert-butyl (S)-(1-oxo-1-((2-oxo-2-(prop-2-yn-1-ylamino)ethyl)amino)-5-(3-((2,2,4,6,7-pentamethyl-2,3-dihydrobenzofuran-5-yl)sulfonyl)guanidino)pentan-2-yl)carbamate (**43a**): obtained from 0.589 g of **41** (0.589 g, MW = 226.08 as TFA salt; 2.61 mmol) and N^α-Boc-N^ω-Pbf-Arg **24** (2.251 g, MW = 526.25; 4.28 mmol) according to *Procedure E*, then purified by flash chromatography (eluent: CHCl$_3 \rightarrow$ CHCl$_3$/MeOH 94:6).

- MW = 620.30; yield 57% from **41**; white solid.
- ^{1}H NMR (CDCl$_3$, 400 MHz) δ_H 7.88 (br t, 1H, N*H* Gly), 7.52 (br, 1H, N*H*-CH$_2$), 6.76 – 6.12 (br, 3H, Gdn), 5.89 (br, 1H, N*H*-Boc), 4.15 (br dt, 1H, C*H*$^\alpha$ Arg), 4.03 – 3.88 (m, 4H, C*H$_2$*$^\alpha$ Gly + NH-C*H$_2$*), 3.39 – 3.14 (m, 2H, C*H$_2$*$^\delta$ Arg), 2.95 (s, 2H, C*H$_2$* Pbf), 2.56, 2.49 (2s, 3H each, 2 x C*H$_3$* Pbf), 2.20 (br t, 1H, alkyne C*H*), 2.08 (s, 3H, C*H$_3$* Pbf), 1.91 – 1.78 (m, 1H, C*H*$^{\beta1}$ Arg), 1.76 – 1.52 (m, 3H, C*H*$^{\beta2}$ Arg + C*H$_2$*$^\gamma$ Arg), 1.46 (s, 6H, (C*H$_3$*)$_2$ Pbf), 1.41 (s, 9H, (C*H$_3$*)$_3$ Boc).
- ^{13}C{^{1}H} NMR (CDCl$_3$, 500 MHz) δ_c 173.9, 169.8, 158.9 (Pbf), 156.6, 156.4 (*C*=NH and *C*ONH Boc), 138.3 (Pbf), 132.4 (Pbf), 132.2 (Pbf), 124.7 (Pbf), 117.6 (Pbf), 86.5 (Pbf), 80.3 (Boc), 79.5 (*C*≡CH), 71.4 (C≡*C*H), 54.7 (*C*$^\alpha$ Arg), 43.2 (Pbf), 43.0 (*C*$^\alpha$ Gly), 40.0 (*C*$^\delta$ Arg), 29.0 (NH-*C*H$_2$), 28.8 (*C*$^\beta$ Arg), 28.6 (Pbf), 28.4 (Boc), 25.5 (*C*$^\gamma$ Arg), 19.3 (Pbf), 18.0 (Pbf), 12.5 (Pbf).
- ESI-MS: m/z 521.2 [M–Boc]H$^+$, 543.2 [M–Boc]Na$^+$, 565.2 [M–C$_4$H$_8$]H$^+$, 621.2 MH$^+$, 643.2 MNa$^+$.

(S)-2-amino-5-guanidino-N-(2-oxo-2-(prop-2-yn-1-ylamino)ethyl) pentanamide trifluoroacetate salt (**43b**): obtained from **43a** according to *Procedure D*.

- MW = 382.18 as TFA salt; yield 84% from **43a**; white to pale yellow glue.
- ^{1}H NMR ((CD$_3$)$_2$SO, 500 MHz) δ_H 8.67 (br t, 1H, CON*H* Gly), 8.44 (br t, 1H, N*H*-CH$_2$), 8.09 – 6.70 (br m, 8H, protonated Gdn + N*H$_3^+$*), 3.95 – 3.65 (m, 5H, NH-C*H$_2$* + C*H$_2^\alpha$* Gly + C*H$^\alpha$* Arg), 3.15 – 3.04 (m, 3H, alkyne C*H* + C*H$_2^\delta$* Arg), 1.68 (br, 2H, C*H$_2^\beta$* Arg), 1.52 (br, 2H, C*H$_2^\gamma$* Arg).
- ^{13}C{^{1}H} NMR ((CD$_3$)$_2$SO, 500 MHz) δ_c 169.5, 168.5, 157.2 (*C*=NH), 81.3 (*C*≡CH), 73.6 (C≡*C*H), 52.3 (*C$^\alpha$* Arg), 42.2 (*C$^\alpha$* Gly), 40.3 (overlapped to the signal of DMSO, *C$^\delta$* Arg), 28.6 (*C$^\beta$* Arg), 28.4 (NH-*C*H$_2$), 24.2 (*C$^\gamma$* Arg).
- ESI-MS: m/z 269.1 MH$^+$.

Compounds **44a-b**
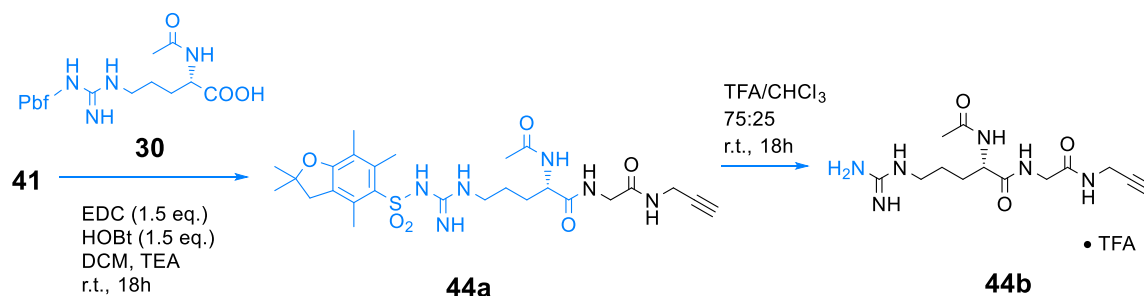
(S)-2-acetamido-N-(2-oxo-2-(prop-2-yn-1-ylamino)ethyl)-5-(3-((2,2,4,6,7-pentamethyl-2,3-dihydrobenzofuran-5-yl)sulfonyl)guanidino)pentanamide (**44a**): obtained by reacting **41** (0.289 g, MW = 226.08 as TFA salt; 1.28 mmol) with N$^\alpha$-Acetyl-N$^\omega$-Pbf-Arg **30** (1.006 g, MW = 468.20; 2.14 mmol) according to *Procedure E,* then purified by flash chromatography (eluent: CHCl$_3$ → CHCl$_3$/MeOH 95:5).

- MW = 562.26; yield 68% from **41**; white solid.

- ^{1}H NMR (CDCl$_3$, 400 MHz) δ_H 8.10 (br t, 1H, NH Gly), 7.74 (br, 2H, NH Ac + NH-CH$_2$), 6.95 – 6.23 (br m, 3H, Gdn), 4.38 (br dt, 1H, CH^α Arg), 4.01 – 3.87 (m, 4H, C$H_2{}^\alpha$ Gly + NH-CH_2), 3.35 – 3.15 (m, 2H, C$H_2{}^\delta$ Arg), 2.95 (s, 2H, CH_2 Pbf), 2.55, 2.48 (2s, 3H each, 2 x CH_3 Pbf), 2.24 (t, J = 2.3 Hz, 1H, alkyne CH), 2.08 (s, 3H, CH_3 Pbf), 2.03 (s, 3H, CH_3 Ac), 1.95 – 1.53 (m, 4H, C$H_2{}^\beta$ Arg + C$H_2{}^\gamma$ Arg), 1.45 (s, 6H, (CH_3)$_2$ Pbf).

- ^{13}C{^{1}H} NMR (CDCl$_3$, 400 MHz) δ_c 173.6, 172.3, 169.9, 158.8 (Pbf), 156.7 (C=NH), 138.2 (Pbf), 132.5 (Pbf), 132.1 (Pbf), 124.8 (Pbf), 117.6 (Pbf), 86.5 (Pbf), 79.6 (C≡CH), 71.5 (C≡CH), 53.9 (C^α Arg), 43.2 (Pbf), 43.0 (C^α Gly), 40.1 (C^δ Arg), 29.0 (NH-CH$_2$), 28.6 (2C, Pbf + C^β Arg), 25.5 (C^γ Arg), 22.9 (CH$_3$ Ac), 19.3 (Pbf), 18.0 (Pbf), 12.5 (Pbf).

- ESI-MS: m/z 563.2 MH$^+$, 585.2 MNa$^+$, 601.2 MK$^+$.

(S)-2-acetamido-5-guanidino-N-(2-oxo-2-(prop-2-yn-1-ylamino)ethyl)
pentanamide trifluoroacetate salt (**44b**): obtained from **44a** according to *Procedure D.*

- MW = 424.20 as TFA salt; yield 77% from **44a**; white to pale yellow glue.

- ^{1}H NMR ((CD$_3$)$_2$SO, 400 MHz) δ_H 8.38 – 8.14 (m, 3H, 3 x NH), 7.93 – 6.74 (br m, 5H, protonated Gdn), 4.19 (br, 1H, CH^α Arg), 3.83 (br, 2H, NH-CH_2), 3.65 (br, 2H, C$H_2{}^\alpha$ Gly), 3.07 (br, 3H, alkyne CH + C$H_2{}^\delta$ Arg), 1.85 (s, 3H, CH_3 Ac), 1.74 – 1.33 (m, 4H, C$H_2{}^\beta$ Arg + C$H_2{}^\gamma$ Arg).

- ^{13}C{^{1}H} NMR ((CD$_3$)$_2$SO, 500 MHz) δ_c 172.5, 170.3, 169.1, 157.2 (C=NH), 81.4 (C≡CH), 73.4 (C≡CH), 52.8 (C^α Arg), 42.3 (C^α Gly), 40.7 (C^δ Arg), 29.1 (C^β Arg), 28.3 (NH-CH$_2$), 25.3 (C^γ Arg), 23.0 (CH_3 Ac).

- ESI-MS: m/z 311.2 MH$^+$.

Compound **45a**
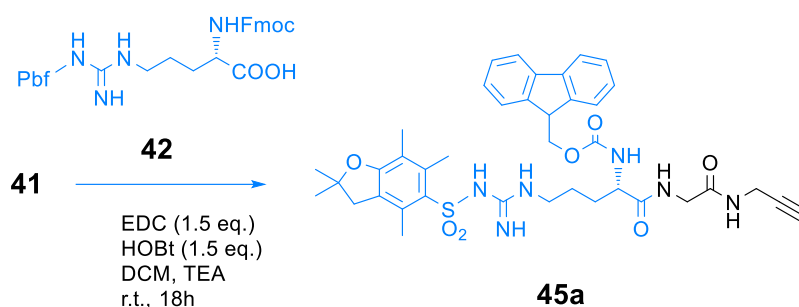
*(9H-fluoren-9-yl)methyl (S)-(1-oxo-1-((2-oxo-2-(prop-2-yn-1-ylamino)ethyl)
amino)-5-(3-((2,2,4,6,7-pentamethyl-2,3-dihydrobenzofuran-5-yl)sulfonyl)guanidino)
pentan-2-yl)carbamate* (**45a**): obtained from 0.368 g of **41** (MW = 226.08 as TFA
salt; 1.63 mmol) and 1.774 g of N^α-Fmoc-N^ω-Pbf-Arg **42** (MW = 648.26;
2.74 mmol) according to *Procedure E*, then purified by flash chromatography
(eluent: CHCl₃ → CHCl₃/MeOH 92:8).

- MW = 742.31; yield 59% from **41**; white solid.

- ^{1}H NMR (CDCl₃, 500 MHz) δ_H 7.94 (br t, 1H, N*H* Gly), 7.69 (app d, 2H,
  Ph*H* Fmoc), 7.53 (app t, 2H, Ph*H* Fmoc), 7.47 (br t, 1H, N*H*-CH₂), 7.35 – 7.29
  (m, 2H, Ph*H* Fmoc), 7.23 – 7.17 (m, 2H, Ph*H* Fmoc), 6.64 – 6.24 (br m, 4H,
  Gdn + N*H*-Fmoc), 4.37 – 4.21 (m, 3H, C*H₂* Fmoc + C*H*$^\alpha$ Arg), 4.10
  (t, J = 7.0 Hz, 1H, C*H* Fmoc), 3.99 – 3.83 (m, 4H, C*H₂*$^\alpha$ Gly + NH-C*H₂*),
  3.37 – 3.09 (m, 2H, C*H₂*$^\delta$ Arg), 2.87 (s, 2H, C*H₂* Pbf), 2.56, 2.48 (2s, 3H each,
  2 x C*H₃* Pbf), 2.06 (br t, 1H, alkyne C*H*), 2.04 (s, 3H, C*H₃* Pbf), 1.94 – 1.81
  (m, 1H, C*H*$^{\beta1}$ Arg), 1.77 – 1.66 (m, 1H, C*H*$^{\beta2}$ Arg), 1.66 – 1.51 (m, 2H, C*H₂*$^\gamma$
  Arg), 1.40 (s, 6H, (C*H₃*)₂ Pbf).

- ^{13}C{^{1}H} NMR (CDCl₃, 500 MHz) δ_c 173.6, 169.7, 158.9 (Pbf), 156.9, 156.5
  (*C*=NH and *C*ONH Fmoc), 143.7 (Fmoc), 141.2 (Fmoc), 138.4 (Pbf), 132.3
  (Pbf), 127.7 (Fmoc), 127.1 (Fmoc), 125.1 (Fmoc), 124.8 (Pbf), 119.9 (Fmoc),
  117.7 (Pbf), 86.5 (Pbf), 79.4 (*C*≡CH), 71.5 (C≡*C*H), 67.2 (Fmoc),
  54.9 (*C*$^\alpha$ Arg), 47.0 (Fmoc), 43.1 (Pbf), 43.1 (*C*$^\alpha$ Gly), 40.0 (*C*$^\delta$ Arg), 29.0

(NH-CH_2), 28.9 (C^β Arg), 28.5 (Pbf), 25.4 (C^γ Arg), 19.4 (Pbf), 18.0 (Pbf), 12.5 (Pbf).

- ESI-MS: m/z 743.3 MH$^+$, 765.3 MNa$^+$, 781.3 MK$^+$.

Compounds 48a-b
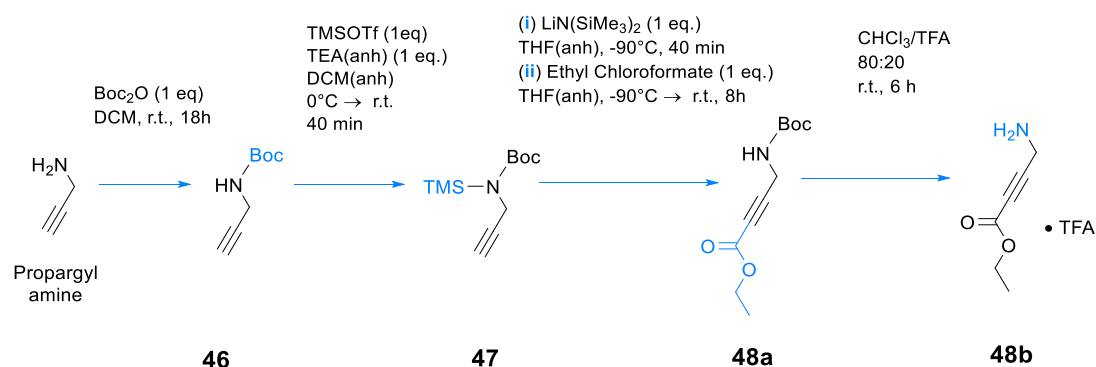
tert-butyl prop-2-yn-1-ylcarbamate (**46**): 2.2 mL of propargylamine (MW = 55.08; *d* = 0.86 g/mL; 34 mmol) and 9.815 g of Boc$_2$O (MW = 218.25; 44.97 mmol) were dissolved in 40 mL of dichloromethane. The resulting mixture was stirred overnight and subsequently evaporated under vacuum to afford the crude product **46**, which was directly used in the next step.

- MW = 155.09; yield 97% from propargylamine; yellow oil.
- ^{1}H NMR (CDCl$_3$, 400 MHz) δ_H 4.96 (br, 1H, NH-Boc), 3.92 (br, 2H, NH-CH_2), 2.21 (t, *J* = 2.5 Hz, 1H, alkyne CH), 1.45 (s, 9H, Boc (CH_3)$_3$).

tert-Butyl prop-2-yn-1-yl(trimethylsilyl)carbamate (**47**): 7.072 g of **46** (MW = 155.09; 45.60 mmol) were dissolved in 10 mL of anhydrous dichloromethane and 7.0 mL of anhydrous triethylamine (MW = 155.09; *d* = 0.726 g/mL; 50 mmol) at 0°C under Ar flow. After 5 minutes, 9.5 mL of TMSOTf (MW = 22.26; *d* = 1.228 g/mL; 52 mmol) were slowly added dropwise to the reaction mixture, which was stirred at 25°C for 30 minutes. The reaction was quenched with NaHCO$_{3(sat)}$, then the organic layer was dried over Na$_2$SO$_4$ and concentrated *in vacuo* to afford the crude product **47**.

- MW = 227.13; yield 79% from **46**; yellow oil.
- ^{1}H NMR (CDCl$_3$, 500 MHz) δ_H 3.92 (br, 2H, NH-C*H$_2$*), 2.14 (t, *J* = 2.5 Hz, 1H, alkyne C*H*), 1.48 (s, 9H, Boc (C*H$_3$*)$_3$), 0.29 (s, 9H, TMS (C*H$_3$*)$_3$).

Ethyl 4-((tert-butoxycarbonyl)amino)but-2-ynoate (**48a**): an oven-dried round bottom flask was charged with 10 mmol of lithium bis(trimethylsilyl)amide in anhydrous THF under Ar flow. The temperature of the system was cooled to – 90°C using a liquid N$_2$/acetone bath, then a solution of 2.239 g of **46** (MW = 227.13; 9.86 mmol) in 15 mL of dry THF was slowly added dropwise over 15 min by a dropping funnel, and the resulting mixture was left on stirring at – 90°C. After 25 minutes, 1.2 mL of ethyl chloroformate (MW = 108.52; *d* = 1.135 g/mL; 13 mmol) were added dropwise over three minutes. The flask was removed from the bath and allowed to warm to 20°C, then stirred for 8 additional hours. When the conversion was complete (TLC), the reaction was quenched with 2 mL of water, and concentrated *in vacuo* to approximately half of its volume. The mixture was subsequently re-diluted with 30 mL of water and finally extracted 3 x with CHCl$_3$. The combined organic phases were dried over Na$_2$SO$_4$, evaporated *in vacuo*, and the crude mixture was purified by flash chromatography (eluent: hexane/ethyl acetate 99:1 → 94:6) affording pure **48a.**

- MW = 227.12; yield 28% from **47**; yellow oil.
- ^{1}H NMR (CDCl$_3$, 400 MHz) δ_H 4.85 – 4.66 (br, 2H, N*H*-Boc), 4.22 (q, *J* = 7.1 Hz, 2H, O-C*H$_2$*), 4.07 (d, *J* = 5.6 Hz, 2H, NH-C*H$_2$*), 1.44 (s, 9H, Boc), 1.30 (t, *J* = 7.1 Hz, 3H, O-C*H$_2$*).

Ethyl 4-aminobut-2-ynoate trifluoroacetate salt (**48b**): obtained from **48a** according to *Procedure B*.

- MW = 241.08 as TFA salt; quantitative yield from **48a**; yellow oil.
- ^{1}H NMR (CDCl$_3$, 400 MHz) δ_H 8.36 – 7.60 (m, 3H. N*H$_3^+$*), 4.27 (q, *J* = 7.1 Hz, 2H, O-C*H$_2$*), 4.04 (br s, 2H, NH-C*H$_2$*), 1.31 (t, *J* = 7.1 Hz, 3H, O-C*H$_2$*).

Compounds **49a-b**
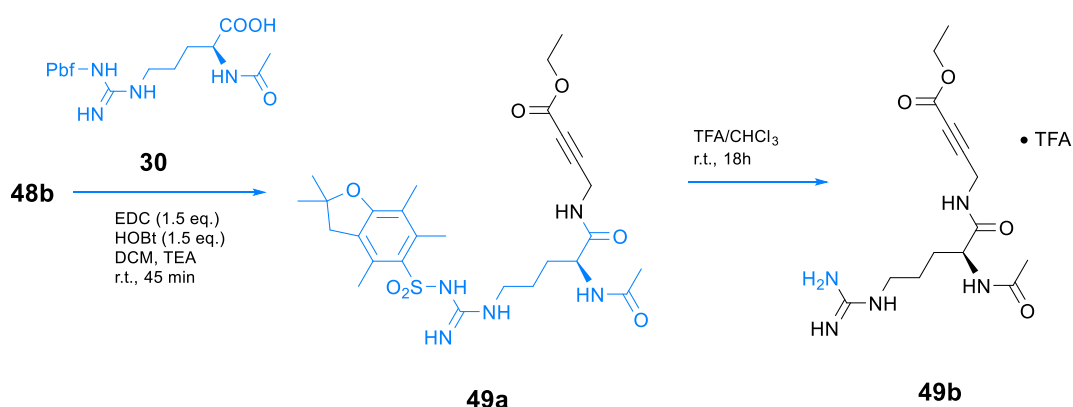
Ethyl (S)-4-(2-acetamido-5-(3-((2,2,4,6,7-pentamethyl-2,3-dihydrobenzofuran-5-yl)sulfonyl)guanidino)pentanamido)but-2-ynoate (**49a**): obtained from **48b** (0.336 g, MW = 241.08 as TFA salt; 1.39 mmol) and N$^\alpha$-Acetyl-N$^\omega$-Pbf-Arg **30** (0.976 g, MW = 468.20; 2.08 mmol) according to *Procedure E*, then purified by flash chromatography (eluent: CHCl$_3$/MeOH 99:1 → 95:5).

- MW = 577.26; yield = 40% from **48b**; pale yellow solid.
- ^{1}H NMR (CDCl$_3$, 400 MHz) δ_H 7.11 (br, 1H, N*H* Ac), 6.87 (app s, 1H, N*H*-CH$_2$), 6.39 – 6.02 (m, 3H, Gdn), 5.13 (dt, *J* = 7.4, 6.6 Hz, 1H, C*H*$^\alpha$ Arg), 4.18 (q, *J* = 7.1 Hz, 2H, O-C*H*$_2$), 3.70 (br s, 2H, NH-C*H*$_2$), 3.27 – 3.11 (m, 2H, C*H*$_2$$^\delta$ Arg), 2.94 (s, 2H, C*H*$_2$ Pbf), 2.55, 2.48 (2s, 3H each, 2 x C*H*$_3$ Pbf), 2.11 – 1.80 (m, 8H, Pbf C*H*$_3$ + C*H*$_3$ Ac [2.08, 2.01 (2s)] + C*H*$_2$$^\beta$ Arg), 1.63 – 1.49 (m, 2H, C*H*$_2$$^\gamma$ Arg), 1.45 (s, 6H, (C*H*$_3$)$_2$ Pbf), 1.27 (t, *J* = 7.1 Hz, 3H, CH$_2$C*H*$_3$).
- ^{13}C{^{1}H} NMR (CDCl$_3$, 500 MHz) δ_c 170.8, 168.5, 163.5, 158.7 (Pbf), 156.7 (*C*=NH), 145.4, 138.2 (Pbf), 132.8 (Pbf), 132.1 (Pbf), 124.7, 124.6 (Pbf), 117.5 (Pbf), 86.4 (Pbf), 61.6 (O-*C*H$_2$), 47.3 (*C*$^\alpha$ Arg), 43.2 (Pbf), 40.6 (*C*$^\delta$ Arg), 31.5 (NH-*C*H$_2$), 30.7 (*C*$^\beta$ Arg), 28.6 (Pbf), 25.4 (*C*$^\gamma$ Arg), 22.8 (*C*H$_3$ Ac), 19.2 (Pbf), 17.9 (Pbf), 14.1 (*C*H$_3$), 12.4 (Pbf).
- ESI-MS: m/z 578.3 MH$^+$, 600.3 MNa$^+$, 616.2 MK$^+$.

Ethyl (S)-4-(2-acetamido-5-guanidinopentanamido)but-2-ynoate trifluoroacetate salt (**49b**): obtained from **49a** according to *Procedure D*.

- MW = 439.20 as TFA salt; yield = 40% from **49a**; yellow glue.
- ^{1}H NMR ((CD$_3$)$_2$SO, 400 MHz) (mixture of rotamers) δ_H 8.42 (d, J = 8.5 Hz, 1H, Ac N*H*), 7.45 (t, J = 5.7 Hz, 1H, N*H*-CH$_2$), 7.53 – 6.50 (br m, 5H, protonated Gdn), 5.01 – 4.89 (m, 1H, C*H*$^\alpha$ Arg), 4.09, 3.72 (2q, J = 7.1 Hz each, 2H in total, O-C*H*$_2$) 3.83 (br s, 2H, NH-C*H*$_2$), 3.14 – 3.03 (m, 2H, C*H*$_2$$^\delta$ Arg), 1.84 (s, 3H, Ac C*H*$_3$), 1.75 – 1.61 (m, 1H, C*H*$^{\beta 1}$ Arg), 1.55 – 1.33 (m, 3H, C*H*$^{\beta 2}$ Arg + C*H*$_2$$^\gamma$ Arg), 1.17, 1.08 (2t, J = 7.1 Hz each, 3H in total, C*H*$_3$).
- ^{13}C{^{1}H} NMR ((CD$_3$)$_2$SO, 400 MHz) (mixture of rotamers) δ_c 170.5, 170.3, 169.0, 163.6, 163.4, 157.0 (*C*=NH), 146.6, 146.0, 125.0, 124. 8, 62.5, 61.4 (2 x O-*C*H$_2$), 46.6, 40.7 (2 x *C*$^\delta$ Arg), 31.5, 31.3 (2 x NH-*C*H$_2$), 30.1 (*C*$^\beta$ Arg), 25.3 (*C*$^\gamma$ Arg), 22.7 (*C*H$_3$ Ac), 15.3, 14.3 (2 x *C*H$_3$ ester).
- MS: m/z 326.2 MH$^+$.

Compound **50b**

tert-butyl (E)-(3-(phenylsulfonyl)allyl)carbamate (**50a**): 0.122 g of NaH (60% dispersion in mineral oil; MW = 24.00; 3.05 mmol) were dissolved in 10 mL of anhydrous THF and cooled to 0° C under Ar, then 0.575 g of diethyl (phenylsulfonyl)methylphosphonate (MW = 292.29; 1.97 mmol) were added to the reaction mixture, which was left on stirring at 0°C. After 20 minutes, a solution of 0.303 g of **34** (MW 159.09; 1.90 mmol) in 5 mL of dry THF was slowly added. After five minutes the reaction was quenched with sat. $Na_2CO_{3(aq)}$ and extracted 4 x with $CHCl_3$. The organic layer was dried over Na_2SO_4 and evaporated under vacuum. Separation of the crude product by flash chromatography (eluent: $CHCl_3$) gave pure **50a.**

- MW = 297.10; yield = 56% from **34**; white solid.
- ^{1}H NMR (CDCl$_3$, 400 MHz) δ_H 7.99 – 7.81 (m, 2H, Ph*H*), 7.70 – 7.46 (m, 3H, Ph*H*), 6.94 (dt, *J* = 15.1, 4.5 Hz, 1H, =C*H*-CH$_2$), 6.45 (dt, *J* = 15.1, 1.9 Hz, 1H, =C*H*-SO$_2$), 4.73 (br, 1H, N*H*-Boc), 4.04 – 3.81 (m, 2H, NH-C*H*$_2$), 1.40 (s, 9H, Boc).

(E)-3-(phenylsulfonyl)prop-2-en-1-amine trifluoroacetate salt (**50b**): obtained from **50a** according to *Procedure B*.

- MW = 311.07 as TFA salt; quantitative from **50a**; white sticky solid.
- ^{1}H NMR ((CD$_3$)$_2$SO, 400 MHz) δ_H 8.12 – 7.94 (m, 3H, NH_3^+), 7.89 – 7.84 (m, 2H, PhH), 7.78 – 7.73 (m, 1H, PhH), 7.70 – 7.65 (m, 2H, PhH), 7.02 (dt, J = 15.1, 1.9 Hz, 1H, =CH-SO$_2$), 6.86 (dt, J = 15.1, 4.5 Hz, 1H, =CH-CH$_2$), 3.76 – 3.69 (m, 2H, NH-CH_2).

Compounds **51a-b**

(S,E)-2-acetamido-5-(3-((2,2,4,6,7-pentamethyl-2,3-dihydrobenzofuran-5-yl) sulfonyl)guanidino)-N-(3-(phenylsulfonyl)allyl)pentanamide (**51a**): prepared from 0.513 g of **50b** (MW = 311.07 as TFA salt; 1.65 mmol) and 0.945 g of N$^\alpha$-Acetyl-N$^\omega$-Pbf-Arg **30** (MW = 468.20; 2.02 mmol) according to *Procedure E*, then purified by flash chromatography (eluent: CHCl$_3$/MeOH 99:1 → 95:5).

- MW = 647.24; yield = 43% from **50b**; white solid.
- ^{1}H NMR (CDCl$_3$, 500 MHz) δ_H 7.94 – 7.79 (m, 3H, 2 x PhH + NH), 7.66 – 7.45 (m, 3H, PhH), 7.07 (br, 1H, NH Ac), 6.91 (dt, J = 15.2, 4.8 Hz, 1H, CH$_2$-CH=), 6.61 – 6.00 (br m, 4H, Gdn + =CH-SO$_2$ [6.55 (dt, J = 15.2, 1.7 Hz, 1H)]), 4.57 – 4.42 (m, 1H, CH^α Arg), 4.08 – 3.98 (m, 2H, NH-CH_2), 3.36 – 3.19 (m, 2H, CH_2^δ Arg), 2.95 (s, 2H, CH_2 Pbf), 2.54, 2.48, 2.08 (3s, 3H each, 3 x CH_3 Pbf), 1.98 (s, 3H, CH_3 Ac), 1.91 – 1.86 (m, 1H, C$H^{\beta 1}$), 1.76 – 1.50 (m, 3H, C$H^{\beta 2}$ Arg + CH_2^γ Arg), 1.45 (s, 6H, (CH_3)$_2$ Pbf).

- ^{13}C{^{1}H} NMR (CDCl$_3$, 400 MHz) δ$_c$ 172.7, 171.4, 159.0 (Pbf), 156.3 (*C*=NH), 142.9 (CH$_2$-*C*H=), 139.8 (Ar *C*$_q$), 138.4 (Pbf), 133.5 (Ar *C*H), 132.4 (Pbf), 130.8 (=*C*H-SO$_2$), 129.3 (Ar *C*H), 127.6 (Ar *C*H), 124.9 (Pbf), 117.7 (Pbf), 86.6 (Pbf), 53.1 (*C*$^\alpha$ Arg), 43.2 (Pbf), 40.3 (*C*$^\delta$ Arg), 39.4 (*C*H$_2$-CH=), 29.5 (*C*$^\beta$ Arg), 28.6 (Pbf), 25.5 (*C*$^\gamma$ Arg), 23.0 (*C*H$_3$ Ac), 19.4 (Pbf), 18.0 (Pbf), 12.5 (Pbf).
- ESI-MS: m/z 648.3 MH$^+$, 670.3 MNa$^+$, 686.3 MK$^+$.

(S,E)-2-acetamido-5-guanidino-N-(3-(phenylsulfonyl)allyl)pentanamide trifluoroacetate salt (**51b**)*: obtained from **51a** according to *Procedure D*.

- MW = 647.24; yield = 67% from **51a**; white sticky material.
- ^{1}H NMR (CD$_3$OD, 400 MHz) δ$_H$ 8.38 (t, *J* = 5.6 Hz, 1H, N*H*), 7.95 – 7.84 (m, 2H, Ph*H*), 7.74 – 7.56 (m, 3H, Ph*H*), 7.42 – 7.34 (m, 1H, N*H*), 6.92 (dt, *J* = 15.2, 4.3 Hz, 1H, CH$_2$-C*H*=), 6.55 (dt, *J* = 15.2, 1.9 Hz, 1H, =C*H*-SO$_2$), 4.30 – 4.23 (m, 1H, C*H*$^\alpha$ Arg), 4.10 – 3.94 (m, 2H, C*H*$_2$-CH=), 3.24 – 3.14 (m, 2H, C*H*$_2$$^\delta$ Arg), 1.97 (s, 3H, C*H*$_3$ Ac), 1.90 – 1.78 (m, 1H, C*H*$^{\beta 1}$), 1.72 – 1.53 (m, 3H, C*H*$^{\beta 2}$ Arg + C*H*$_2$$^\gamma$ Arg).
- ^{13}C{^{1}H} NMR (CD$_3$OD, 400 MHz) δ$_c$ 173.1, 172.4, 157.1 (*C*=NH), 143.1, 140.3, 133.3, 130.4 (=*C*H-SO$_2$), 129.1, 127.2, 53.4 (*C*$^\alpha$ Arg), 40.5 (*C*$^\delta$ Arg), 39.0 (*C*H$_2$-CH=), 28.3 (*C*$^\beta$ Arg), 24.9 (*C*$^\gamma$ Arg), 21.1 (*C*H$_3$ Ac).

1. INTRODUCTION

2. AIM

3. RESULTS AND DISCUSSION

4. CONCLUSIONS

5. EXPERIMENTAL SECTION

6. SUPPORTING MATERIAL
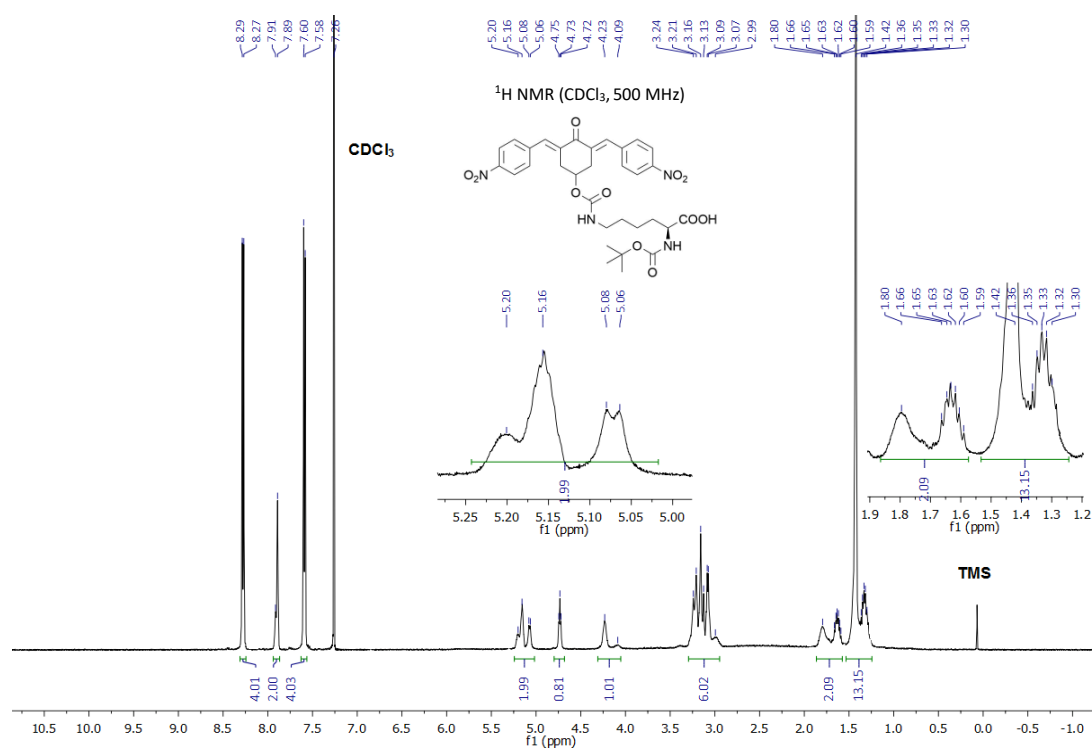
Figure 38

^{1}H NMR of compound **7a**.
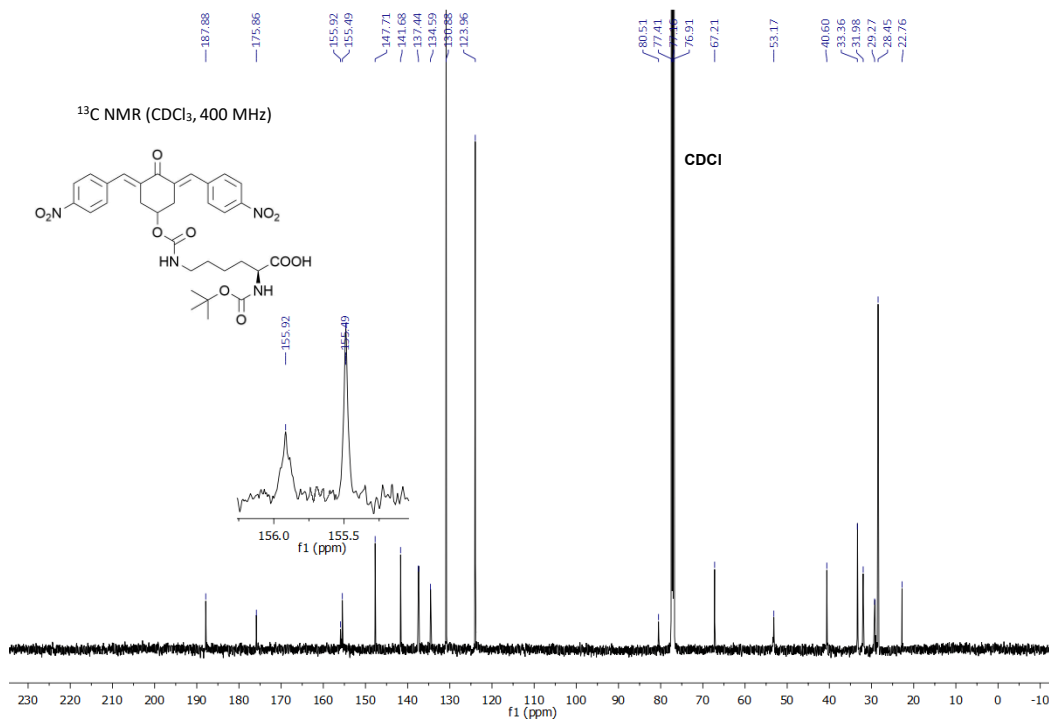
Figure 39

^{13}C NMR of compound **7a**.
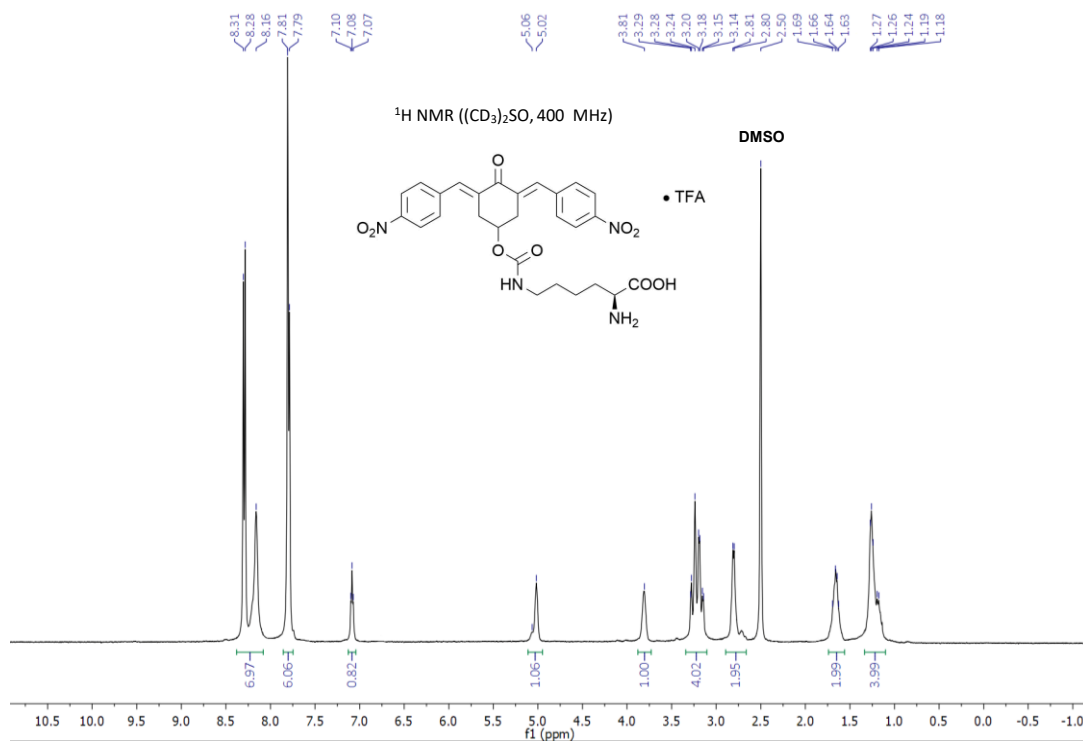
Figure 40

^{1}H NMR of compound **7b**.
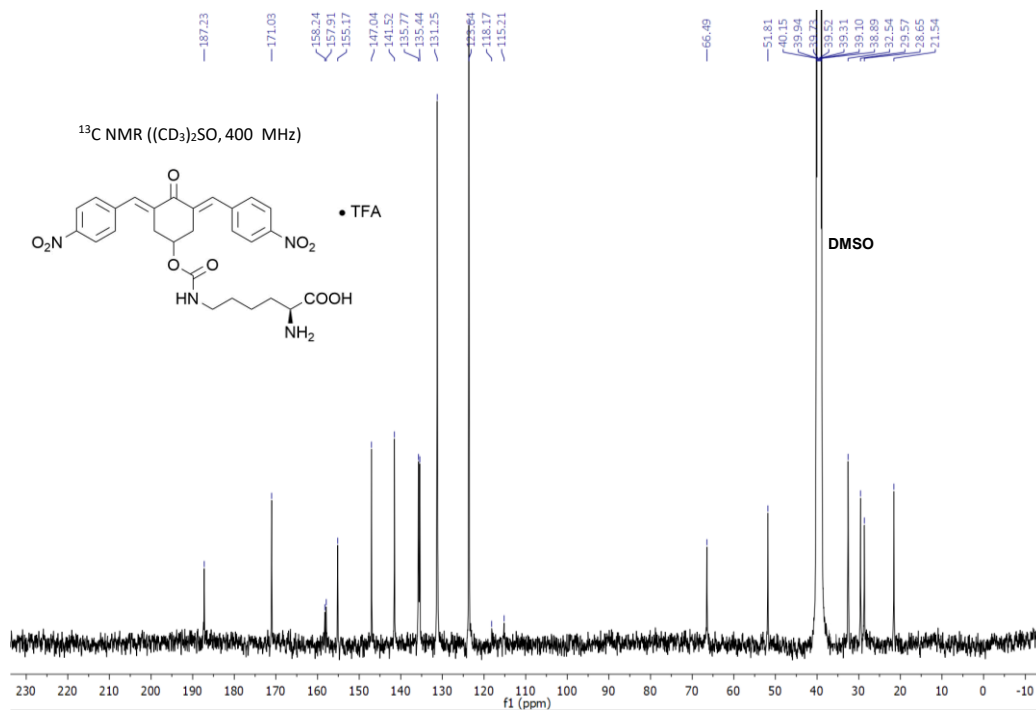
Figure 41

^{13}C NMR of compound **7b**.
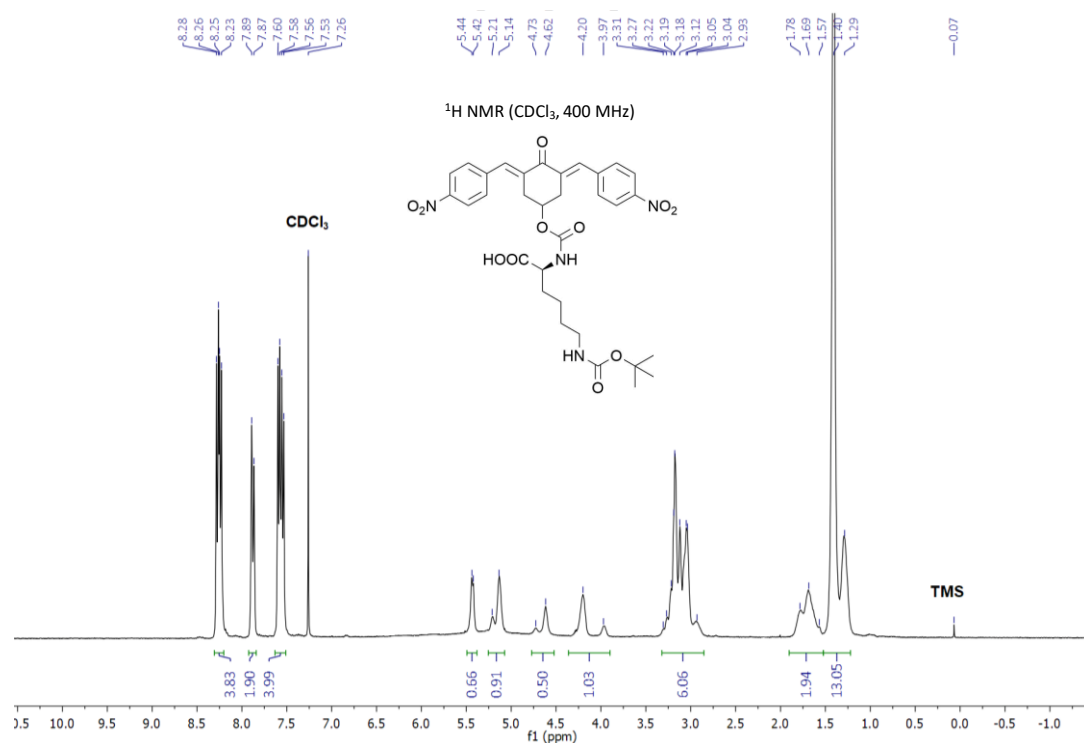
Figure 42

^{1}H NMR of compound **8a**.
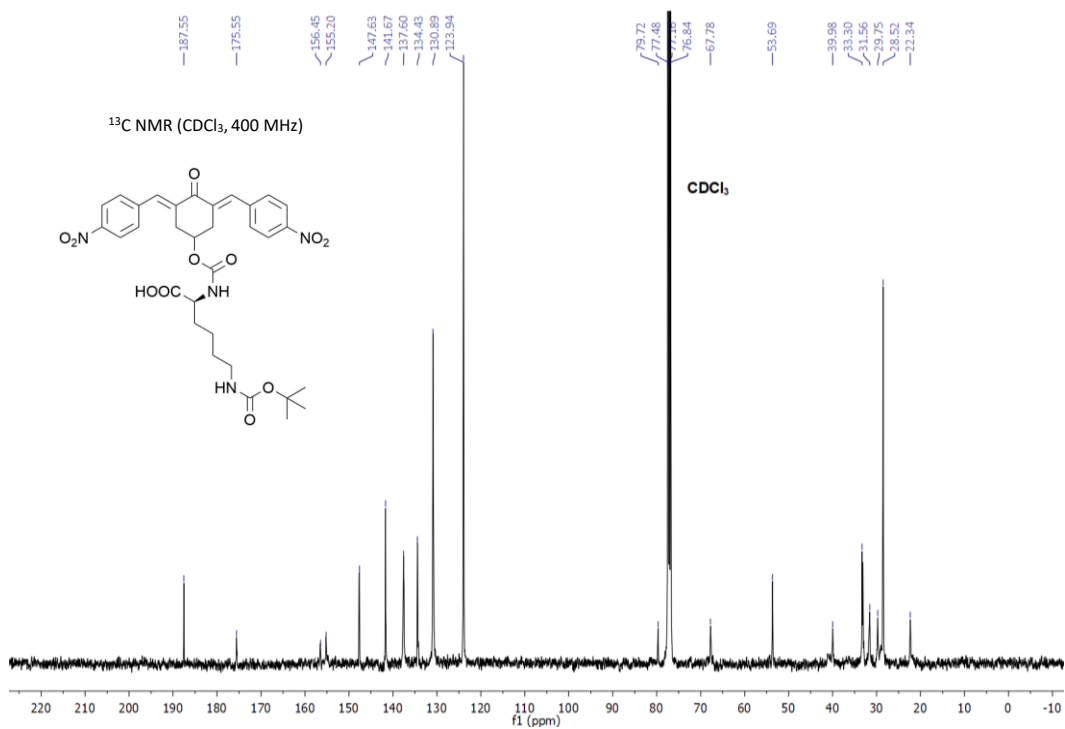
Figure 43

^{13}C NMR of compound **8a**.
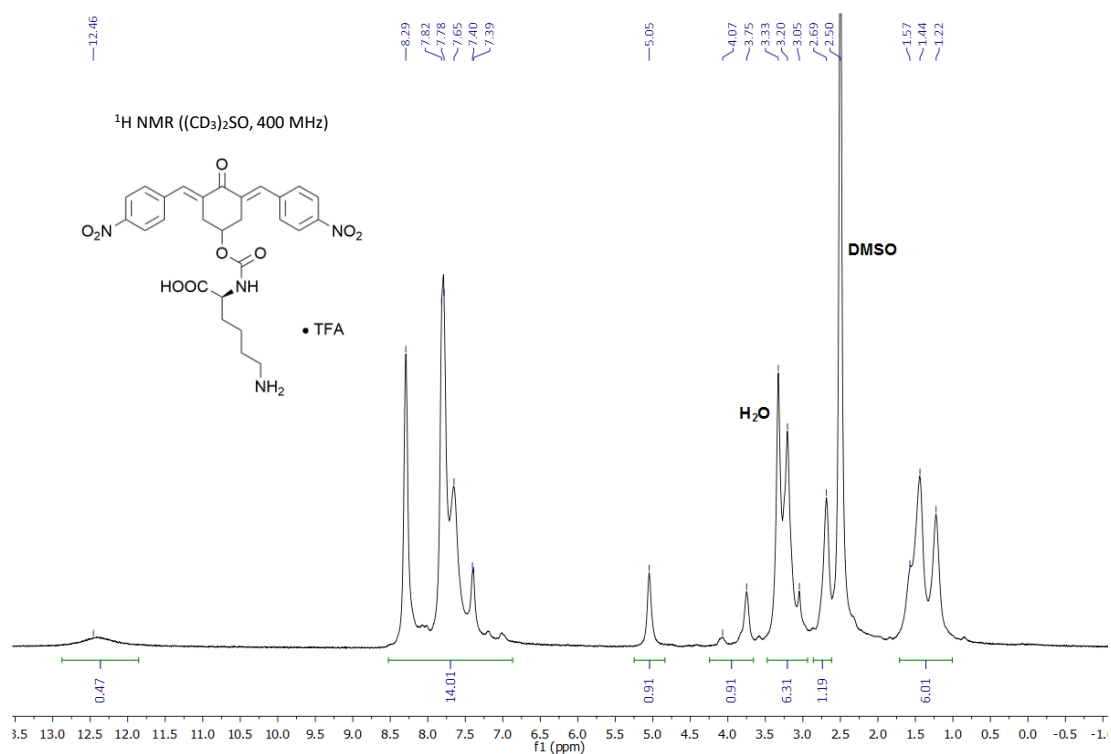
Figure 44

^{1}H NMR of compound **8b**.
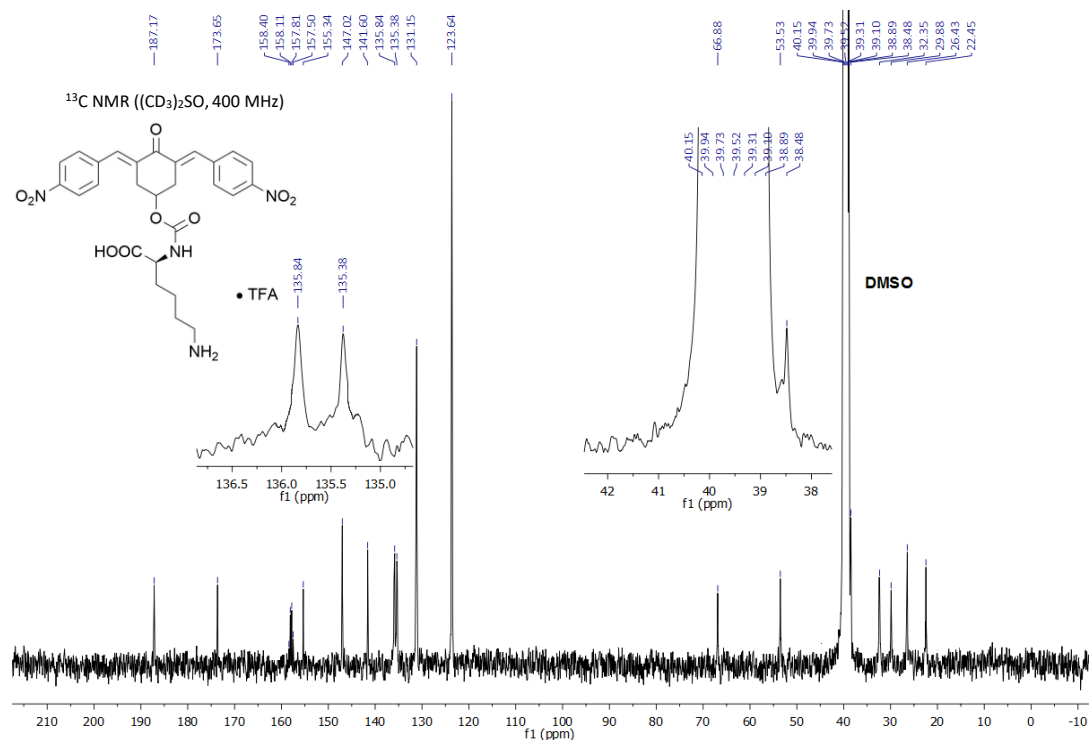
Figure 45

^{13}C NMR of compound **8b**.
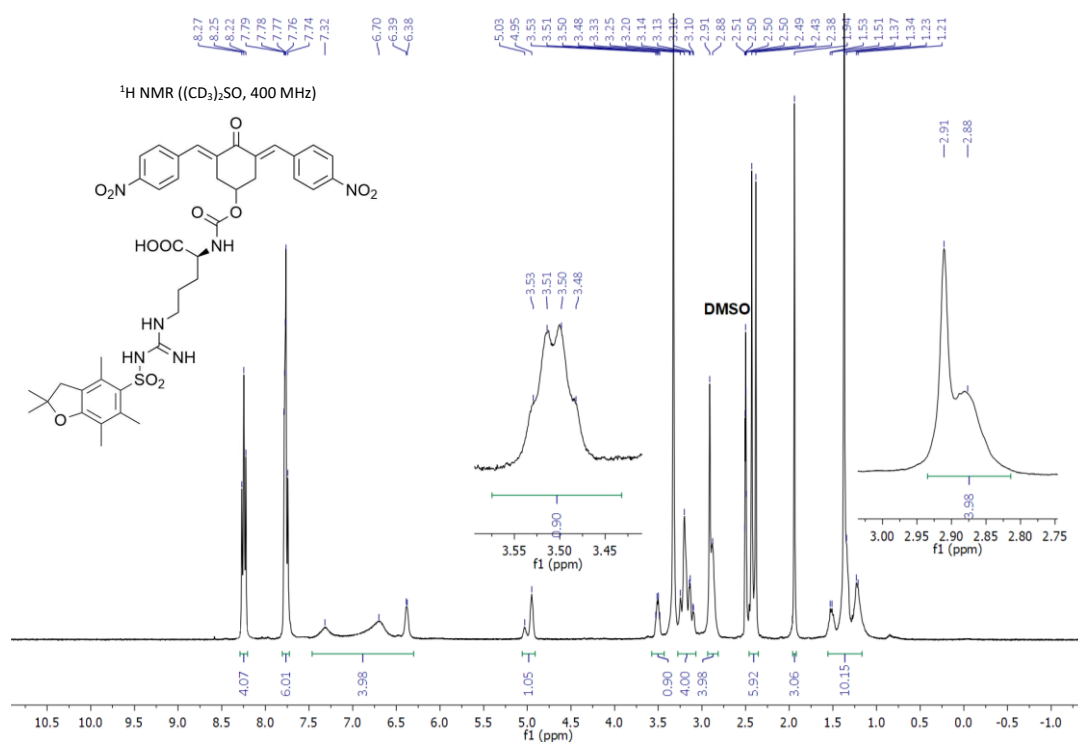
Figure 46

¹H NMR of compound **9a**.
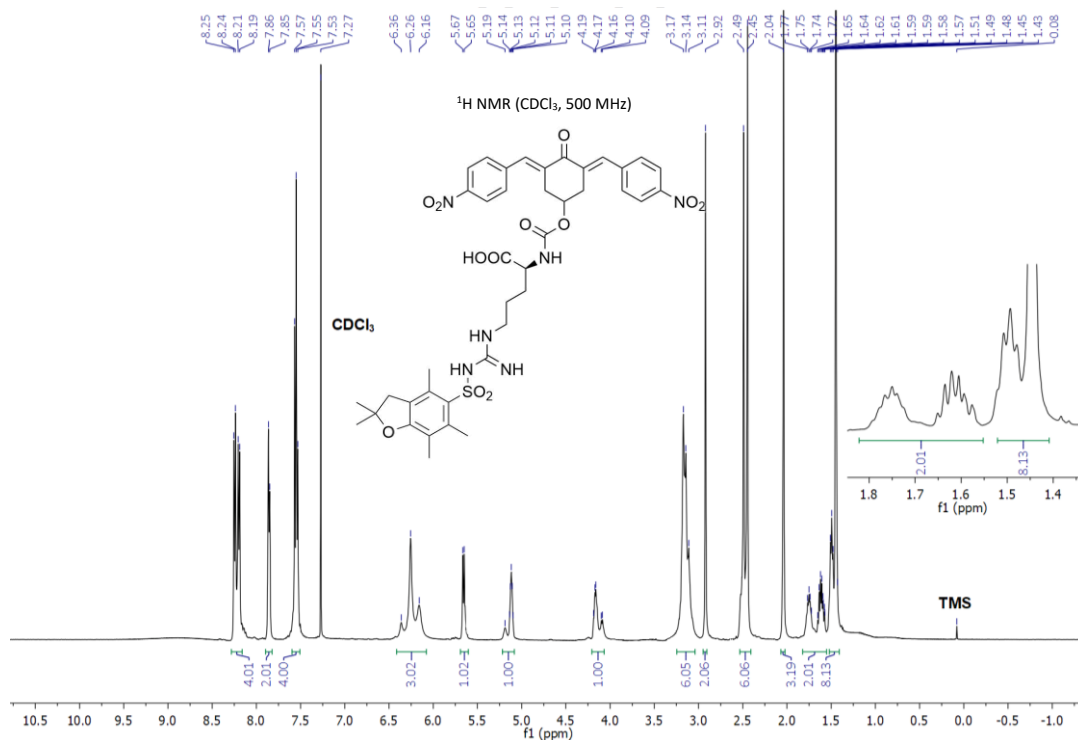
Figure 47

¹³C NMR of compound **9a**.
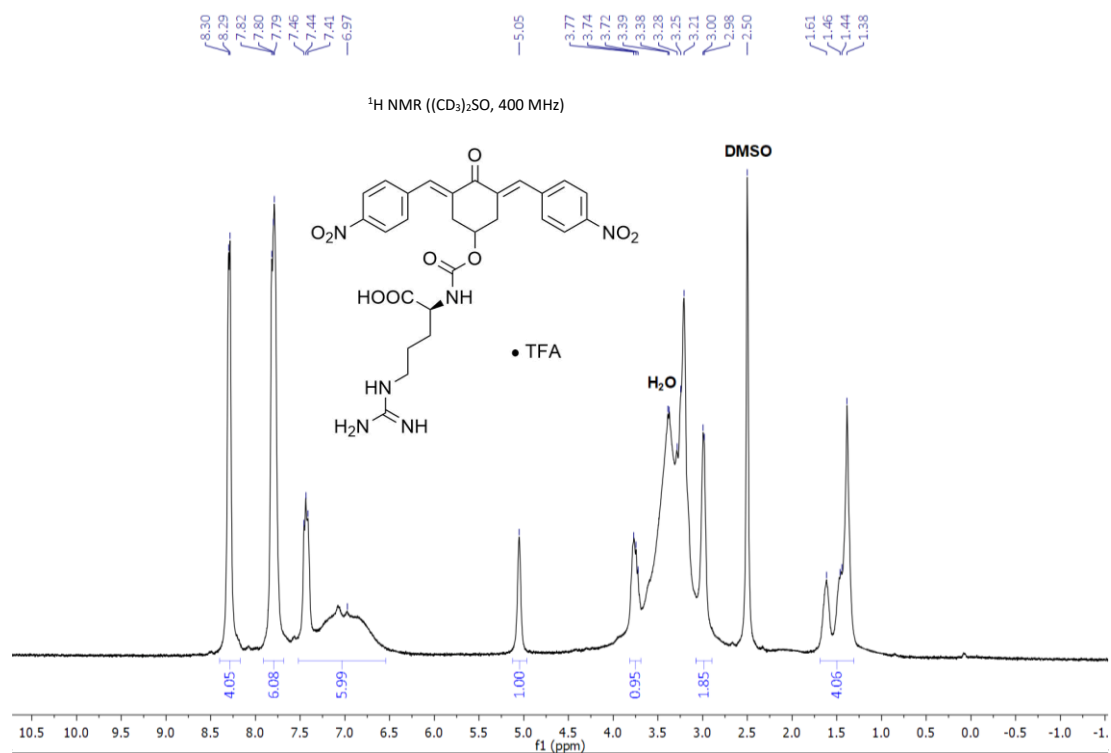
Figure 48

^{1}H NMR of compound **9b**.
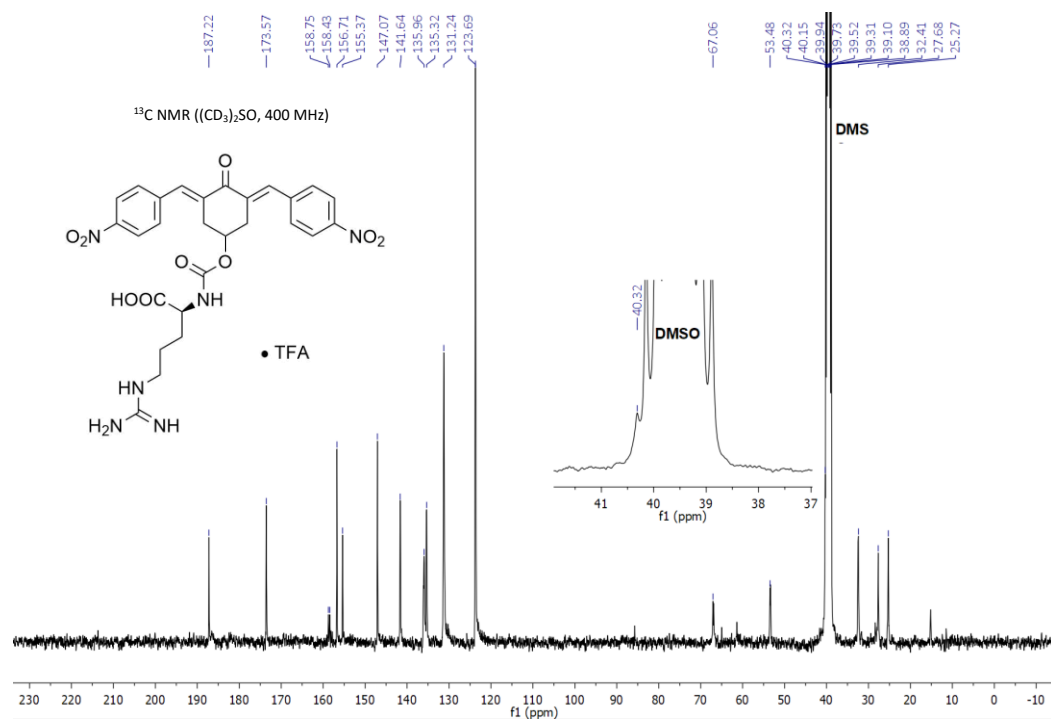
Figure 49

^{13}C NMR of compound **9b**.
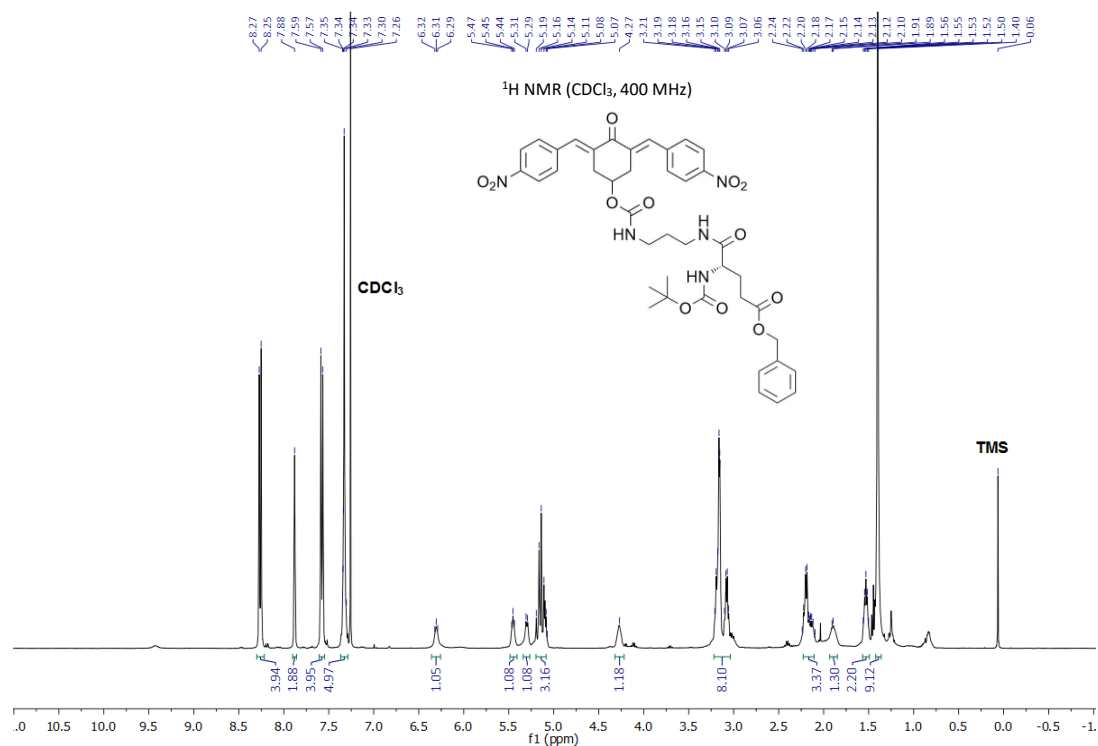
Figure 50

^{1}H NMR of compound **10a**.
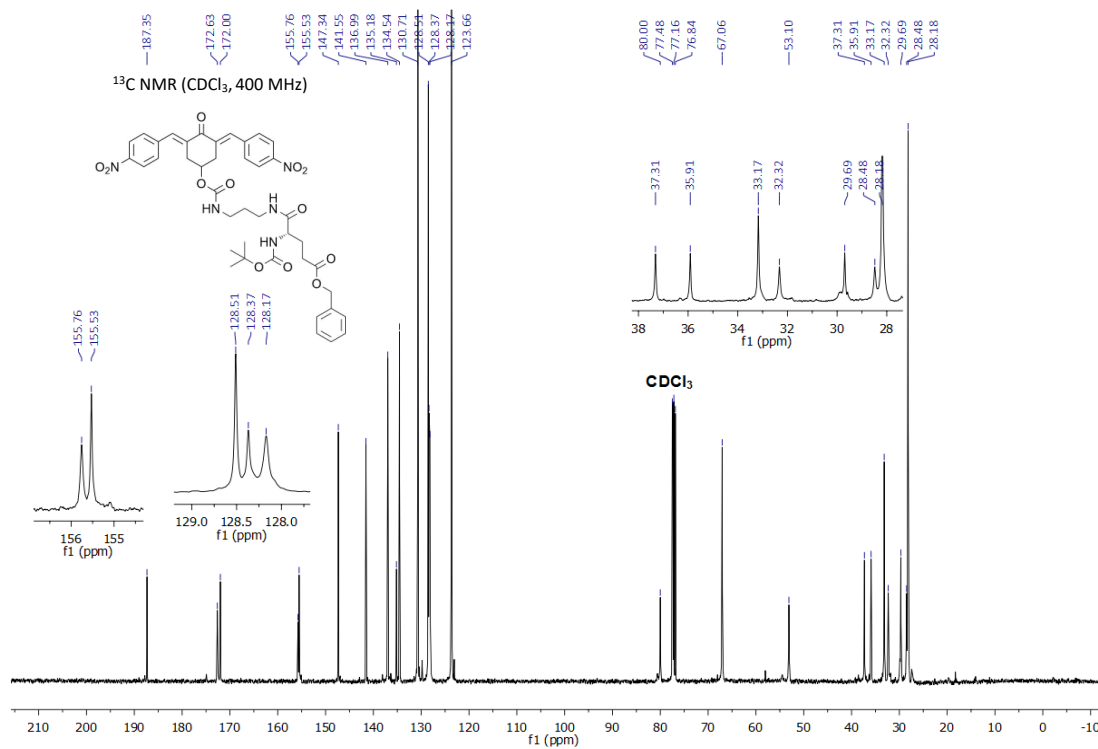
Figure 51

^{13}C NMR of compound **10a**.
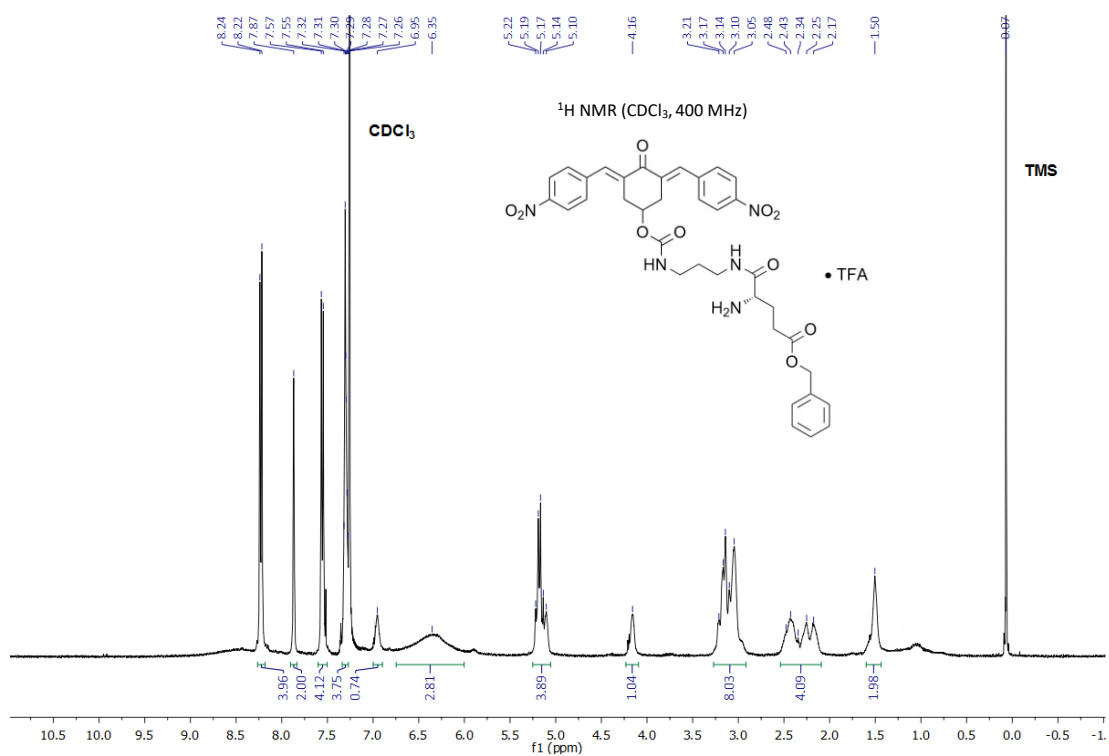
Figure 52

¹H NMR of compound **10b**.
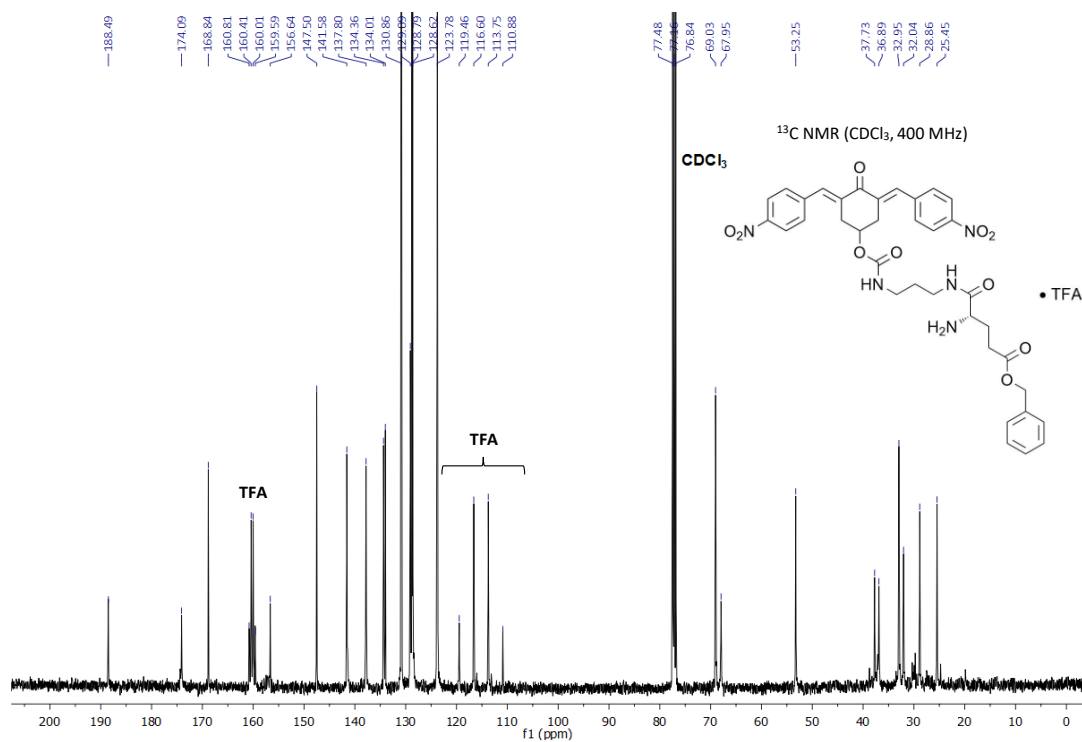
Figure 53

¹³C NMR of compound **10b**.

Figure 54

^{1}H NMR of compound **11a**.

Figure 55

^{13}C NMR of compound **11a.**

Figure 56

^{1}H NMR of compound **11b**.

Figure 57

^{13}C NMR of compound **11b.**
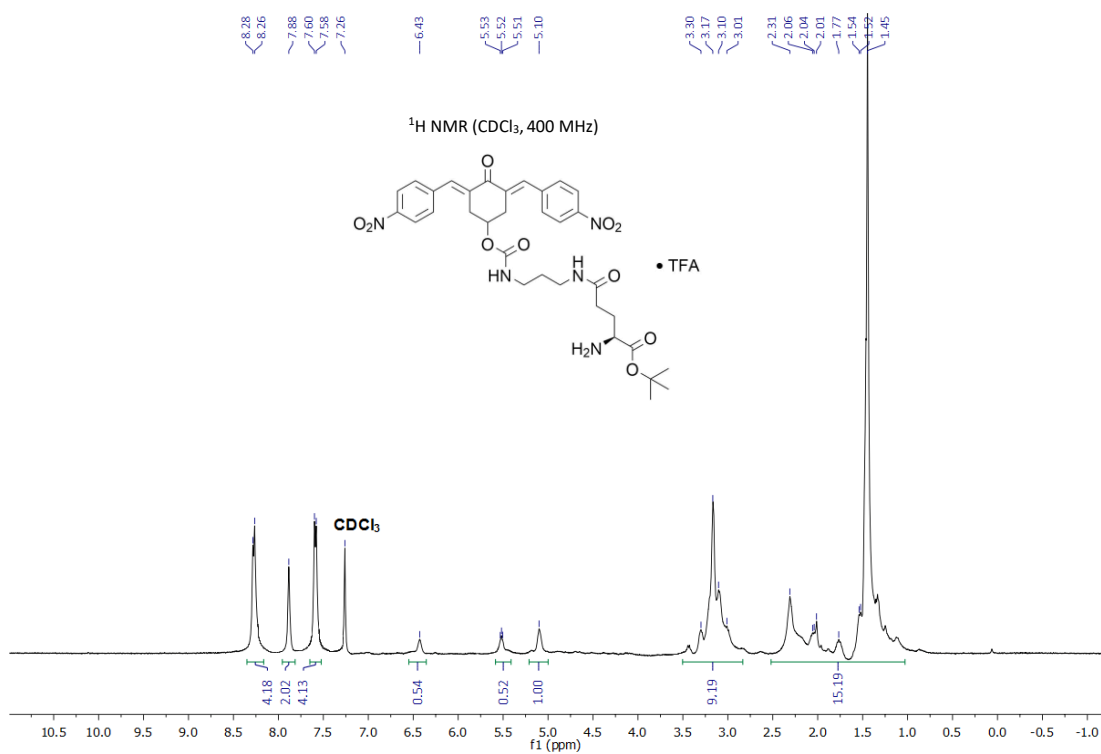
Figure 58

¹H NMR of compound **11c**.
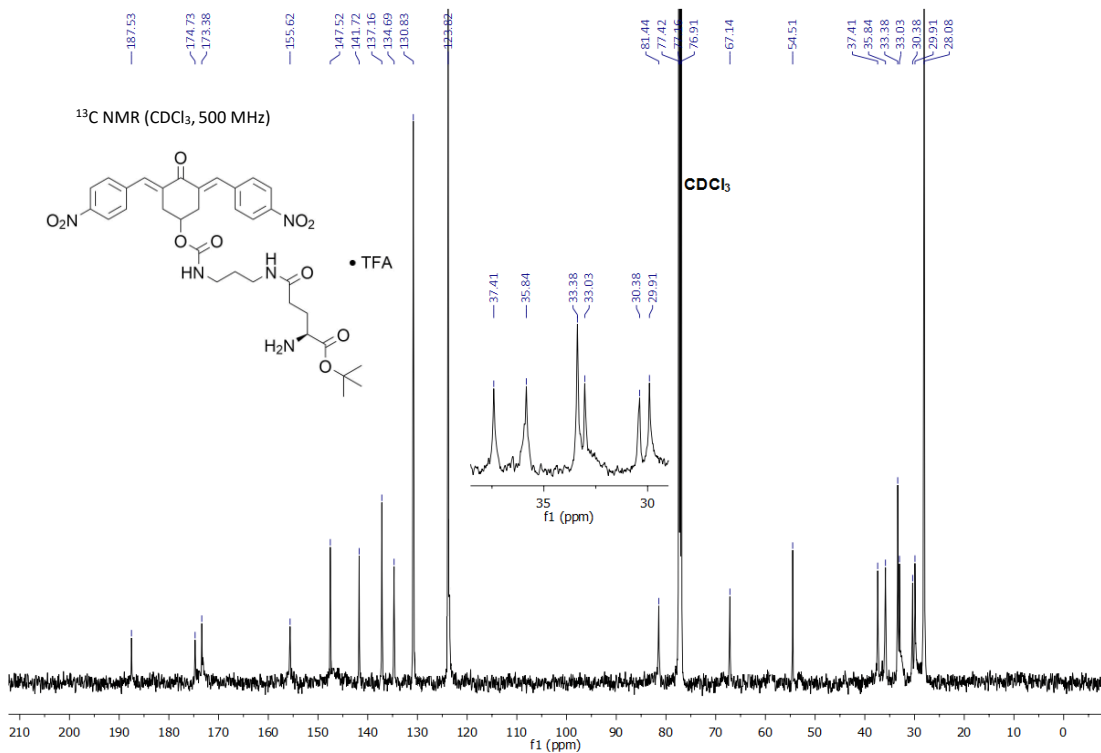
Figure 59

¹³C NMR of compound **11c.**

Figure 60

^{1}H NMR of compound **12a**.

Figure 61

^{13}C NMR of compound **12a.**
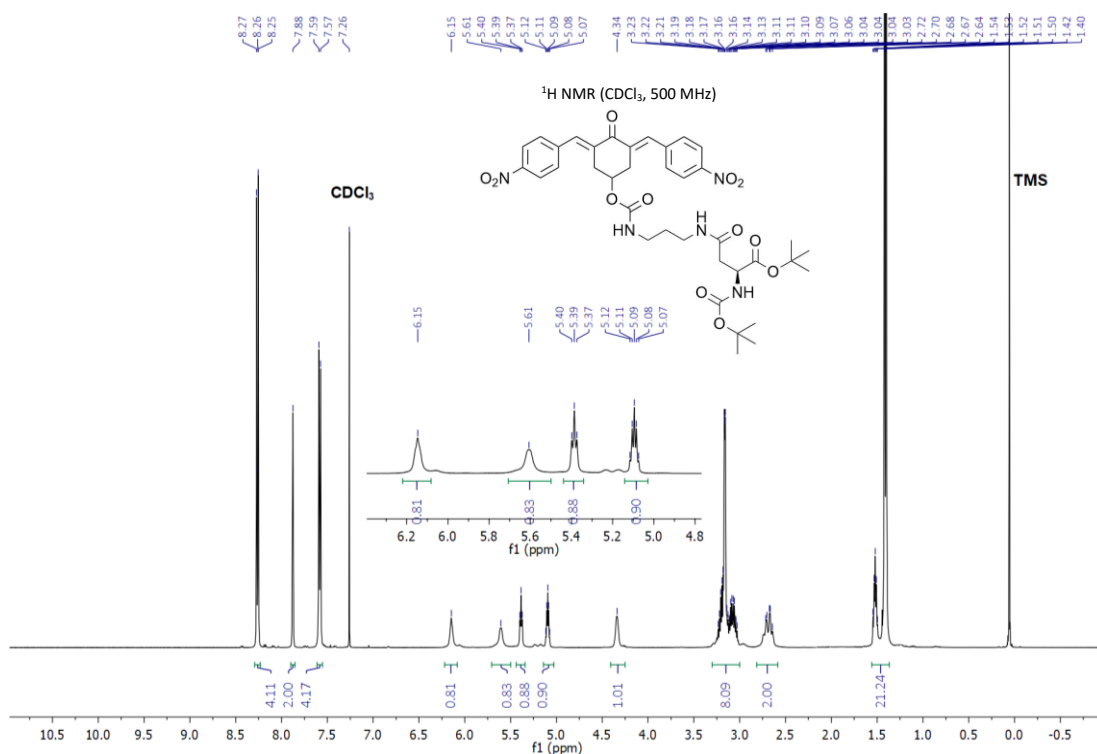
Figure 62

^{1}H NMR of compound **13a**.
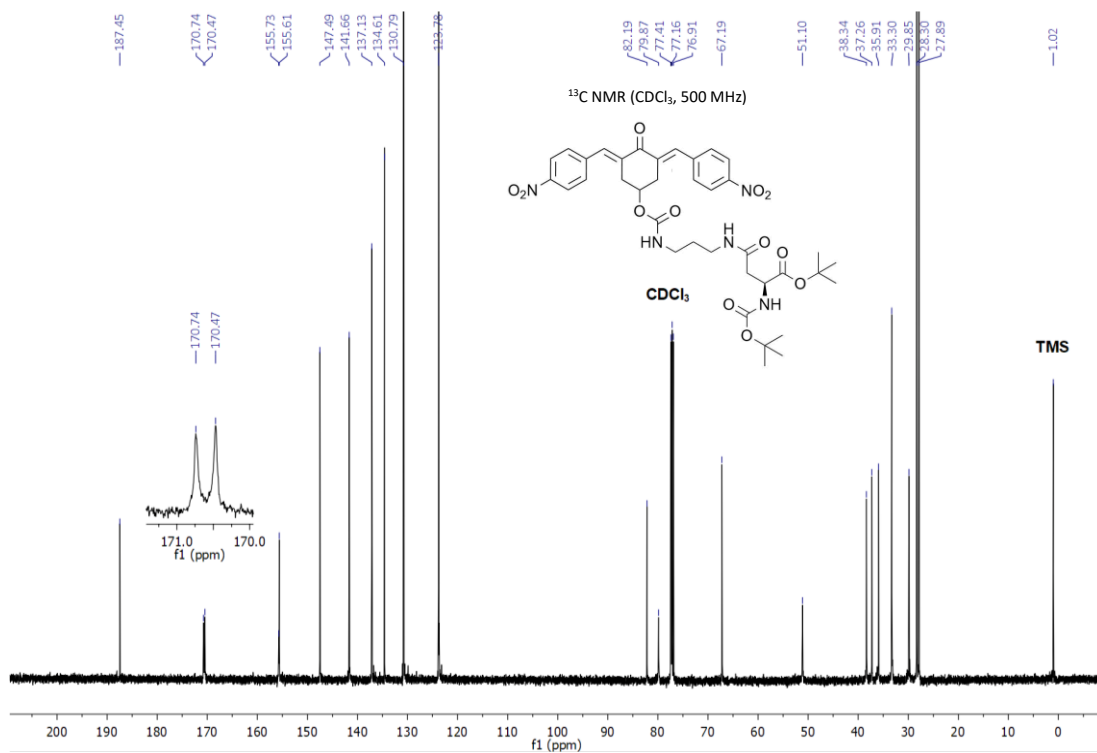
Figure 63

^{13}C NMR of compound **13a.**
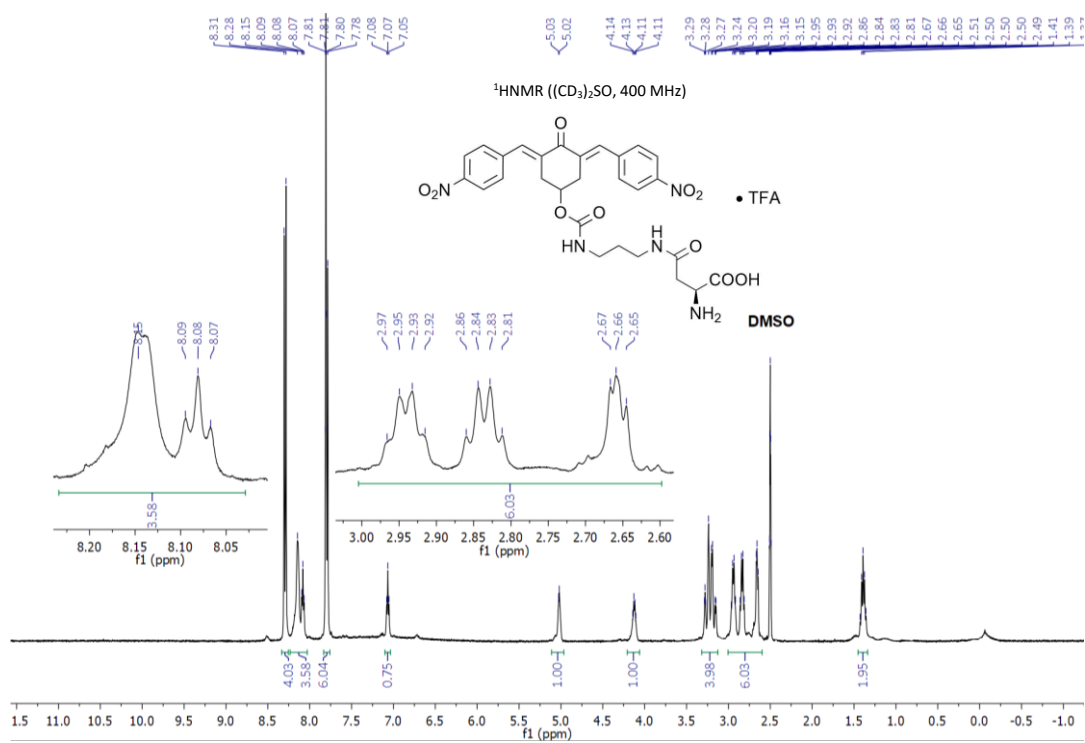
Figure 64

¹H NMR of compound **13b**.
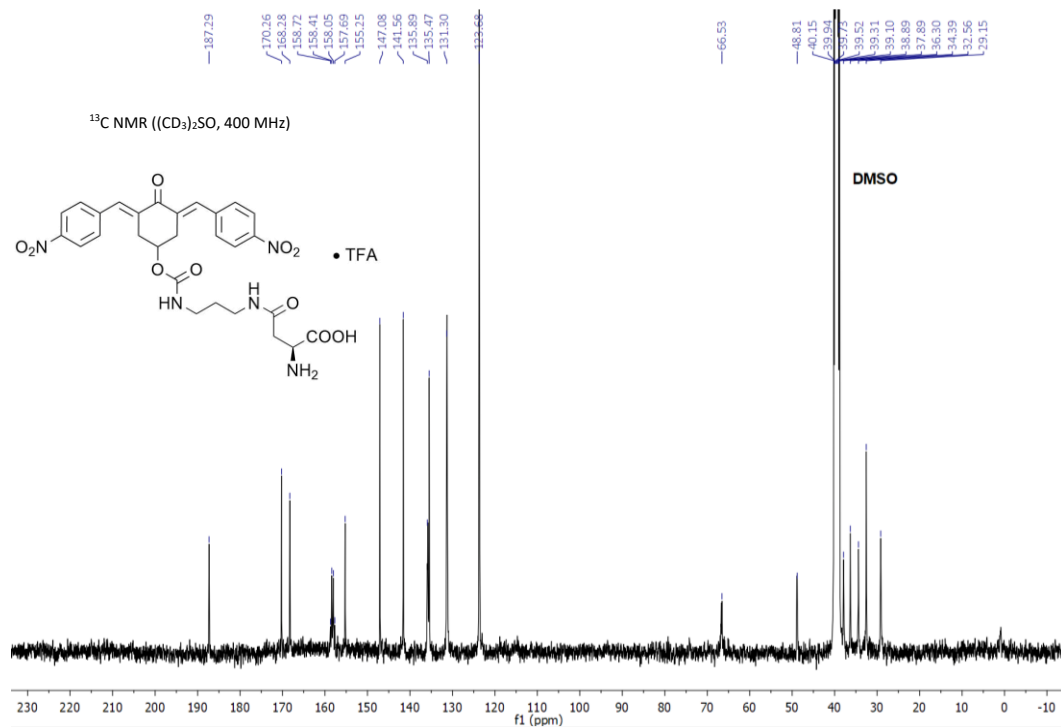
Figure 65

¹³C NMR of compound **13b.**
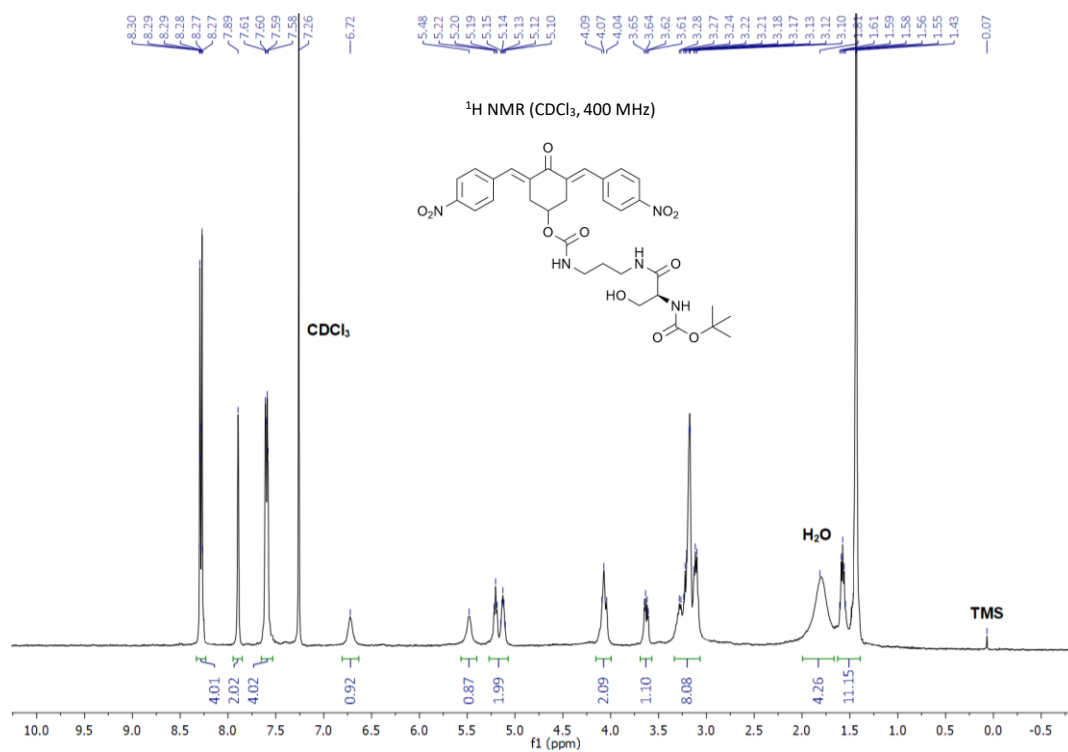
Figure 66

^{1}H NMR of compound **15a**.
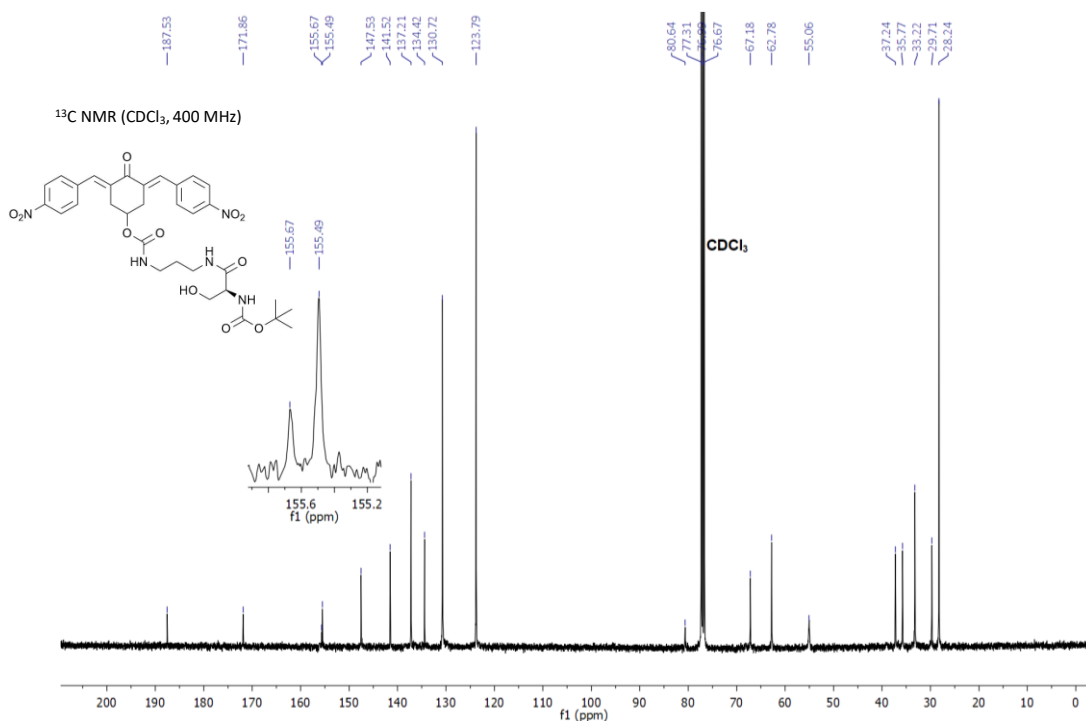
Figure 67

^{13}C NMR of compound **15a.**
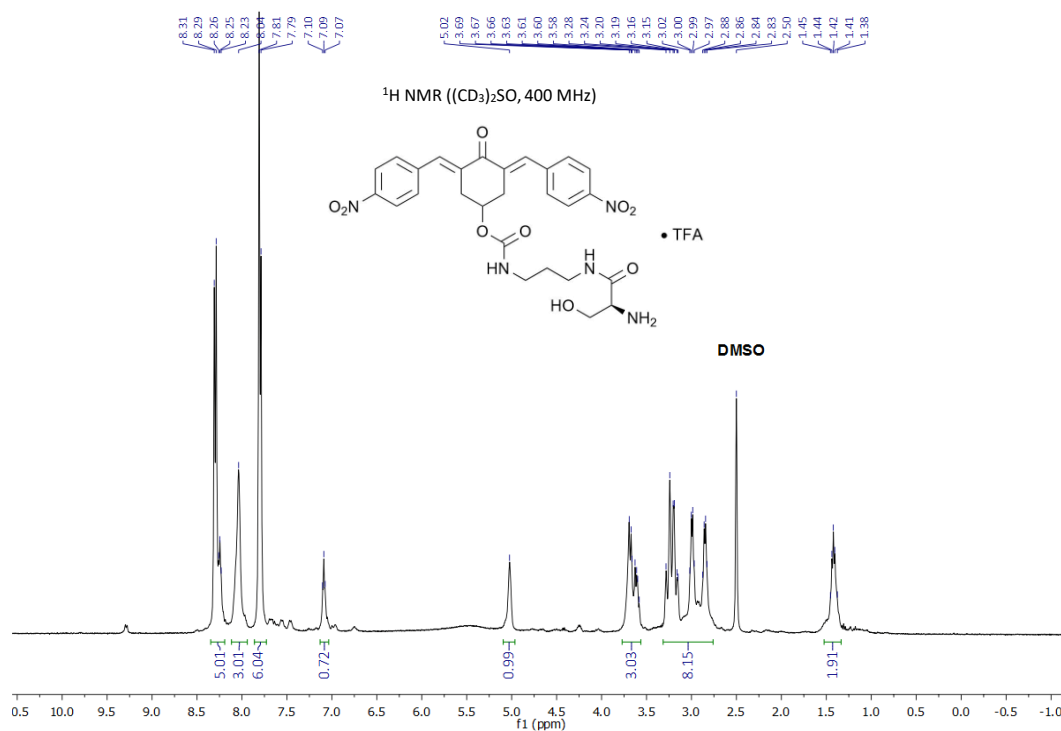
Figure 68

^{1}H NMR of compound **15b**.
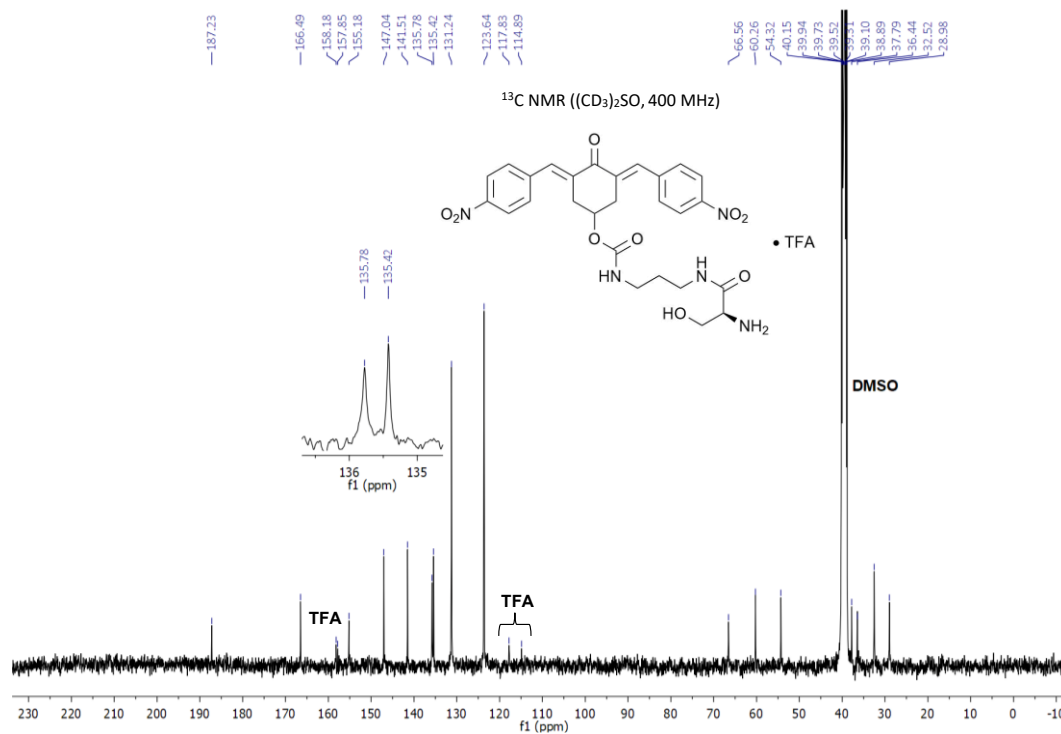
Figure 69

^{13}C NMR of compound **15b.**
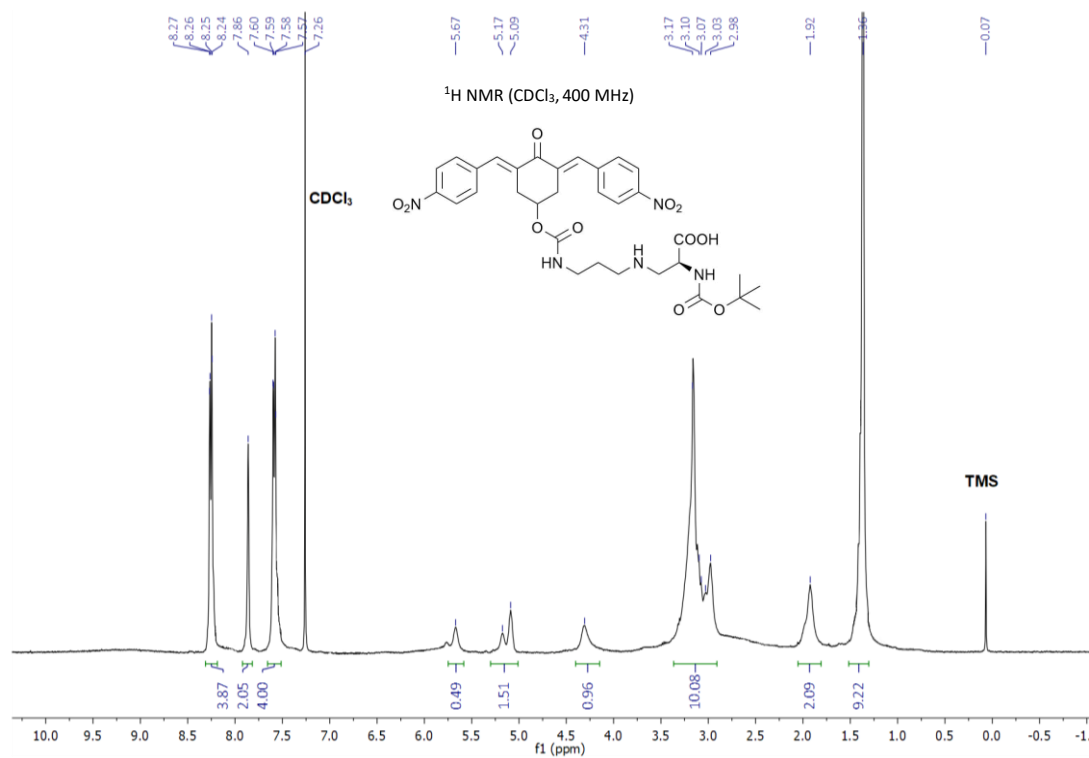
Figure 70

¹H NMR of compound **16a**.
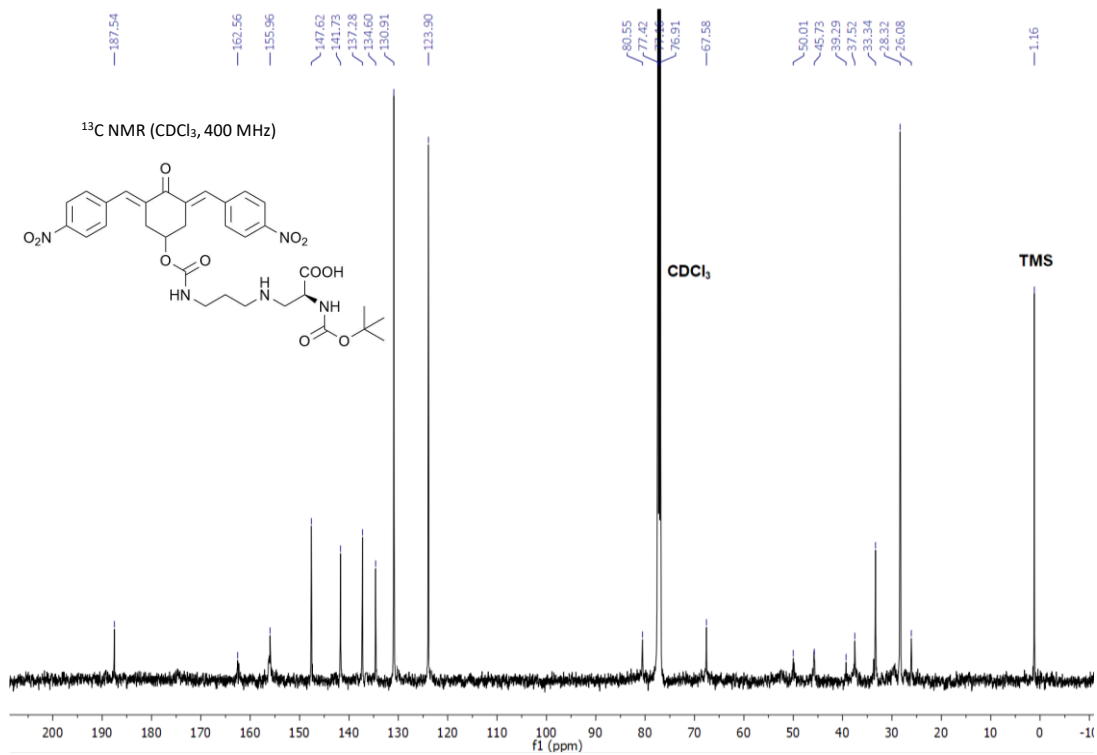
Figure 71

¹³C NMR of compound **16a.**

^{1}H NMR ((CD$_3$)$_2$SO, 500 MHz)
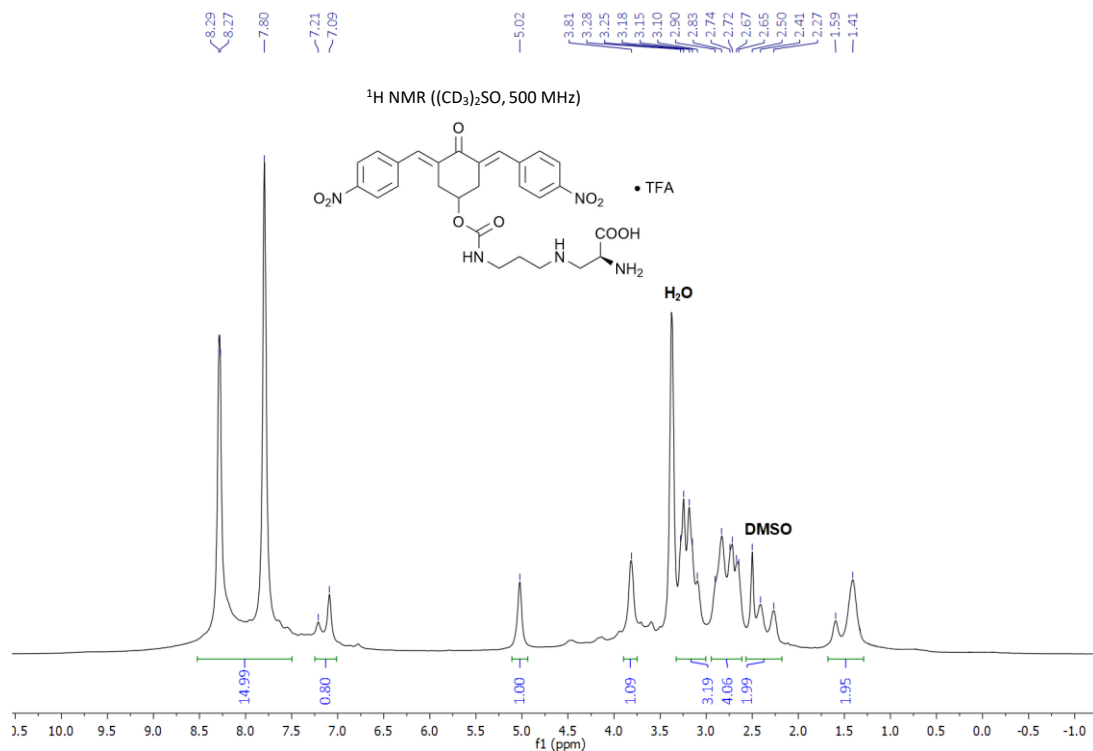
Figure 72

^{1}H NMR of compound **16b**.

^{13}C NMR ((CD$_3$)$_2$SO, 500 MHz)
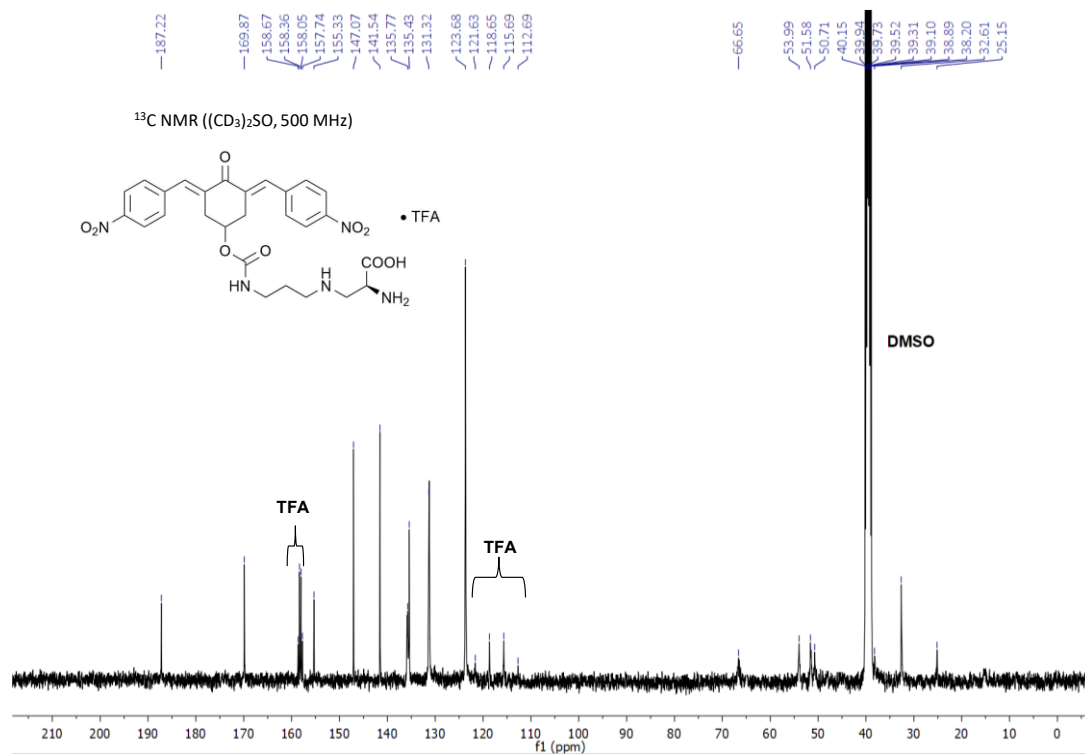
Figure 73

^{13}C NMR of compound **16b.**
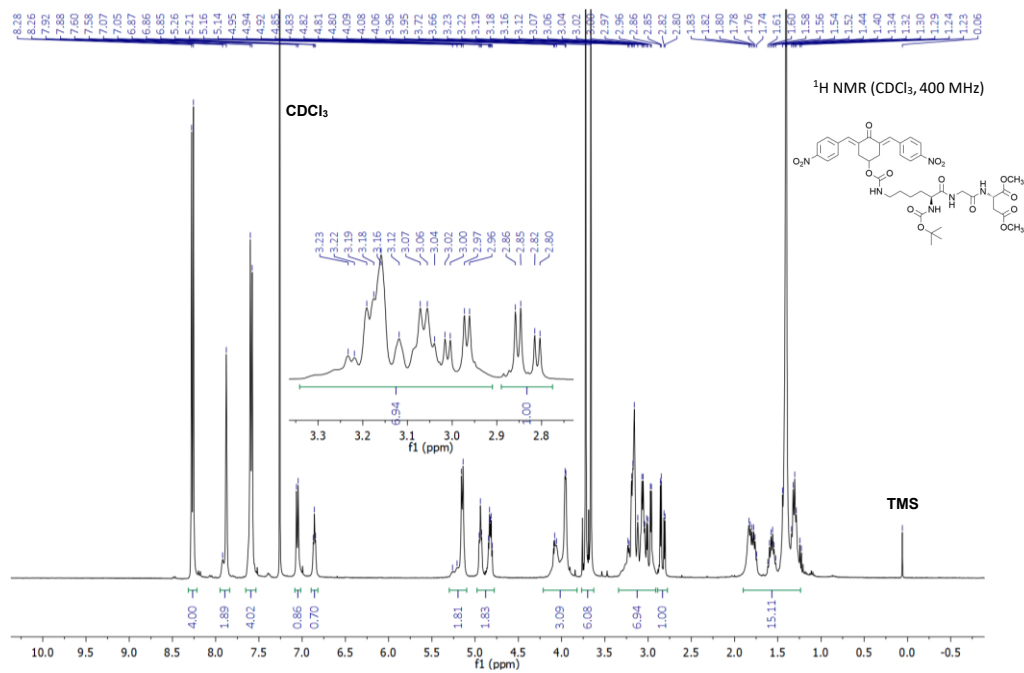
Figure 74

^{1}H NMR of compound **18a**.
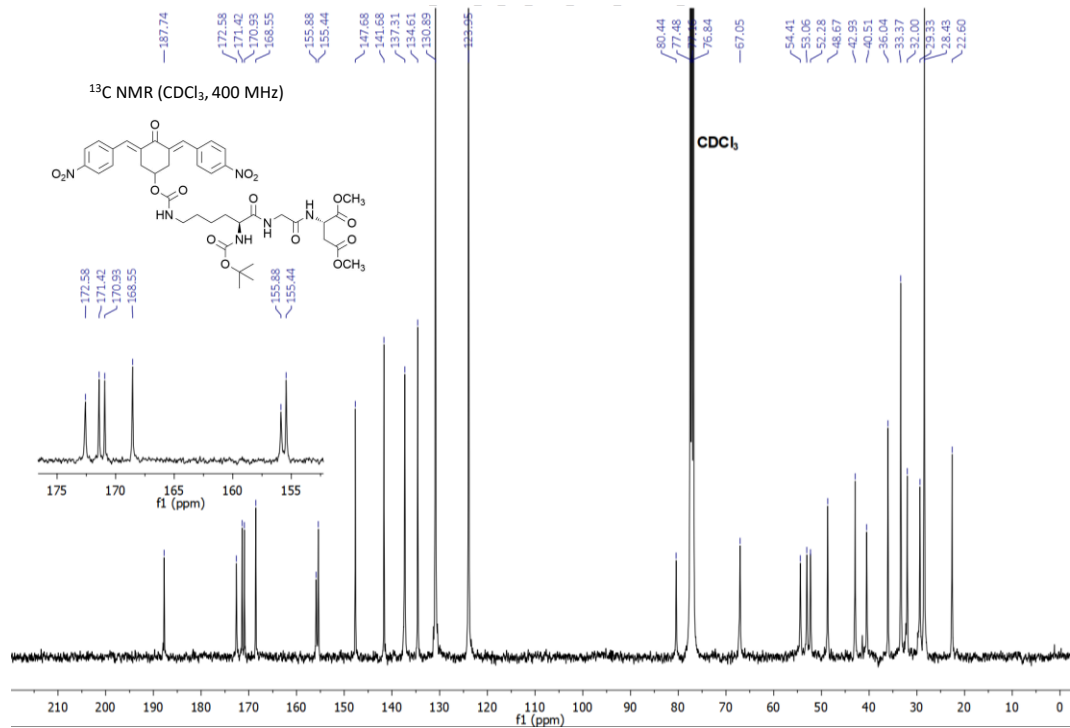
Figure 75

^{13}C NMR of compound **18a.**

Figure 76

^{1}H NMR of compound **18b**.

Figure 77

^{13}C NMR of compound **18b.**
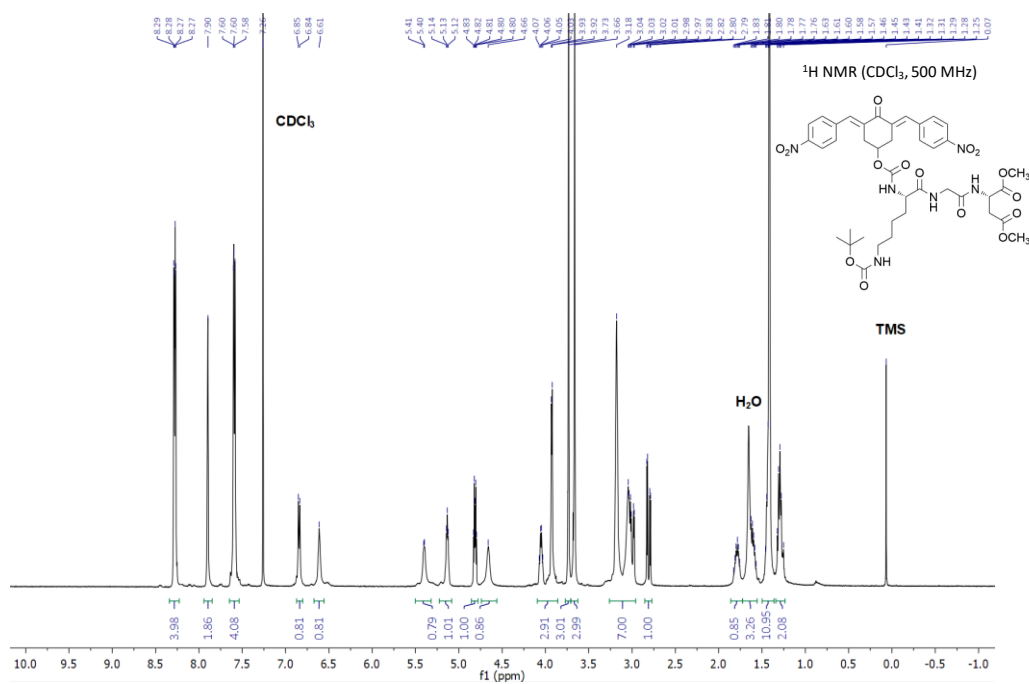
Figure 78

^{1}H NMR of compound **19a**.
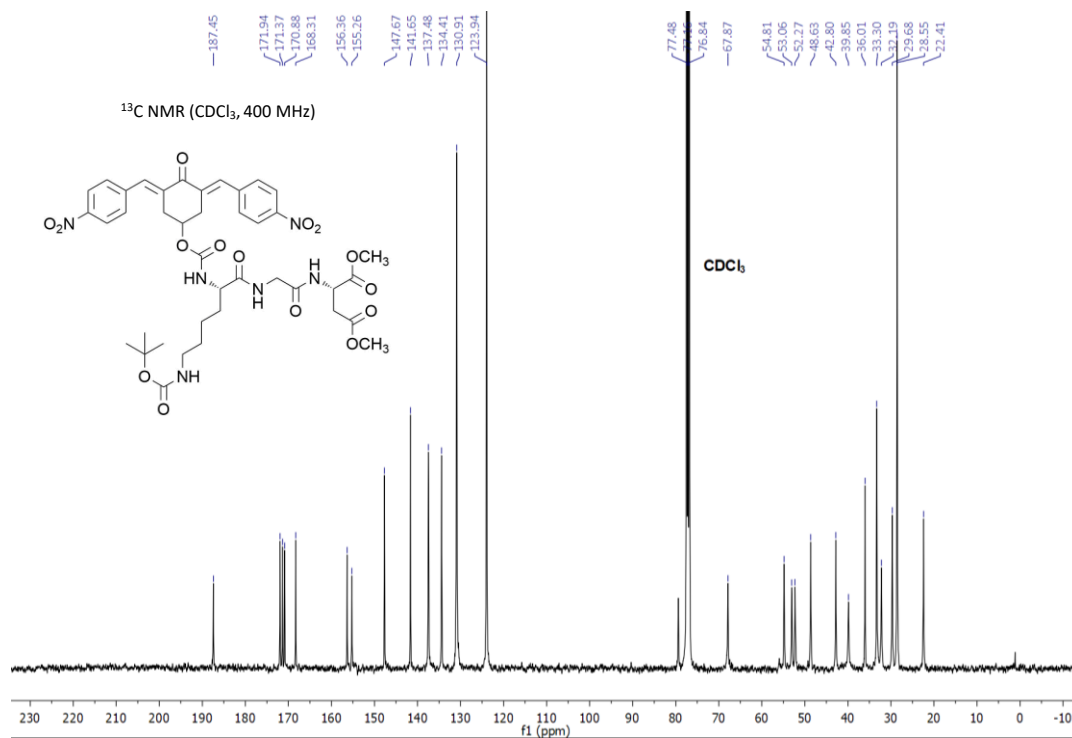
Figure 79
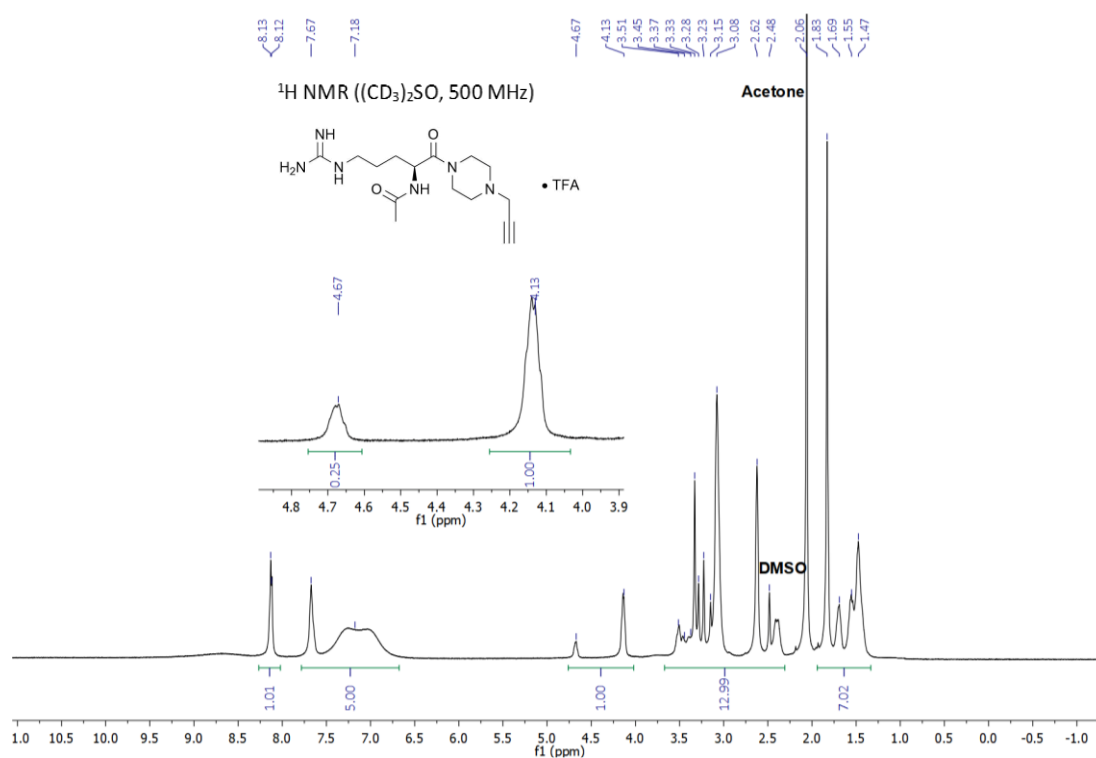
^{13}C NMR of compound **19a.**
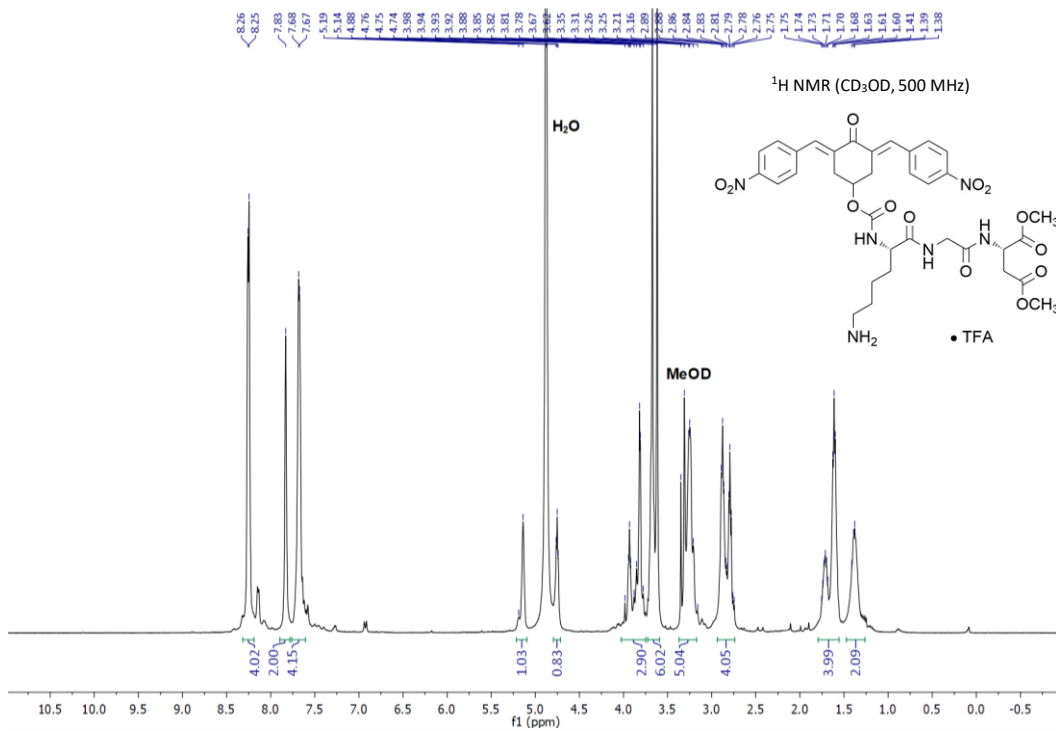
Figure 80

¹H NMR of compound **19b**.
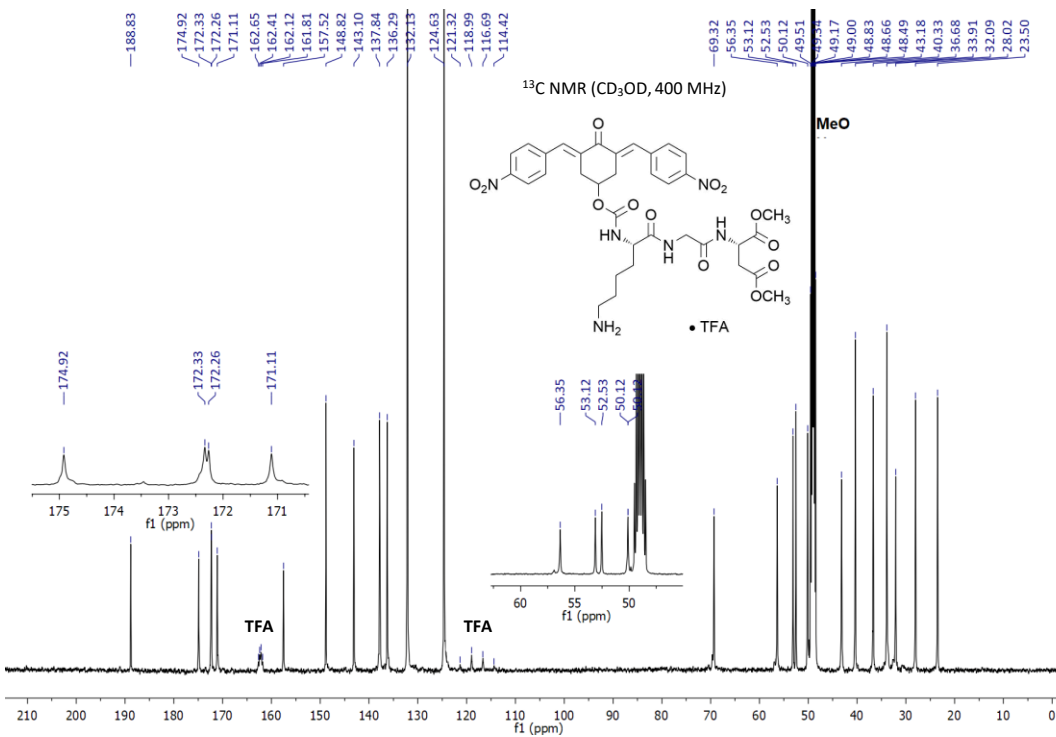
Figure 81

¹³C NMR of compound **19b.**
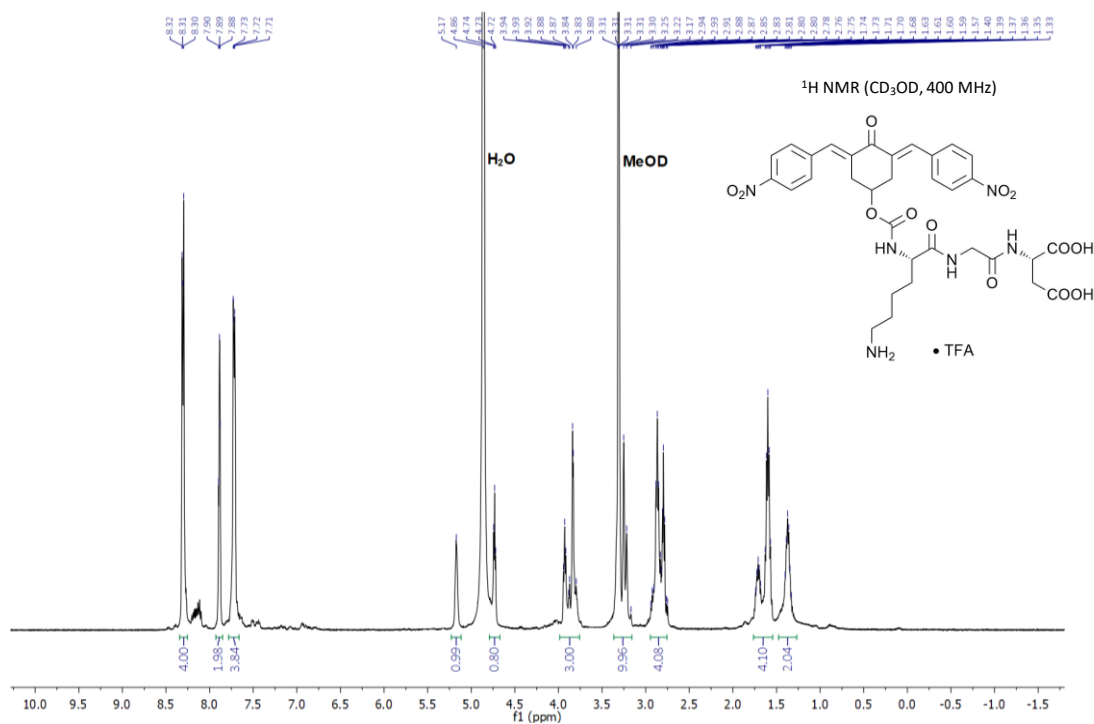
Figure 82

¹H NMR of compound **19c**.
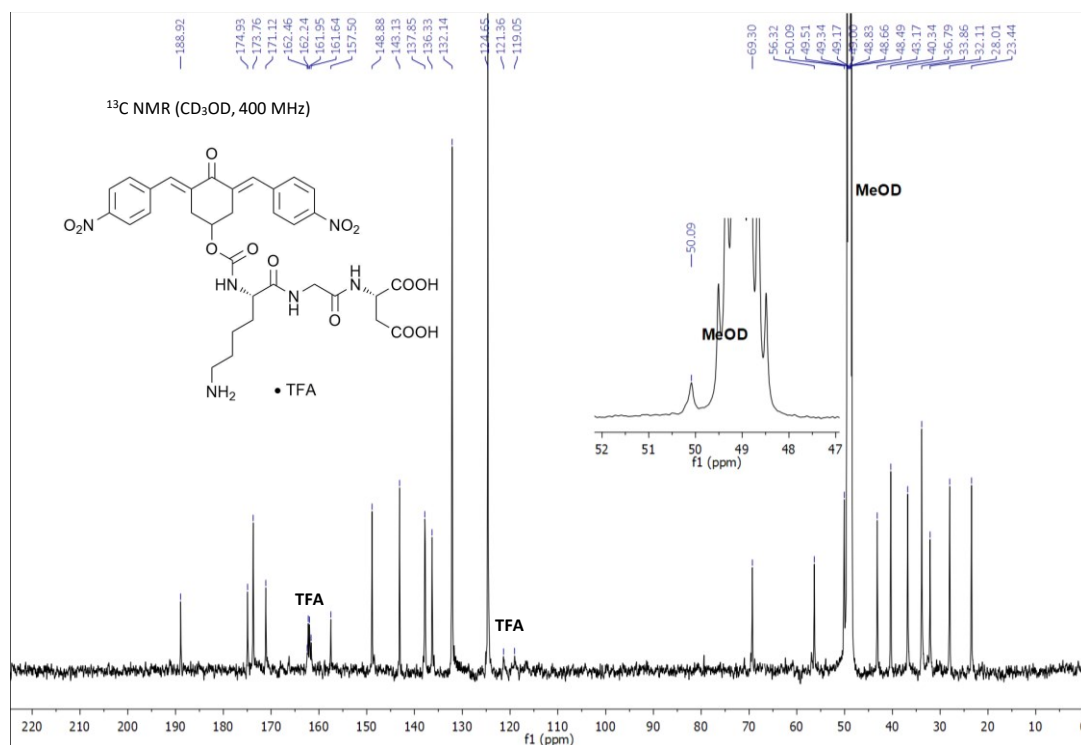
Figure 83

¹³C NMR of compound **19c.**
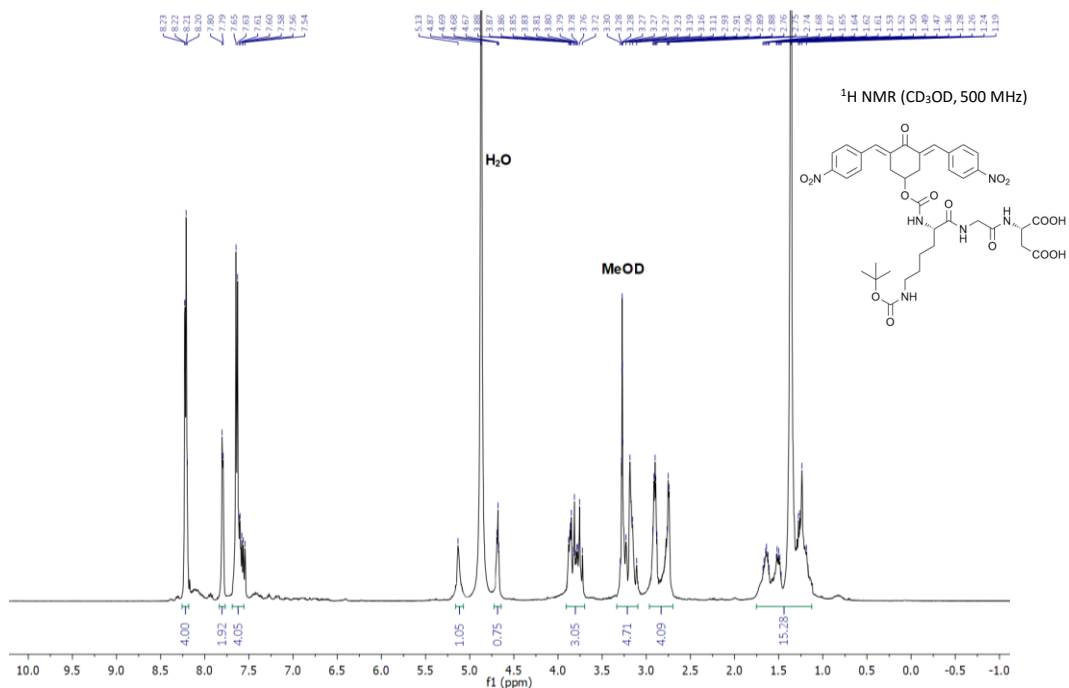
Figure 84

^{1}H NMR of compound **21c**.
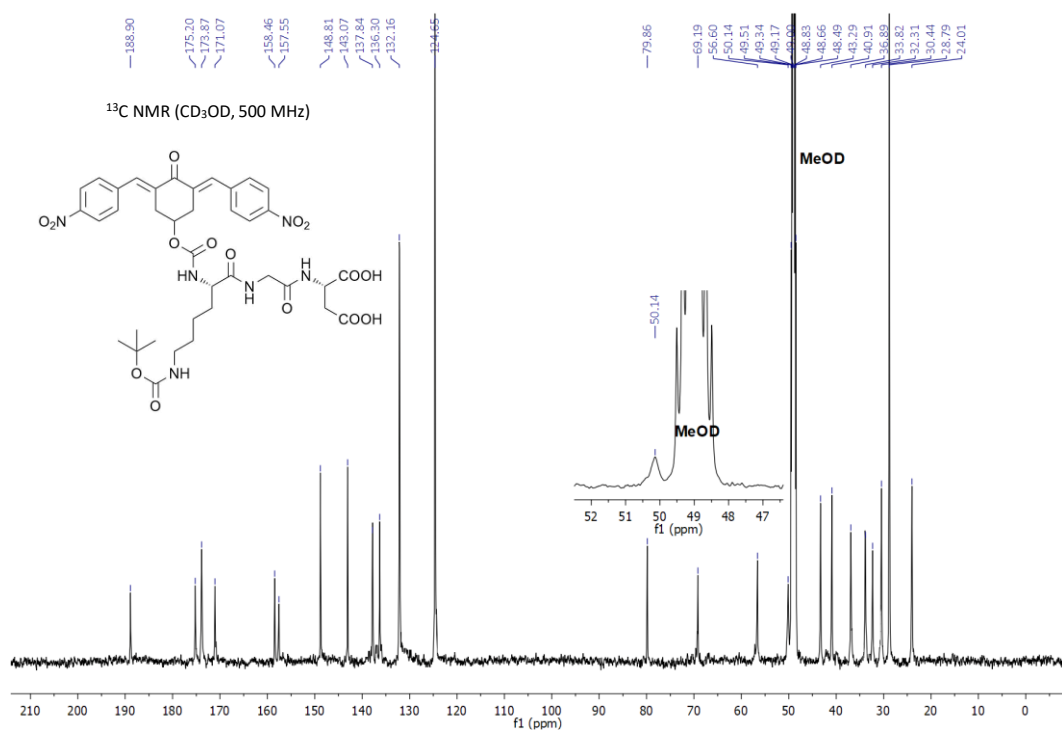
Figure 85

^{13}C NMR of compound **21c**.

Figure 86

^{1}H NMR of compound **22a**.

Figure 87

^{13}C NMR of compound **22a.**
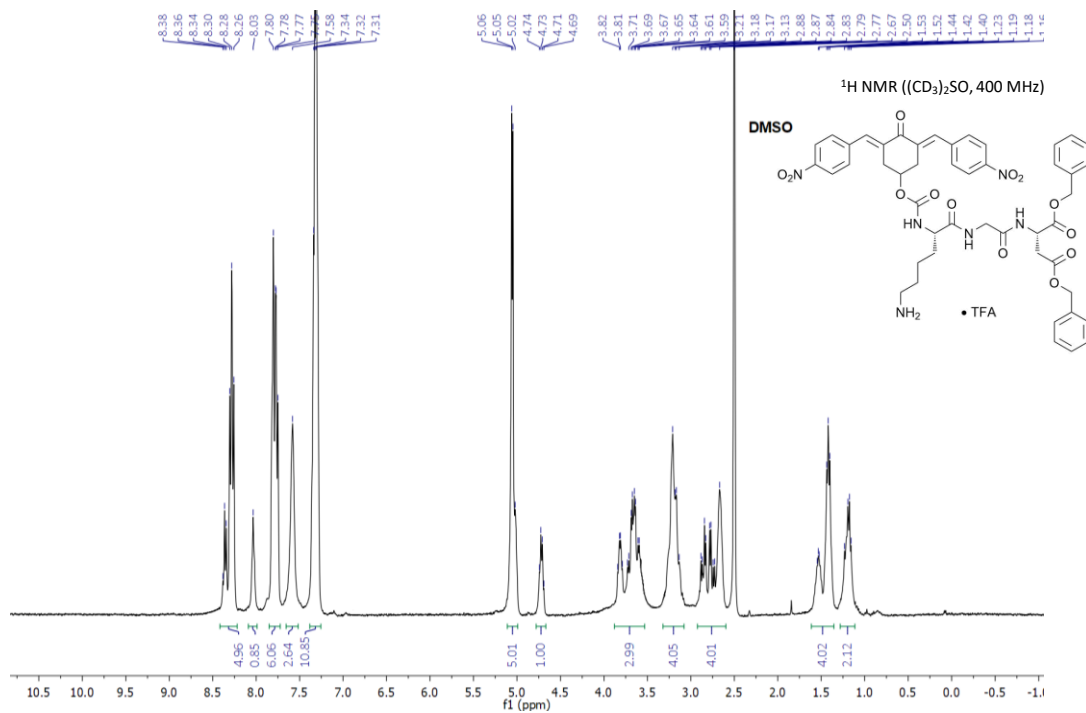
Figure 88

^{1}H NMR of compound **22b**.
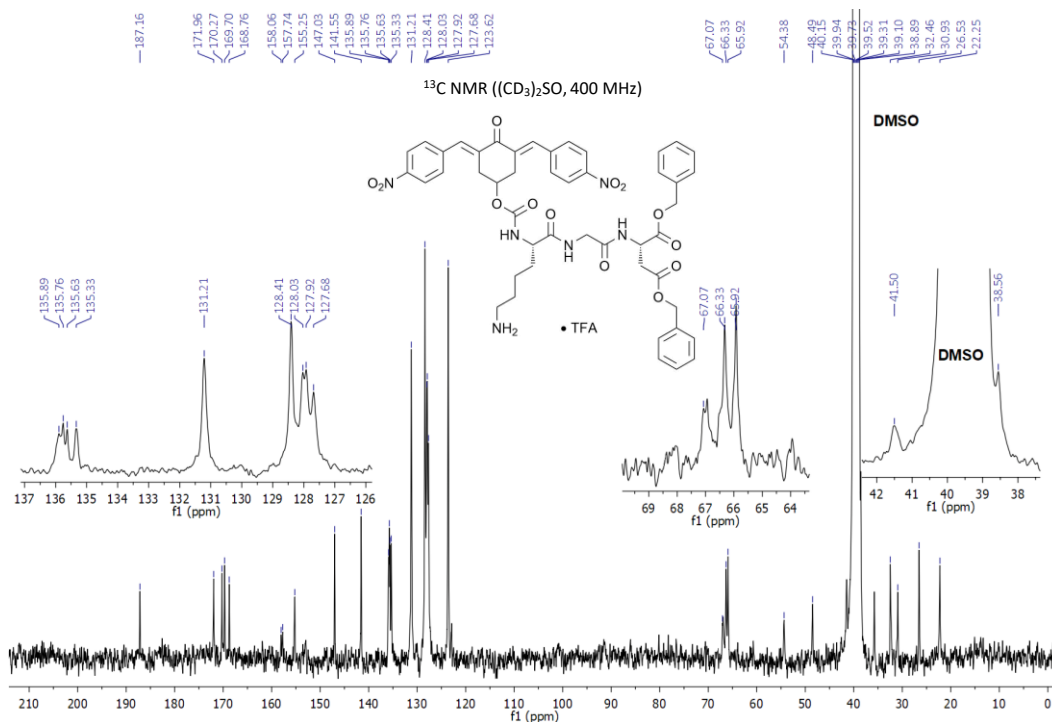
Figure 89

^{13}C NMR of compound **22b.**
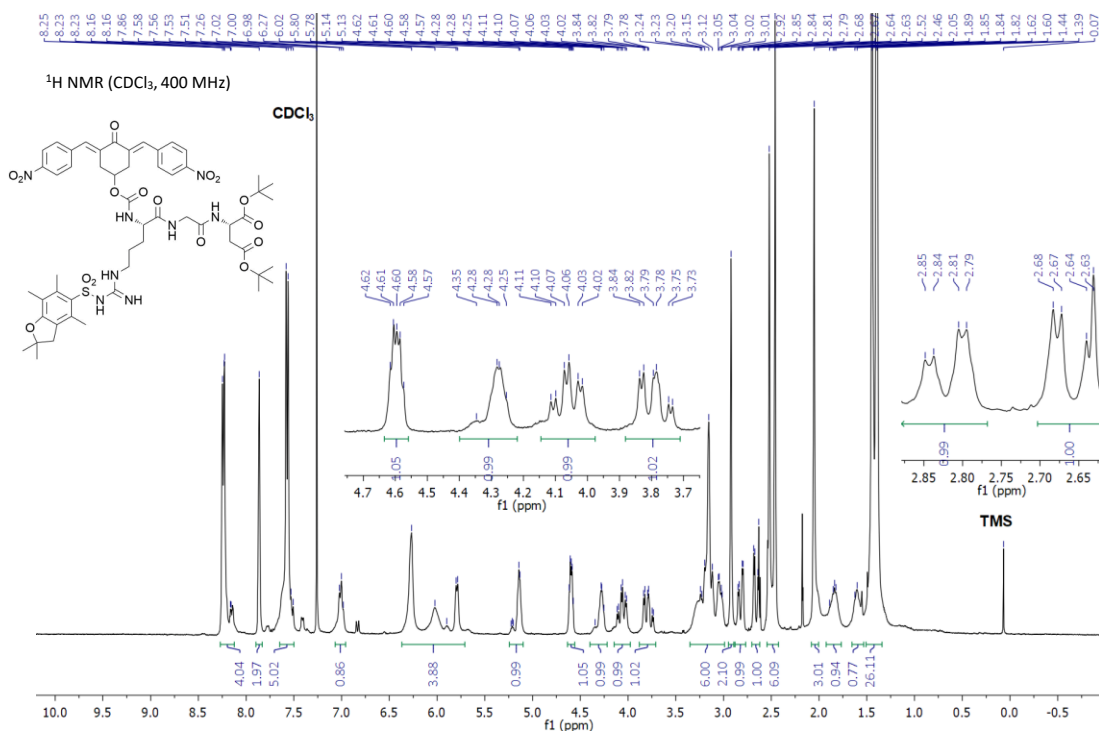
Figure 90

^{1}H NMR of compound **23a**.
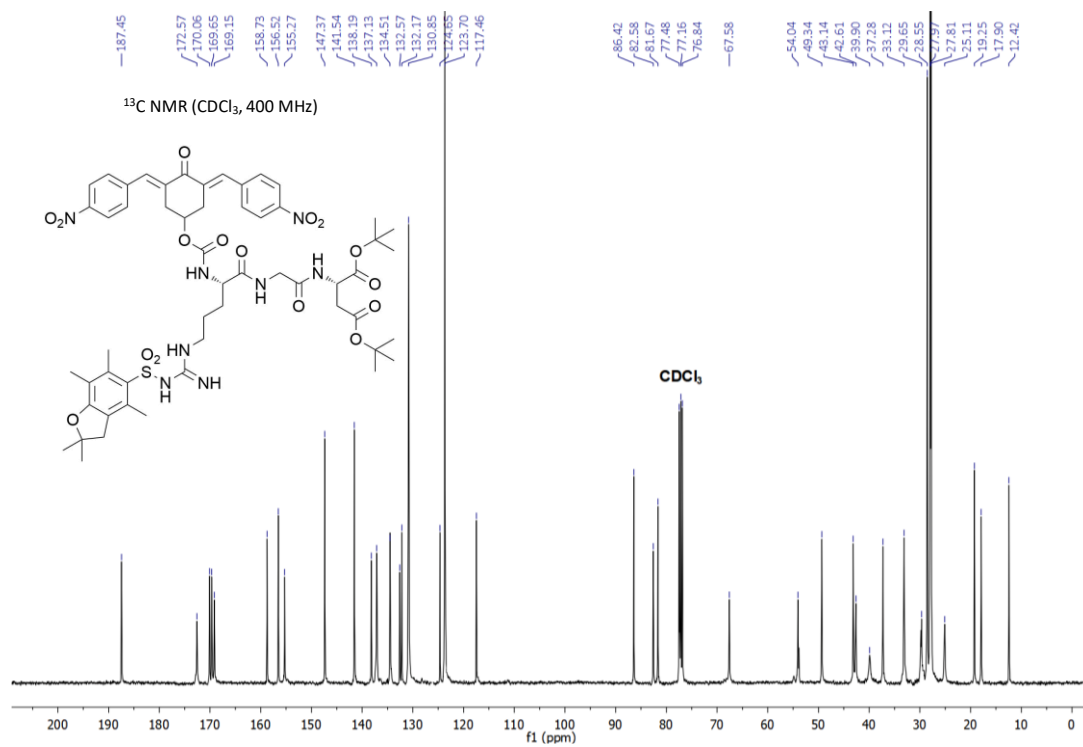
Figure 91

^{13}C NMR of compound **23a.**
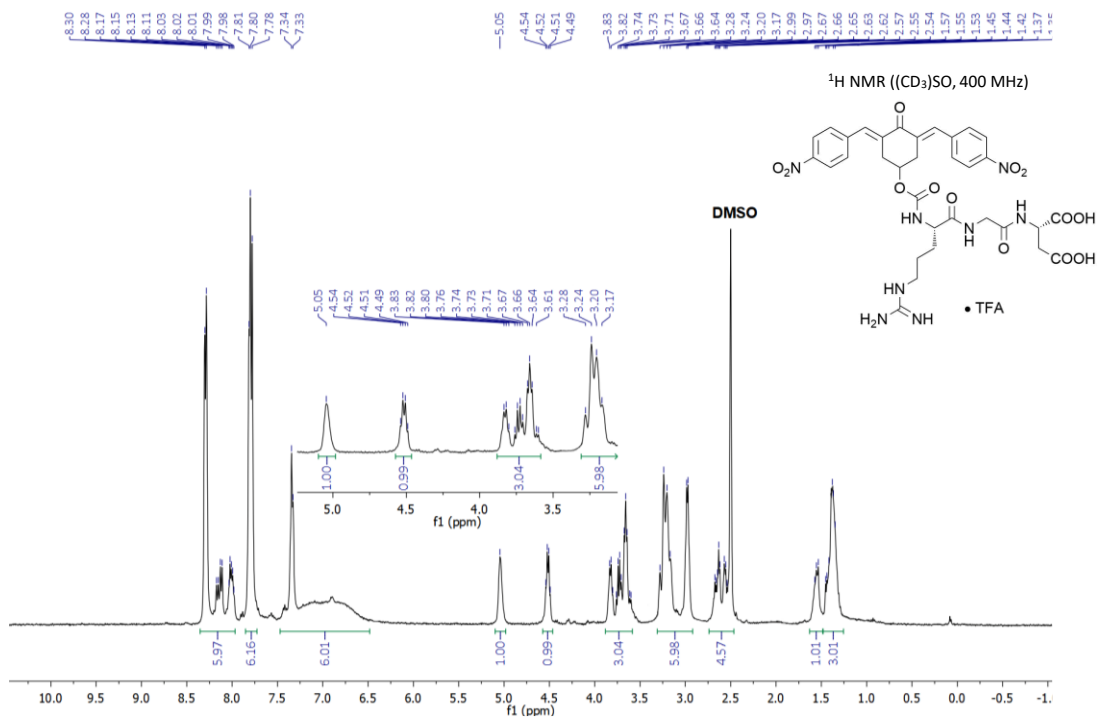
Figure 92

^{1}H NMR of compound **23b**.
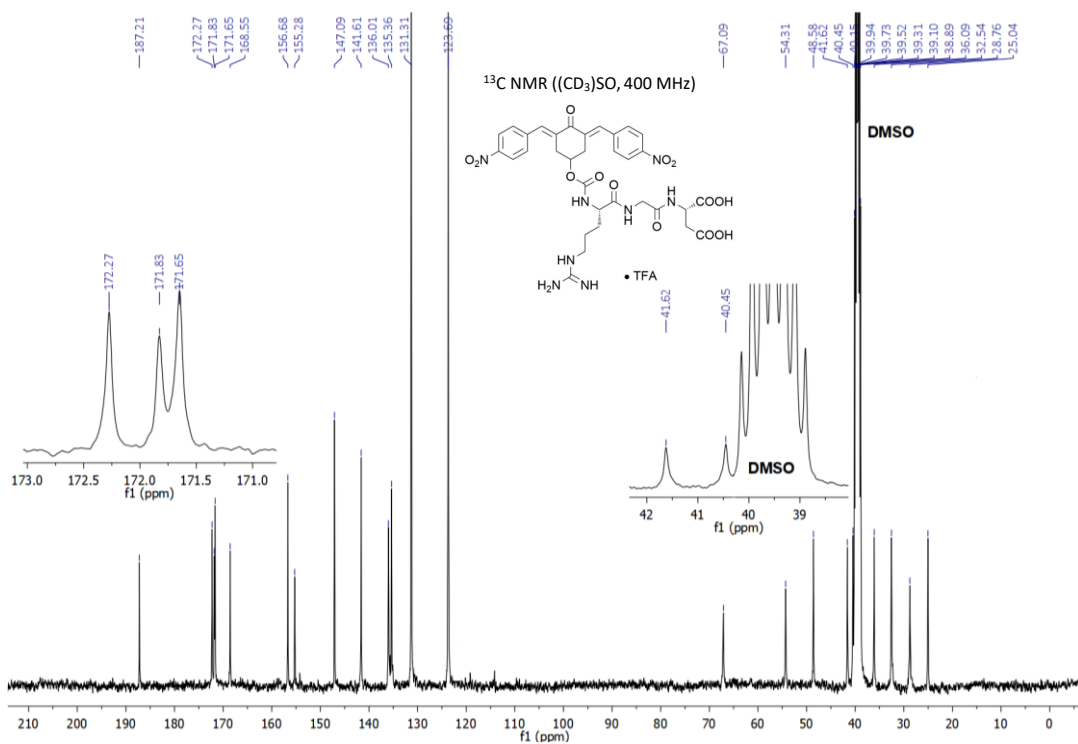
Figure 93

^{13}C NMR of compound **23b.**
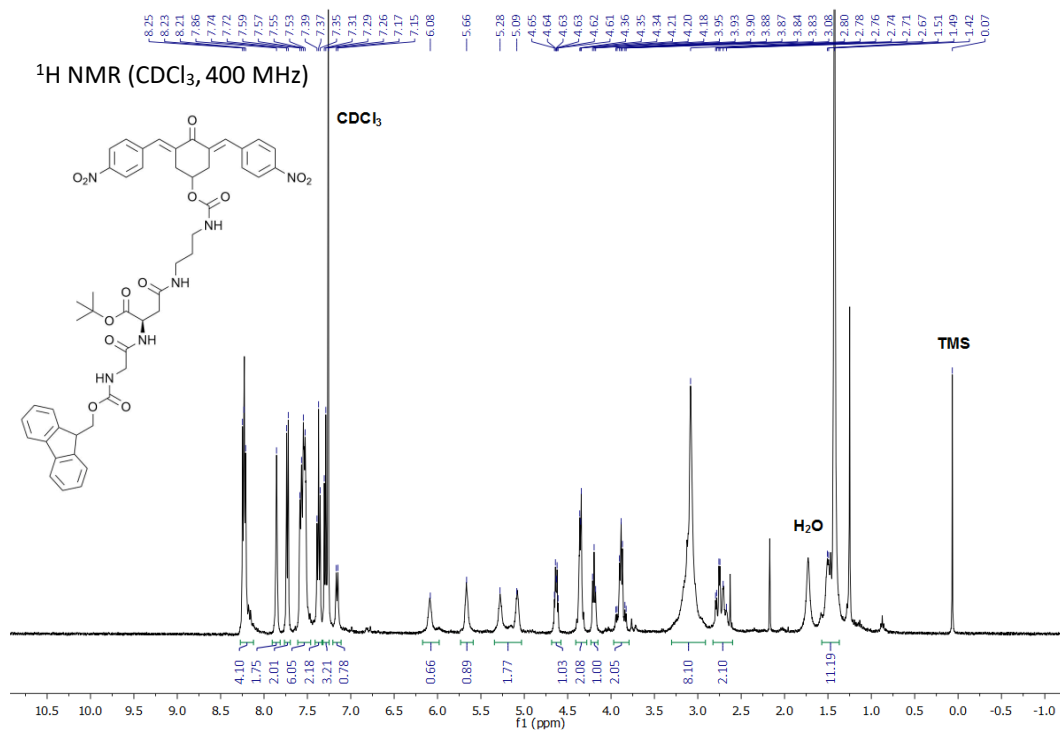
Figure 94

^{1}H NMR of compound **24a**
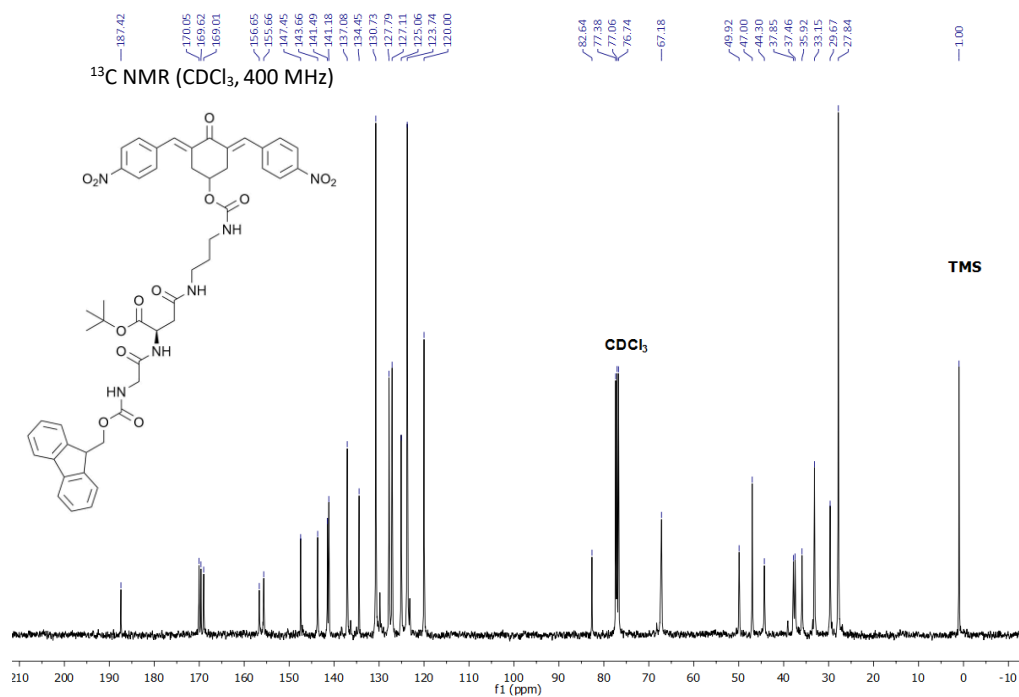
Figure 95

^{13}C NMR of compound **24a.**
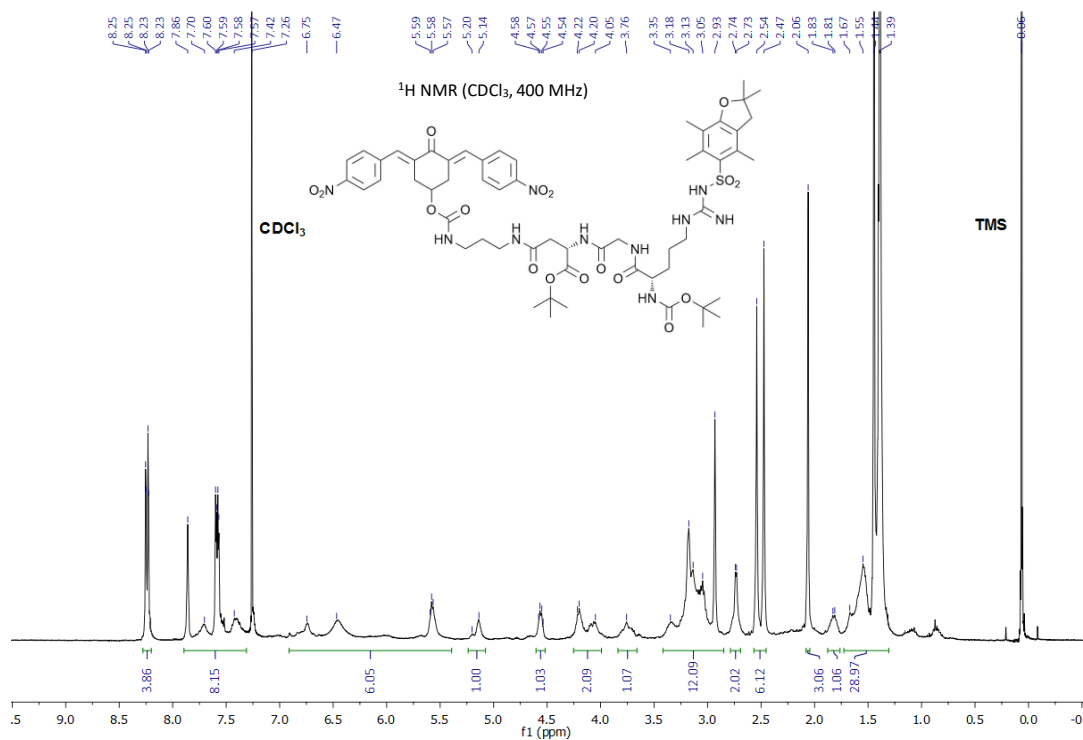
Figure 96

^{1}H NMR of compound **24b**
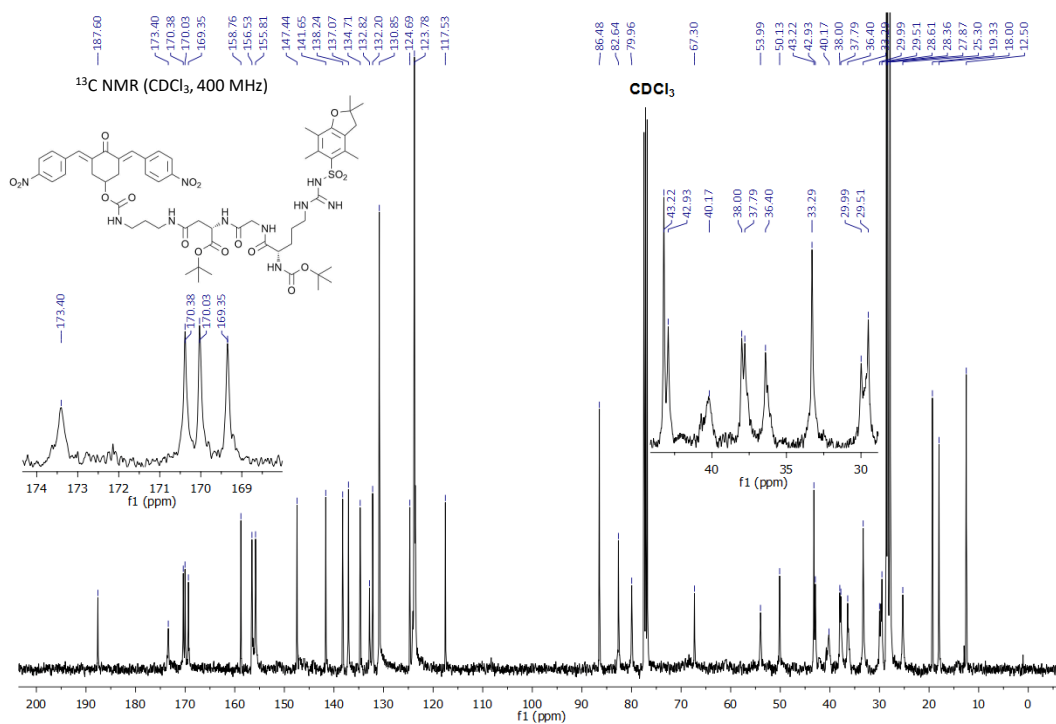
Figure 97

^{13}C NMR of compound **24b.**

^{1}H NMR ((CD$_3$)SO, 500 MHz)

8.94
8.29 8.28 8.21 7.96 7.80 7.57 7.22 7.03
5.02
4.19 3.83 3.50 3.34 3.07 2.93 2.87 2.84 2.50 2.41
1.81 1.76 1.56 1.36 1.24

H$_2$O

DMSO

0.88   20.83   0.78   0.81   3.23   6.06

f1 (ppm)
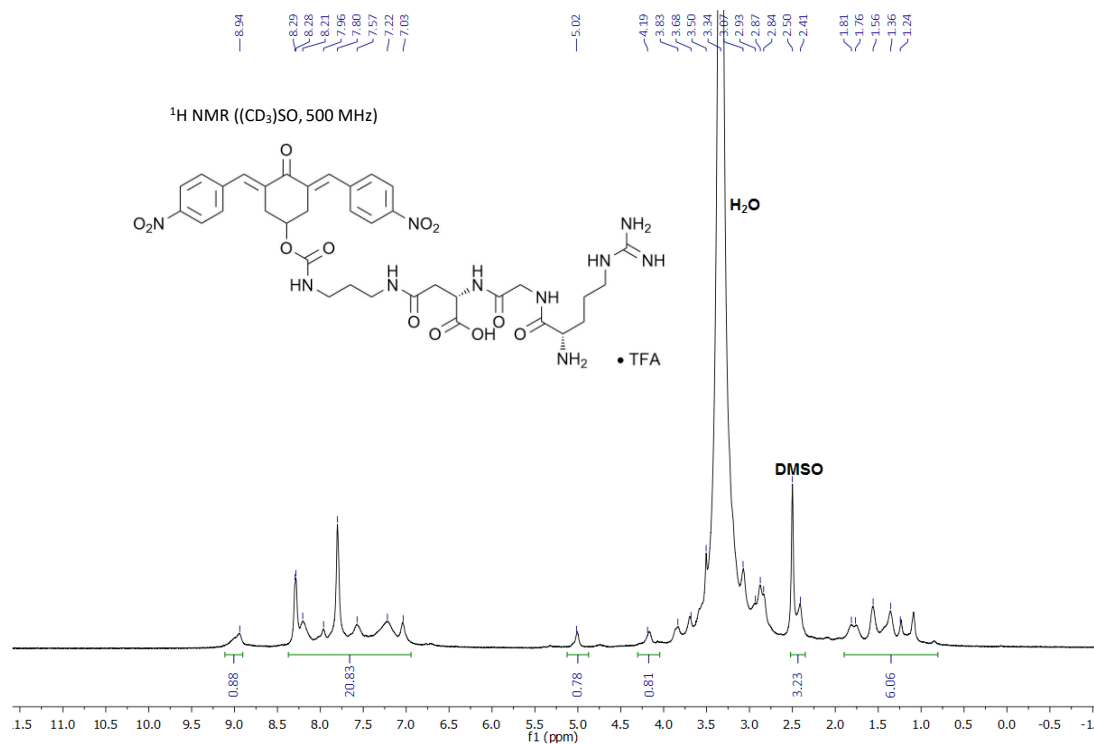
Figure 98

^{1}H NMR of compound **24c**.

187.23
173.55 169.46 169.38 167.96
157.02 155.17
147.02 141.51 135.79 135.43 131.24
123.62
66.55
51.80 50.15 42.21 40.02 39.85 39.69 39.52 39.35 39.19 39.02 37.79 36.09 32.56 29.14 28.26 23.26

^{13}C NMR ((CD$_3$)SO, 500 MHz)

DMSO

173.55   169.46 169.38   167.96

174 173 172 171 170 169 168 167
f1 (ppm)

f1 (ppm)
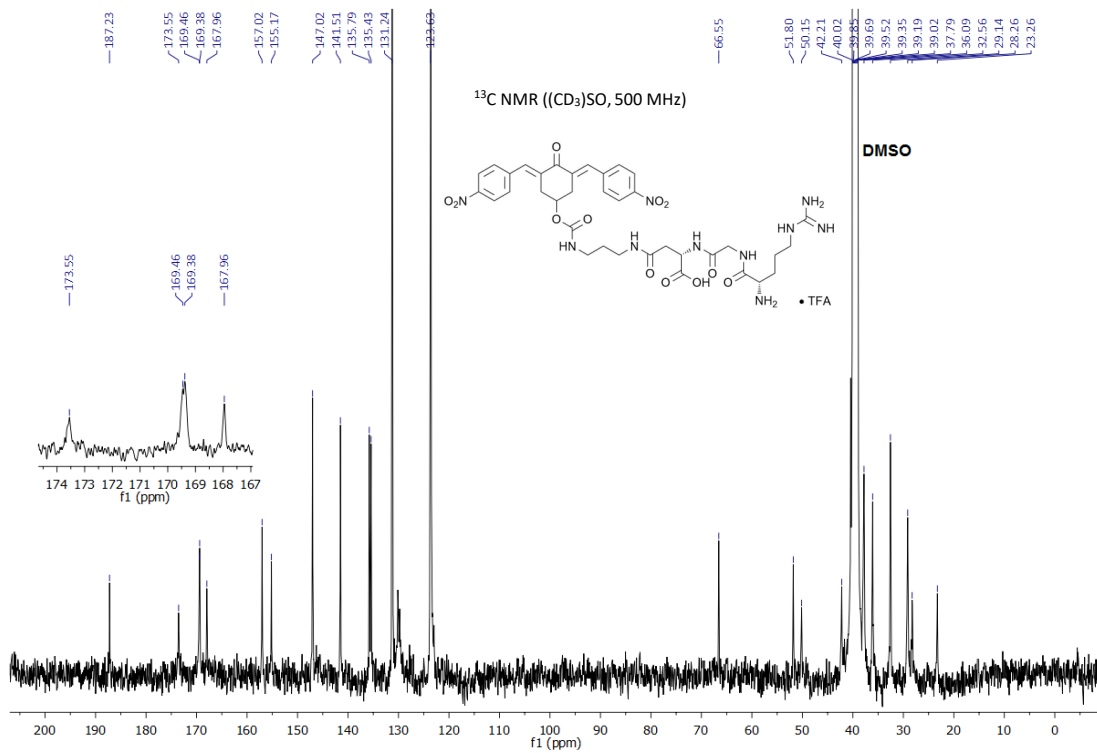
Figure 99

^{13}C NMR of compound **24c.**
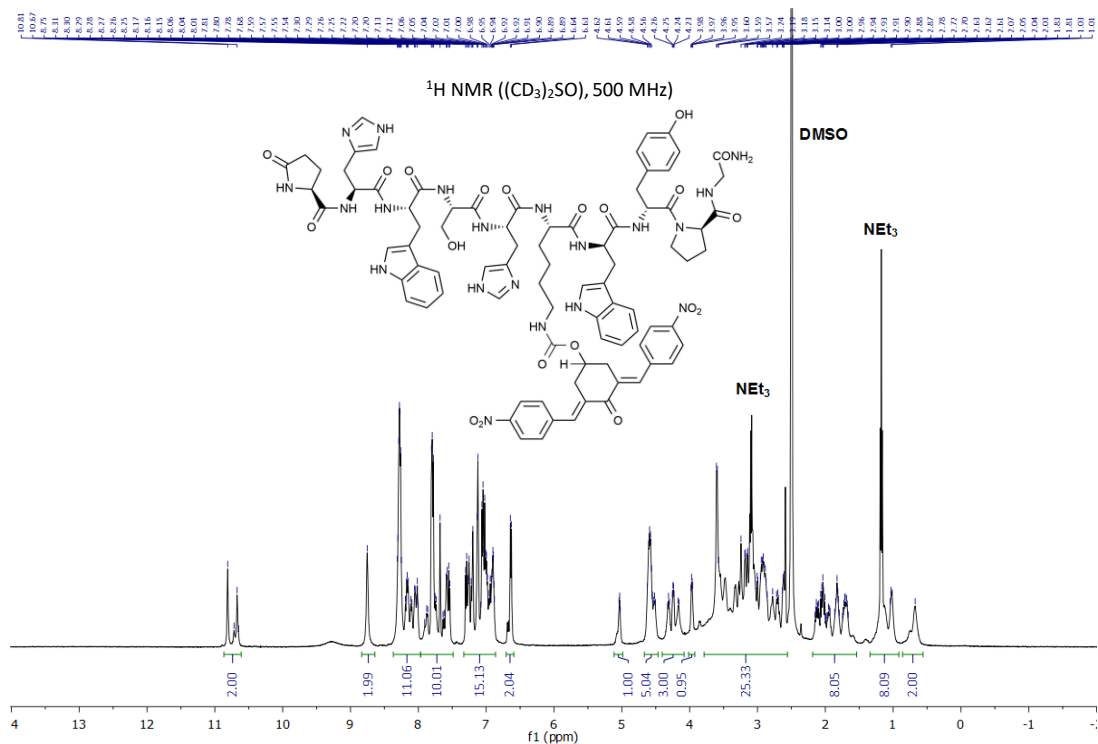
Figure 100

^{1}H NMR of compound **25a**.
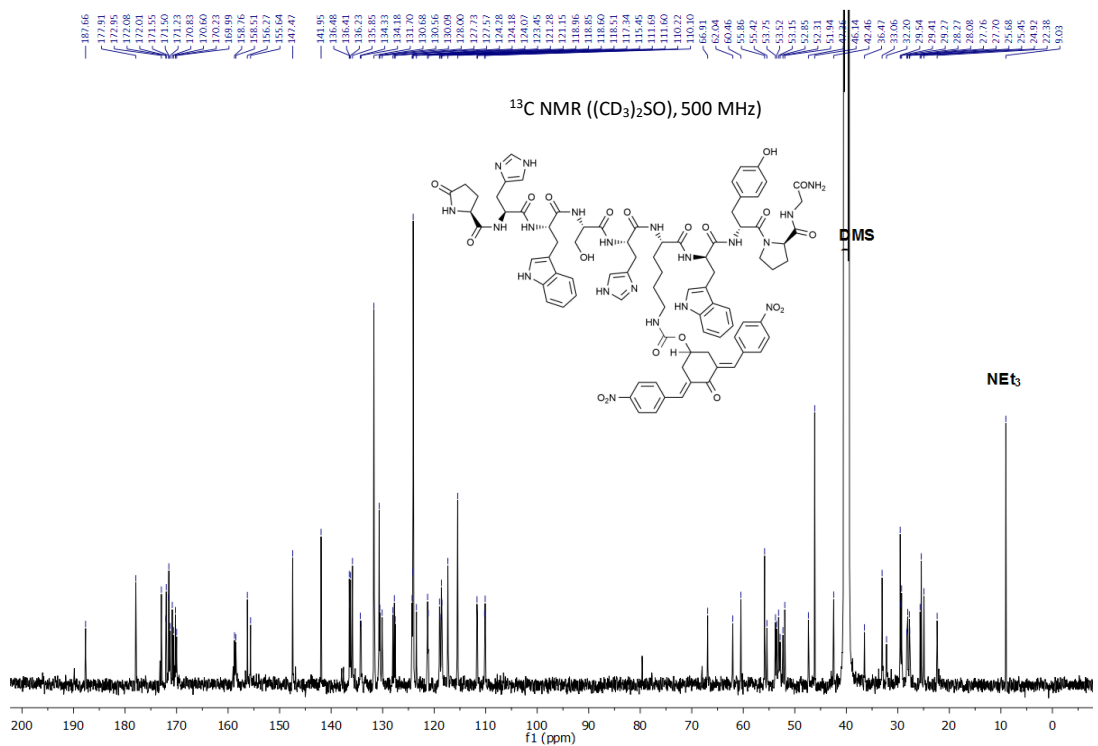
Figure 101

^{13}C NMR of compound **25a.**

Figure 102

^{1}H NMR of compound **31a**.

Figure 103

^{13}C NMR of compound **31a**.
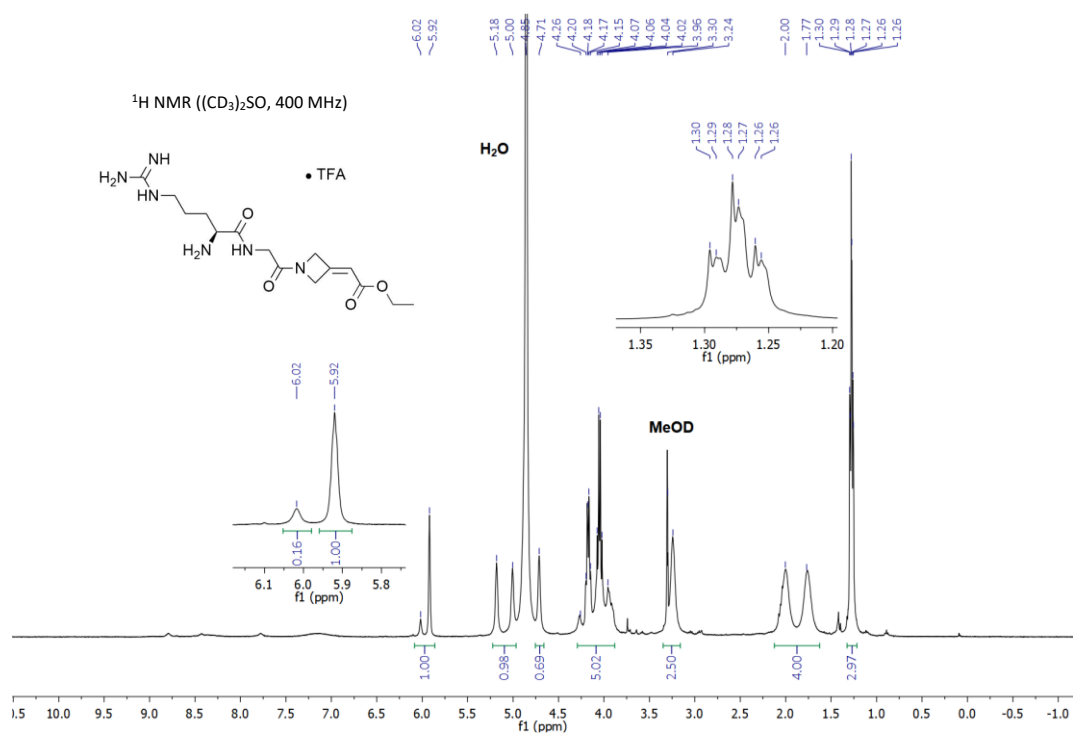
Figure 104

¹H NMR of compound **31b**.
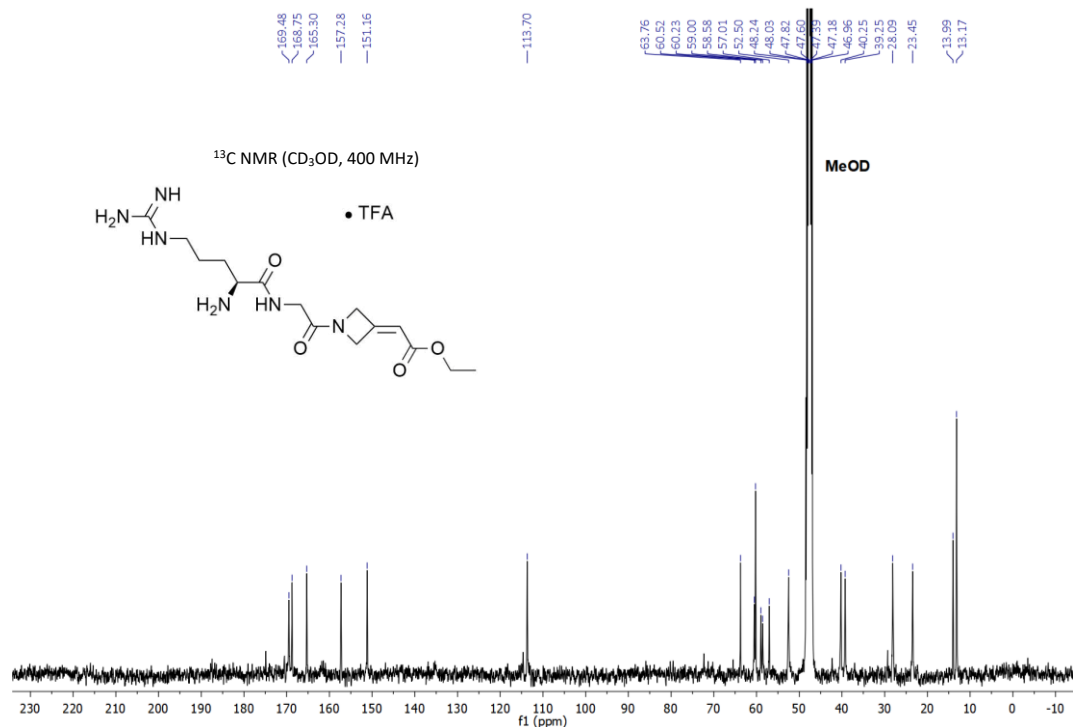
Figure 105

¹³C NMR of compound **31b**.
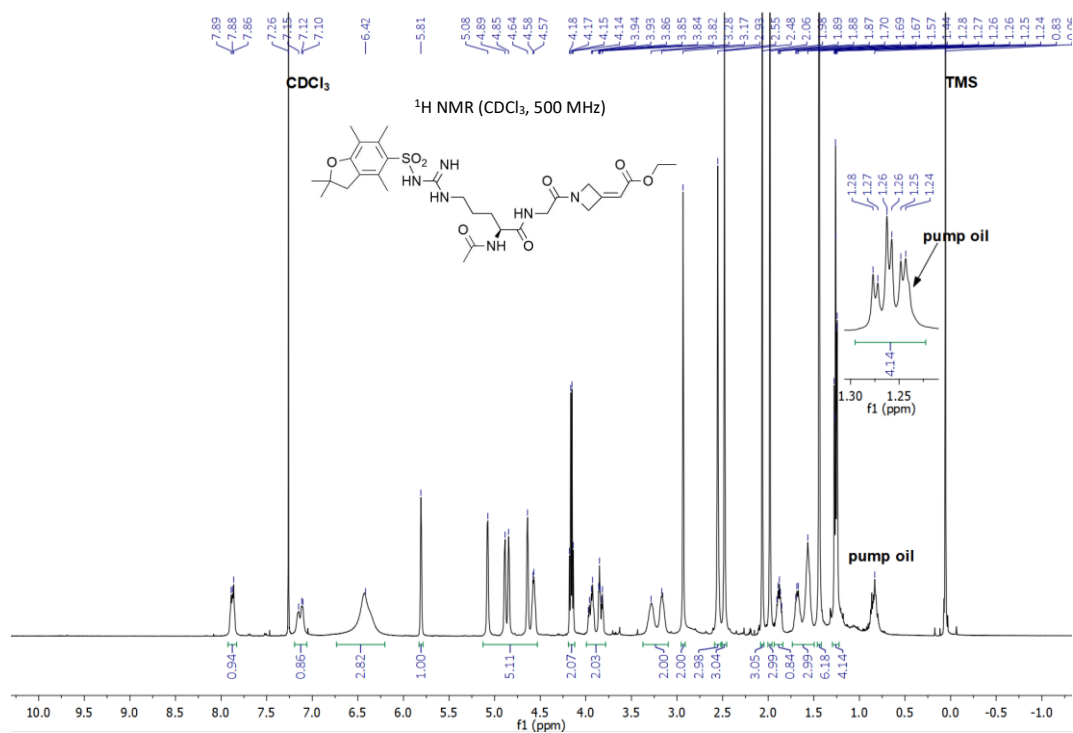
Figure 106

^{1}H NMR of compound **32a**.
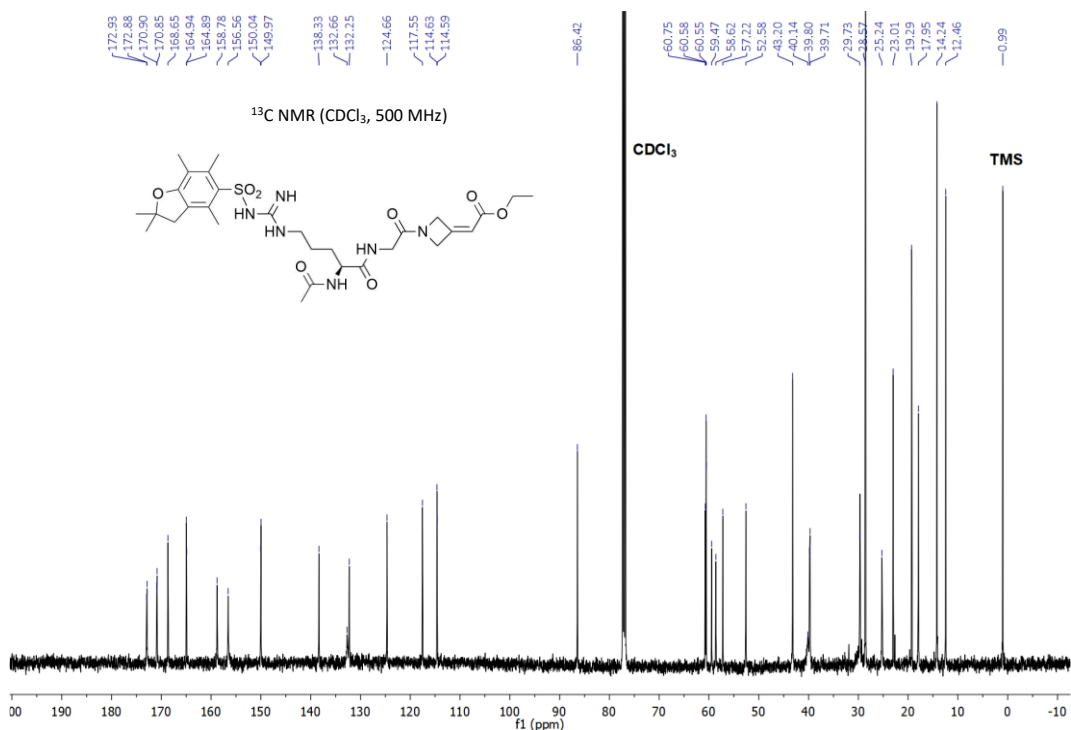
Figure 107

^{13}C NMR of compound **32a**.
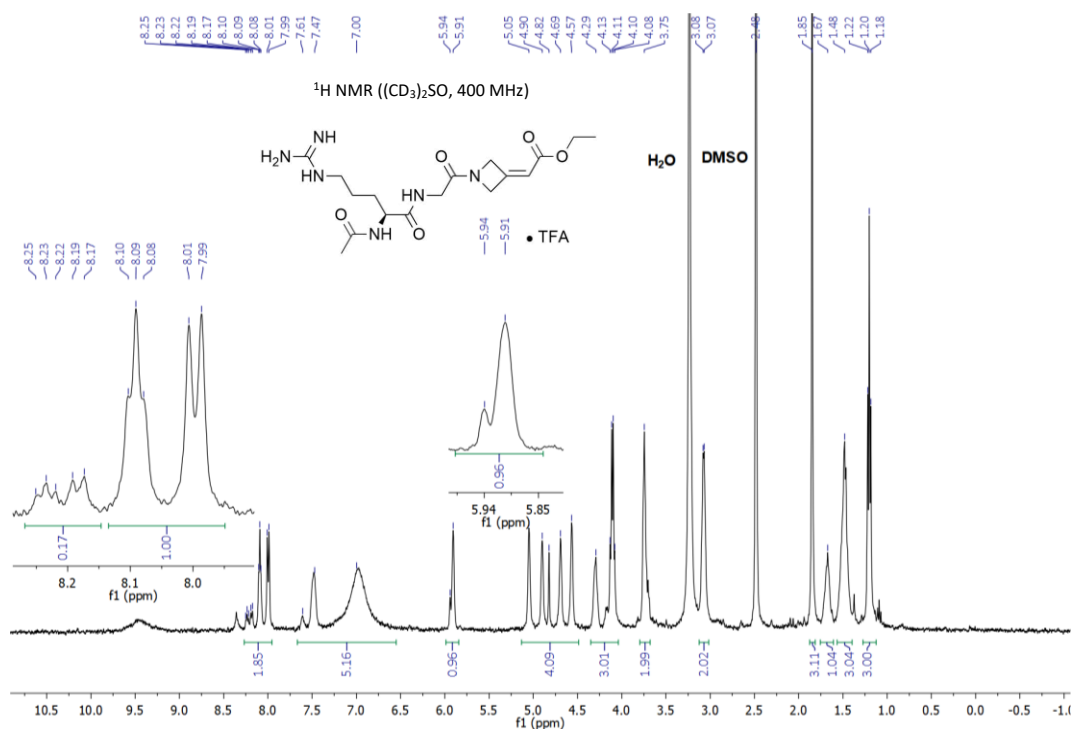
Figure 108

^{1}H NMR of compound **32b**.
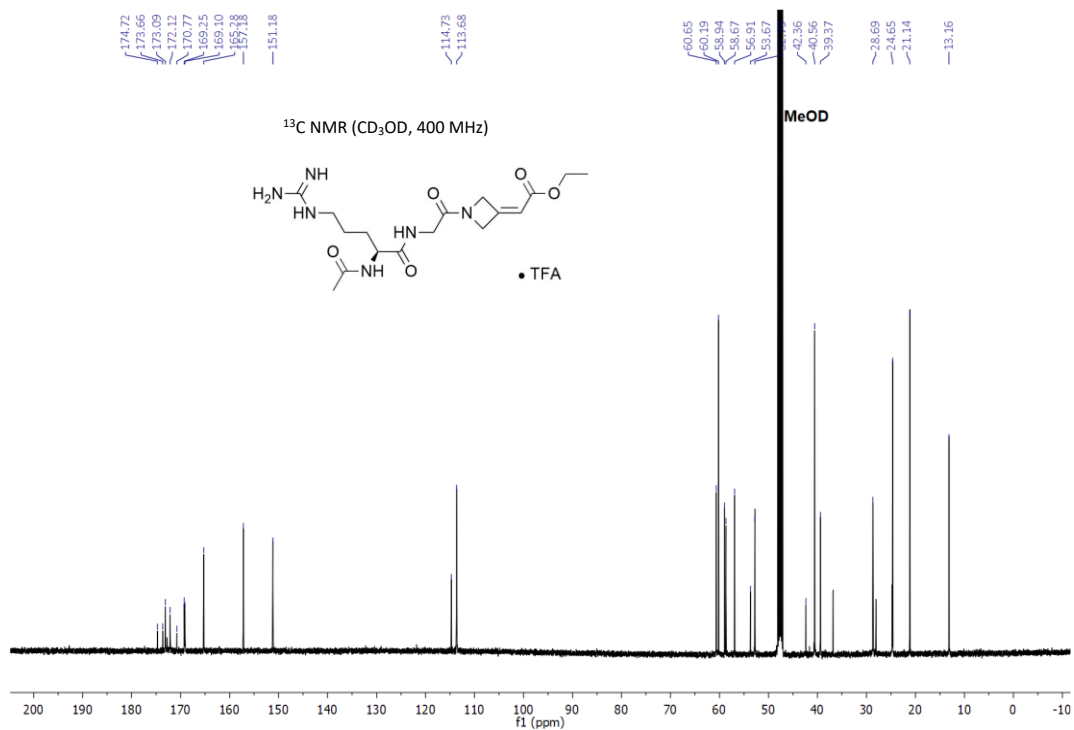
Figure 109

^{13}C NMR of compound **32b**.
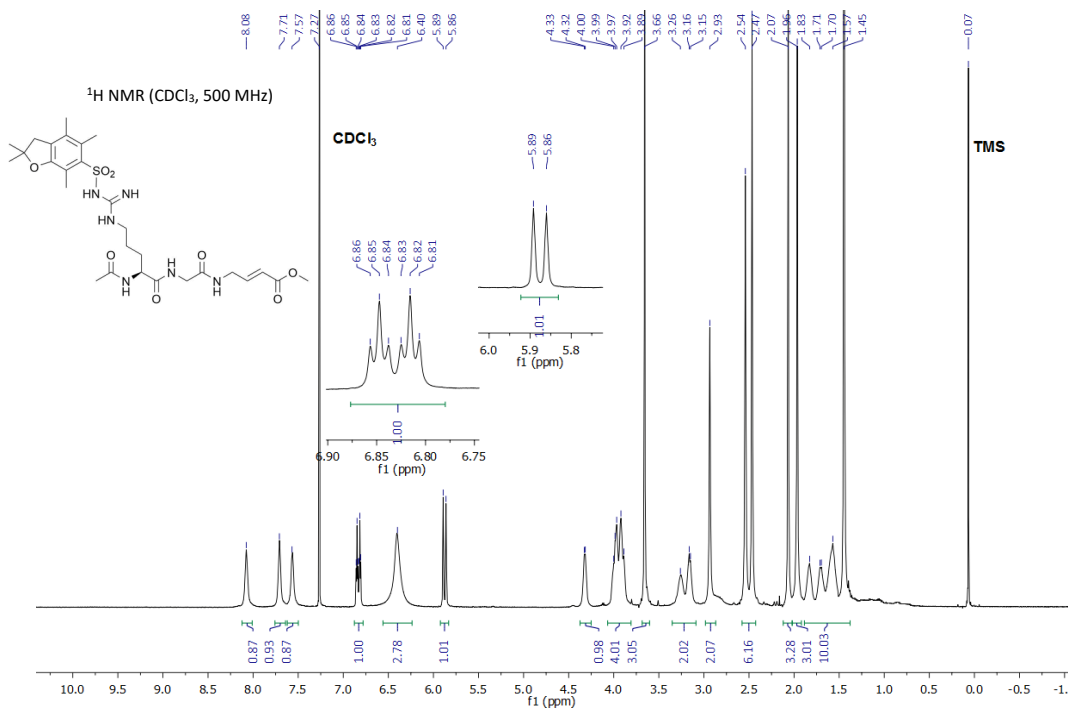
Figure 110

¹H NMR of compound **37a**.
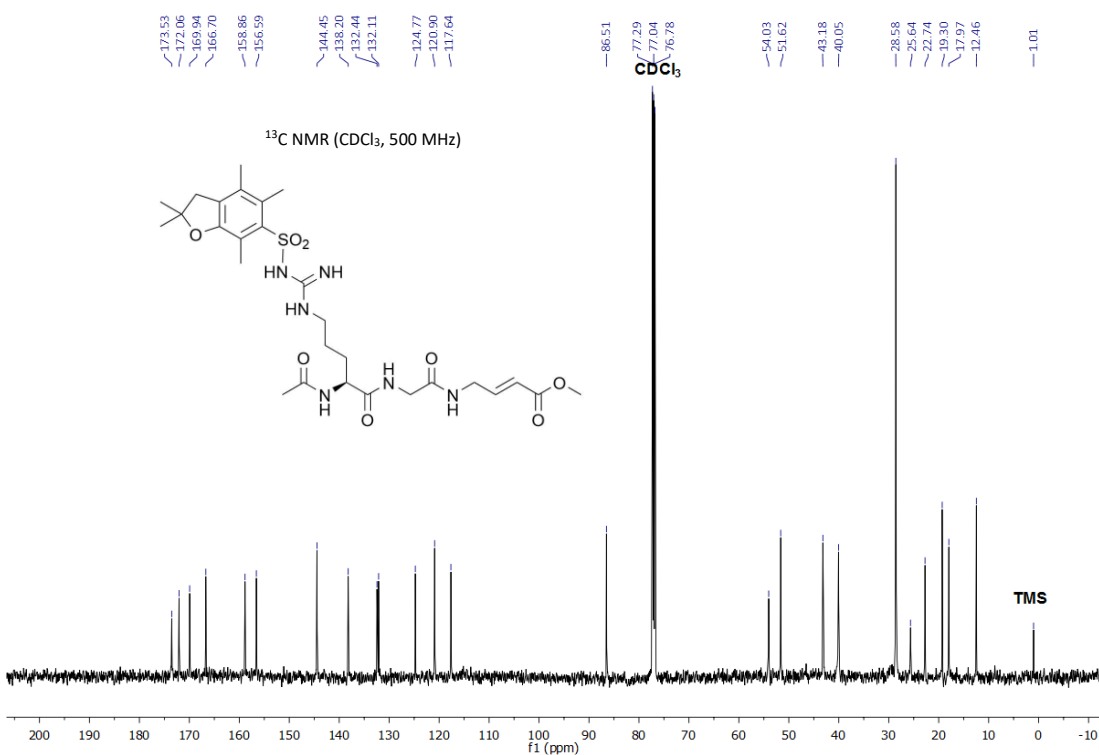
Figure 111

¹³C NMR of compound **37a**.
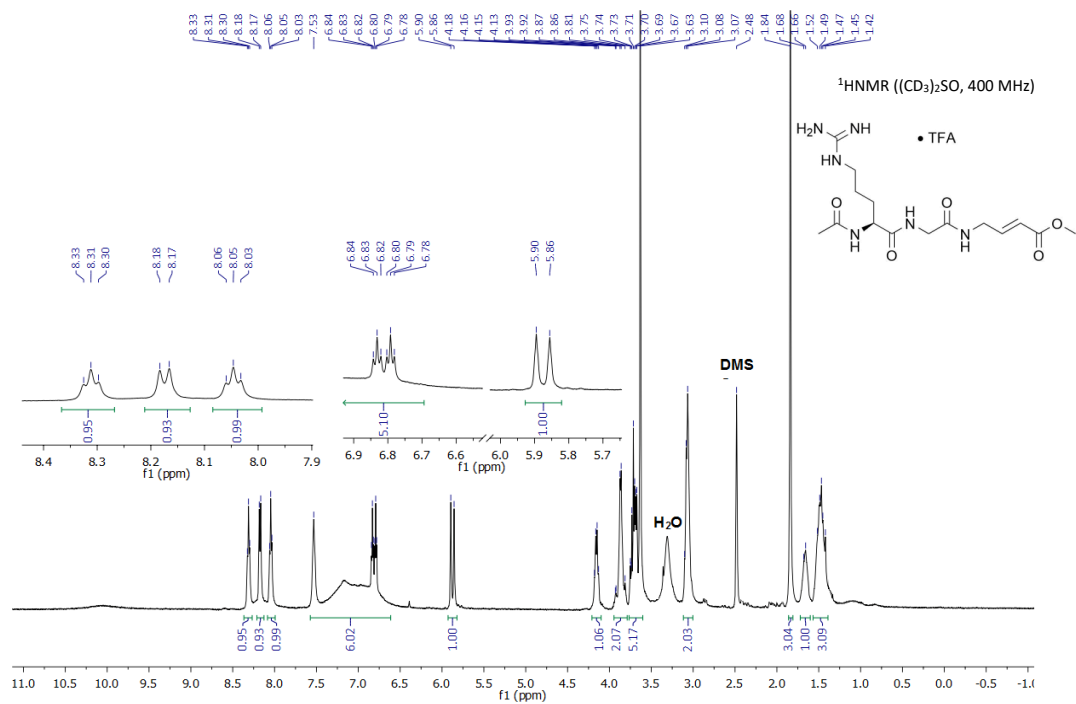
Figure 112

^{1}H NMR of compound **37b**.
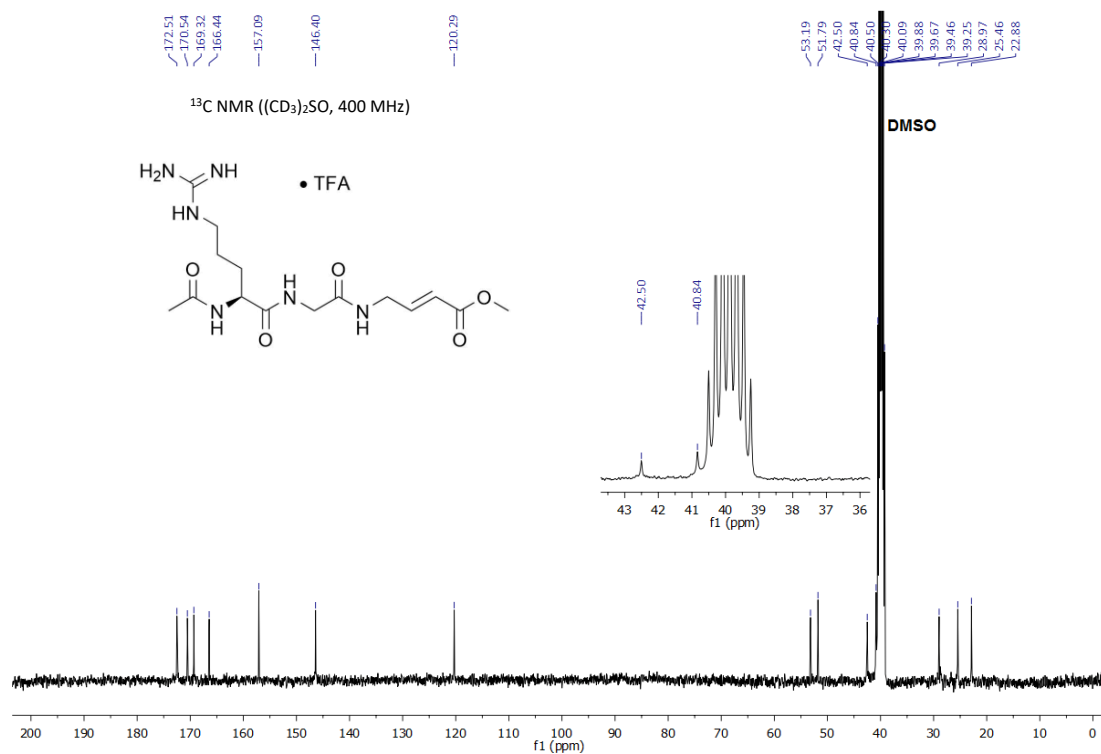
Figure 113

^{13}C NMR of compound **37b**.
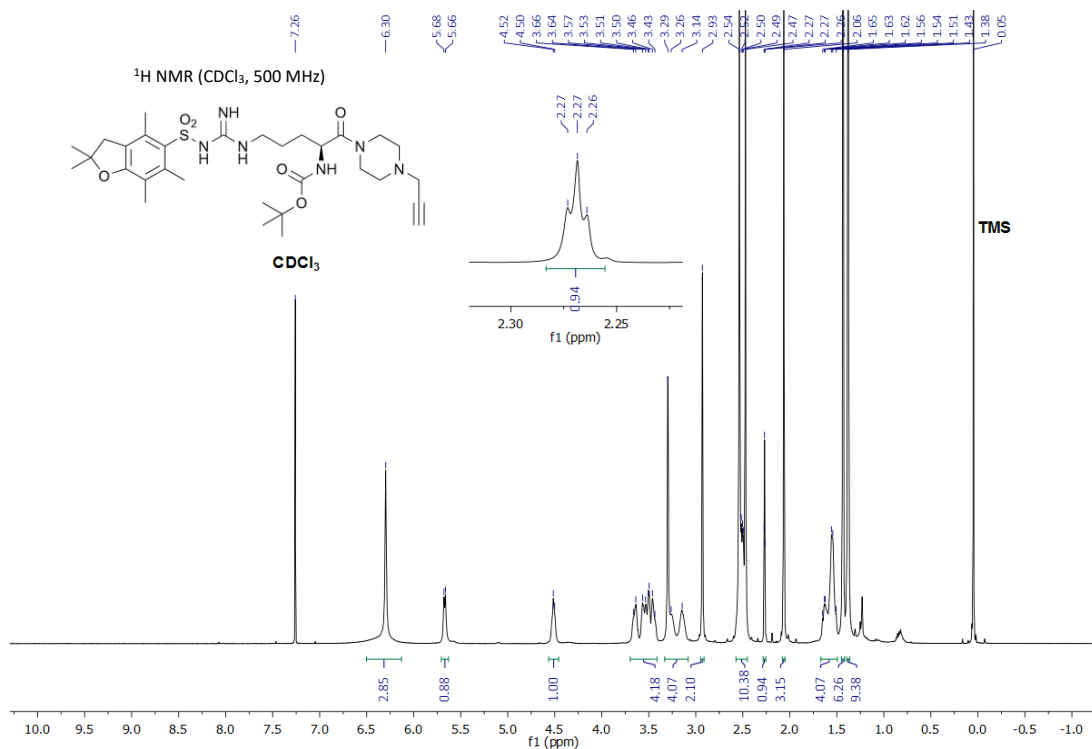
Figure 114

^{1}H NMR of compound **39a**.
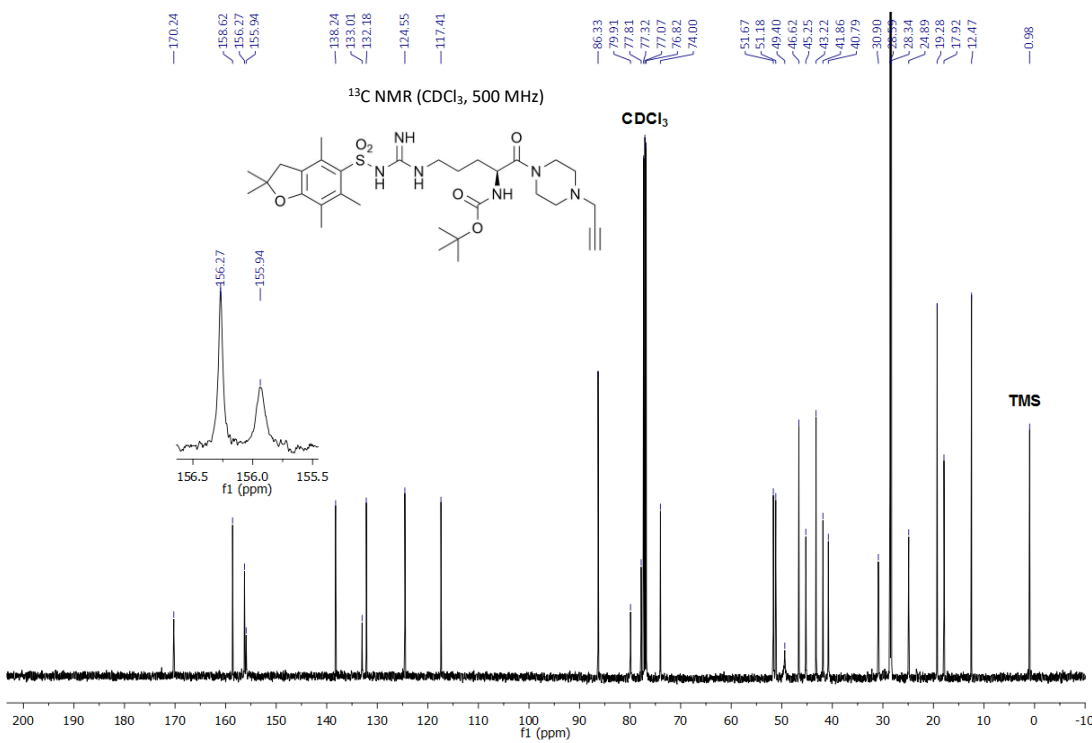
Figure 115

^{13}C NMR of compound **39a**.
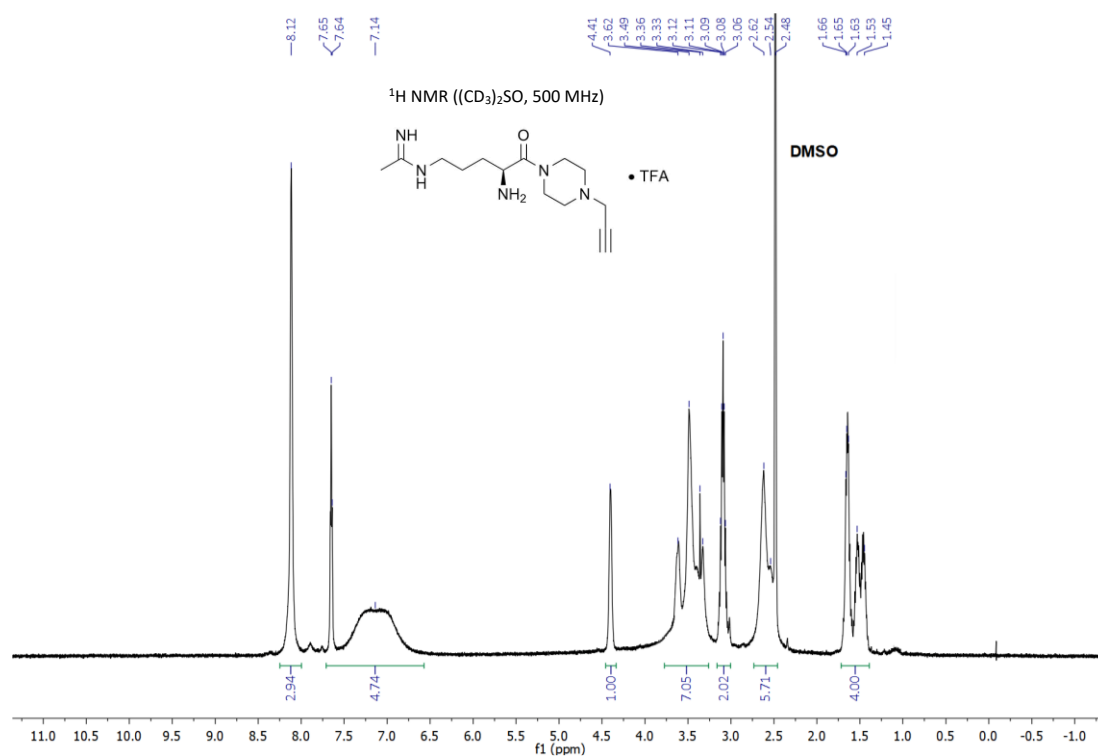
Figure 116

^{1}H NMR of compound **39b**.
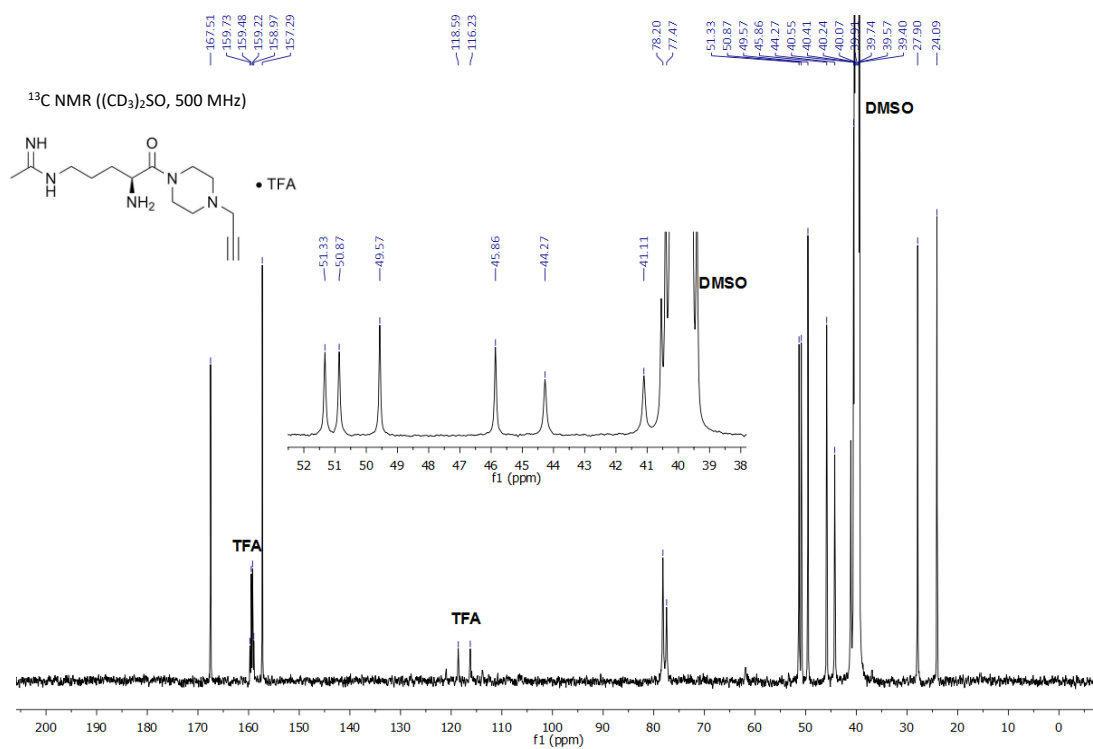
Figure 117

^{13}C NMR of compound **39b**.
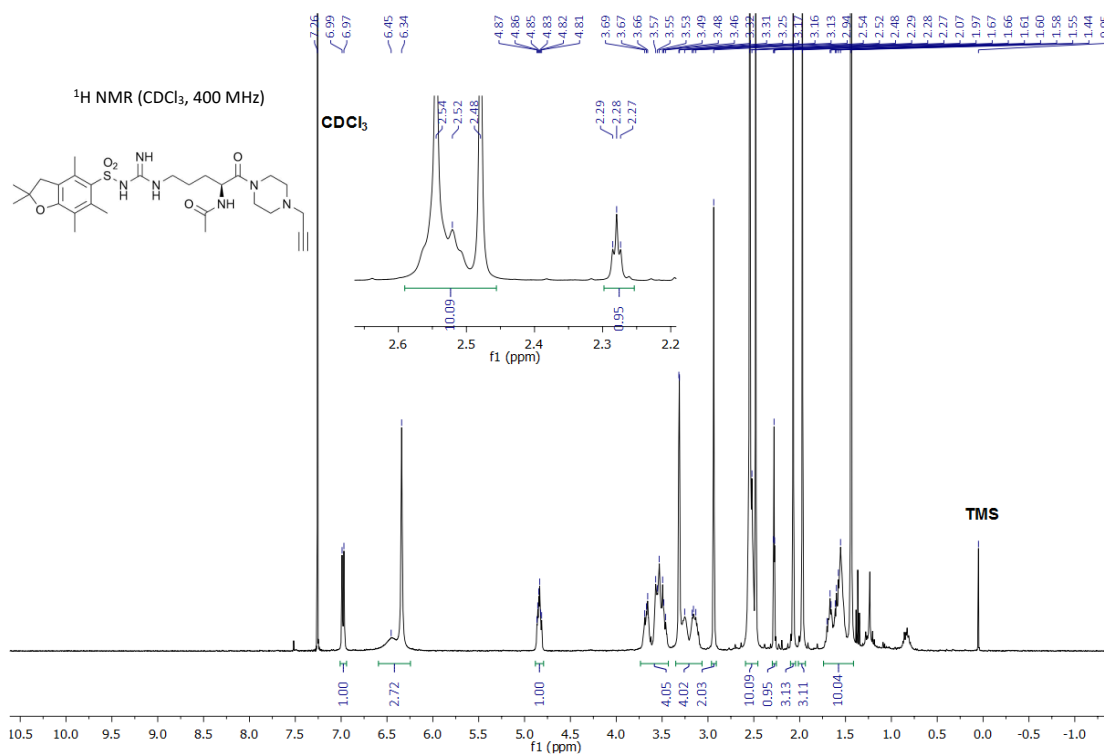
Figure 118

^{1}H NMR of compound **40a**.
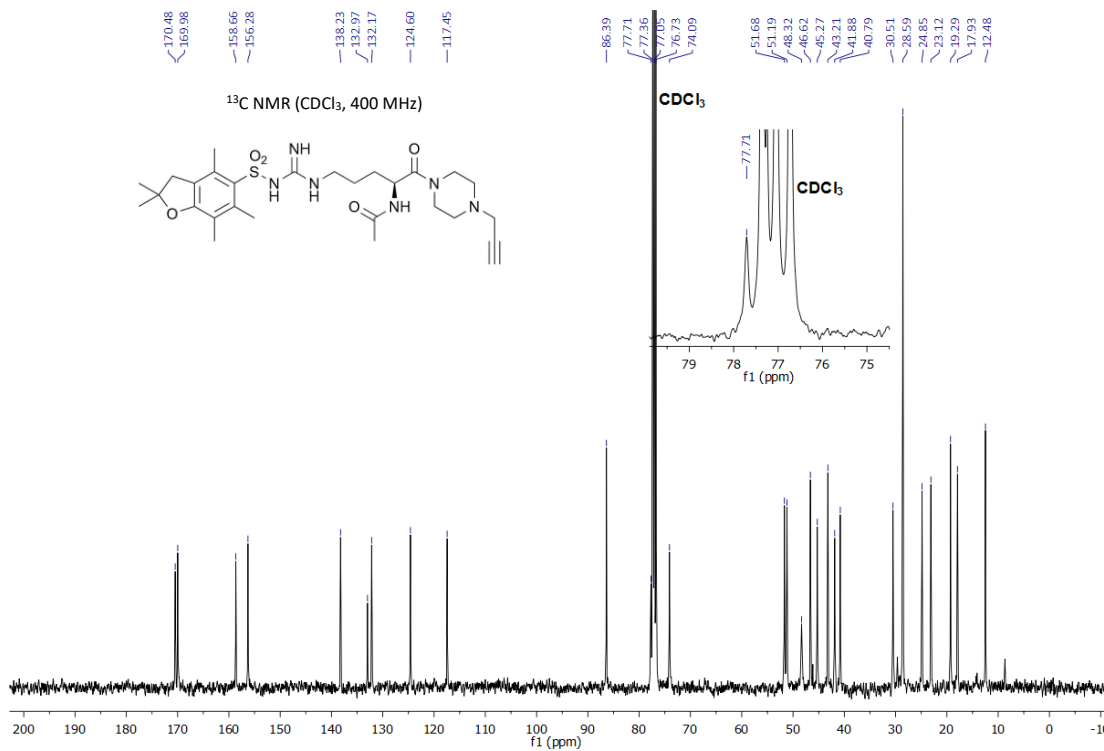
Figure 119

^{13}C NMR of compound **40a**.

Figure 120

¹H NMR of compound **40b**.
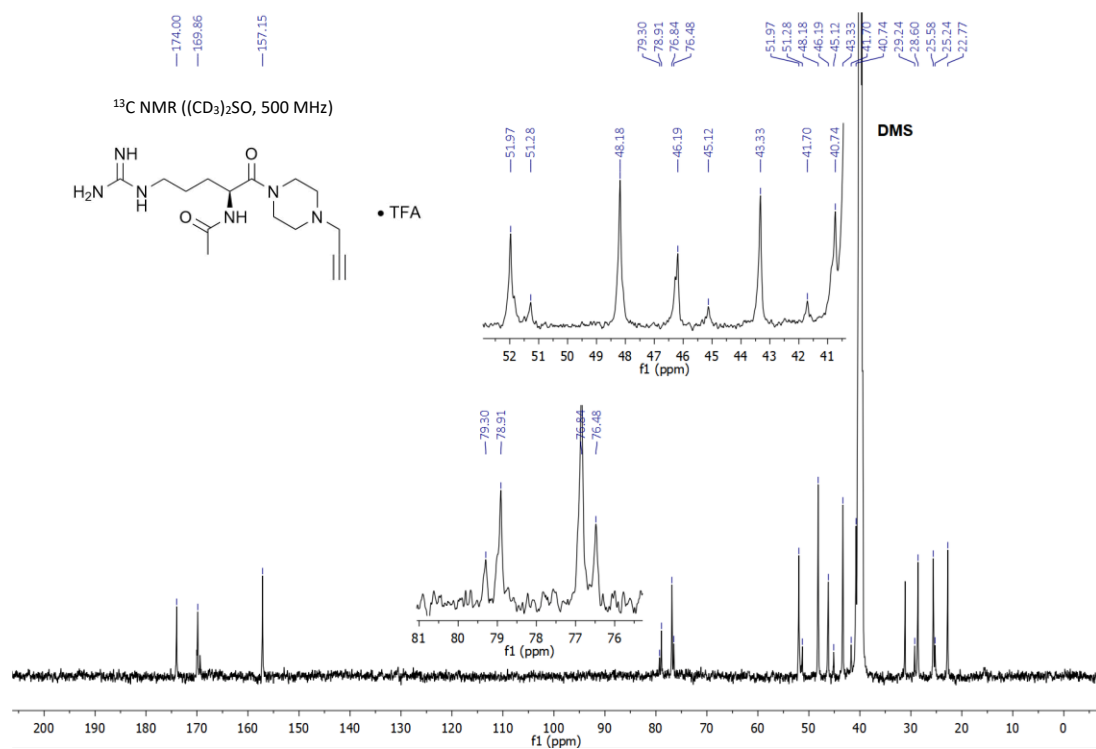
Figure 121

¹³C NMR of compound **40b**.
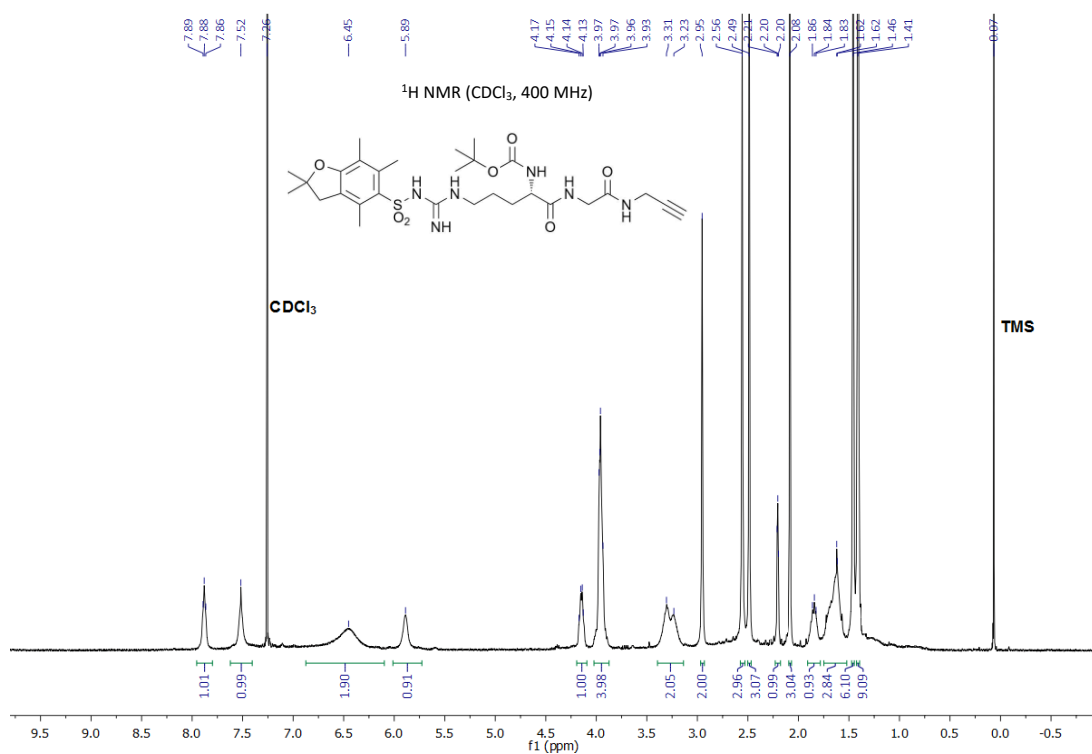
Figure 122

^{1}H NMR of compound **43a**.
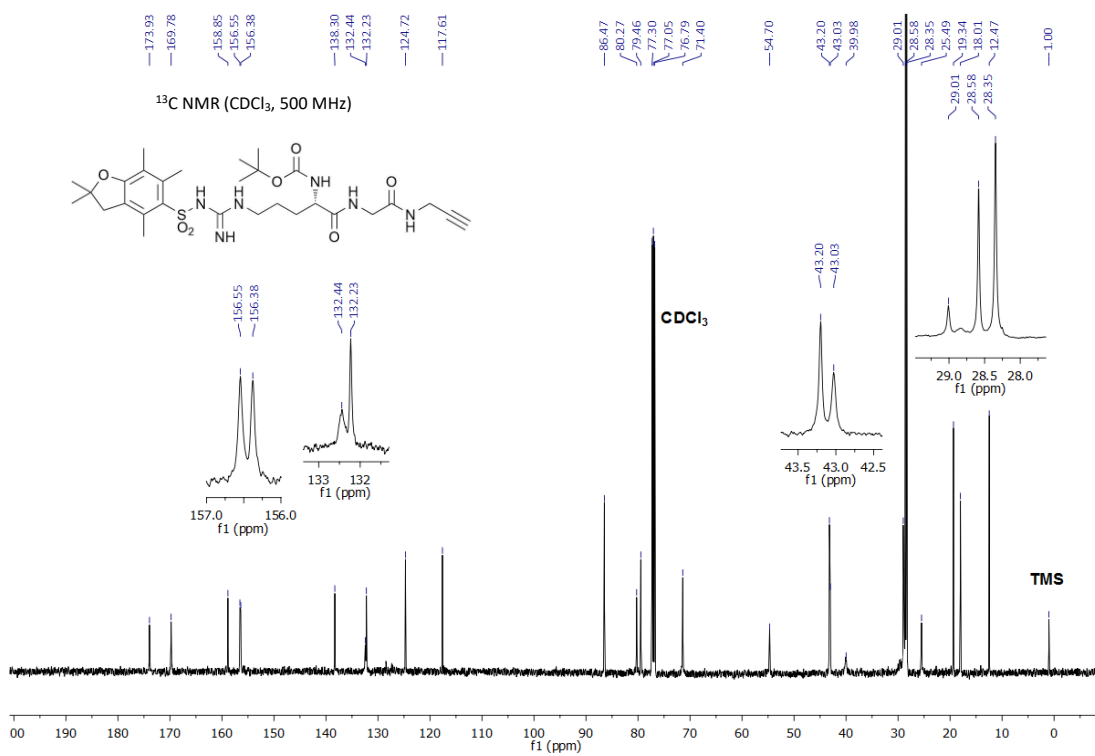
Figure 123

^{13}C NMR of compound **43a**.

^{1}H NMR ((CD$_3$)$_2$SO, 500 MHz)

H$_2$O

DMSO
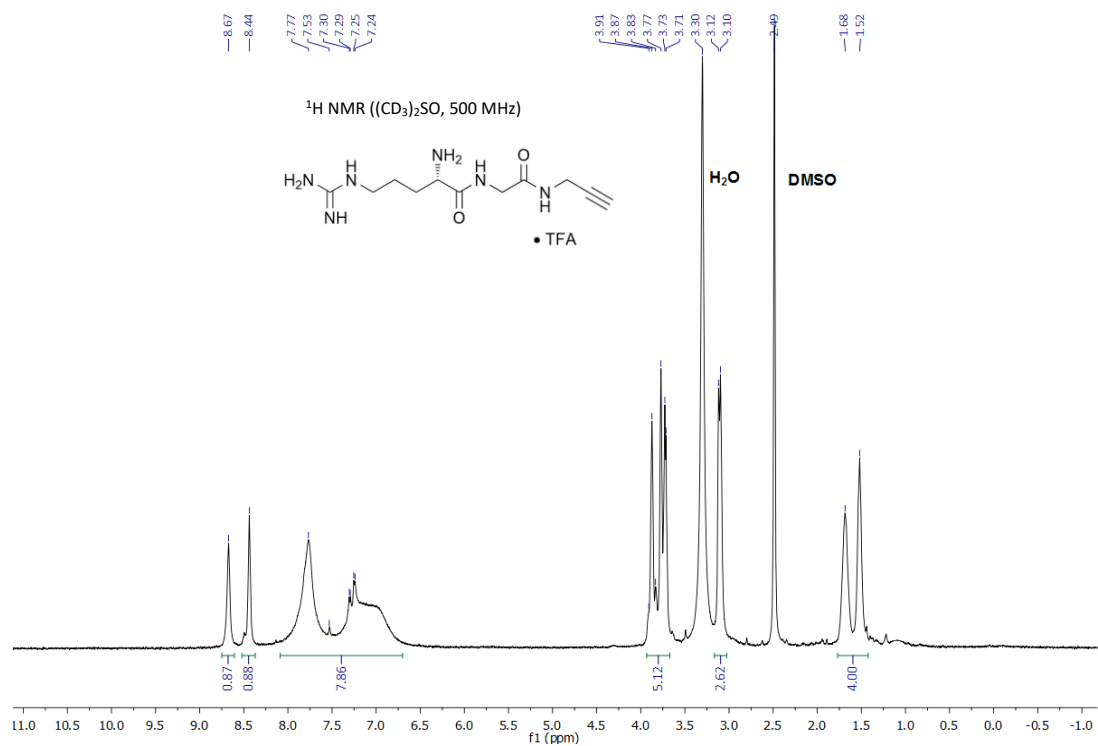
Figure 124

^{1}H NMR of compound **43b**.

^{13}C NMR ((CD$_3$)$_2$SO, 500 MHz)

DMSO

TFA

TFA
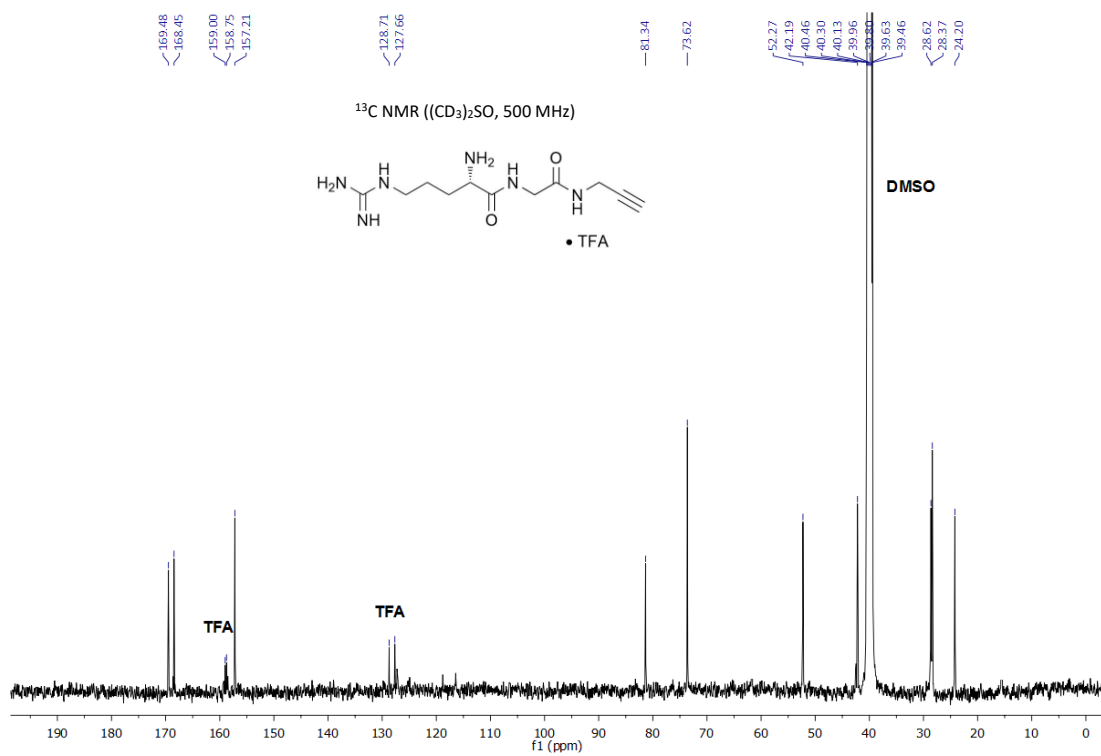
Figure 125

^{13}C NMR of compound **43b**.
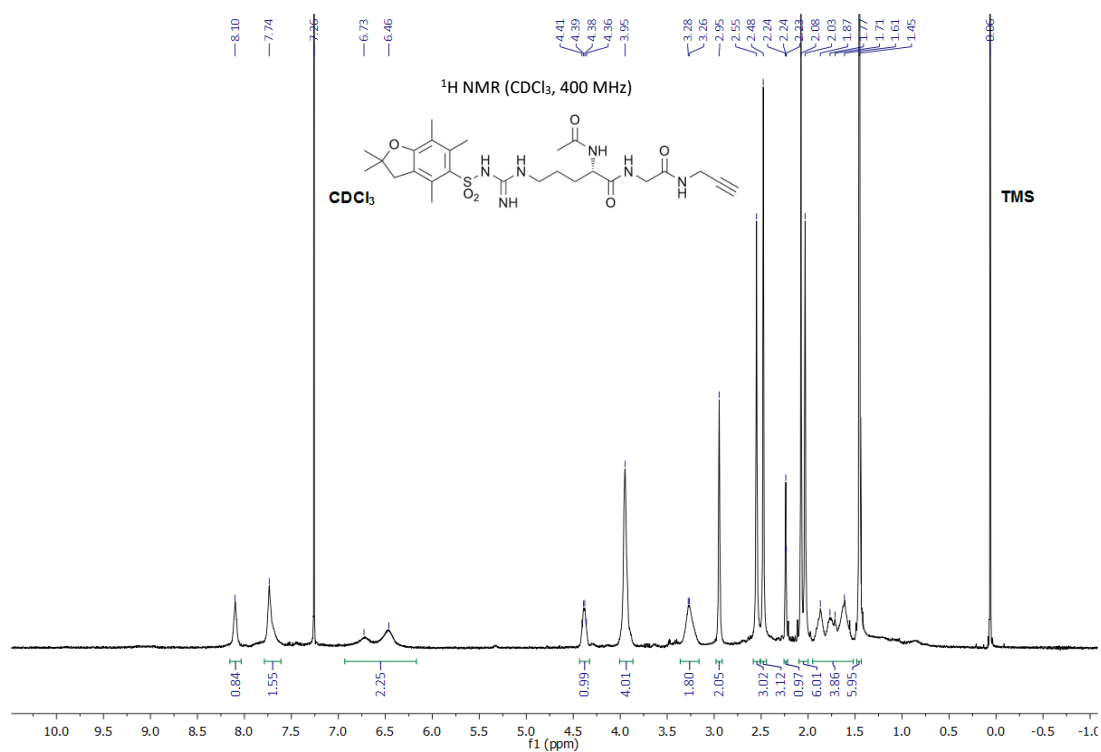
Figure 126

¹H NMR of compound **44a**.
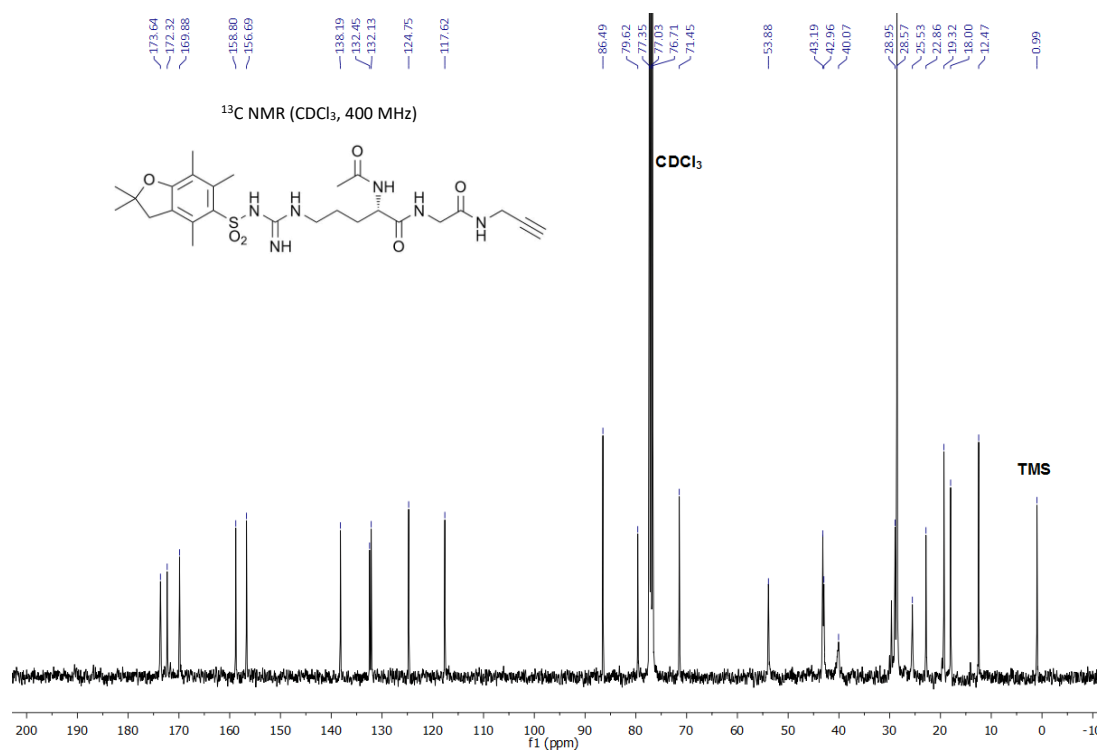
Figure 127

¹³C NMR of compound **44a**.
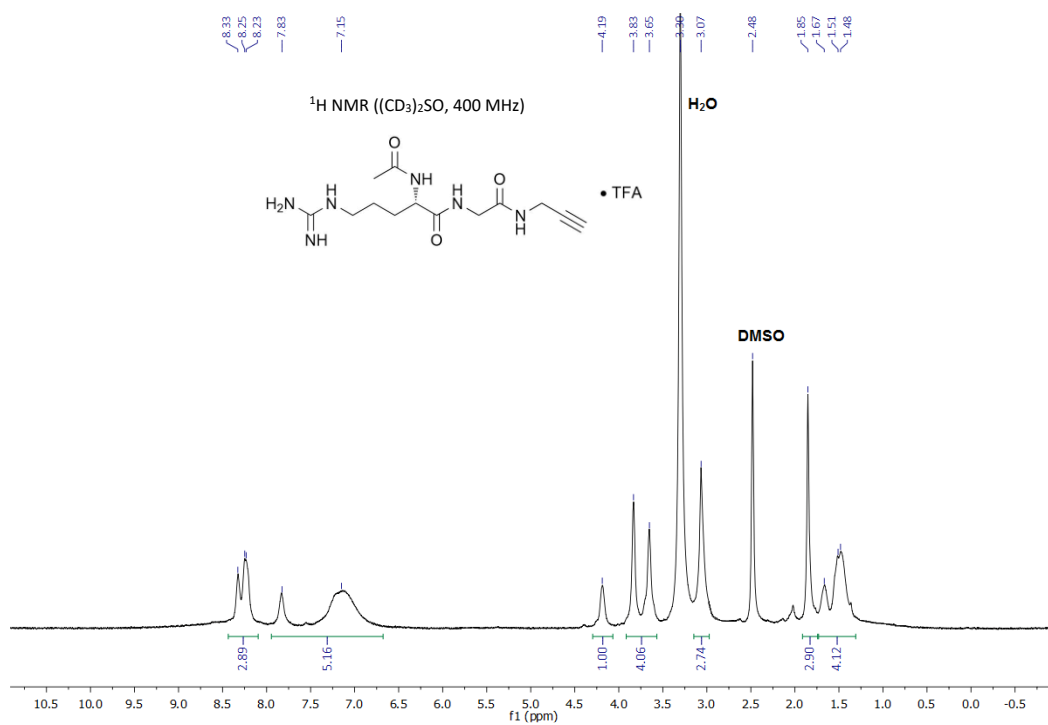
Figure 128

^{1}H NMR of compound **44b**.
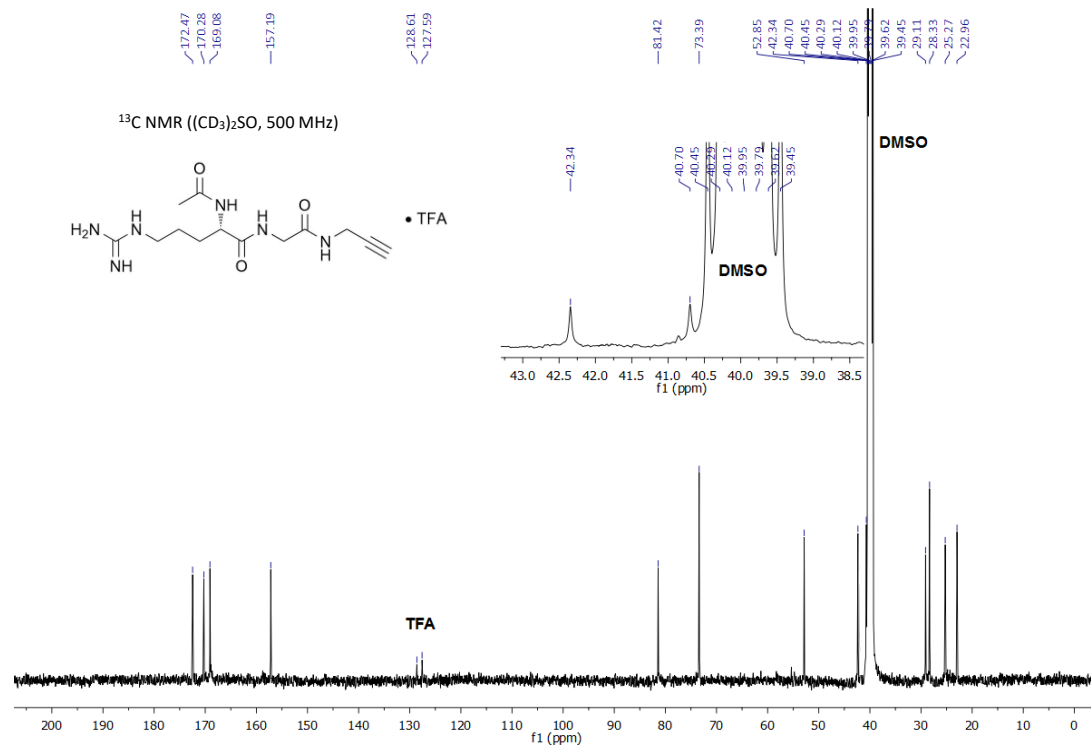
Figure 129

^{13}C NMR of compound **44b**.
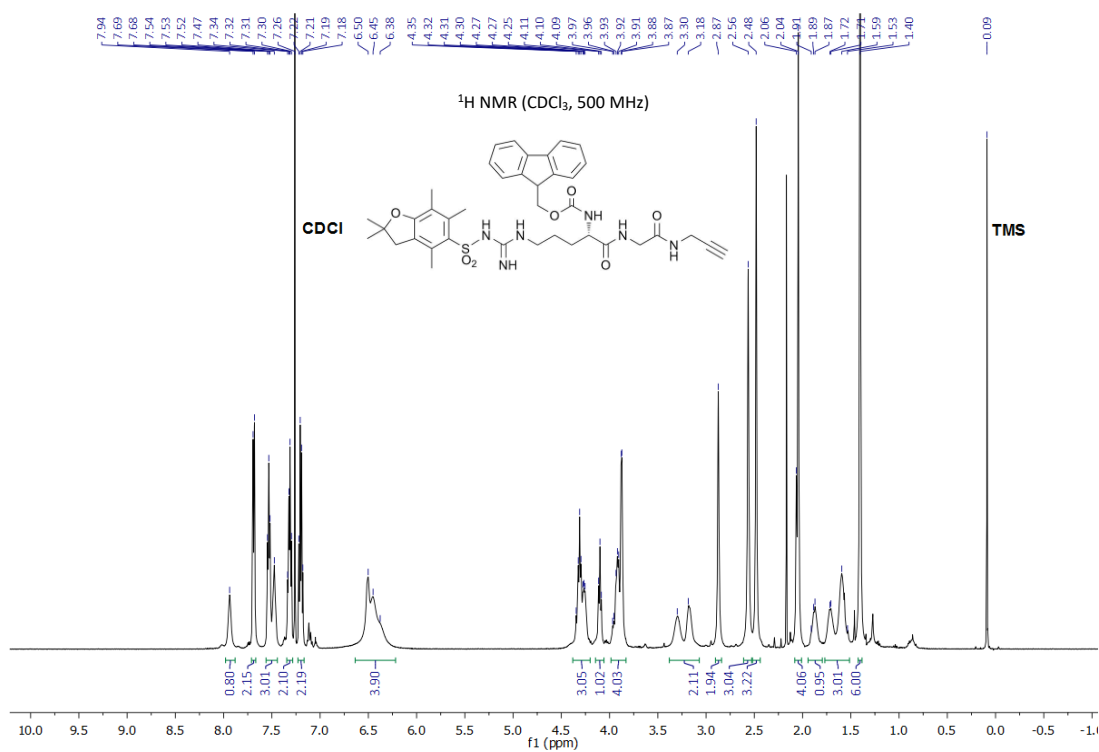
Figure 130

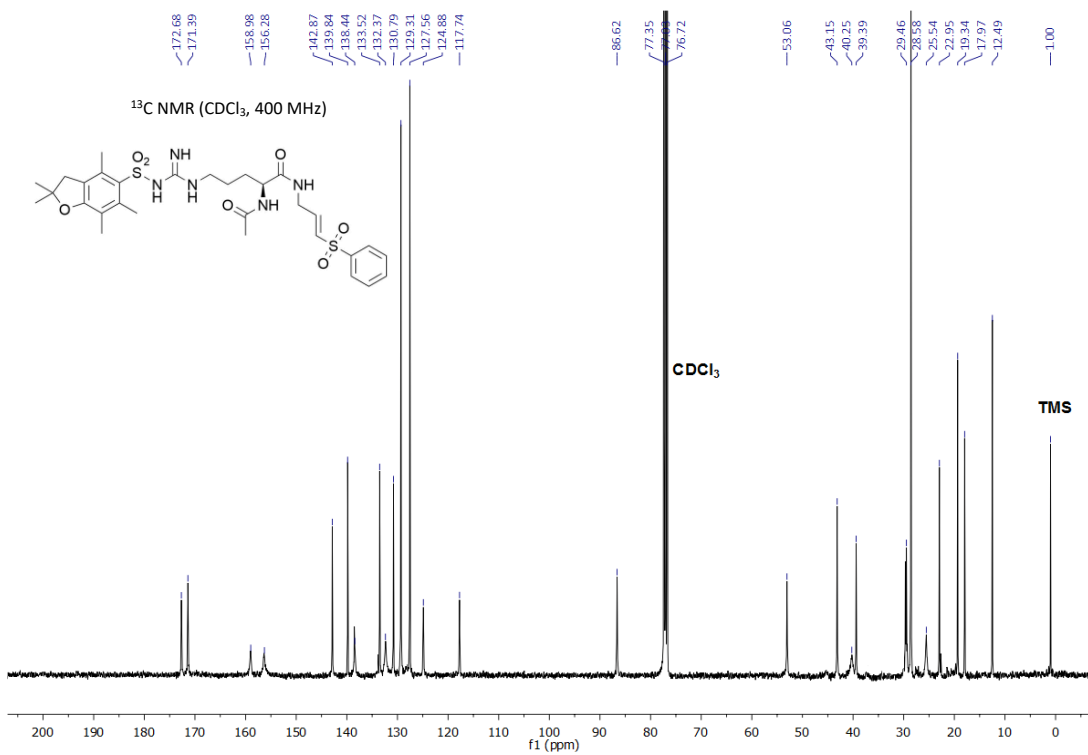¹H NMR of compound **49a**.
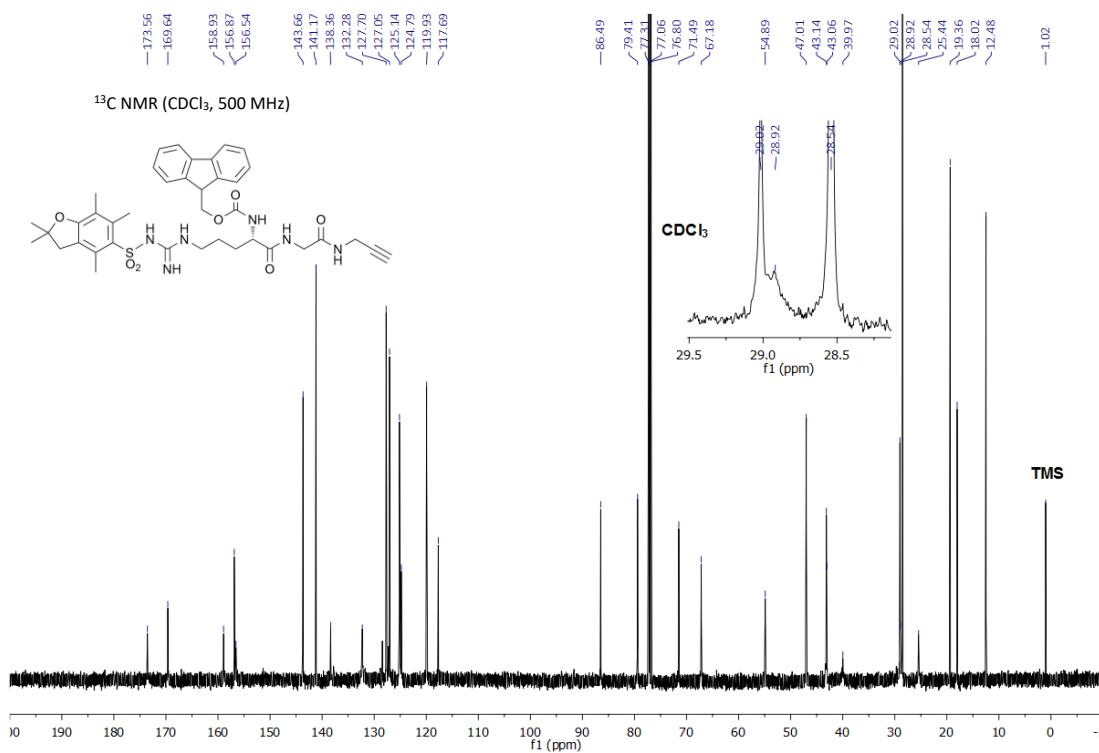
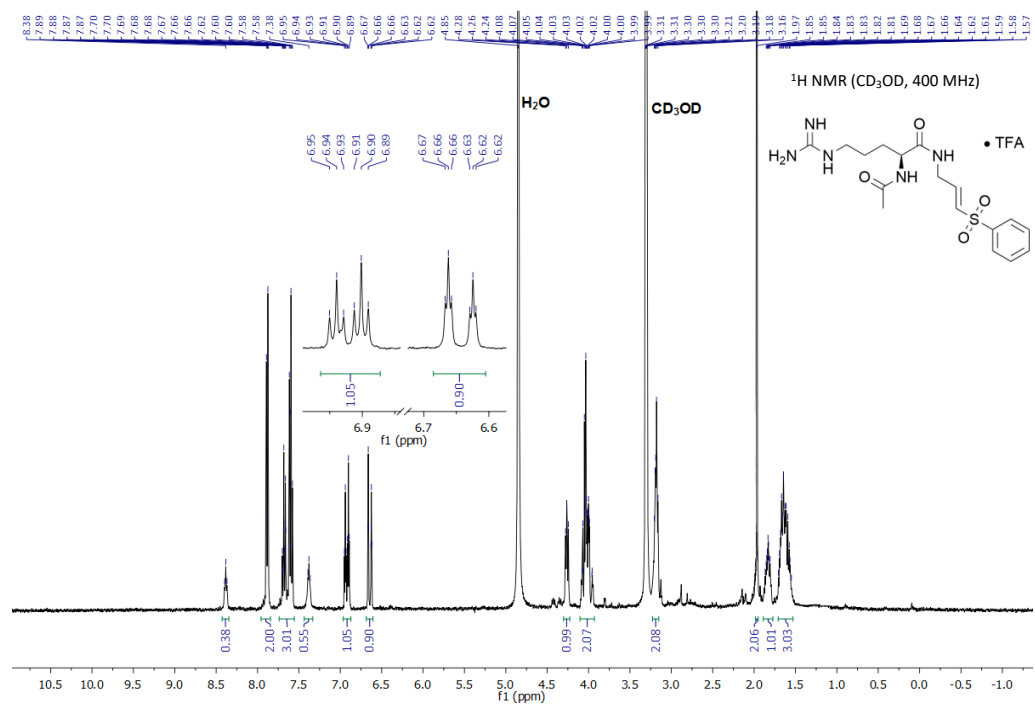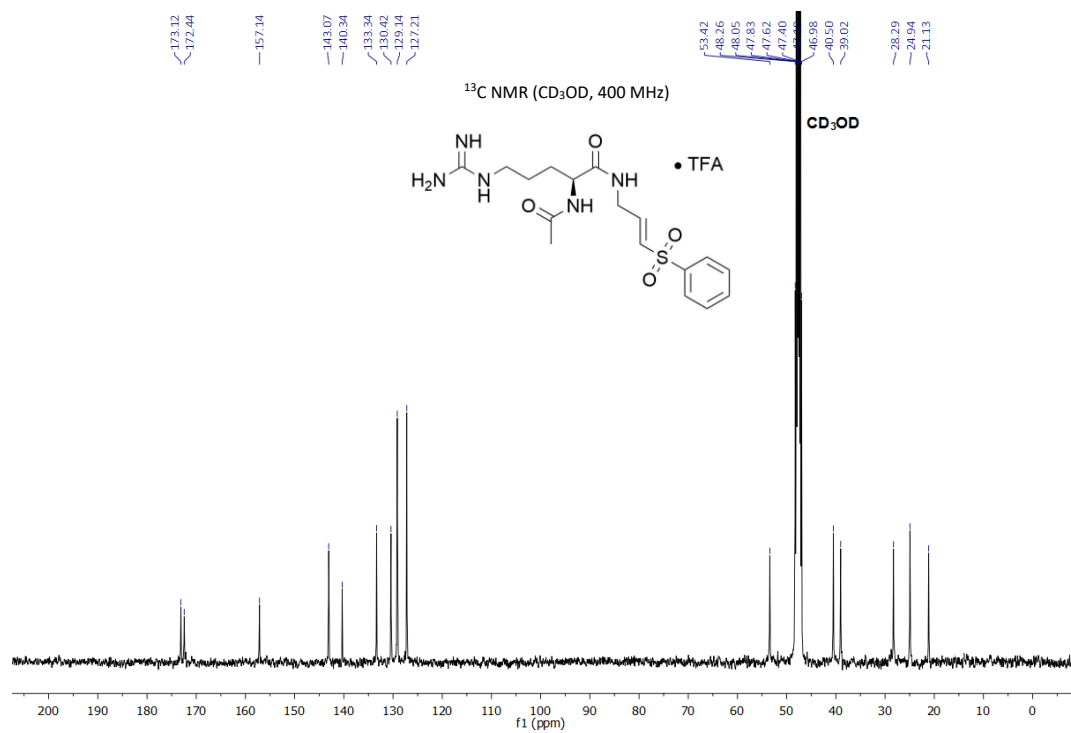## Figure 131

¹³C NMR of compound **49a**.
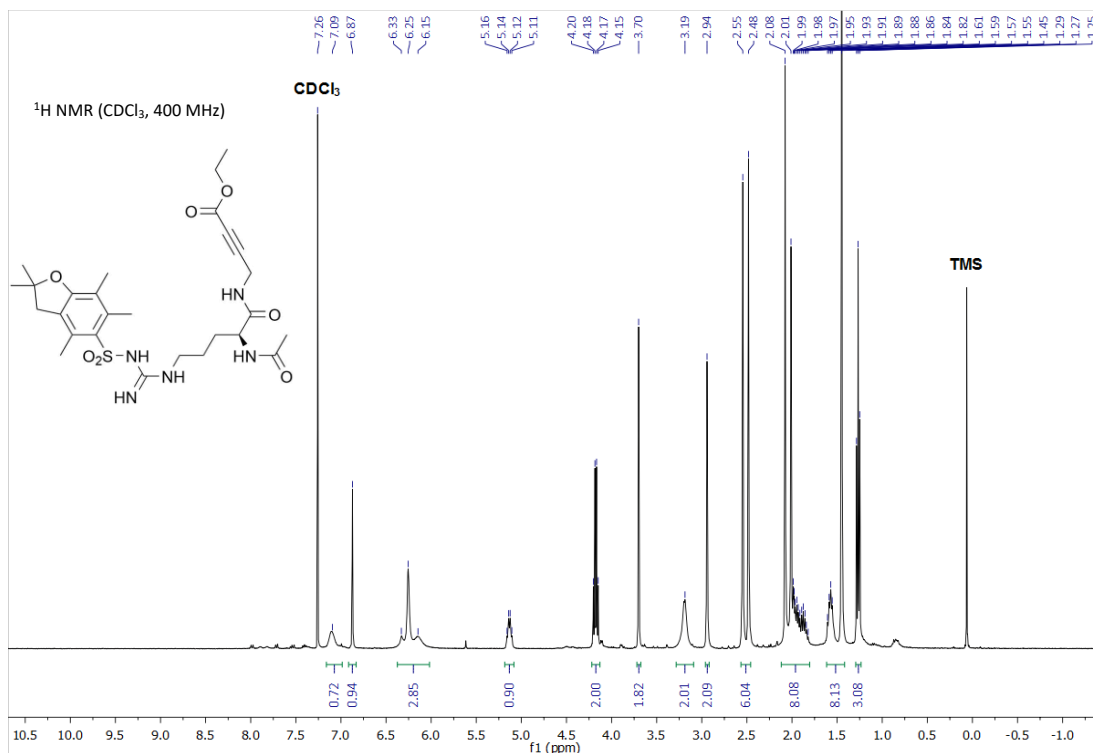
Figure 132

¹H NMR of compound **49b**.
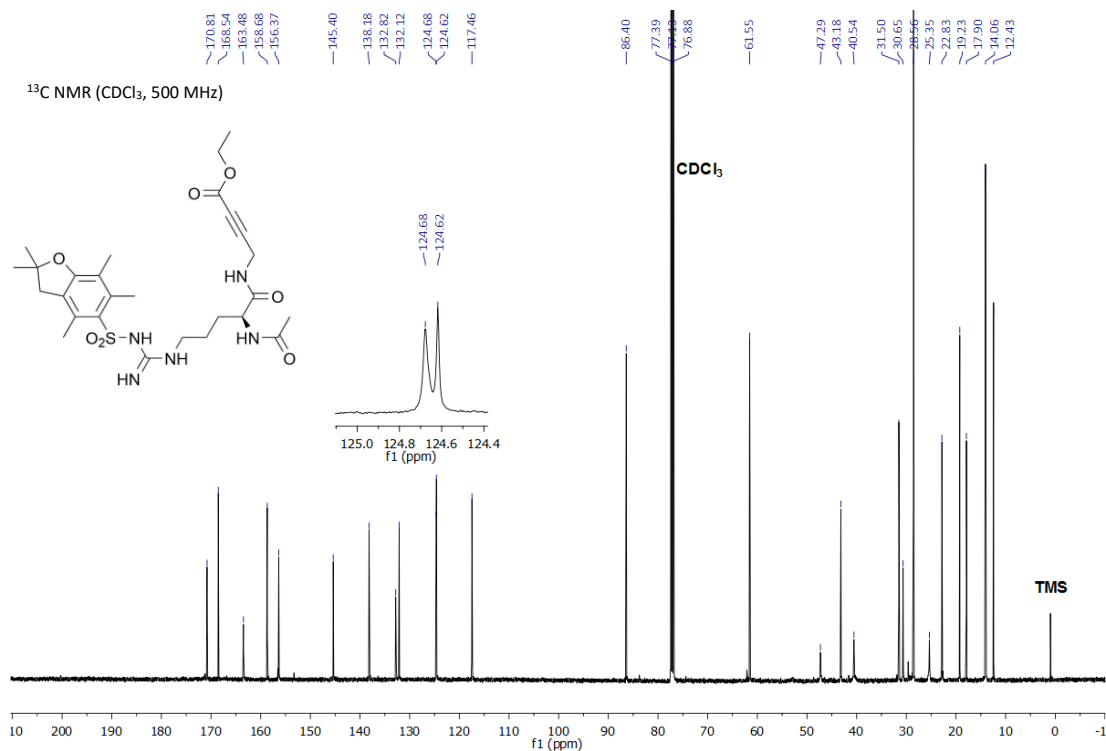
Figure 133

¹³C NMR of compound **49b**.
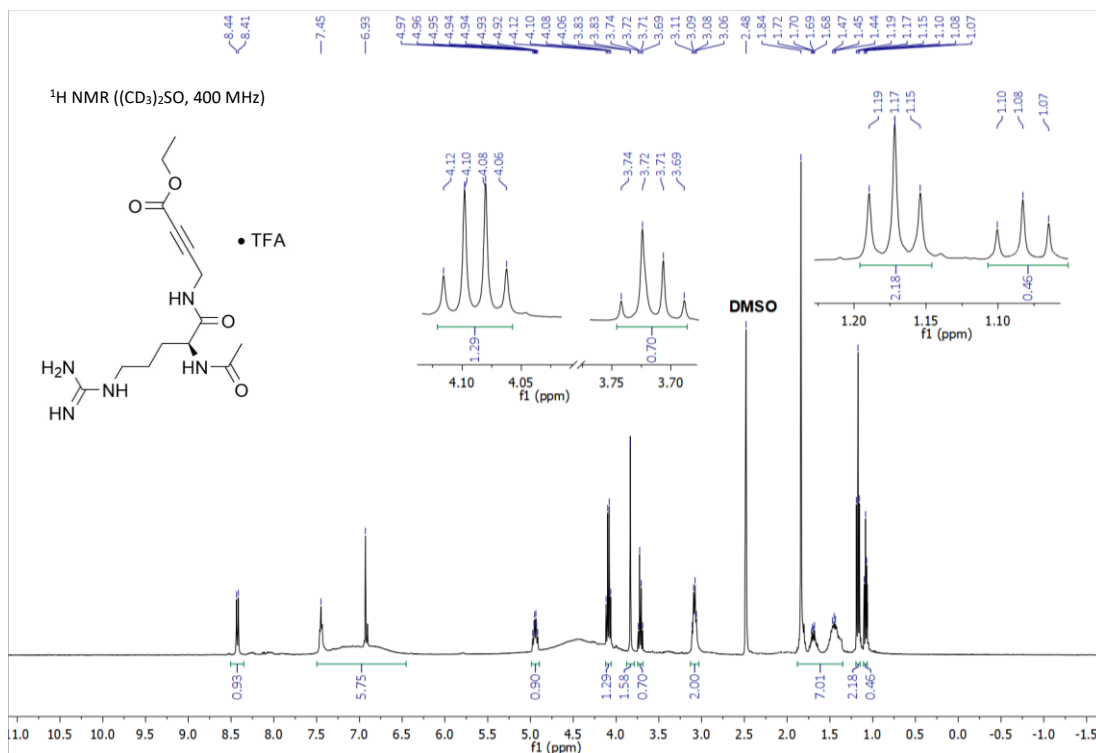
Figure 134

^{1}H NMR of compound **45a**.
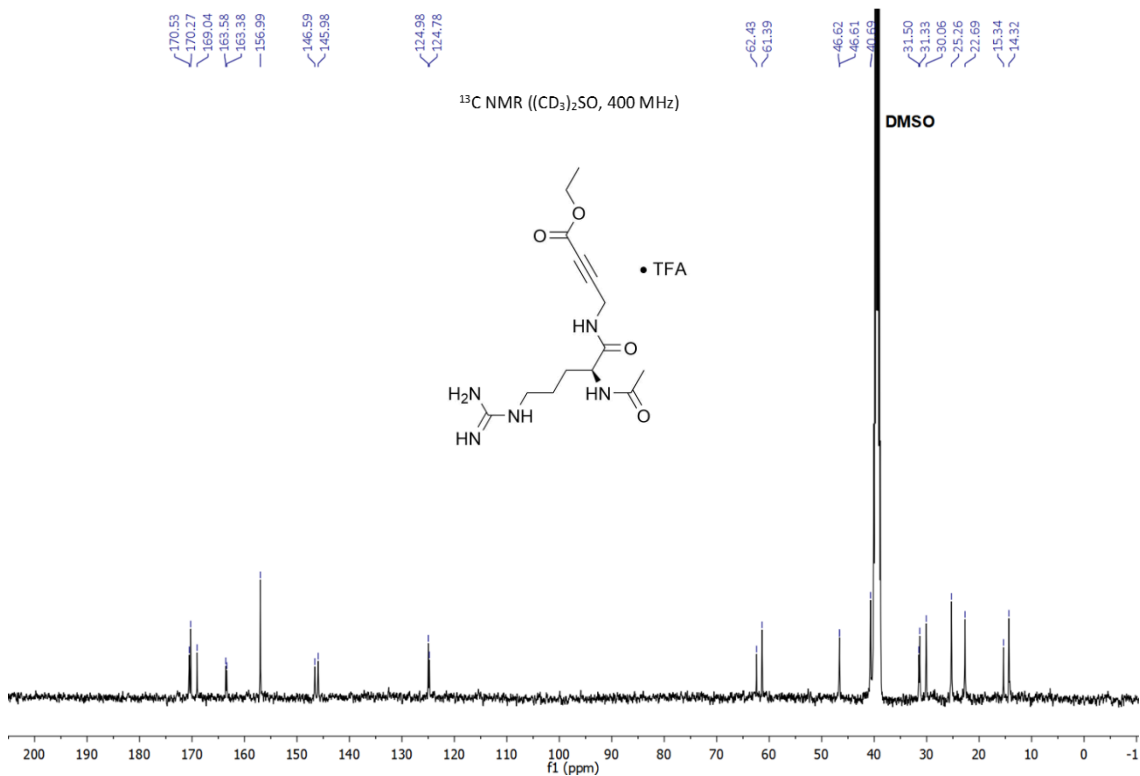
Figure 135

^{13}C NMR of compound **45a**.
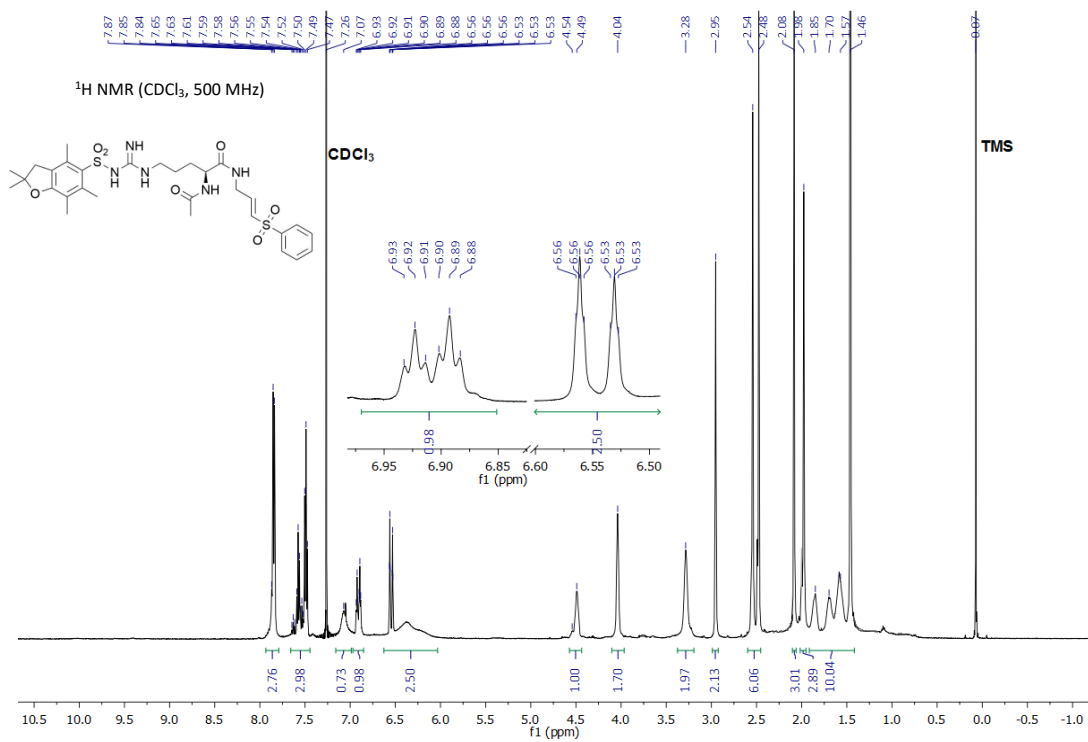
Figure 136

¹H NMR of compound **51a**.

Figure 137

¹³C NMR of compound **51a**.

Figure 138

^{1}H NMR of compound **51b**.

Figure 139

^{13}C NMR of compound **51b**.